Techniques for condition monitoring using cyclo-non-stationary signals

Barbini, Leonardo

Award date:
2018

Awarding institution:
University of Bath

Techniques for condition monitoring using cyclo-non-stationary signals

submitted by

Leonardo Barbini

for the degree of Doctor of Philosophy

of the

University of Bath

Department of Mechanical Engineering

September 2017

This thesis is dedicated to all those who are dear to me.

Acknowledgements

I would like to express my gratitude to the academics and researchers who helped me during this research work and to the University of Bath for the financial support. A special thanks goes to my supervisor Dr. J. L. du Bois for giving me both guidance and freedom, to Dr. A. Ompusunggu for the numerous discussions and to Dr. M. Eltabach for providing valuable expertise. I would also like to thank Flanders Make in Belgium, the National Renewable Energy Laboratory in the United States and the Centre Technique des Industries Mécaniques and Safran in France for sharing their data.

Summary

Condition based maintenance is becoming increasingly popular in many industrial contexts, offering substantial savings and minimising accidental damage. When applied to rotating machinery, its most common tool is vibration analysis, which relies on well-established mathematical models rooted in the theory of cyclo-non-stationary processes. However, the extraction of diagnostic information from the real world vibration signals is a delicate task requiring the application of sophisticated signal processing techniques, tailored for specific machines operating under restricted conditions. Such difficulty in the current state of the art of vibration analysis forces the industry to apply methods with reduced diagnostic capabilities but higher adaptability. However in doing so most of the potential of vibration analysis is lost and advanced techniques becomes of use only for academic endeavours. The aim of this document is to reduce the gap between industrial and academic applications of condition monitoring, offering ductile and automated tools which still show high detection capabilities. Three main lines of research are presented in this document. Firstly, the implementation of stochastic resonance in an electrical circuit to enhance directly the analog signal from an accelerometer, in order to lower the computational requirements in the next digital signal processing step. Secondly, the extension of already well-established digital signal processing techniques, cepstral prewhitening and spectral kurtosis, to a wider range of operating conditions, proving their effectiveness in the case of non-stationary speeds. Thirdly, the main contribution of the thesis: the introduction of two novel techniques capable of separating the vibrations of a defective component from the overall vibrations of the machine, by means of a threshold in the amplitude spectrum. After the separation, the cyclic content of the vibration signal is extracted and the thresholded signals provide an enhanced detection. The two proposed methods, phase editing and amplitude cyclic frequency decomposition, are both intuitive and of low computational complexity, but show the same capabilities as more sophisticated state of the art techniques. Furthermore, all these tools have been successfully tested on numerically simulated signals as well as on real vibration data from different machinery, lasting from laboratory test rigs to wind turbines drive-trains and aircraft engines. So in conclusion, the proposed techniques are a promising step toward the full exploitation of condition based maintenance in industrial contexts.

Keywords: vibration analysis - condition monitoring - cyclo-non-stationary vibrations - variable speed - phase editing - amplitude cyclic frequency decomposition.

Contents

List of Figures

List of Tables

Chapter 1

Introduction

Nomenclature			
$\boldsymbol{b(t)}$	vibrations from bearings	$\boldsymbol{g(t)}$	vibrations from gears
$\boldsymbol{n(t)}$	vibrations from other components	$\boldsymbol{v(t)}$	total vibrations
$\boldsymbol{T_{im,p}(t)}$	occurrence time of p^{th} impact	$\boldsymbol{\Theta}$	angular separation between impacts
$\boldsymbol{\Psi}$	random angular jitter between impacts	$\boldsymbol{\overline{f}_{sh,k}(t)}$	mean shaft rotational speed
$\boldsymbol{m_b(t)}$	impulse response of single impact	$\boldsymbol{w(t)}$	white noise
$\boldsymbol{h(t)}$	impulse response of band pass filter	$\boldsymbol{f_l, f_h}$	cut off frequencies
$\boldsymbol{a}$	exponential decay constant	$\boldsymbol{D_p}$	random amplitude of impact
$\boldsymbol{e^{A,B}(t)}$	vibrations from wheels A,B	$\boldsymbol{m(t)}$	vibrations from meshing of wheels
$\boldsymbol{E^{A,B}}$	amplitude of vibrations from wheels	$\boldsymbol{r_e}$	harmonic order of A,B
$\boldsymbol{\alpha, \theta, \beta, \gamma}$	phases of vibrations	$\boldsymbol{f_{A,B}}$	rotational speed of A,B
$\boldsymbol{N_{A,B}}$	number of teeth	$\boldsymbol{M}$	amplitude of meshing
$\boldsymbol{r_m}$	harmonic order of meshing	$\boldsymbol{r_c}$	harmonic order of phase modulation
$\boldsymbol{r_d}$	harmonic order of amplitude modulation	$\boldsymbol{C^{A,B}}$	amplitude of phase modulation
$\boldsymbol{D_{A,B}}$	amplitude of amplitude modulation	$\boldsymbol{m_g(t)}$	impulse response of vibrations from gears
$\boldsymbol{S_{vv}(l, f)}$	spectral correlation of $v(t)$	$\boldsymbol{SES_v(l)}$	squared envelope spectrum of $v(t)$
$\boldsymbol{SK_v^w}$	spectral kurtosis of $v(t)$	$\boldsymbol{rc_v(q)}$	real cepstrum of $v(t)$
$\boldsymbol{cpw_v(t)}$	cepstral prewhitening of $v(t)$	$\boldsymbol{r_k m}$	Kramers rate
$\boldsymbol{\Delta U}$	height of potential barrier	$\boldsymbol{T_\Omega}$	period of forcing
$\boldsymbol{\vec{F}\,[v(t), t_u]}$	vector of features	$\boldsymbol{t_u}$	utilisation time

1.1 Motivation

The constant demand for a stable economy and high living standards has motivated technological developments to ensure the reliability and the efficiency of industrial assets. In this context, maintenance has a pivotal role ensuring the maximal performance of all the machines within the asset and avoiding their failure, or ultimately a com-

plete breakdown. Historically, maintenance was implemented following a preventive strategy: interventions on the machines are carried out at predetermined intervals, according to criteria recommended by the machine supplier, such that the likelihood of failure between maintenance interventions is minimised. However preventive maintenance has evident economical disadvantages. As a matter of fact the full life of the various components is not exhausted, because interventions are scheduled more frequently than needed, resulting in a greater use of spare parts and added maintenance costs. For this reason, in a wide range of industries, the strategy is changing from preventive to condition based maintenance. As the name suggests, the idea consists of scheduling maintenance interventions based on the technical condition of machines, while they are in operation. The advantages with respect to the traditional preventive strategy, besides the economical ones, are an increased reliability and real-time monitoring [Al-Najjar, 2007]. Condition based maintenance needs methods able to both:

1. determine the current condition of the machine, i.e. condition based monitoring
2. give an indication on its remaining useful life, i.e. prognostics

The condition of the machine is monitored by means of a three step procedure. Firstly, data are gathered using transducers to measure different physical characteristics of the machines such as vibrations, temperature, acoustic emissions. Secondly, the acquired data are mapped into a feature space using digital signal processing algorithms. Finally, features are classified based on the previous history of the machine and the condition is determined [Jardine et al., 2006]. On the other hand, prognostic information is estimated from data driven approaches applied to the feature space or from physics based models for the evolution of failures [Heng et al., 2009b]. Based on this information it is then possible to schedule a maintenance intervention to ensure the proper operational conditions of the machine. Figure 1.1 shows a schematic overview of condition based maintenance and emphasises how this new strategy can be seen as a system of systems engineering and the focus of research could be each block, or conversely the relationship between different blocks [Vachtsevanos et al., 2006]. Within the framework of condition based maintenance, this thesis focuses on improving one of these blocks. Specifically, the research work was on condition monitoring, with the objective of developing signal processing methods for monitoring bearings using vibration data. The following outlines the motivations which led to a focus on this topic in particular.
The focus on vibration analysis among other techniques is motivated by the fact that by far it is the most commonly used. The reasons are both historical, with some classical books on vibration analysis more than 30 years old [Braun, 1986], and practical,

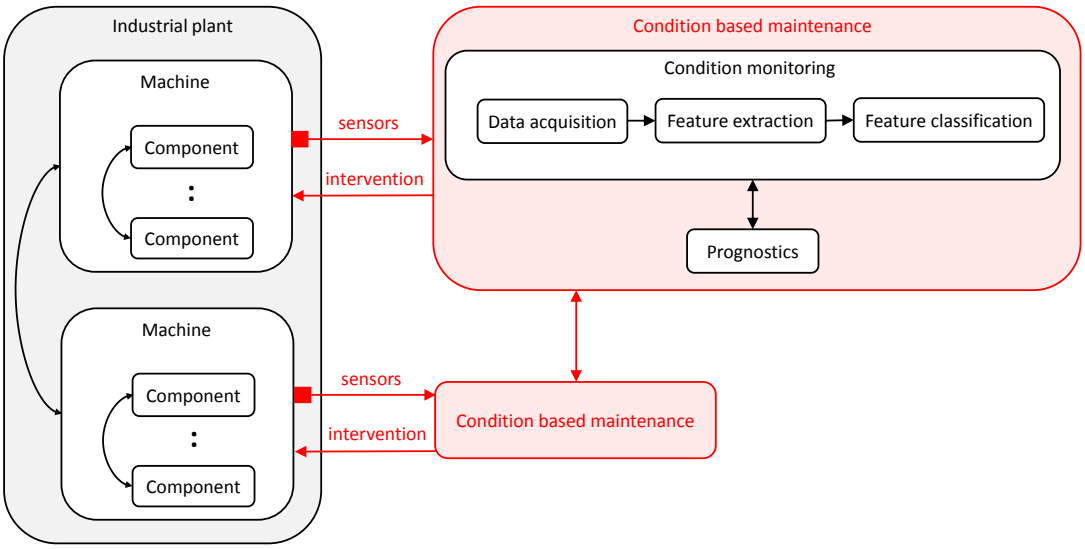

Figure 1.1: Schematics of condition based maintenance

with a large class of machines producing vibrations which carry diagnostic information and ease of positioning of vibration transducers. The sources of these vibrations are directly linked to events in the operation of the machine. Typical examples are rotating shafts and bearings, meshing of gears, rotating magnetic fields and combustion events. The machine in good condition has its typical vibration signature and the presence of a malfunction in one of its components yields a change in this signature, which carries all the diagnostic information necessary to drive the maintenance intervention. In addition, vibration signals from real world machines, comprising engines [Safran, 2017] or gearboxes in electrical power generators [Sheng, 2012], are available online for research purposes. These data sets have been studied thoroughly in several papers [Antoni et al., 2017a, Peeters et al., 2016, Siegel et al., 2014], therefore they offer the possibility of comparing the performance of the signal processing methods proposed in this thesis with that of state of the art techniques.

Among all the machines producing vibration carrying diagnostic information, rotating machines are the most commonly used, existing in a wide variety of industrial applications such as power production, vehicle transportation, process manufacturing. For such a class of machines, the events producing vibrations occur periodically with respect to the rotating components, and the presence of a malfunction can be effectively monitored by means of spectral analysis. In a rotating machine the most common component is the bearing, transferring the working load from the rotating element to the body, with small motion resistance and good positioning. Bearings operate continuously for a long time, under various conditions of load and speed hence they wear

out, causing friction processes which create point and surface faults in one or multiple of their parts. In contrast to other components of a rotating machine, the bearing does not produce significant vibrations when it operates in healthy conditions and the weak vibration signal produced by the defective bearings is likely to be masked by the underling vibration signature of the machine and further result in a missed detection. In addition, it is recognised that the malfunctioning of a bearing brings longer down times in comparison to other components and can result in catastrophic failures [Ribrant and Bertling, 2007]. For these reason, this research work focuses on condition based maintenance of bearings using vibration data.

After definition of this specific diagnostic objective potential avenues for improving condition based maintenance capabilities, referring to Fig. 1.1, are either condition monitoring or prognostics. As a matter of fact, the development of prognostic methods requires data for all the life span of the machine which is of the scale of years, in contrast to a few seconds of vibration signals needed in condition monitoring. The condition based maintenance community is trying to address this intrinsic complexity in the evaluation of prognostic methods and has developed experimental setups where bearings are used in abnormal conditions and undergo an accelerated degradation [IMS, 2017, Nectoux et al., 2012, Gebraeel et al., 2004] or where defects are seeded both electronically or mechanically in the bearings [Singleton et al., 2017, Elforjani and Mba, 2008]. However, these accelerated life tests do not reproduce the real world evolution of the defect and the research on prognostics suffers from a fundamental limitation until appropriate databases become available. For this reasons, this thesis focuses on the task of condition monitoring, in order to develop methods that can be thoroughly tested on vibration data from machines operating in real conditions. As stated above these data are currently available from a variety of sources for research purposes.

Two aspects of condition monitoring are interesting from a research point of view: mathematical modelling of the vibration signals in order to define which features can provide diagnostics information, and development of signal processing methods for feature extraction and classification. In the condition monitoring community, it is well established that vibrations from rotating machines have to be modelled as cyclostationary and cyclo-non-stationary signals and in the last decade several mathematical models have been proposed [Antoni et al., 2004, Abboud, 2015]. This resulted in the identification of features calculated from cyclic-spectral analysis as the best candidates for gathering all the necessary diagnostic information. On the other hand, there is still disagreement on which signal processing method is both applicable to a wide class of vibration signal and is reliable from the point of view of real industrial applications. Feature extraction and classification is indeed a delicate task, because an error at this

stage can result in a missed detection of a defective component and then a subsequent failure in the machine.
The features commonly used in condition monitoring can be divided in three classes, which are, in order of increasing computational complexity [Samuel and Pines, 2005]:

1. temporal
2. spectral
3. temporal/spectral
4. spectral/spectral.

Of these classes, typical examples are root mean square calculated on the time domain signals, the amplitude at certain frequencies in the spectrum of the signal or in the cepstrum, patterns in the short time Fourier transform, wavelet decomposition or in the spectral correlation. The diagnostic information extracted by the features differs between classes, and its selection is based on the specific diagnostic needs. Over recent years, the literature has seen an increasing number of signal processing methods to extract diagnostic features from vibration signals, driven both by the higher computational capabilities and growing interest from industries. An interesting aspect of the research in this field, is that many of the proposed methods accomplish higher diagnostics capability only by increasing the number of signal processing steps. However this adds computational complexity and raises the possibility of errors, therefore it is not suitable for real industrial applications. In addition, traditionally, feature selection and classification was done by a trained operator, with expertise in the particular area of the application. Nowadays the strategy is changing towards the use of semi automated or fully automated methods, the advantages being avoidance of human errors and savings in the condition monitoring systems. Therefore the use of signal processing methods involving several steps results in a difficult automation. For instance, methods used in commercially available condition monitoring systems offer lower diagnostics capabilities compared to those developed in the academic context, but are easy to implement and automate, and have higher reliability [Samuel and Pines, 2005, Hedin, 2014]. Another drawback of the signal processing methods currently used in condition monitoring, is that they are developed for stationary vibration signals, but in real world scenarios, there are many circumstances where stationarity is violated, due to machines operating at both varying speed and load, resulting in a deteriorated performance in the extraction of features [Borghesani et al., 2013b, Zimroz et al., 2014]. However, the mathematical modelling of vibration signals in non-stationary operation has been recently introduced [Abboud, 2015], opening new possibilities of research for

the community of condition based maintenance, some of which are investigated in this research work.
To summarise, the field of condition based maintenance with its broad range of tasks and high impact in the running costs of the industrial assets, is the objective of many research activities. Among which, this thesis focuses on vibration data for practical reasons, on monitoring the condition of bearings for applicability reasons while on development of signal processing methods because current techniques still have remaining challenges to address. In such a way it may maximise the possibility of applying the methods presented hereafter in machines from different industrial scenarios, with the hope of offering to the condition based maintenance community reliable and ductile tools.

1.2 Tutorial example of condition based maintenance

This section shows with a tutorial example the application of the condition based maintenance strategy on a simple machine. The data are artificial, and not from a real experimental situation and serves only for an illustration.
The machine which is monitored consists of a variable speed motor, a single stage gear, two rolling element bearings and a load applied to the output shaft of the gear. For this simple machine it is supposed that the analysis of its vibrations will provide all the necessary diagnostic information. Vibrations are measured by means of an accelerometer mounted on the housing of one of the bearings as shown in Fig. 1.2. Measurements are taken at fixed intervals of utilisation time t_u, which are decided considering factors such as history of failures, importance of the machine in the industrial asset, cost of repair. The utilisation time of the machine is much longer than the time t of the dynamics of the vibroacoustic processes $v(t)$. On the other hand, the length of each measurement is defined to ensure enough resolution based on the lowest cyclic frequency of interest, within the range of operating speed of the machine, usually corresponding to one of the fault frequencies of the bearings.

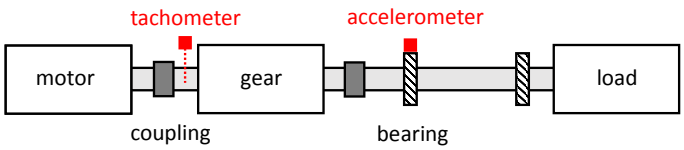

Figure 1.2: Schematics of tutorial example

Following the scheme of Fig. 1.1, the condition of the machine is then monitored studying the evolution of the norm of the features calculated on the vibration measurements $\|\vec{F}\,[v(t), t_u]\,\|$. The definition of the norm in the feature space depends on the history of failures of the machine, for example kurtosis would have a higher weight with respect to root mean square if the machine had a history of faulty bearings compared to gears [Randall, 2011]. The norms used in practice range from the simple Euclidean to statistical-based distances [Cardona-Morales et al., 2014]. In addition, features might be correlated and some authors propose to reduce the dimension of $\vec{F}[v(t), t_u]$ using principal component analysis, however in the new space the features lose their intuitive physical interpretation [Malhi and Gao, 2004].
The diagnostic information extracted by the condition monitoring step is then used as the input for the prognostic methodology implemented in the condition based maintenance program. Prognostic methods provide an estimation of the probability of failure of the machine [Heng et al., 2009a]. Figure 1.3 shows the condition based maintenance steps, on the top showing the evolution of the norm of the features of the vibration signal and on the bottom the probability of failure at two particular utilisation times.

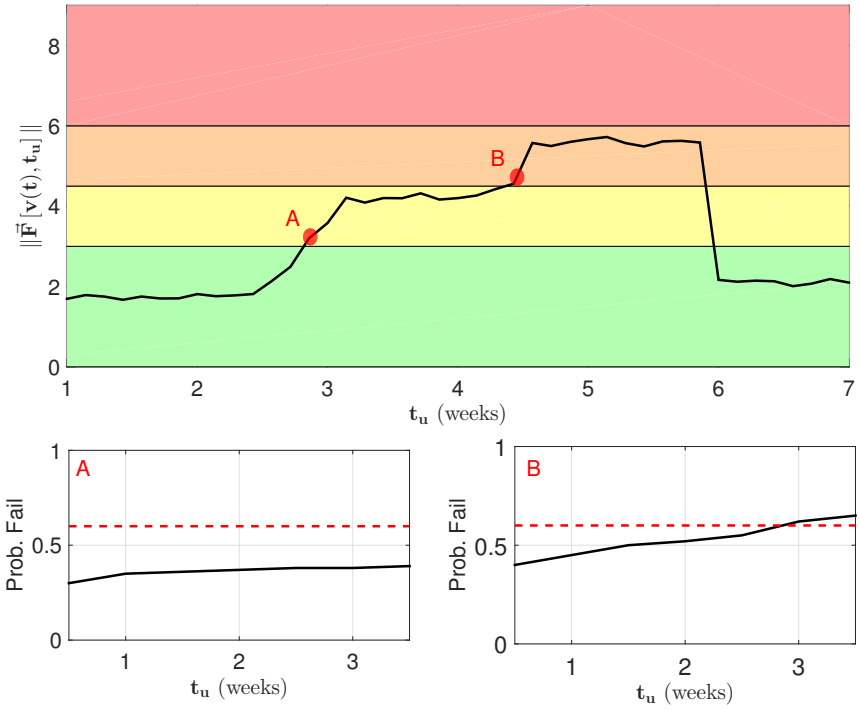

Figure 1.3: Trend of the norm of the vector of features calculated from vibration measurements, against the utilisation time of the machine (Top). Probability of failure of the machine calculated at utilisation times of points A and B (Bottom).

In Fig. 1.3 the regions from green to red correspond respectively to healthy, two warning regions and a failure region while the red dotted lines represent a threshold above which maintenance is required. The values of the thresholds are based on statistics of the machine failures or expertise of the condition monitoring technician.
In this tutorial example, let us suppose that after installation all the components of the equipment are working in healthy condition and $\|\vec{F}[v(t), t_u]\|$ shows low values and that after only a few weeks of operation the diagnostic metric reaches the first warning level A. It is in this situation that the work presented in the thesis finds its place. Since the machine is operating in an abnormal way, complex signal processing methods are applied to the measured vibration signal to determine which specific components are causing the malfunction. In regards to the specific diagnostic objective of the thesis, the state of the art methods currently used for detection of defective bearings will be described in Section 1.3.3, while Chapter 4 and Chapter 5 will introduce the novel methods proposed by this research work.
Let us suppose that for the warning A of Fig. 1.3, the condition monitoring analysis does not give a clear indication of defects from any of the components of the machine, thus the increase in $\|\vec{F}[v(t), t_u]\|$ is attributed to normal operating wear of the machine. In addition the probability of failure calculated from the prognostic methods is likely to be below the threshold for the next weeks, therefore no maintenance intervention is planned on the machine. However, after a further few weeks of operation $\|\vec{F}[v(t), t_u]\|$ reaches a warning of the second level B. Again, complex signal processing methods are applied to detect the origin of such malfunctioning. For example, there is a clear indication of impulsive behaviour at one of the cyclic frequencies of a bearing and an increased kurtosis level of the time domain signal, furthermore prognostic methods indicate that a failure is likely to occur within the next three weeks. For this reason the maintenance technician schedules an intervention, direct inspection of the bearing confirms the presence of a defect, and the component is replaced. After the intervention $\|\vec{F}[v(t), t_u]\|$ goes back to nominal levels and the condition based maintenance procedure starts again.
This tutorial example emphasises the importance of the signal processing methods used for the determination of which specific component needs intervention. As a matter of fact, $\|\vec{F}[v(t), t_u]\|$ monitors the overall condition of the machine and the prognostics methods suggest the appropriate maintenance procedure. Thus they are effective in minimising the risks of catastrophic failures, however they are unable to drive the maintenance intervention. Furthermore, both for economic and practical reasons, the analysis of vibration signals is preferred to disassembling the machine and checking the health of each component when a warning is triggered. For this reason, when a

malfunction is observed [Sheng, 2012] the machine is stopped for precaution and more accurate vibration analysis , as studied in this research, is undertaken.

1.3 Literature review

This thesis is conceived in the framework of condition based maintenance, focusing on monitoring the condition of bearings from the analysis of vibration data, as explained above.
With this objective in mind, the following literature review firstly introduces mathematical models for vibrations signals generated by rotating machines, with particular emphasis on the cyclo-stationary an cyclo-non-stationary cases. Then it describes the state of the art signal processing methods currently used by the condition monitoring community, against which those proposed by the thesis will be bench-marked. Finally, it details the vibration transducers commonly used in the field.

1.3.1 Mathematical model for the vibration signal

The literature offers a wide range of mathematical models for the vibration signal produced by rotating machines. This section introduces the modelling theory that has been used in the numerical simulations in this research work.
The vibration recorded by a transducer placed on the housing of a machine is modelled as the superposition of three components: vibrations from the rolling elements bearings $b(t)$, vibrations from the gears $g(t)$ and random vibrations $n(t)$.
The vibration produced by a rolling element bearing is modelled following [Randall et al., 2001, Stack et al., 2006, Borghesani et al., 2013b, Abboud, 2015]. The mechanical elements of the bearing are the inner race, the outer race, the cage and the rollers. The bearing produces vibrations when there are defects in one or multiple parts of its elements. The defect is due to manufacturing imperfections or utilisation wear. Throughout the rotation the defective component impacts the other components of the bearing and produces a shock which propagates towards the vibration transducer. The impacts are locked at fixed angular increments plus a small random angular jitter due to slippage in the rotation. The reason for the slip is that the ratio of axial to radial load for individual rollers varies with their position in the bearing, hence they are trying to roll at different speeds while the cage forces them to maintain a uniform

mean separation. The occurrence time of the p^{th} impact is then

$$T_{im,p}(t) = \sum_{k=1}^{p} \frac{\Theta}{2\pi \overline{f}_{sh,k}(t)} + \Psi_p \tag{1.1}$$

where $\overline{f}_{sh,k}(t)$ is the mean shaft rotational speed between the kth and kth-1 impacts. Θ is a constant depending on the geometry of the bearing, number of rollers and type of defect, i.e. in the outer race, inner race or roller. Ψ is a random number reproducing the effect of the slip. The structural resonance excited by each impact is modelled as impulsive noise decaying exponentially:

$$m_b(t) = (w(t) * h(t))\, e^{-t/a} \tag{1.2}$$

where $*$ is the convolution operator, $w(t)$ is white noise and $h(t)$ the impulse response of a band pass filter. The cutoff frequencies of the filter f_l f_h, define the spectral band of the resonance. The time constant of the decay is $a < \max_k (T_{im,k})$, ensuring separation between consecutive impacts. Making use of Eq. 1.1 and Eq. 1.2, the vibration produced by the sequence of impacts is then modelled as:

$$b(t) = m_b(t) * \left\{ \sum_p D_p \delta \left[t - T_{im,p}(t) \right] \right\} \tag{1.3}$$

where D_p is the random amplitude of each impulse and $\delta(t - t^*)$ is an unitary Dirac delta function.

The vibration produced by toothed gears is modelled following [McFadden and Smith, 1985, Cempel, 1991, Randall, 2011]. The mechanical elements of the gear are: a slow speed shaft rotating at speed $f_A(t)$, a high speed shaft rotating at $f_B(t)$ and corresponding toothed wheels A and B with N_A and N_B number of teeth. The vibration from the rotation of the wheels is the superposition of sinusoids at $f_{A,B}(t)$ and harmonics:

$$e^{A,B}(t) = \sum_{r_e} E^{A,B}_{r_e} \cos \left(2\pi r_e \int_0^t f_{A,B}(z) dz + \alpha^{A,B}_{r_e} \right) \tag{1.4}$$

where r_e is the index of the harmonic order, α is the phase and $E^{A,B}$ the amplitude. In addition the gear produces vibrations at the harmonic frequencies of meshing

$f_M(t) = f_A(t)N_A = f_B(t)N_B$, amplitude and phase modulated at harmonics of $f_{A,B}(t)$:

$$m(t) = \sum_{r_m} M_{r_m} \cos\left(2\pi r_m \int_0^t f_M(z)dz + \theta^A_{r_m} + c^A_{r_m}(t) + c^B_{r_m}(t)\right) \times \left[1 + d^A_{r_m}(t) + d^B_{r_m}(t)\right] \quad (1.5)$$

where the phase and amplitude modulation terms are:

$$\begin{aligned} c^{A,B}_{r_m}(t) &= \sum_{r_c} C^{A,B}_{r_m r_c} \cos\left(2\pi r_c \int_0^t f_{A,B}(z)dz + \beta^{A,B}_{r_m r_c}\right) \\ d^{A,B}_{r_m}(t) &= \sum_{r_d} D^{A,B}_{r_m r_d} \cos\left(2\pi r_d \int_0^t f_{A,B}(z)dz + \gamma^{A,B}_{r_m r_d}\right). \end{aligned} \quad (1.6)$$

In Eq. 1.5, Eq. 1.6 r_m, r_c and r_d are the indexes of the harmonic orders, θ, β and γ the corresponding phases and $M, C^{A,B}, D^{A,B}$ the amplitudes. The vibration produced by the gear, comprising all its mechanical elements, is then modelled as:

$$g(t) = m_g(t) * \left[e^A(t) + e^B(t) + m(t)\right] \quad (1.7)$$

where $m_g(t)$ models the impulse response of the transmission path of the vibrations from the excitation to the sensor. The number of harmonics, the phase and the amplitude of each of the components of the vibration from the gear are not known a priori and are considered as random. However indications can be given in accordance with the state of the gear. For example a gear with wear defects, as a smeared tooth, will show vibrations characterised by a high number of r_m, r_c, r_d and large values of the amplitude and phase modulation terms $C^{A,B}, D^{A,B}$ resulting in many sidebands at f_M around harmonics of f_M. Finally, making use of Eq. 1.3 and Eq. 1.7 the expected vibration signal is given by:

$$v(t) = b(t) + g(t) + n(t) \quad (1.8)$$

where $n(t)$ is additive noise.
From Eq. 1.8 is possible to derive the following set of observations, of fundamental importance for selection of the proper signal processing tools.

- When the machine is operating at a speed $f_{sh}(t)$ which varies with time, $b(t)$ and $g(t)$ become non-stationary.
- The signal $b(t)$ is intrinsically random due to the presence of the slip.

- The spectral content of the impacts from the defective bearing $m(t)$ is not known a priori and depends on factors such as the wear state of the machine.
- The amplitude spectrum of $g(t)$ is characterised by a high number of peaks, at harmonics and sidebands of known frequencies.
- If $\frac{1}{T_{im}(t)} \simeq f_{A,B}(t)$ or one of their harmonics, $g(t)$ and $b(t)$ would be characterised by the same temporal scale.

1.3.2 The cyclo-non-stationary signal

The model for the vibration signal introduced in the previous section has two sources of non-stationarity and one source of randomness. The first source of non-stationarity is the periodically time varying energy, contributed by the series of impacts from the defective bearing and by the amplitude and frequency modulations in the vibrations from the gears. The second source of non-stationarity is the shaft rotational speed which can be time varying, while the source of randomness is the slip term in Eq. 1.1. In the following, a numerical simulation shows how the vibration signal and its amplitude spectrum are affected differently by these three aspects.
Non-stationary signals that exhibit some hidden periodicity, such as the time-varying energy of the vibration signal, are mathematically called cyclo-stationary [Gardner, 1994]. When analysed with ad-hoc techniques, cyclo-stationary signals reveal their periodicity in the cyclic frequency domain. A cyclo-stationary signal can be seen as an amplitude modulated signal that contributes sidebands in the amplitude spectrum. These sidebands are spaced around the modulated frequency component by a number equal to the modulation frequency. Therefore there is a hidden structure in the amplitude spectrum, which can be discovered by correlating the spectrum with itself. The correlation is non-zero for displacements equal to discrete multiples of the spacing of the sidebands: the cyclic frequency of the signal [Randall, 2011]. An excellent review on cyclostationarity with examples and engineering applications is [Antoni, 2009]. Section 1.3.3 in the following, introduces signal processing methods to extract the cyclic information.
The cyclo-stationarity is an intrinsic property of Eq. 1.8 while the shaft rotational speed can either be stationary or non-stationary. Therefore two cases of vibration signal can be encountered: the cyclo-stationary and cyclo-non-stationary. In the numerical simulation showed hereafter the jitter term Ψ in Eq. 1.1 is both set to zero or not, resulting in a total of four different types of signals. However, in real world scenarios Ψ is always present [Randall, 2011] and here it is set to zero only to show how it changes the

vibration signal.
The simulated signal is modelled using Eq. 1.7 and Eq. 1.3. It comprises vibrations produced by a gear, constituted by wheels A-B, and a series of impacts from a defect on the bearing which supports the shaft rotating at $f_A(t)$. The length of the signal is 10 seconds and the sampling frequency is $Fs = 20$ kHz. The following values are used for the vibrations from the gear $g(t)$:

$$\begin{array}{ccc} N_A = 20 & N_B = 40 & C^{A,B}_{r_m,r_c} = 0 \\ E^A_1 = 1 & E^B_4 = 1.5 & D^A_{2,5} = 0.8 \\ D^B_{1,6} = 0.7 & M_1 = 1.3 & M_2 = 1.5 \end{array} \tag{1.9}$$

and all the phases $\theta^{A,B}_{r_m} = \alpha^{A,B}_{r_e} = \beta^{A,B}_{r_m,r_c} = \gamma^{A,B}_{r_m,r_d} = 0$. The following values are used for the vibrations from the bearing $b(t)$:

$$\begin{array}{ccc} \Theta = \pi\ rad & D_p = 5 & a = 5e-4\ s \\ f_l = 1.2\ kHz & f_h = 1.5\ kHz & \end{array} \tag{1.10}$$

In the stationary case the speed is fixed at $f_A = 15$ Hz, while in the non-stationary case it increases linearly from $f_A(0) = 15$ Hz to $f_A(10) = 16$ Hz. When the jitter term ψ_p is considered, it is a normally distributed random number with zero mean and variance 5% of Θ [Randall and Antoni, 2011]. The overall vibration signal is then obtained, as in Eq. 1.8, adding white Gaussian noise with SNR=2 dB. Results are shown in Fig. 1.4, Fig. 1.5, Fig. 1.6 and Fig. 1.7. Each figure displays at the top a zoomed in section of the signals in the time domain and at the bottom the Welch power spectrum using a Hamming window of 0.3 s with 50% overlap. In red is shown only the signal from the bearing while in black the total signal.
Figure 1.4 shows the cyclo-stationary case with the jitter set to zero. In this case the spectrum is composed of a set of discrete components. At low frequencies it is possible to see the peaks contributed by the vibrations from the gears. As an example, the second harmonic of the meshing frequency and a sideband of the first harmonic have been indicated with arrows. In the resonant band excited by the defective bearing, it is possible to notice peaks spaced at the occurrence frequency of the impacts $1/T_{im}$. The signature of the cyclo-stationary signal is the absence of peaks at $1/T_{im}$ and harmonics, in the low part of the spectrum of Fig. 1.4(b) in red , i.e. in the frequency domain they are present only as sidebands. In contrary, they would be present in the cyclic-frequency domain.
Figure 1.5 shows the cyclo-stationary case when there is jitter. The spectrum shows discrete components only for vibrations from the gears and in contrast to the previous

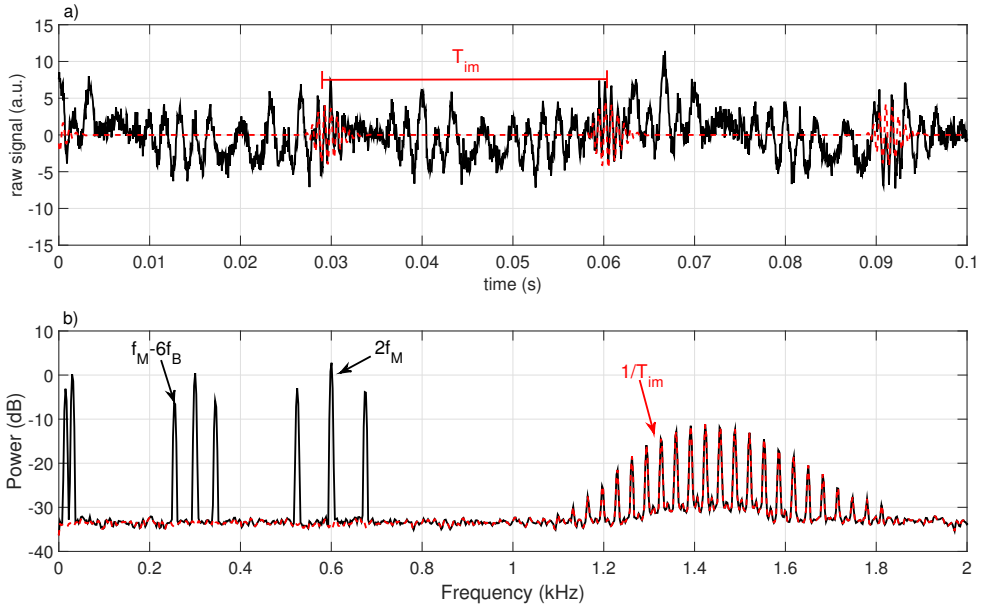

Figure 1.4: Example of vibration signal in the cyclo-stationary case with no jitter. In black the vibration $v(t)$ and in red only the component $b(t)$ from the bearing.

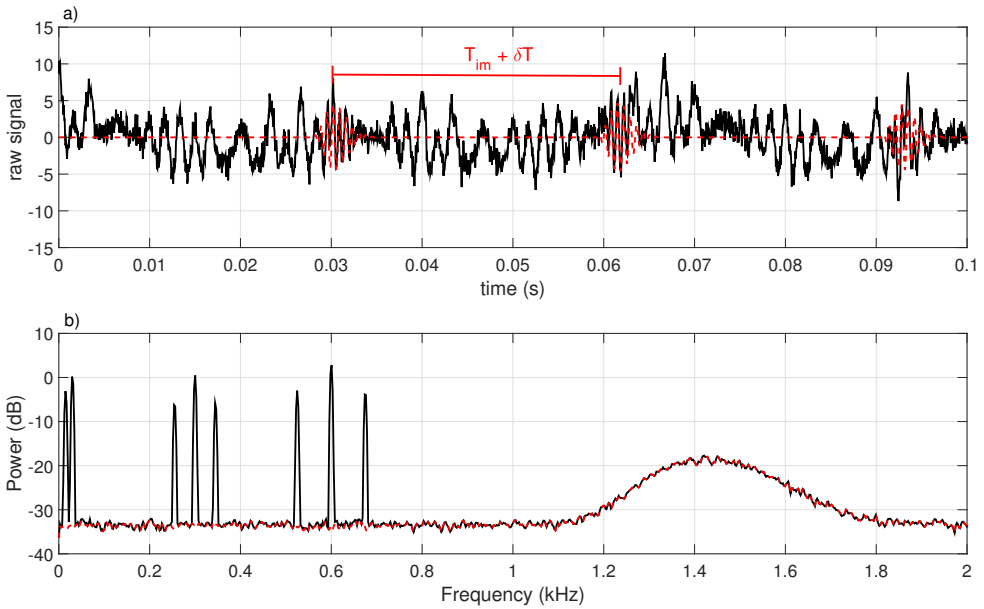

Figure 1.5: Example of vibration signal in the cyclo-stationary case with jitter. In black the vibration $v(t)$ and in red only the component $b(t)$ from the bearing.

case, a continuous spectrum for the vibrations from the bearing. Comparing the time signal with Fig. 1.4, it is possible to see how a small change δT in the occurrence times

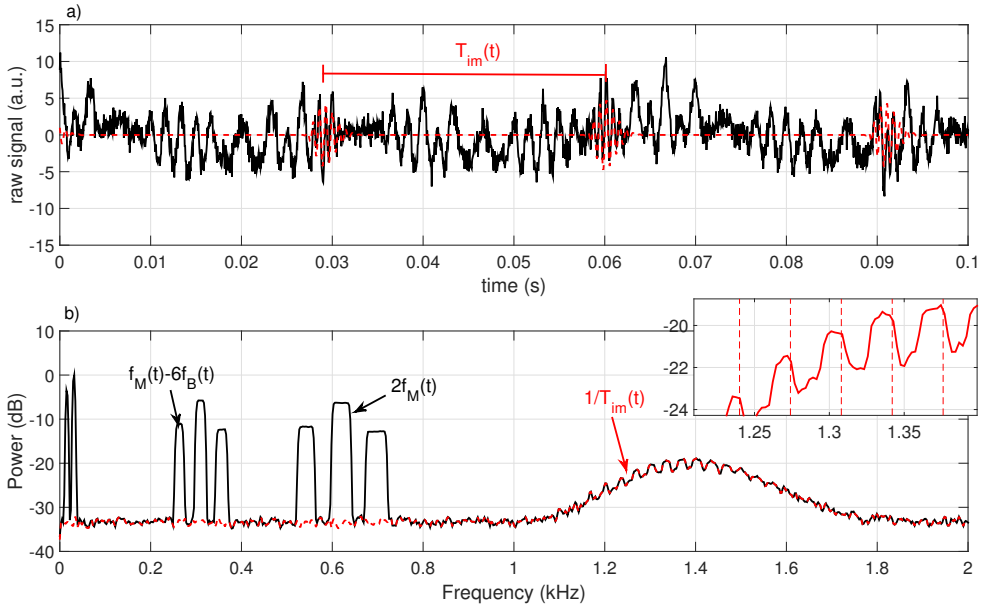

Figure 1.6: Example of vibration signal in the cyclo-non-stationary case with no jitter. In black the vibration $v(t)$ and in red only the component $b(t)$ from the bearing.

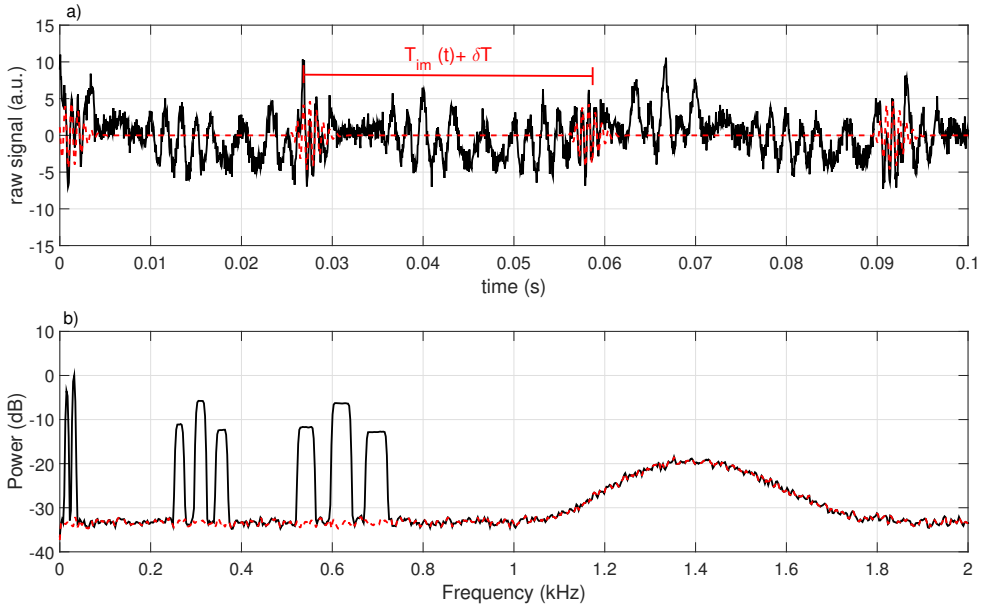

Figure 1.7: Example of vibration signal in the cyclo-non-stationary case with jitter. In black the vibration $v(t)$ and in red only the component $b(t)$ from the bearing.

of the impacts can drastically modify the spectrum. It is of fundamental importance to notice that Fig 1.5(b) does not show an indication of events occurring at $1/T_{im}$. Hence

the combination of cyclo-stationarity and randomness jeopardises the use of classical spectral analysis in monitoring the condition of a bearing and cyclic-spectral analysis is needed.
Figure 1.6 shows the cyclo-non-stationary case when the jitter is set to zero. As expected from the stationary case, the spectrum is composed by a set of discrete but smeared components, both for the vibrations from the gears and the bearing. The zoomed in section shows that the frequency of the impacts is still visible in this case, with the vertical dotted lines at harmonics of $1/T_{im}$. In this case $T_{im}(t)$ varies within two consecutive impacts, however the speed varies by only 1 Hz in 10 s, therefore this difference is not noticeable in Figure 1.6(a)
Finally, Fig. 1.7 shows the cyclo-non-stationary case when there is jitter. The spectrum is composed of a set of discrete and smeared components only for the vibrations from the gears, while the vibrations from the bearing contribute a continuous spectrum. As with the stationary speed case, it is possible to notice how small is the change in the occurrence time of the impacts δT.

1.3.3 Signal processing methods

This Section introduces the background literature relating to common signal processing methods applied in vibration based condition monitoring. The methods address the set of observations outlined at the end of Section 1.3.1 and the cyclostationarity of the vibration signal as shown in Section 1.3.2.

Spectral correlation

The numerical simulation of Section 1.3.2 showed how the intrinsic cyclic property of Eq. 1.3 combined with the random slip jeopardise the use of classical spectral analysis to detect a defective bearing from vibration data. In order to extract the cyclic information hidden in the vibration signal it is necessary to compute the correlation of the spectrum with itself: the Spectral Correlation (SC) .
Given the cyclo-stationary signal $v(t)$, the spectral correlation $S_{vv}(l, f)$ is defined as the two dimensional Fourier Transform of the time varying auto-correlation function function [Randall, 2011]:

$$S_{vv}(l, f) = \lim_{W\to\infty} \frac{1}{W} \int_{-W/2}^{W/2} \int_{-\infty}^{\infty} \mathbf{E}[v(t - \tau/2)v(t + \tau/2)]e^{-j2\pi(f\tau+lt)}d\tau dt \qquad (1.11)$$

where $\mathbf{E}$ is the ensemble averaging operator, f is the spectral frequency and l is the cyclic frequency. An alternative form of expressing SC, which gives insight on its name, is [Antoni, 2007a]:

$$S_{vv}(l,f) = \lim_{W\to\infty} \frac{1}{W}\mathbf{E}[\hat{v}_W(f+l/2)\hat{v}^*_W(f-l/2)] \tag{1.12}$$

where $\hat{\cdot}_W$ denotes the Fourier Transform over a time interval of duration W: $\hat{v}_W(z) = \int_{-W/2}^{W/2} v(t)e^{-j2\pi zt}$.

The SC of the simulated cyclo-stationary signal with random jitter from Section 1.3.2 is shown in Fig.1.8. The spectral correlation is discrete in the cyclic frequency domain, with non-zero values only at those cyclic frequencies related to time-varying energy contributed by the impacts from the bearing: $1/T_{im}$ and harmonics. Therefore SC reveals the presence of the defective bearing. In the frequency domain the SC shows discrete peaks at the frequencies of the gear, while the resonant band excited by the bearing is continuous due to the presence of the jitter term, similarly to Fig. 1.5.

Equation 1.12 is applied on cyclo-stationary signals. In the case of a machine operating at varying speed the SC of the cyclo-non-stationary signal is computed as the two dimensional Fourier Transform of the angle-time auto-correlation function[Abboud et al., 2016a]:

$$S_{vv}(l,f) = \lim_{U\to\infty} \frac{1}{U}\int_{-U/2}^{U/2}\int_{-\infty}^{\infty} \mathbf{E}[v(t(\theta)-\tau/2)v(t(\theta)+\tau/2)]e^{-j2\pi(f\tau+l\theta)}d\tau d\theta \tag{1.13}$$

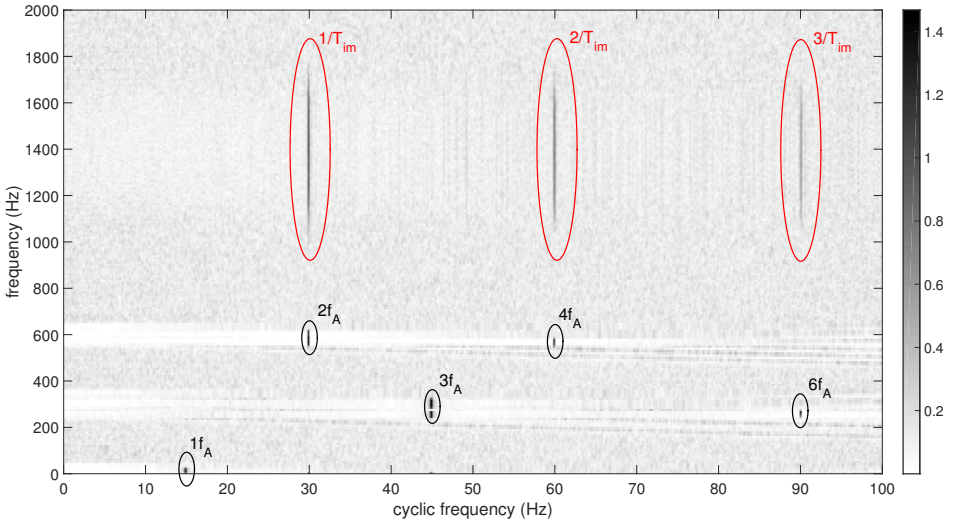

Figure 1.8: Spectral correlation of the cyclo-stationary vibration signal of Fig. 1.5.

where the relationship $t(\theta)$ is found inverting Eq. 1.16. The SC of the simulated cyclo-non-stationary signal with random jitter of Section 1.3.2 is not displayed here, being the same as Fig. 1.8 with only the cyclic order instead of the cyclic frequency.
The spectral correlation is the most versatile and reliable tool for vibration based condition monitoring, with the only drawback being the computational cost. In this respect, the fast algorithm for its computation recently introduced by [Antoni et al., 2017b] represents an important step towards its use in commercially available condition monitoring software. In Chapter 5 the performance of a novel methodology developed during this research work will be compared to that of SC.

Squared envelope spectrum

The cyclic content of the vibration signal can also be identified in the Spectrum of the Squared Envelope (SES). Conventionally the envelope of the signal is calculated using the absolute value of the analytic representation of the signal

$$\tilde{v}(t) = v(t) + j\tilde{v}(t) \tag{1.14}$$

where $\tilde{\cdot}$ denotes the Hilbert transform. The difference between SES and SC is that the latter is a two dimensional map of frequency vs cyclic frequency, while the first shows only the cyclic frequencies. Specifically, it was proved [Randall et al., 2001] that the SES corresponds to the integral over all the frequencies of the SC:

$$SES_v(l) = \int_{-\infty}^{\infty} \mathbf{E}\left[|\tilde{v}(t)|^2\right] e^{-2\pi l t} = \int_{-\infty}^{\infty} S_{vv}(l, f)df. \tag{1.15}$$

Interestingly, the SES was recognised as being one of the most effective diagnostic tool for bearings well before the introduction of cyclostationarity, under the name of *high-resonance frequency technique* or *demodulated resonance analysis* [McFadden and Smith, 1984, Dyer and Stewart, 1978]. In other words, the SES can be seen as a quick way of gathering the cyclic information extracted by the SC, without the need of actually computing it [Antoni, 2007b]. The advantage is that computation of the SES uses only the FFT algorithm, two times for calculation of the envelope and one time for calculation of the spectrum, and results in a much less computationally expensive scheme than SC. For instance the computation time for the SES for the 2×10^6 point signal of Section 1.3.2 is 0.11 seconds while that of the SC is 11.3 seconds[1]. However the reduction from a two dimensional map to the one dimensional SES has two disad-

[1]Using the fast-SC algorithm with $N_w = 2^{12}$

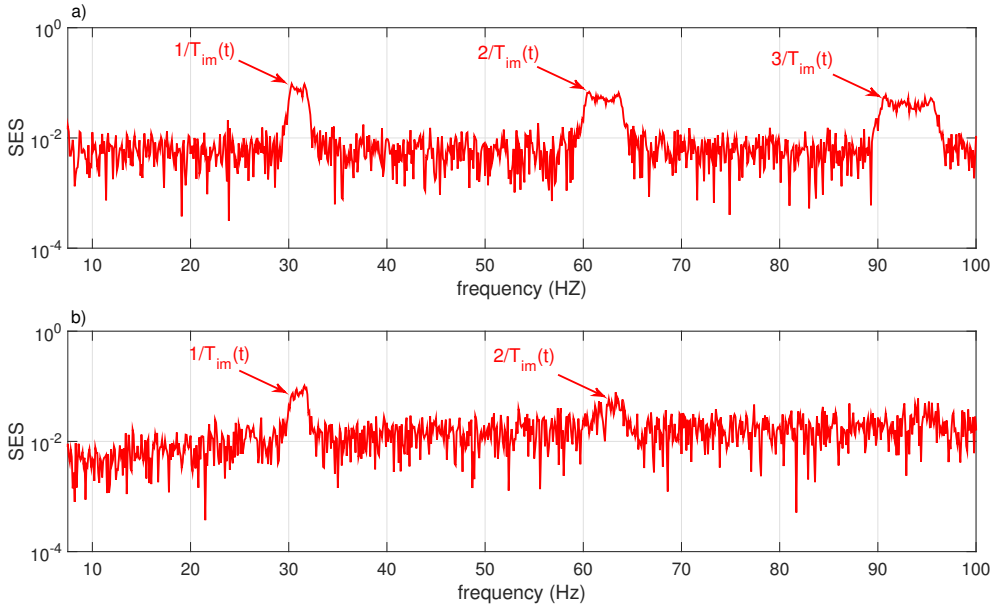

Figure 1.9: Squared envelope spectrum of the cyclo-non-stationary vibration signal, comprising only vibrations from a bearing. (a) Case with no jitter. (b) Case with jitter. Shaft speed varying of 1 Hz in 10 seconds.

vantages.

The first drawback of the SES is that different components contributing vibrations at the same cyclic-frequency are not distinguished. For example the integral over f of the SC of Fig. 1.8 shows peaks at $1/T_{im}$ and harmonics which coincide with f_A and harmonics, because $\Theta = \pi$ and the SES does not detect the defective bearing. Therefore signal pre-processing algorithms for the separation of the vibrations from the gears and from the bearing have to implemented before the SES. Common methods are: time synchronous averaging [McFadden and Smith, 1985], self adaptive noise cancellation [Widrow et al., 1986], linear prediction [Antoni and Randall, 2004], spectral kurtosis and cepstral prewhitening. In the following sections, the last two of these algorithms are discussed in detail. The comparison on the performance of these techniques is studied in [Randall et al., 2011, Kilundu et al., 2014] and it is found that cepstrum editing outperforms the other methods. Furthermore spectral kurtosis not only separates vibrations from the gears and from the bearing, but it also identifies the resonance band excited by the impacts. Thus these two techniques have been preferred and used in the rest of this work.

The second drawback of the SES is that when applied to cyclo-non-stationary signals it shows smeared peaks at the cyclic frequencies of interest. Figure 1.9 shows the SES of the simulated cyclo-non-stationary signals of Section 1.3.2. Specifically Fig. 1.9(a) of

the signal from the defective bearing in the case of jitter term set to zero, corresponding to Fig. 1.6 in red. While Fig. 1.9(b) of the signal from the defective bearing when there is jitter, corresponding to Fig. 1.7 in red. It can be noticed how in both cases the SES shows smeared peaks at cyclic frequency $1/T_{im}$ and harmonics, furthermore the presence of the jitter term acts as a low pass filter in the cyclic domain. This drawback of the SES is conventionally addressed by means of a re-sampling procedure, as introduced in the next section.

Order tracking

In a real world scenario a machine operates at variable speed and as a consequence its vibrations are cyclo-non-stationary. The classical approach to address this issue is a re-sampling operation: Order Tracking (OT) [Fyfe and Munck, 1997]. Specifically the signal is re-sampled from constant increments Δt in the time domain to constant increments $\Delta\theta$ in the angular domain.
The reference signal for the instantaneous speed of the machine is needed to perform OT. This signal is usually acquired by means of a tachometer placed on one of the shafts. If it is not possible to place an additional sensor, the instantaneous speed is reconstructed from the vibration signal. The classical approach is to band pass filter the Fourier transform around one of the meshing frequencies and then obtain the phase from the analytic signal calculated using the Hilbert transform [Bonnardot et al., 2005]. Recently, [Leclere et al., 2016] propose a probabilistic approach based on the short-time Fourier transform while [Randall and Smith, 2016a] the use of the Teager Kaiser energy operator.
The angular position is then defined from the shaft speed as:

$$\theta(t) = 2\pi \int_0^t f(z)dz \tag{1.16}$$

and the operation of re-sampling in the angular domain corresponds to the substitution of Eq. 1.16 in Eq. 1.7 and Eq. 1.3. Digitally this is done by means of numerical interpolation.
The effect of order tracking is different for the vibration from the gears and from the bearing. For example if a tachometer is placed on the shaft where the wheel A is mounted, the vibration due to rotation of the wheel B of Eq.1.4, becomes

$$e^B(\theta_A(t)) = \sum_{r_e} E^B_{r_e} \cos\left(r_e \frac{N_B}{N_A}\theta_A(t) + \alpha^B_{r_e}\right). \tag{1.17}$$

Therefore, in the angular domain, the vibration from the gear is a superposition of sinusoids. The same applies to Eq. 1.5 and Eq. 1.7 and spectral analysis can be applied to the resampled signal, independently from the variations in operating speed of the machine. Conversely, considering a defect on the bearing supporting the shaft rotating at $f_A(t)$, OT yields:

$$b(\theta_A(t)) = m(\theta_A(t)) * \left[\sum_p D_p \delta \left(\theta_A(t) - \Psi_p - p\Theta \right) \right]. \tag{1.18}$$

Equation 1.18 corresponds to a series of impacts occurring at constant, plus random jitter Ψ, angular increments Θ for which the spectral content changes accordingly to the shaft speed. In other words, the resonance frequency excited by each of the impacts becomes non-stationary. This aspect is based on the model assumption that only the occurrence time of the impacts is locked at fixed angular position of the shaft, while the excited resonance does not depend on the rotational speed as shown in Eq. 1.2. More details on how this drawback of OT affects the task of monitoring the condition of the machines are discussed in Chapter 3.

Spectral kurtosis

The Spectral Kurtosis (SK) is a method to determine which frequency band contains events of maximum impulsivity [Dwyer, 1983] and in vibration based condition monitoring is used to extract the vibrations from a defective bearing $b(t)$ from $v(t)$ [Antoni and Randall, 2006].
The SK is calculated from the Short Time Fourier Transform (STFT) of the signal $v(t)$ as [Antoni, 2006]

$$SK_v^w(f) = \frac{\left\langle |STFT_v^w(\tau, f)|^4 \right\rangle_\tau}{\langle |STFT_v^w(\tau, f)|^2 \rangle_\tau} - 2 \tag{1.19}$$

where ω denotes the window function of the STFT and $\langle \cdot \rangle_z$ the averaging in z. For a white Gaussian noise the result of Eq. 1.19 is 0 for all the frequencies, while in the case of an impulsive signal as the impacts from the bearing of Eq. 1.3, returns positive values for the frequencies of the excited resonant band $[f_l, f_h]$.
The length of the window N_w used in the computation of the STFT of Eq. 1.19 has to be shorter than T_{im} and longer than the exponential decay a of Eq 1.2. However the optimal length giving the maximum value of SK is not known a priori and is found by a blind search on a set of N_w. The resulting two dimensional map is called the kurtogram [Antoni, 2007d], for which a fast computation algorithm is available at

[Spectral Kurtosis, 2017].
The kurtogram of the simulated cyclo-stationary signal in the presence of jitter, of Section Ref. 1.3.2 is shown in Fig. 1.10. The vertical scale shows a set of levels related to the length of the window by

$$N_w = \frac{2^{k+1}}{Fs} \tag{1.20}$$

The kurtogram correctly identifies that the resonance excited by the impacts has a bandwidth of $\simeq$ 400 Hz and central frequency of $\simeq$ 1.4 kHz. Therefore the signal $b(t)$ can be separated by the vibrations from other components by means of band pass filtering, and the SES calculated on the filtered signal reveals diagnostics information on the defective bearing.
The SK is applied on cyclo-stationary signals, while on the cyclo-non-stationary case its computation follows a first operation of OT[Randall and Antoni, 2011]. In the following, Chapter 3 shows that if the machine undergoes large speed variation the operation of OT jeopardises the use of the SK.

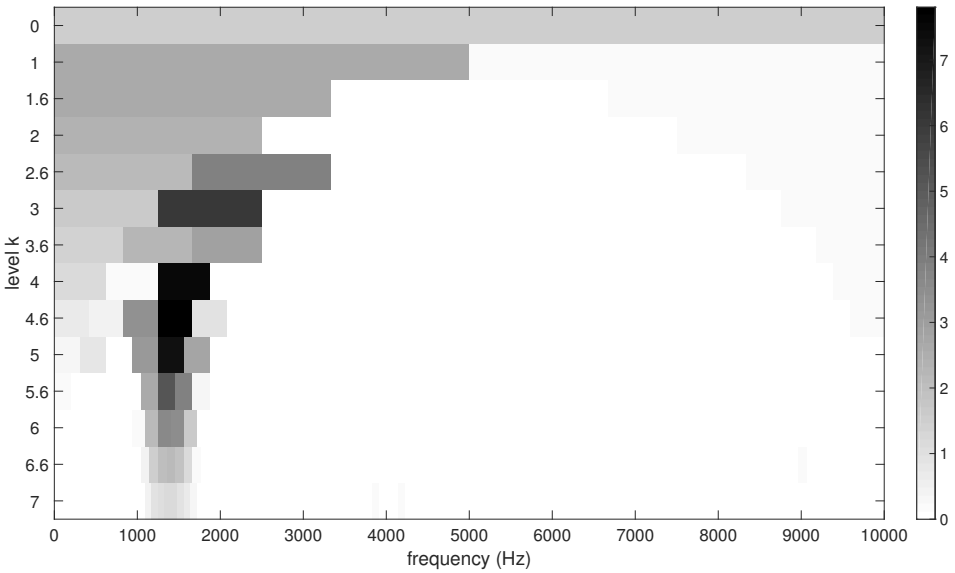

Figure 1.10: Example of kurtogram of cyclo-stationary signal.

Real cepstrum

Vibrations from the gears as introduced in Eq. 1.7 produce a spectrum[2] characterised by a series of peaks at harmonics of $f_{A,B,M}$ with sidebands at $f_{A,B}$, as shown in Fig. 1.4. This characteristic can be exploited in two ways: indication of the health of the gear, and separation between deterministic and random sources of vibration, i.e. gears and impacts from the bearing. The real cepstrum is a technique commonly used in vibration based condition monitoring to accomplish these tasks. An excellent review on cepstral methods is [Randall, 2016]. The real cepstrum is defined as the Inverse Fourier Transform (IFT) of the log amplitude spectrum:

$$rc_v(q) = IFT\left\{log\left|\hat{v}(t)\right|\right\} \tag{1.21}$$

where the new variable q is called quefrency and has physical dimension of seconds or radiant, depending on whether the cepstrum is computed on the time or angular domain signal. Equation 1.21 checks for periodicity in the amplitude spectrum and if a peak is present at $rc_v(q^*)$, the amplitude spectrum of the signal $v(t)$ has peaks occurring periodically at $\Delta f = 1/q^*$.
A numerical example on the application of the real cepstrum is shown in Fig. 1.11. The signal is the same as in the cyclo-stationary case of Section 1.3.2, with the only difference a higher number of sidebands around the second harmonic of the meshing frequency:

$$D^A_{2,[1,\cdots,8]} = 0.8.$$

The real cepstrum is shown in Fig. 1.11(a). Clear peaks are observed at the quefrency of $1/f_A$ and harmonics, giving an indication of a high number of harmonics spaced at f_A. The health of a gear is then easily monitored tracking the amplitude of peaks at particular quefrencies. If the real cepstrum is notch filtered at $rc_v(q^*)$, the corresponding peaks spaced at $\Delta f = 1/q^*$ in the amplitude spectrum are highly suppressed [Randall and Sawalhi, 2011]. As a consequence, editing the real cepstrum can be used as method to remove vibrations from the gears. In addition, [Sawalhi and Randall, 2011] introduced the cepstral prewhitening (CPW) as an easy implementation of cepstral editing. The method consists of setting all the cepstral coefficients to zero. More recently, it was proved [Borghesani et al., 2013a] that CPW corresponds to the computation of the

[2]For machines operating at stationary speed the peaks are visible in the spectrum calculated on the signal in the time domain, while in the case of non-stationary speed in the spectrum of the angular domain signal after the operation of OT.

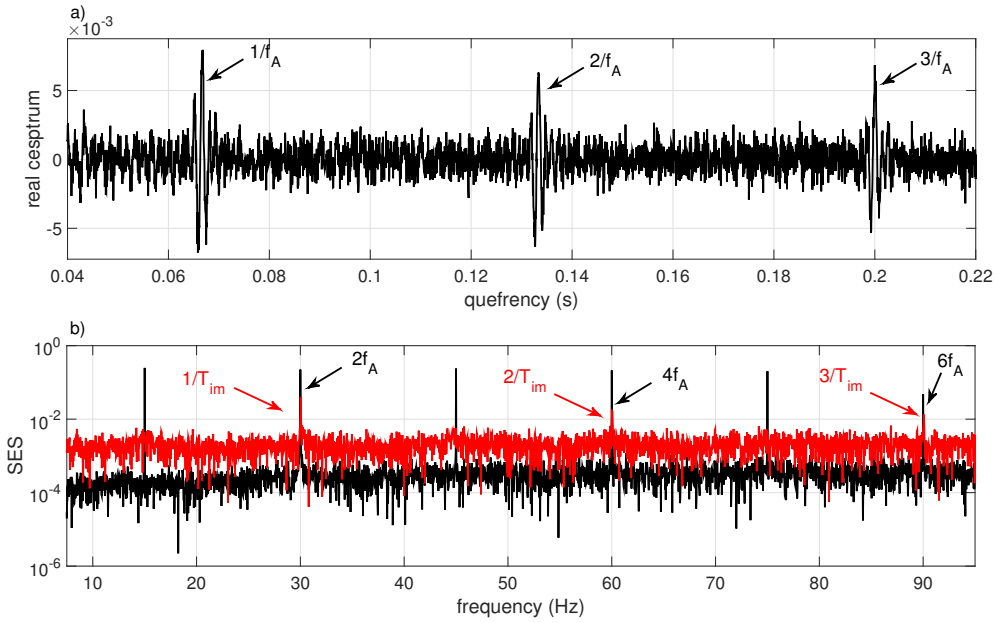

Figure 1.11: Real cepstrum applied on a numerical simulation. (a) real cepstrum. (b) SES computed on $v(t)$ (black) and on $cpw_v(t)$ (red).

IFT on the signal with all the spectral amplitudes set to one :

$$cpw_v(t) = IFT\left\{\hat{v}(t)/\left|\hat{v}(t)\right|\right\} \tag{1.22}$$

A review on the performance of cepstral editing methods is [Peeters et al., 2017]. The effect of Eq. 1.22 on the signal is shown in Fig. 1.11(b). Specifically, in black it shows the SES calculated on the raw signal $v(t)$ and in red on $cpw_v(t)$. The signal from the defective bearing is characterised by impacts occurring at integer orders of f_A therefore vibrations from the gears and from the defective bearing contribute a peak at the same cyclic frequency $1/T_{im} = 2f_A$ and harmonics. In such cases the SES calculated on the full band raw signal loses its detection capabilities. Conversely, as shown in Fig. 1.11(b) CPW effectively removes the unwanted vibrations from the gear and the presence of the defective bearing is revealed by the peaks at $1/T_{im}$ and harmonics. In the literature cepstral editing is applied on stationary or cyclo-stationary signals, while on the non-stationary case its computation follows a first operation of OT. Chapter 3 extends the existing body of work to show that cepstral prewhitening is effective also on cyclo-non-stationary signals, when the cepstrum does not present any peak.

Stochastic resonance

The last signal processing method which has been investigated in this research is a synchronisation phenomenon which acts as a non linear filter: Stochastic Resonance (SR). SR was introduced to explain the noise driven amplification of weak signals in nonlinear systems [Benzi et al., 1981]. The interest in SR from the point of view of condition monitoring is based on the similarity between the signal amplified by the SR and the vibration signal described in Section 1.3.1. In the vibration signal, $b(t)$ corresponds to the weak component and $g(t)+n(t)$ to the masking noise. The literature on SR is abundant and an excellent review paper is [Gammaitoni et al., 1998]. In the following its working principle is explained.

The classic SR is described by a one dimensional dynamical system with a bi-stable symmetric potential function $U(x)$ perturbed by a Gaussian noise of variance σ and zero mean. The noise triggers random transitions between the stable states which occur according to the Kramers rate r_{kr}:

$$r_{kr}\left[\Delta U, \sigma\right] \propto exp\left(\frac{-\Delta U}{\sigma}\right) \tag{1.23}$$

where ΔU is the height of the potential barrier between the two stable states. SR studies the response of this system when it is subjected to a weak forcing of amplitude A and period T_Ω, which alone has not enough energy to trigger a transition between the two stable states. The effect of the forcing is that of periodically raising and lowering the potential barrier of $\delta(A)$. Since Eq. 1.23 depends exponentially on the height of the barrier, a small change of ΔU is sufficient to trigger a transition with probability 1 at:

$$\frac{T_\Omega}{2} = \frac{1}{\langle r_{kr}(\Delta U + \delta(A), \sigma)\rangle}. \tag{1.24}$$

As a result the non-linear system is synchronised with the forcing and the output signal becomes periodic. The peculiar aspect of the SR is that, in contrast to linear filters where an increase in the input noise deteriorates the output, the synchronisation does not occur if σ is too small. In other words, an increase in the level of noise improves the output of the non linear filter.

After the observation of the SR phenomenon in the 1D system as described above, the positive role of noise in non linear systems has been widely investigated. Firstly, it was observed SR also for a system subjected to an aperiodic forcing [Gang et al., 1992], then a SR-like behaviour was found in the case of non-Gaussian noise [Hänggi et al., 1993]. Furthermore, it was observed that the non-linear system can also be a static non-linearity [Chapeau-Blondeau and Godivier, 1997]. Finally, a supra threshold

SR-like phenomenon has been investigated by [Apostolico et al., 1997, Stocks, 2000]. In the field of vibration based condition monitoring the first use of SR is [Klamecki, 2005], where vibration signals of an internal combustion engine were enhanced to monitor the wear of crankshaft bearings. After that a consistent amount of literature can be found on this engineering application of SR [Tan et al., 2009, He et al., 2012, Ompusunggu et al., 2013]. In the following, Section 2.3 discusses the problems related to the use of SR on vibration signals.

Other methods

The signal processing methods introduced so far are the most common in the field of condition monitoring and since they will be used throughout this thesis, they have been treated here with particular attention. Nevertheless, the literature offers a much higher and continuously increasing number of methods, as described in many review papers from the classical [Howard, 1994] to the more recent [El-Thalji and Jantunen, 2015, Akhand and Upadhyay, 2016]. Among these methods can be identified three main approaches which need to be mentioned in a literature review on condition monitoring: Wavelet Decomposition (WD), Empirical Mode Decomposition (EMD) and Higher Order Spectral Analysis (HOSA).

Developed as improvements on the classical short time Fourier Transform, WD [Mallat, 1999] and EMD [Huang et al., 1998] tackle non-stationarity, decomposing the signals into different time scales. The main difference between EMD and WD is that the former is performed adaptively and in a data-driven way, whereas the latter uses a set of pre-defined filters based on the mother wavelet. Both these algorithms act as a dyadic filter bank [Flandrin et al., 2004, Mallat, 1999], where the central frequency and bandwidth of each filter is given by the scale level. The presence of impacts in the resulting band passed signals is then used as diagnostic information [Dalpiaz et al., 2000, Antoniadou et al., 2015]. In contrast to the SC of Section 1.8 which produces a frequency-cyclic frequency map, such methods do not give information on the periodic[3] repetition of the impacts, achieved only with a further Fourier transform giving a scale-frequency decomposition.

On the other hand, HOSA is the generalisation of classical spectral analysis and it was developed to check the presence of non-linear phase coupling between frequency components [Nikias and Mendel, 1993]. The most used tool of HOSA in condition monitoring is the bispectrum, from the classical [Sato et al., 1977] to the more recent [Stack et al., 2004, Guoji et al., 2014]

[3] in the cyclo-stationary case or after OT in the cyclo-non-stationary case

The bispectrum of the signal $v(t)$ is defined as [Collis et al., 1998]:

$$B_v(f_1, f_2) = \int\int \mathbf{E}[v(t)v(t-\tau_1)v(t-\tau_2)]e^{-j2\pi(f_1\tau_1+f_2\tau_2)}d\tau_1 d\tau_2 \qquad (1.25)$$
$$= \lim_{W\to\infty} \frac{1}{W}\mathbf{E}[\hat{v}_W(f_1)\hat{v}_W(f_2)\hat{v}^*_W(f_1+f_2)]$$

and is different from zero only if there is quadratic phase coupling between the frequencies f_1, f_2 and $f_1 + f_2$. In other words, a peak at $B_v(f_1, f_2)$ identifies that the peak at $f_1 + f_2$ in the spectrum is due to a modulation effect. Similarly to $S_{vv}(l, f)$ of Eq. 1.12, $B_v(f_1, f_2)$ decomposes the signal in a two dimensional frequency-frequency map, however the spectral correlation computes the correlation between two frequencies while the bispectrum between three. The performance of the cyclo-stationary and bilinear tools when applied to vibrations, is studied in [Bouillaut, 2001] and it is observed that they simultaneously detect both non-linear and cyclic properties of the signals and offer similar detection capabilities. However the former has to be preferred due to the lower computational complexity and more intuitive interpretation. Furthermore mathematical evidence suggests that the signal from a defective bearing is cyclo-stationary [Antoni, 2007c] and this property has been linked [Randall et al., 2001] to the well established high resonant frequency technique [McFadden and Smith, 1984] for bearing fault detection.

1.3.4 Transducers

The transducer most commonly used in the field of vibration based condition monitoring is the mono-axial piezoelectric accelerometer. Piezoelectric accelerometers have low noise density, in the order of $\mu g/\sqrt{Hz}$, and for this reason they have been historically preferred to MEMS in commercially available systems. However in this respect, Analog Devices has recently introduced MEMS accelerometers ADXL1001 and ADXL1002 with a comparable noise density [Analog Devices, 2017] and a promising commercial future. The dynamic range of the accelerometers used in condition monitoring is of ± 50 g with a ± 3 dB frequency bandwidth up to $\simeq$ 10 kHz and resonant frequency at $\simeq$ 20 kHz, while for measurements at higher frequencies ultrasound sensors [National Instruments, 2017] are used. Between these two types is found the shock pulse transducer, which is an accelerometer with resonant frequency in the band 30-40 kHz [Sohoel, 1985].
When only contactless measurements are possible, microphones are used to record the sound produced by the vibrations, for example [Gryllias and Antoniadis, 2013] pro-

poses a method for instantaneous speed recovery from a microphone record. Recently, microphones arrays combined with beam forming and SK have been proposed as a way to visualise defects on gearboxes [Cardenas Cabada et al., 2017].
Commercially available products which use phenomena different than vibrations to extract diagnostic information from machinery are: infrared cameras and acoustic emission sensors. A review on thermographic methods for condition monitoring is [Bagavathiappan et al., 2013] while an automated method to detect defective bearing from infrared images was recently investigated by [Janssens et al., 2015]. The main disadvantage of thermography, compared to classical vibration analysis, is that diagnostic information can be extracted only at the final stage of the defect, i.e. close to the failure point. On the other hand, acoustic emission sensors are preferred in the case of monitoring machines operating at very low speed and for detection of incipient faults [Mba and Raj, 2006, Al-Ghamd and Mba, 2006], offering a better performance than vibration analysis. As a drawback, acoustic emission sensors are expensive and require signal conditioning, such as pre-amplification and amplification. Finally, in the case of monitoring the bearings of an induction motor, the spectrum of the stator current contains diagnostic information [Schoen et al., 1995] therefore it can be used in condition monitoring.

1.4 Objectives

The thesis is conceived in the framework of condition based maintenance described in Section 1.1 and the general objective is the development of novel signal processing methods for vibration based condition monitoring of bearings in rotating machines, offering adaptable diagnostic capabilities and the possibility of automation. The literature on condition monitoring already offers many signal processing methods for vibration analysis, among which the most commonly used are described in Section 1.3.3. Thus the introduction of novel techniques in such an already well investigated field is not trivial. In this regards, two aspects of the currently used methods were recognised as improvable and have driven the research of this thesis. Firstly, existing techniques are difficult to implement in an automated way because they need the supervision of expert users. Secondly, they are developed for ad hoc situations requiring unlikely real world operating conditions of the machines, such as constant speed and load.
Therefore, with the general objective in mind and considering the weaknesses of the current state of the art methods, the focus throughout the thesis has been on the development of methods which are:

- suitable for automated implementation
- effective on the varying operating conditions of the machines.

Certainly the diagnostic capability of the proposed methods should not be affected by these characteristics and the performance in the detection of defective bearings has to be bench-marked with that of state of the art techniques.
Besides focusing on such requirements for the proposed methods, the research was also aimed towards the development of intuitive algorithms which can be applied in a computationally inexpensive way, with the aim of offering methods attractive for commercial applications.

1.5 Thesis structure

The thesis is divided into six chapters and is written in the Bath University alternative format, i.e. thesis by publication. The number of included publications is five, comprising 3 peer reviewed papers from international conferences and 2 peer reviewed journal papers. Each chapter has an introductory section to establish the link between the included publications and the framework of the research. Each chapter is also concluded with a summary section where the results of the proposed methodologies are compared against the objectives of the thesis.

In more detail:

- Chapter 1 delineates the framework of condition based maintenance in which the thesis is conceived and sets the objectives of this research work. It also introduces the mathematical models used to simulate the cyclo-non-stationary vibration signals and state of the art signal processing techniques currently used in condition monitoring.
- Chapter 2 investigates the performance of a two dimensional stochastic resonance system and applies it to enhance vibration signals [Barbini et al., 2015]. In addition, it introduces a circuit capable of performing stochastic resonance directly on analog signals. It also elaborates on the problems involved in this approach and justifies the conclusions that this method is unsuitable for the problem in hand.
- Chapter 3 investigates the effect that large variations in the operating speed of the machine have on its vibration signature and extends techniques commonly applied to cyclo-stationary vibration signals to cyclo-non-stationary signals [Barbini et al., 2018].

- Chapter 4 presents the core methodology proposed by this research work: phase editing. It is applied on numerical simulated signals and experimental data and its performance is compared to that of state of the art techniques. Phase editing is firstly applied on cyclo-stationary signals [Barbini et al., 2017c] and secondly on cyclo-non-stationary signals [Barbini et al., 2017a].
- Chapter 5 presents a further extension of the proposed methodology: amplitude-cyclic frequency decomposition based on phase editing. Its performance is tested on cyclo-stationary and cyclo-non-stationary vibration signals both from simulated data and experimental data [Barbini et al., 2017b]. Its performance is compared to that of state of the art techniques and it matches the objectives of the thesis.
- Chapter 6 concludes the thesis with considerations on the contributions of this research and presents some perspectives on future work.

Chapter 2

Investigation of stochastic resonance

Nomenclature			
a	2^{nd} order constant of potential	**b**	4^{rd} order constant of potential
(x,y)	variables of dynamical system	$\boldsymbol{\delta}$	coupling constant
A	amplitude of sinusoid	$\boldsymbol{\omega}$	frequency of sinusoid
ε	variance of white noise	**w**	Wiener process
$\boldsymbol{T_R}$	time rescale	$\boldsymbol{S_R}$	spatial rescale
k	rescale constant	$\boldsymbol{\tau}$	mean residence time
$\boldsymbol{\eta}$	derivative Wiener process	**L**	length of signal
γ	constant multypling noise variance	$\boldsymbol{r_\tau}$	degree of SR synchronisation
d(t)	data from defective bearing	**q**	constant multiplying the data
$\boldsymbol{T_i}$	temporal scale of one impact	$\boldsymbol{T_{im}}$	temporal interval between two impacts

2.1 Introduction

This chapter investigates the use of Stochastic Resonance (SR) as a signal processing tool in the field of vibration-based condition monitoring. The general background of SR is discussed in Section 1.3.3.

Despite being introduced as a physical phenomenon to model climate changes [Benzi et al., 1983] SR has rapidly attracted the attention of engineers. In particular it is used as a non-linear filter capable of enhancing a signal too weak to be detected by a sensor

or masked by heavy noise. The most attractive characteristic of the SR mechanism from an engineering point of view is its easy implementation. For instance an analog circuit can reproduce the software based SR system.
Concerning the field of condition monitoring, the model of a vibration signal as described in Section 1.3.1, matches that of the classical SR system in a superficial sense. Specifically, the defective component contributes a weak signal masked by the stronger vibrations from all the remaining components of the machine. Despite this similarity with the classical SR system, the use of this non linear phenomenon to enhance a vibration signal presents one clear difficulty. The noise considered in the classical SR theory has a flat spectrum, i.e. white noise. In contrast, in a machine the background vibrations are concentrated in a set of tonal components. However this aspect only marginally affects the performance of the SR system, as shown by the vast amount of research on its application to vibration data, for example [Klamecki, 2005, He et al., 2012, Ompusunggu et al., 2013] and as a matter of fact 15 papers on the application of SR in the field of vibration based condition monitoring, have been produced only in 2016[1]. The work presented here, firstly investigates from a general point of view the performance of a SR system with two degrees of freedom instead of one, as introduced in [Barbini et al., 2013], in order to verify whether it offers improved enhancing capabilities. Secondly it focuses on the specific application of SR on vibration data and differently from the literature it applies the non linear filter directly on the analog signal from the accelerometer, rather than its digital version, introducing a SR based circuit.
The chapter is organised as follows. Section 2.2 presents the comparison of the classical one dimensional SR system with a two dimensional SR system. Section 2.2 is reproduced from the author's published work in the proceedings of the 23^{rd} European Signal Processing Conference (EUSIPCO) [Barbini et al., 2015]. Section 2.3 presents the analysis carried out to test the performance of the two dimensional SR system directly on vibration data from an experimental setup and discusses the difficulties concerning the use of SR in a realistic application. In addition Section 2.3 introduces an analog circuit implementation of the two dimensional stochastic resonance system and tests its performance on simulated and experimental data.

[1]According to a search on 'web of science' [WoS, 2017]

2.2 Weak signal detection based on two dimensional stochastic resonance

Article published in the Proceedings of the 23^{rd} European Signal Processing Conference (EUSIPCO). Reprinted, with permission, from [Barbini et al., 2015] 2015 IEEE.

Statement of contributions of joint authorship

L. Barbini (candidate): writing and compilation of manuscript, established methodology, data analysis, preparation of tables and figures. Presented results at the conference.

M. O. T. Cole (associate supervisor): editing and co-author of manuscript

A. J. Hillis (associate supervisor): editing and co-author of manuscript

J. L. du Bois (principal supervisor): supervised and assisted with manuscript compilation and offered guidance in the development of the methodology, editing and co-author

Copyright

Weak signal detection based on two dimensional stochastic resonance

L. Barbini[a,1,*], M. O. T. Cole[a], A. J. Hillis[a], J. L. du Bois[a]

[a] *The University of Bath Department of Mechanical Engineering, Claverton Down, Bath, BA2 7AY, UK*

Abstract

The analysis of vibrations from rotating machines gives information about their faults. From the signal processing perspective a significant problem is the detection of weak signals embedded in strong noise. Stochastic resonance (SR) is a mechanism where noise is not suppressed but exploited to trigger the synchronization of a non-linear system and in its one-dimensional form has been recently applied to vibration analysis. This paper focuses on the use of SR in a two-dimensional system of gradient type for detection of weak signals submerged in Gaussian noise. Comparing the traditional one-dimensional system and the two-dimensional used here, this paper shows that the latter can offer a more sensitive means of detection. An alternative metric is proposed to assess the output signal quality, requiring no *a priori* knowledge of the signal to be detected, and it is shown to offer similar results to the more conventional signal-to-noise ratio.

Keywords: stochastic resonance, weak signal detection, non linear signal processing

1. Introduction

The response of a non-linear system to both the effects of noise and a periodic signal can result in a phenomenon of synchronization: stochastic resonance (SR) [1]. In the field of mechanical engineering a problem of great importance is that under operating conditions of many mechanical equipment, signals carrying useful information are submerged by heavy background noise. Conventional methods for the enhancement of the useful signal, so that it can be detected, consist of filtering or masking the noise [2, 3] while in the SR mechanism the noise is used to enhance the signal, reducing the risk of losing the information of interest. In this context the flow of the detection scheme is as follows. The sum of periodic aperiodic or impact signals [4] and an heavy noise is preprocessed [4, 5] and taken as the input of the non linear system, usually a 1D double well. Then will start an algorithm for tuning the parameters of this non-linear system, in order to trigger the SR mechanism. For each combination of the parameters, the output signal will be collected and evaluated with certain criteria, such as maximization of the weighted kurtosis index (KC) or of the signal-to-noise ratio (SNR), so that the best output is found and the signal of interest is detected [4]. The assumption of the adiabatic approximation for the SR mechanism, i.e. small values of frequency, amplitude and noise variance, can be avoided [5] hence in practical applications also high frequency-amplitude signals can be detected (henceforth "large parameter SR"). It is worth noticing that in the above mentioned detection scheme two key roles are the type of non linearity

*Corresponding author

Email address: leo.barbini@bath.ac.uk (L. Barbini)

Preprint submitted to 23rd European Signal Processing Conference

of the system and the optimization criteria; the former because it determines the set of variables that one is able to tune, the latter because it decides the values of those variables.
In the present paper we investigate both of the above mentioned aspects, firstly we will show how switching to a non linear system in more than one dimension will allow us to tune another parameter. Barbini *et al.* [6] investigated the effect of the addition of another degree of freedom to the usual bistable system used for the SR mechanism. It was observed a dependence of the output signal on the coupling constant, due to a change in the transition path among the stable points. Then the number of parameters which can be tuned increases, now being: the height of the potential barrier, the position of the stable points and also the coupling constant. One is tempted to think that for the same input signal, after the tuning process of the parameters, the output of the SR will be the same in the two cases. We investigate this question, comparing the best result of the 2D non-linear system with the mono-dimensional one, for the same input signal when the parameters are tuned in the same range of values. Secondly we propose a new criterion for selecting the best values of the three tuning parameters. Instead of looking at a time-frequency transformation we evaluate the degree of synchronization of the output signal using directly the distribution of the mean residence time in the stable points of the non linear system.
The paper is structured as follows. In section 2 we provide a description of the two dimensional non linear system, as well as the rescaling for extending the large parameter SR to this model. In section 3 we test the efficiency of the new tuning criteria for the parameters, detecting signals using the 1D model. In section 4 we show the dependence of the output in the 2D model on the coupling constant and comparing with the results obtained in the 1D case. Conclusions and an outlook for future development are given in the final section.

2. Normalised two dimensional SR

Let us consider the dynamical system associated to the following potential:

$$U(x,y) = -\frac{a}{2}\left(x^2+y^2\right) + \frac{b}{4}\left(x^4+y^4\right) - \frac{\delta}{2}\left(x^2y^2\right) \tag{1}$$

where a, b, δ are real positive numbers. This potential is the generalization of the one studied in [6], where $a = b = 1$. Throughout the paper we will consider the inertia small compared to other dynamical components.
The origin is an unstable steady point so that if we consider the effect of small fluctuations to the motionless state, i.e. noise, we will observe the system to stabilize in one of the minima, then for increasing values of the fluctuations we will have random transition between those minima symmetrically displaced in the quadrants. The system is two dimensional hence, differently from the usual double well, as a function of a, b, δ we have the possibility to have saddle points as unstable steady states and curved transition paths in the (x, y) plane. Respectively a, b define the height of the potential barrier between the stable steady states and their positions; δ is the coupling. Whether transitions will take place among saddle points or the maxima as well as the rate, depend on both the height of the potential barrier and on the curvature of the potential landscape [7]. In Fig.1 we show the displacement of the steady states and the transitions paths for different values of the coupling in the case $a = b = 1$. In green ($\delta = 0.65$) and red ($\delta = -0.65$) stable states lie on the axes of the plane and transitions occur through an unstable steady state at $(0, 1)$. Due to the symmetry of (1) such transitions could take place also between the $I - II, II - III$ and $III - IV$ quadrants (not shown). When the value of the coupling constant is lower than $\delta < -1$ there is a

change in the stability of the steady states of the potential, in Fig.1 we show in blue transitions in the case $\delta = -1.5$. It can be noticed that unstable steady states are now situated on the axes of the plane while steady states are at $(0, -1)$ and $(1, 0)$ respectively. The same considerations on

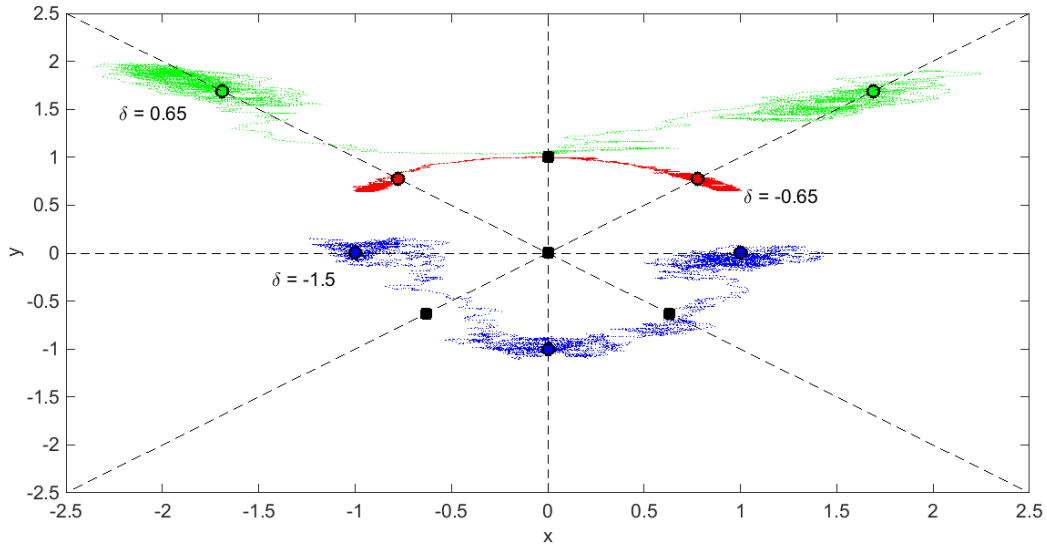

Figure 1: Paths on the $x - y$ plane for different values of δ: blue -1.5, red -0.65 and green 0.65. Circles and squares are respectively stable and unstable steady states

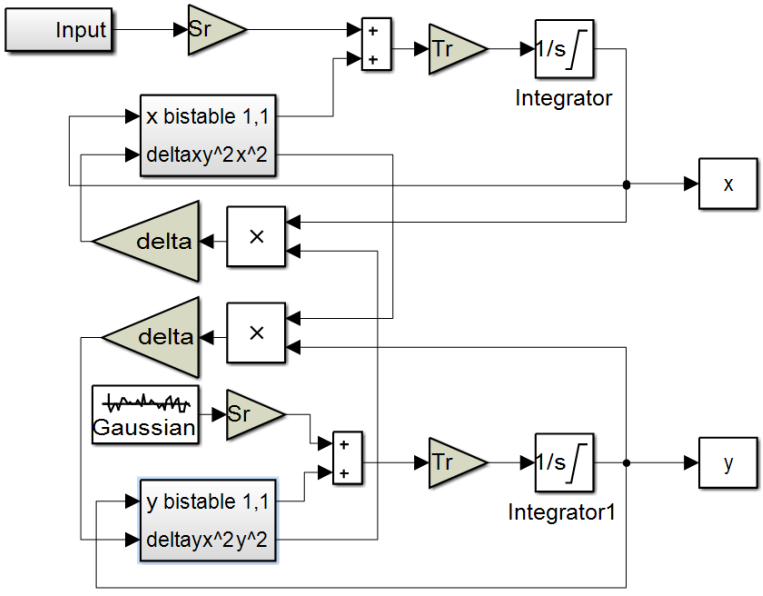

Figure 2: Model of the two dimensional SR detector

the symmetry apply in this case.
Let us consider now the effect of a periodic forcing on the dynamical system of stochastic differential equations obtained from the potential defined in (1). We add a periodic component $Acos(\omega t)$, of amplitude A and frequency ω, on the first of the two equations:

$$\begin{cases} dx = \left[ax - bx^3 + \delta xy^2 + Acos(\omega t)\right] dt + \varepsilon_x^{1/2} dw_x \\ dy = \left(ay - by^3 + \delta yx^2\right) dt + \varepsilon_y^{1/2} dw_y \end{cases} \tag{2}$$

where $dw_{(\cdot)}$ are independent Wiener processes and $\varepsilon_{(\cdot)}$ the variances of the noise. The effect of the periodic component in the first of (2) is that of modulate the potential (1), i.e. the height of the barrier between stable states changes implying a periodicity in the transition rates [1]. This synchronization phenomenon is the result of the cooperative effect of the periodic component and the noise, hence the transition rates are a function of both A, ω, ε, as well as the parameters of the non linear system a, b, δ.
The theory of stochastic differential equations provides an estimate of the mean exit time from the basins of attractions of the stable points in the limit of small parameters A, ω, ε [1, 7]. Nevertheless for a good use of SR in signal detection these limitations on the characteristic of the analysed signal must be avoided. Then following [5] we extend the rescale transformation to (2). For $a, b > 0$ we take a constant $k > 0$, we let and $\hat{x} = x\sqrt{b/a}, \hat{y} = y\sqrt{b/a}, \hat{\delta} = \delta/b, \hat{t} = t/k$; hence (2) reduces to the following system which preserves the gradient type structure:

$$\begin{cases} d\hat{x} = T_R \left\{ \left(\hat{x} - \hat{x}^3 + \hat{\delta}\hat{x}\hat{y}^2 \right) d\hat{t} + S_R \left[Acos\left(\Omega \hat{t}\right) d\hat{t} + \varepsilon_x^{1/2} d\hat{w}_x \right] \right\} \\ d\hat{y} = T_R \left[\left(\hat{y} - \hat{y}^3 + \hat{\delta}\hat{y}\hat{x}^2 \right) d\hat{t} + S_R \varepsilon_y^{1/2} d\hat{w}_y \right] \end{cases} \tag{3}$$

where $T_R = ak$ is the time rescale, $S_R = b^{1/2} a^{-3/2}$ is the spatial rescale, $\Omega = k\omega$ is the new signal frequency and the Wiener process $d\hat{w}$ keeps the statistical conditions $\langle d\hat{w} \rangle = 0, \langle d\hat{w}, d\hat{w}' \rangle = \delta(\hat{t} - \hat{t}')$; in the following we will omit the $\hat{\cdot}$ for simplicity.In practical application of SR as a signal detection method, the input of the nonlinear system is a noisy signal and the main objective is to analyze whether a periodic component is present or not. Referring to (3) the input is the sum of the last two terms of the first equation, with unknown A, ω, ε_x . In system (3) the values of the frequency and of the amplitude of the input signal can be taken without constraints, being multiplied respectively by S_R, k and the position of the stable points in the (x, y) plane and the height of the potential barrier are now fixed, being now the dependence on a, b in $S_R(a, b)$. The detection problem is then reduced to finding the values of T_R, S_R, δ providing a 2D SR mechanism giving an output signal x which shows a transition rate highly synchronized to the periodic component of the input. According to the order of magnitude expected for the frequency and amplitude of the periodic component we will decide the range of values for the parameters T_R and S_R. Then we will test all those for a selected range of values of the coupling constant δ, so that we will have to select the best output from a total number of $n_{T_R} \times n_{S_R} \times n_\delta$. In the present paper we propose to study directly the distribution of the transition rates τ i.e. the exit times from the basins of attraction of stable steady states of (3). Those are obtained from the array of the times of the x-mode zero crossing for each of the output signals. When the system is out of resonance, the times of the transitions between stable states are random, then the distribution of τ depicts no structure and decays exponentially. In [8] Benzi *et al.* showed that the moments for τ are given by:

$$\langle \tau^n \rangle \approx n! \langle \tau \rangle^n \tag{4}$$

In contrast, when we have SR the distribution of τ is peaked at the time being half period of the periodic forcing. In the present paper we use the ratio r_τ between the square of the mean and the variance of τ in order to evaluate the degree of the SR: $r_\tau = \langle\tau\rangle^2 / \left(\langle\tau^2\rangle - \langle\tau\rangle^2\right)$. The control parameter r_τ has to be independent from the time scale at which it is evaluated; this is why it is normalized with the mean here. According to (4) when the system shows completely random jumps r_τ reaches the value 1, while in the SR case $r_\tau \to \infty$ for a perfect identification of the signal frequency. The detection ends finding the maximum from all the r_τ, the measure of success of the procedure is that of detecting the signal carrying the useful information, for which the ratio $r = A/\varepsilon_x$ is the lowest.

3. Numerical results: test of r_τ

In this section we test the use of r_τ as a control parameter for the SR, all our numerical results are taken from a Simulink model reproducing system (3), the model is shown in Fig.2, the input block models the addition of periodic signals and a Gaussian noise:

$$Input = \sum_n A_n sin\left(\omega_n t\right) + \varepsilon_x^{1/2}\eta(t) \tag{5}$$

being $\eta(t) = dw/dt$, and n the number of components. Within this section we restrict our analysis to the 1D system, i.e the first equation of (3) with $\delta = 0$. We test the model with an input signal constructed as follows: $n = 3$; the amplitudes and frequencies of the periodic components are chosen randomly in the ranges of values 0.01 to 1 and 0.001 to 1000 Hz respectively; the variance of the noise is taken as the result of multiplication of the highest of the A_i for a random

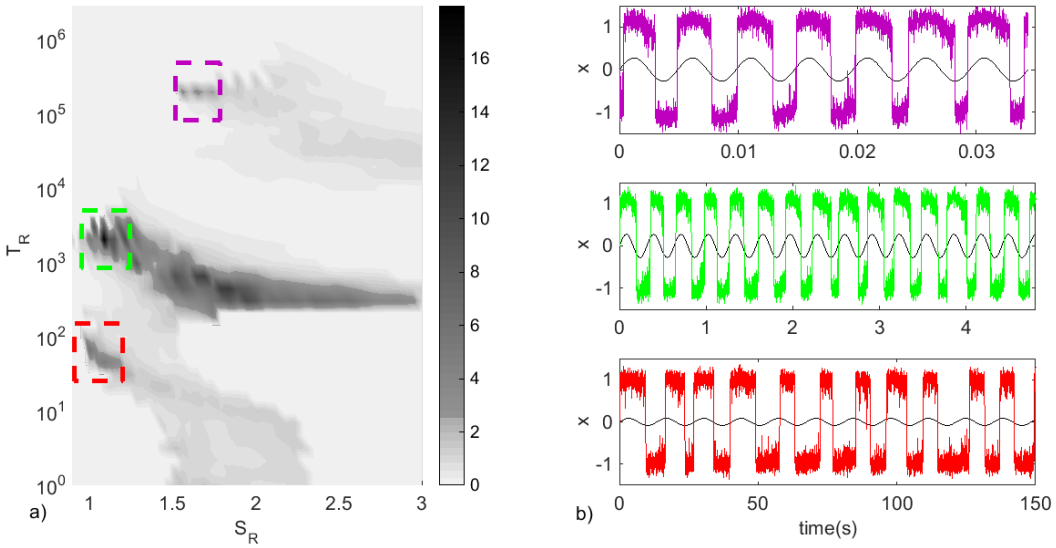

Figure 3: a) contour plot of r_τ for the 1D detector; b) three output signals obtained for the values of S_R, T_R giving the maxima of r_τ. In black the periodic components of the input: top $(A_3, \omega_3) = (0.2794, 203.6811)$, middle $(A_2, \omega_2) = (0.2727, 3.1748)$ and bottom $(A_1, \omega_1) = (0.0845, 0.0741)$

number in the range 5 to 10 so that we ensure that the periodic signals are heavily buried into noise. The following values for the input signal were found: $(A_1, \omega_1) = (0.0845, 0.0741), (A_2, \omega_2) = (0.2727, 3.1748), (A_3, \omega_3) = (0.2794, 203.6811)$ and $\varepsilon_x = (2.3497)^2$. The tuning parameters T_R, S_R are tested in the range 1 to 10^6, 0.01 to 15 respectively and we decide increment steps so that we end up in a matrix of dimensions $n_{T_R} \times n_{S_R} = 40 \times 250$. In the simulations for each T_R we change both the integration time step $dt = 2^{-6}/T_R$ and the time length of the analyzed signals $L = 10000/T_R$, while we keep fixed the number of samples and we sub-sample the output of 27, so that we end up with signals of 5000 samples. In Fig.3(a) we show the contour plot of the values of r_τ for each of the tuning parameter, we have recognized the areas, red green and purple, for the peaks corresponding to the three periodic components of the input signal.In Fig.3(b) we show a comparison between the periodic components, black signals, and the three output x obtained setting S_R, T_R as for the maxima of r_τ; the time scales of the plots are different and after the SR we can appreciate the time decomposition of the three components of the input. We show the classical signal to noise ratio (SNR) metric calculated for the output values for each of the tuning parameter in Fig.4(a), SNR is defined as the ratio between the power of the spectral line at the periodic input frequency and that of the noise background [5], we notice that the areas corresponding to the three input frequencies are visible and comparable with those of r_τ and that a good comparison is possible. In Fig.3(a) we notice the displacement of the peaks in the S_R dimension due both to the ratio $r_i = A_i/\varepsilon_x$ and the superposition of the signals at different frequencies. In order to quantify the dependence of r_τ on the ratio r without such a superposition we test an input signal where there is only one periodic component, $n = 1$ in (5). Following the above mentioned construction procedure we found the following values for the amplitude and frequency $(A, \omega) = (0.2749, 31.6426)$ and for the variance $\varepsilon_x = (5.4976)^2$. Then we modify the

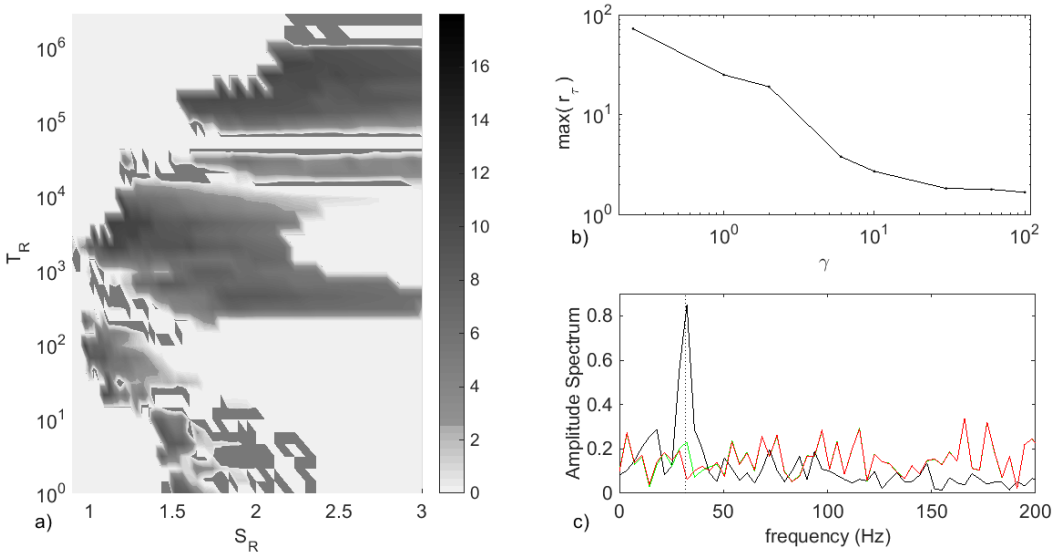

Figure 4: a) contour plot of SNR for the 1D detector; b) dependence of maximum of r_τ on the amplitude $\gamma\varepsilon_x^{1/2}$ of the input noise; c) amplitude spectra of input noise (red) for $\gamma = 6, \varepsilon_x = (5.4976)^2$, input noise plus sinusoid (green) in the case $(A, \omega) = (0.2749, 31.6426)$, output of 1D SR detector (black)

ratio r multiplying the variance for $\gamma = 0.25, 1, 2, 6, 1, 10, 30, 60, 100$ while we keep the values of the periodic component fixed:

$$Input = Asin\,(\omega t) + \gamma \varepsilon_x^{1/2} \eta(t) \tag{6}$$

In Fig.4(b) we show the maximum values of r_τ for each of the inputs as a function of γ; in Fig.4(c) we show the spectral amplitudes for the case $\gamma = 6$, black green and red are respectively the output, the input and only the noise content of the input. A dotted line is plot at the input frequency value, the presence of periodicity is completely not detectable before SR, being the difference in spectra of the noise and sine wave plus noise negligible hence the input signal before SR filtering could be characterized as white noise.

4. Numerical results: the comparison

In this section we use the 2D model, system (3). The value of the variance of the Gaussian noise ε_y of the second degree of freedom will always be taken $\varepsilon_y \ll \varepsilon_x$ so that the motion will displace in the (x, y) plane but any transition in the y-mode, being the jumps between stable states of the x-mode. Firstly we test the dependence of the 2D detector on the value of the coupling constant δ with the input signal as in equation (6). We want to compare the results of this detector with the 1D one then we use same values A, ω, ε_x as in the precedent section and $\gamma = 2$. In Fig.5 we show the contour plot of r_τ for each of the T_R, S_R parameters, top left is the 1D case while all the others are the 2D case for different values of δ, respectively $\delta = -5, -1.5, -0.95, -0.65, -0.25, 0.25, 0.65, 0.95$. We notice the dependence of the position of the peaks in the (T_R, S_R) space on the value of the coupling. Furthermore due to the change on the stability of the steady states of (3) as a function of δ, we notice a difference on the area of r_τ over a threshold, i.e. the area covered by peaks visible in Fig.5. It increases with the coupling constant value varying from $-\infty < \delta < -1$ then occurs the change in the position of the steady states at $\delta = -1$ and the area covered by the peaks

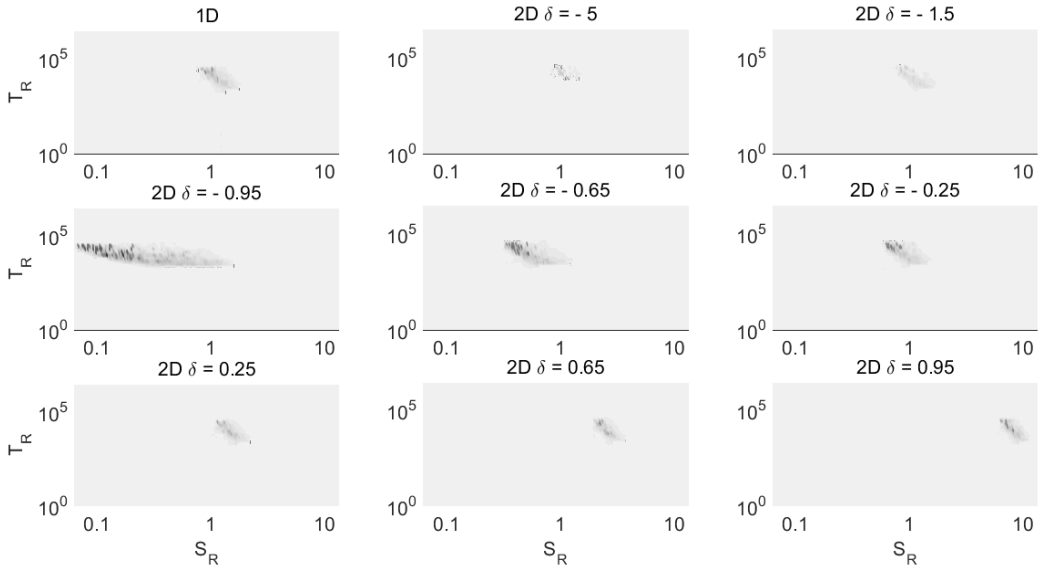

Figure 5: contour plot of r_τ: top left 1D detector, all the others are for the 2D detector with different δ

reaches a maximum for $\delta = -0.95$, hence for (3) approaching the case of a dynamical hysteresis [9], while decreases for $-1 < \delta < 1$. The same dependence on the coupling is found as well on the maximum values of r_τ, in Fig.6 we show such maxima as a function of δ for different values of the ratio r, plots with different vertical scales. The input signal (6) is taken for four different values of γ, respectively $\gamma = 0.25, 1, 2, 6$, while A, ω, ε_x are as in the previous simulation. We notice that the increase in the degree of synchronization of the output signal due to the 2D feature of (3) is related to the stability change in the (x, y) plane and that the maxima are found for $\delta > -1$, i.e. transitions path as in the red and green cases in Fig.1. The maxima of r_τ for the 1D case are blue constant lines in Fig.6, within certain values of δ we notice that the 2D detector outperforms the 1D one. In order to investigate such performance we show the comparison between the output signals of the 1D and 2D detectors for the input signal taken with $\gamma = 2$ and A, ω, ε_x as in the previous simulation. In Fig.7(a) we show the time domain, respectively blue red and black are the outputs in the 1D, 2D case and the periodic component of the input multiplied by a factor 3. Firstly we notice that in the 2D signal the variance of the output around the stable steady states is lower in respect to the one in the 1D signal; furthermore we notice that the accordance between the jumps times and the maximum values reached by the sinusoidal component is greater in the 2D case, corresponding in a fixed phase lag. In Fig.7(b) the two output signals are shown in the frequency domain, blue and red are the 1D and 2D case, dotted vertical lines are plot at the values of ω and at the first two odd harmonics. The values of the steady states in the 1D case are greater in respect to the 2D one, amplitude of output signals in Fig. 7 (a), nevertheless we notice that in the output signal of the 2D detector the power in the range 20 to 40 Hz is lower, this feature is better noticed in the first odd harmonic, which is visible in the 2D case while it is not in the 1D one; at the frequency value of 5ω the peak cannot be easily observed even in the 2D case.

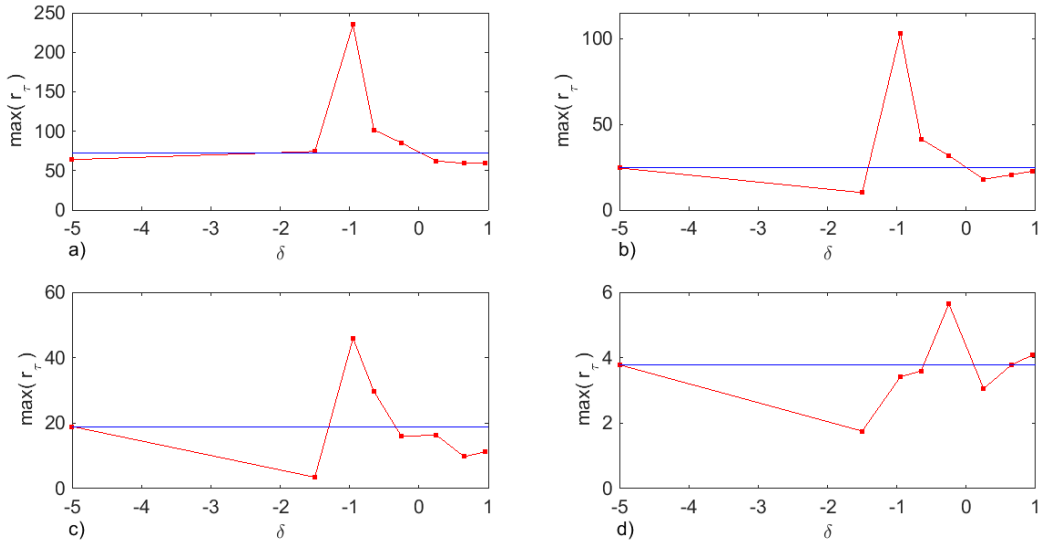

Figure 6: maxima of r_τ for the 2D detector (red) as a function of δ: a)$\gamma = 0.25$, b) $\gamma = 1$, c) $\gamma = 2$, d) $\gamma = 6$; in blue 1D

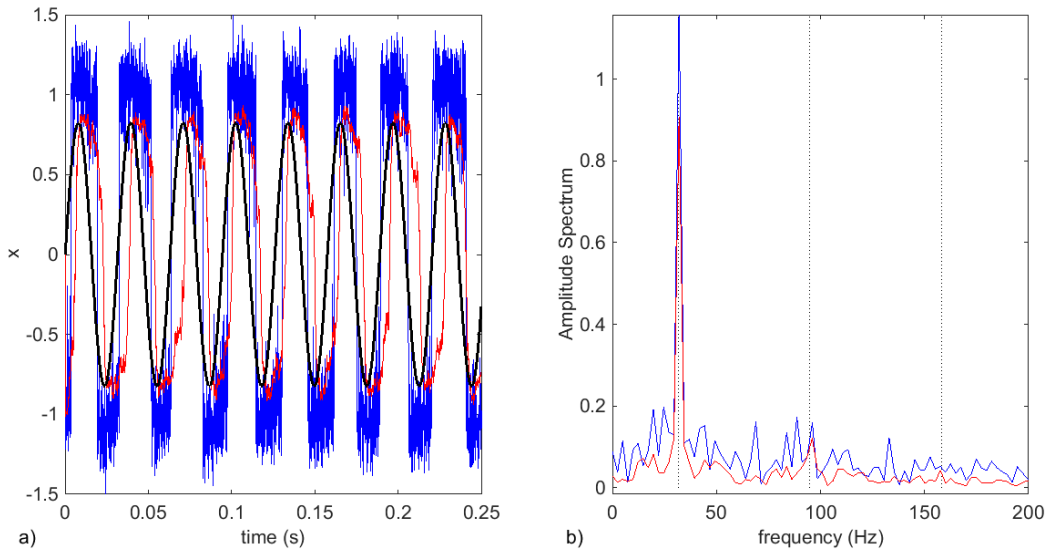

Figure 7: comparisons of the best outputs of the 1D (blue) and 2D (red) detectors, for $\gamma = 1$, input sinusoid multiplied for a factor 3 (black): a) time signals b) amplitude spectra

5. Conclusion

This paper introduced a model based on a two dimensional SR mechanism for the detection of weak periodic signals, of random frequency and amplitude, buried in heavy background noise. A new measurement index was proposed, calculated directly from the vector of the zero crossing of the output signal without the need for a time-frequency transformation or *a priori* knowledge of the input signal. The new index was first shown to convey similar information to that of the signal-to-noise ratio, and was then used to evaluate the periodic content in the output signal from the SR detector. It was shown that the presence of the coupling constant δ, used as a tuning parameter in the proposed two dimensional SR model, results in a better capacity for the detection of weak signals when compared with the usual mono-dimensional model. The best results in the two dimensional detector are found when the value of the coupling is close to $\delta = -1$ corresponding to the case of a limit cycle for the dynamics of the model. The mechanism of operation in this case appears to consist of a dynamical hysteresis where transitions occur deterministically as a function of the amplitude and frequency of the periodic forcing, and further studies are in progress to explore the nature of this mechanism. Future work will involve the experimental application of the techniques developed here in the field of condition monitoring, in particular the detection of weak fault signals in rotating machines.

References

[1] R. Benzi, A. Sutera, A. Vulpiani, The mechanism of stochastic resonance, Journal of Physics A: Mathematical and General 14 (11) (1981) L453. doi:10.1088/0305-4470/14/11/006.
URL http://iopscience.iop.org/0305-4470/14/11/006

[2] J. Lin, M. Zuo, Gearbox fault diagnosis using adaptive wavelet filter, Mechanical Systems and Signal Processing 17 (6) (2003) 1259–1269. doi:10.1006/mssp.2002.1507.
URL http://www.sciencedirect.com/science/article/pii/S0888327002915074

[3] J. Hongkai, H. Zhengjia, D. Chendong, C. Peng, Gearbox fault diagnosis using adaptive redundant lifting scheme, Mechanical Systems and Signal Processing 20 (8) (2006) 1992–2006. doi:10.1016/j.ymssp.2005.06.001.
URL http://www.sciencedirect.com/science/article/pii/S0888327005000944

[4] J. Li, X. Chen, Z. He, Adaptive stochastic resonance method for impact signal detection based on sliding window, Mechanical Systems and Signal Processing 36 (2) (2013) 240–255. doi:10.1016/j.ymssp.2012.12.004.
URL http://www.sciencedirect.com/science/article/pii/S0888327012004736

[5] Q. He, J. Wang, Y. Liu, D. Dai, F. Kong, Multiscale noise tuning of stochastic resonance for enhanced fault diagnosis in rotating machines, Mechanical Systems and Signal Processing 28 (2012) 443–457. doi:10.1016/j.ymssp.2011.11.021.
URL http://www.sciencedirect.com/science/article/pii/S0888327011005139

[6] L. Barbini, I. Bordi, K. Fraedrich, A. Sutera, The stochastic resonance in a system of gradient type, European Physical Journal Plus 128 (2013) 13. doi:10.1140/epjp/i2013-13013-5.
URL http://adsabs.harvard.edu/abs/2013EPJP..128...13B

[7] R. Benzi, A. Sutera, A. Vulpiani, Stochastic resonance in the landau-ginzburg equation, Journal of Physics A: Mathematical and General 18 (12) (1985) 2239. doi:10.1088/0305-4470/18/12/022.
URL http://iopscience.iop.org/0305-4470/18/12/022

[8] R. Benzi, A. Sutera, The mechanism of stochastic resonance in climate theory, in: Proceedings of the International School of Physics E. Fermi, 1985, pp. 403–423.

[9] Jung, Gray, Roy, Mandel, Scaling law for dynamical hysteresis, Physical Review Letters 65 (15) (1990) 1873–1876.

2.3 Stochastic resonance applied to vibration signals

In Section 2.2 SR was tested on a numerically simulated signal consisting of a sum of sinusoids buried in noise, as shown in Eq. 5. In order to investigate the applicability of SR as a tool for vibration-based condition monitoring, and specifically detection of a defective bearing, in this section tests are conducted on a vibration signal from an experimental setup. The data are collected from a test rig consisting of a variable speed motor, a gearbox and a braking system. The motor drives through a flexible coupling the input shaft of the gearbox and after a two stage speed reduction, the load is applied to the output shaft of the gearbox by the braking system. A mono-axial piezoelectric accelerometer is finally mounted on the gearbox cage to measure its vibrations. The shaft rotational speed of the motor can be varied from 0 to 3000 rpm while the load can vary from 0 to 50 Nm. A schematic overview of the setup can be found in Fig. 2.8 with the bearings B1 to B6 supporting the three shafts, the two gear reductions GR, the coupling in yellow and the accelerometer in red.
The analysed vibration signal is collected when the shaft rotational speed is stationary at 2.9 Hz, the load is of 6 Nm and B5 presents a fault in the inner cage. Figure 2.9(a) shows a portion of the raw accelerometer data d(t) believed to comprise two impacts from the defective bearing. The impacts from the defective bearing are present around 10 ms and 75 ms. Before processing the signal with the SR system, a normalised version is calculated as:

$$\tilde{d}(t) = q\left(2\frac{|d(t)|^2}{\max_t |d(t)|^2} - 1\right) \tag{2.1}$$

where q is a constant chosen by the user to produce a sub threshold or a supra threshold signal. The threshold of the SR system corresponds to the height of the potential barrier between two stable states. The signal is normalised in such a way in order to enhance

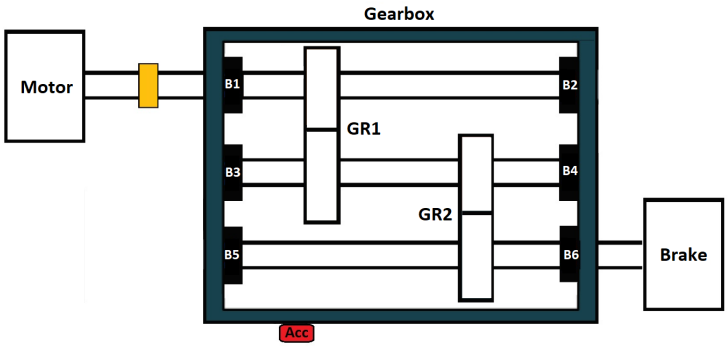

Figure 2.8: Experimental setup for testing the use of SR on vibration data

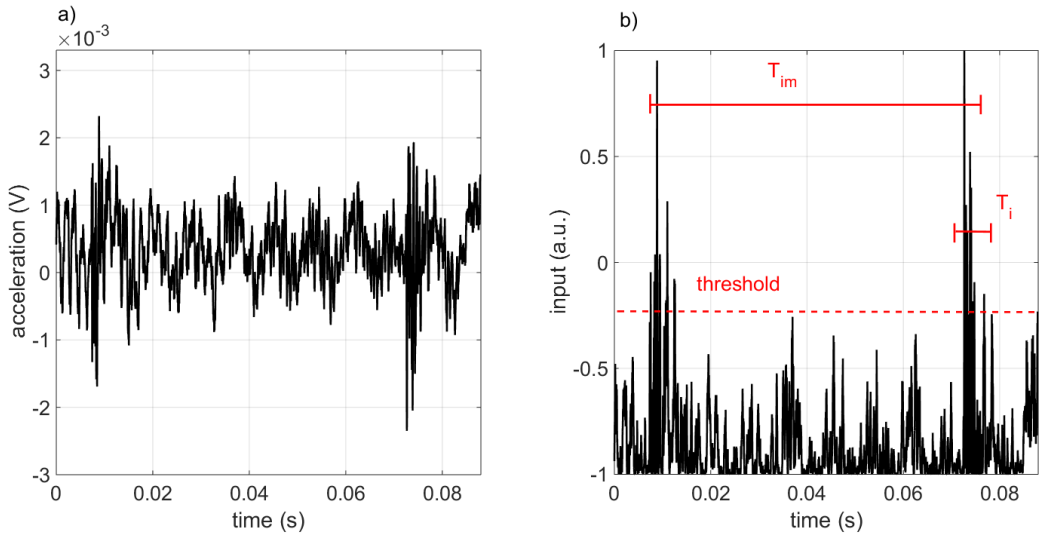

Figure 2.9: (a) The raw signal $d(t)$ acquired by the accelerometer. (b) The normalised version of the signal $\tilde{d}(t)$ used as input for the SR system.

the impacts from the defective bearings and to simplify the selection of the spatial rescale parameter S_R. Figure 2.9(b) shows $\tilde{d}(t)$ corresponding to the selected portion of data from the accelerometer for the constant $q = 1$. The threshold is shown with the red dotted line and corresponds to the height of the potential barrier of the dynamical system.

The normalised signal $\tilde{d}(t)$ is then input in the two dimensional SR system of Eq. 3 instead of the sinusoidal component $Acos(\Omega\hat{t})$, yielding:

$$\begin{cases} d\hat{x} = T_R \left\{ \left(\hat{x} - \hat{x}^3 + \hat{\delta}\hat{x}\hat{y}^2 \right) d\hat{t} + S_R \left[\tilde{d}(\hat{t}) d\hat{t} + \varepsilon_x^{1/2} d\hat{w}_x \right] \right\} \\ d\hat{y} = T_R \left[\left(\hat{y} - \hat{y}^3 + \hat{\delta}\hat{y}\hat{x}^2 \right) d\hat{t} + S_R \varepsilon_y^{1/2} d\hat{w}_y \right] \end{cases} \tag{2.2}$$

where $\hat{x} = x\sqrt{b/a}, \hat{y} = y\sqrt{b/a}, \hat{\delta} = \delta/b, \hat{t} = t/k$ with a, b, k positive constants and $S_R = b^{1/2}a^{-3/2}$ the spatial rescale parameter and $T_R = ak$ the time rescale parameter to be tuned. In such a way the temporal scale of the impacts can be changed accordingly, therefore the assumption of the adiabatic approximation for the SR mechanism, i.e. small values of frequency, is avoided. All the results discussed in the following are obtained using the Euler-Matuyama method [Kloeden and Platen, 1992] for integration of stochastic differential equations.

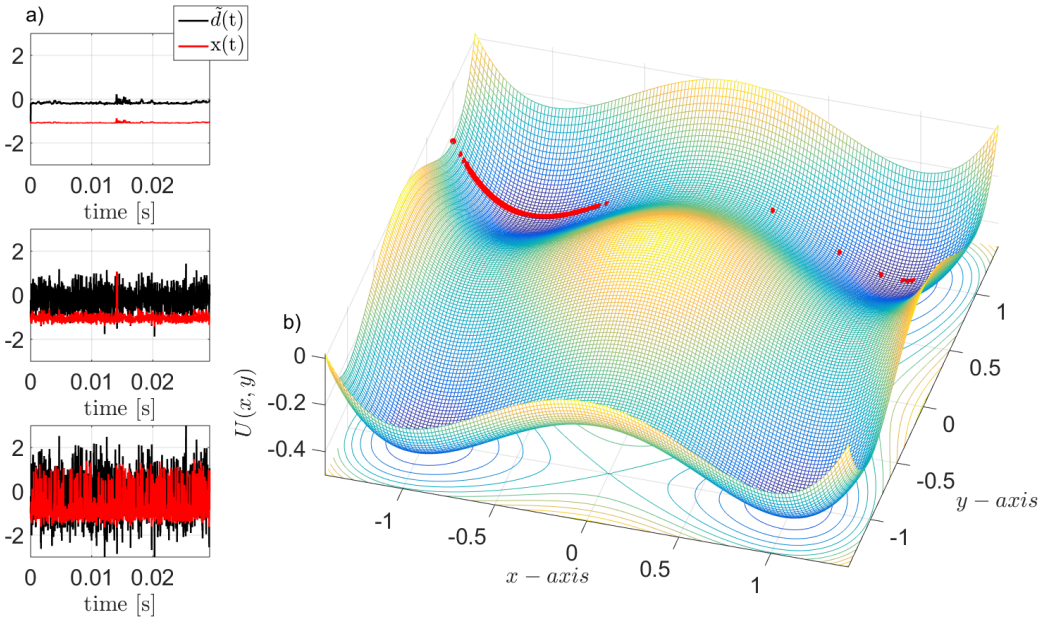

Figure 2.10: Test of the SR system on vibration data $\tilde{d}(t)$. Numerical simulation with $\delta = 0$. (a) Input signal in black and output x(t) in red for three different levels of noise. (b) Potential and output of the system when synchronised.

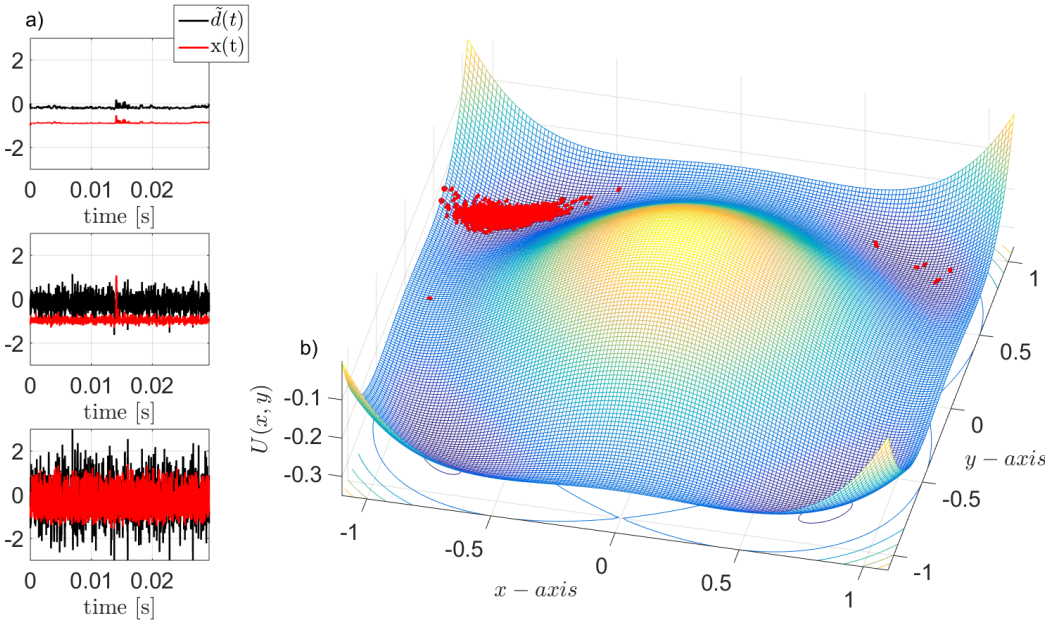

Figure 2.11: Test of the SR system on vibration data $\tilde{d}(t)$. Numerical simulation with $\delta = -0.65$. (a) Input signal in black and output x(t) in red for three different levels of noise. (b) Potential and output of the system when synchronised.

2.3.1 Results

The analysis is restricted to a single impact, using only the first 1500 data points of $\tilde{d}(t)$, corresponding to $\simeq 0.29$ s in Fig. 2.9(a). The SR mechanism in the case of a sub threshold signal is proved to work for four different values of the coupling constant $\delta = \{0,\ -0.65,\ 0.3,\ -1.3\}$. The first case analysed is for $\delta = 0$ and there is no coupling between the two modes of the dynamical system. Therefore Eq. 2.2 corresponds to the one dimensional SR. In order to have a sub threshold signal $q = 0.2$ in Eq. 2.1 and the parameters a and b of the dynamical system are considered unitary, giving $S_R = 1$ and $T_R = k$ in Eq. 2.2.

Figure 2.10(a) shows the results obtained for three different levels of input noise, respectively $\varepsilon_x^{1/2} = \{0.01, 0.25, 0.5\}$ from top to bottom. The constant k for the time rescale was estimated[2] from Fig. 2.3, specifically considering that the temporal scale is $T_i \simeq T_{im}/200 \simeq 3\ kHz$. The value used for the time rescale is $k = 383$, yielding a final integration step of $d\tilde{\tau} = 5 \times 10^{-8}$.

In Fig. 2.10(a) the classical dependence of the SR system on the noise can be observed. For instance on the top plot the noise level is not sufficient for triggering a transition between two stable states. While in the middle plot the increase in the level of noise allows the transition, which occurs around 15 ms, exactly at the time of the impact from the defective bearing. The further increase in the noise level as in the bottom plot, results in a higher number of transitions occurring at spurious times. Figure 2.10(b) shows the potential $U(x, y)$ with the points superimposed in red corresponding to the output of the SR system for $\varepsilon_x^{1/2} = 0.25$. Because the coupling is $\delta = 0$ the y variable is constantly unitary and the two dimensional system corresponds to the one dimensional double well system with the transition occurring at (0,1).

The next test is for $\delta = -0.65$ and $q = 0.1$ in Eq. 2.1, in order to have a sub threshold SR. The results are shown in Fig. 2.11. Three different levels of input noise $\varepsilon_x^{1/2} = \{0.01, 0.2, 0.6\}$ are tested and the constant for the time rescale is selected as $k = 383$. The classical SR behaviour is observed also in this case of a two dimensional system. Specifically, Fig. 2.11(a) shows that an increase in the variance of the noise enhances the detection of the impact from the defective bearing. Figure 2.11(b) shows the potential $U(x, y)$ for $\varepsilon_x^{1/2} = 0.2$ when the SR system is synchronised. In this case of a two dimensional system, in comparison with Fig. 2.10(b), the superimposed red points depict the two dimensional behaviour. Specifically the points are not in the one dimensional line at y=1. They are distributed in the (x,y) plane, in the basin of

[2]From Fig. 2.3 a rule of thumb is that the integration step has to be around $1/(10^4 \times f_{sinusoid})$. Please notice that in Fig. 2.3 the initial integration step is 2^{-6}, while for the the experimental data analysed in this section it is 1/51200

attraction around the stable points calculated from Eq. 2.2:

$$(\pm x_s, \pm y_s) = \left(\frac{1}{\sqrt{1-\delta}}, \frac{1}{\sqrt{1-\delta}} \right) \simeq (0.78, 0.78). \tag{2.3}$$

The curved transition path between the stable points is equivalent to Fig. 2.1 for the case shown in red.
Similar results of Fig. 2.11 are obtained for the other two values of the coupling constant $\delta = \{0.3, -1.3\}$, demonstrating the effectiveness of the SR system for bearing fault detection.

2.3.2 Analog circuit model

The last part of this research on SR focuses on the implementation of a circuit corresponding to the analog version of the two dimensional SR system. Currently SR is applied to vibration signals after digital to analog conversion, either using computer software [He et al., 2012, Ompusunggu et al., 2013] or embedded systems with dedicated digital signal processing units [Lu et al., 2016, Lu et al., 2014]. For instance the methodology of Section 2.3 corresponds to the application of two dimensional SR on the digital version of the accelerometer data using computer software.
The observation of SR in electric circuits dates back to 1983, when [Fauve and Heslot, 1983] used an analog comparator to enhance a sinusoid buried in noise. Afterwards a diode circuit [Godivier et al., 1997] implementing a static non linearity was used to test the SR phenomenon. More recently, an electrical circuit implementing the one dimensional SR system has been proposed in [Luchinsky et al., 1999a, Luchinsky et al., 1999b, Dai et al., 2011, Dai and He, 2012]. However in the literature there is no direct application of SR to the analog signal from an accelerometer. Research in this direction lies in the field of distributed intelligent sensors. For instance when condition monitoring is applied in industrial contexts, there is the need to place several transducers. An example is monitoring the condition of a farm of wind turbines. In such cases each sensor sends the collected raw data to a central server unit which provides analog to digital conversion and implements digital signal processing algorithms. Afterwards digital data is sent to a remote server and further analysed by trained technicians [Pylvänen and Elfström, 2013]. When the signal from hundreds of sensors needs to be sent to a central unit two main problems arise:

- computational power of the server
- transfer of large amount of data.

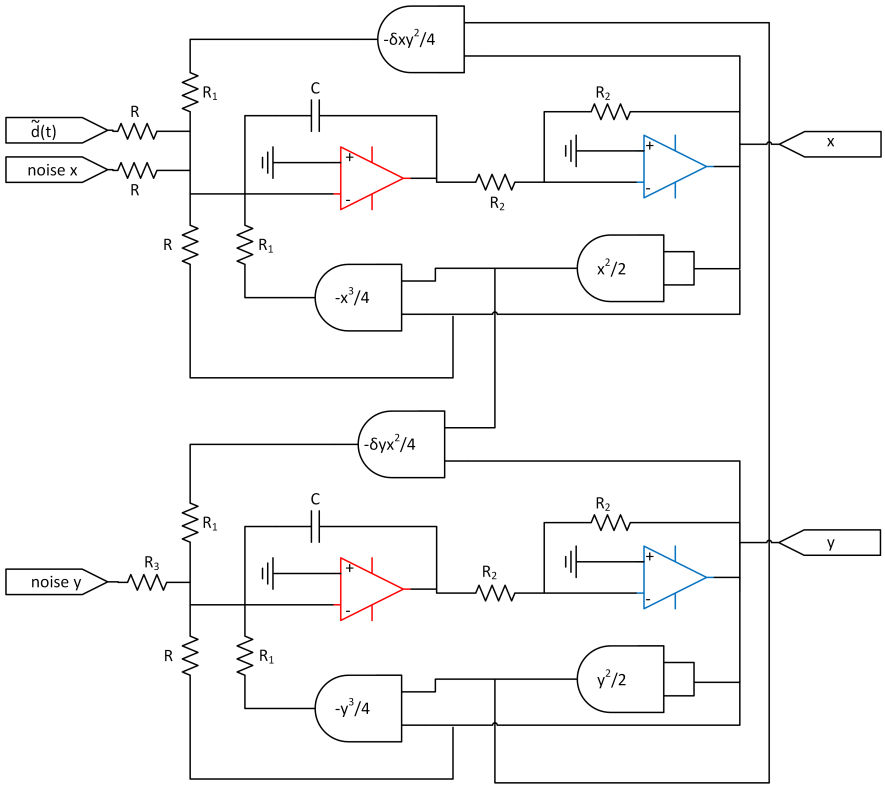

Figure 2.12: The schematics of the two dimensional SR analog circuitry

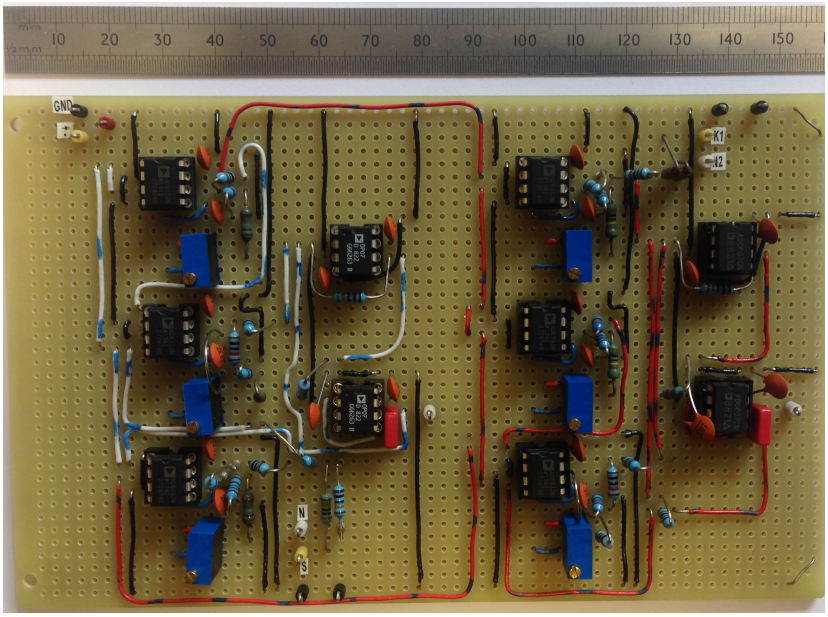

Figure 2.13: Photograph of the realised analog circuitry

In this context distributed intelligent sensors find their role. In order to have a low cost condition monitoring architecture there is the need to develop sensors with the ability to directly implement basic signal processing algorithms [Lumme, 2012].
Figure 2.12 shows the schematic of the circuit corresponding to the integral version of Eq. 2 with a=b=1. Integration is implemented using an operational amplifier, shown in red, while an analog multiplier AD633 is used to have the second and third order terms. The use of variable resistors allows the selection of the coupling constant δ, when AD 633 is used in the variable scale factor configuration [AD, 2017]. In addition AD 633 allows change of sign, for the negative third order term. In each multiplication a scale factor of 2 is selected to prevent the product voltage exceeding the specified maximum of the AD 633. Subsequently resistors R_1 are chosen as $4R_1 = R$. Therefore the time constant of the circuit of Fig. 2.12 is given by RC. Resistor values should be chosen in the range 1 to 100 $k\Omega$ and capacitance of at least 22 pF, in view of the typical stray capacitance of a few pF [Luchinsky et al., 1999a].
The inputs of the circuit are the signal $\tilde{d}(t)$ and the white noise for the x and y variables. Outputs are taken after the analog inverter circuit, shown with the blue operational amplifiers. Analog noise can be realised using commercial generators, simple electronic components [Moss and McClintock, 1988], or by a computer and then digital to analog converted. In the following experiments the noise was generated using the latter of these methods. Resistor $R_3 = 500R$ in order to have a greater noise in the driving variable x.
As a first test of the circuit, a sinusoid of amplitude 0.1 V and frequency 80 Hz is selected as input. Figure 2.13 shows the picture of the realised circuit, the component values used are R=20 $k\Omega$ and C=220 pF, giving a time constant $RC = 4.4\mu s$, which allows synchronisation with the sinusoid. The blue components are variable resistors used to fine tune the output of the multipliers. The coupling constant is chosen as $\delta = -0.4$. Results obtained from this circuit are shown in Fig. 2.14(a) for three different levels of the input noise. The typical SR mechanism is observed. A small amount of noise does not allow synchronisation, as shown in the top plot, while an increase in the level of noise results in transitions occurring at the frequency of the sinusoid, as shown in the second plot. In the bottom plot the further increase in the level of noise results in uncontrolled transitions. Figure 2.14(b) shows transition between the two stable states in the potential landscape, for the case of synchronisation of the SR circuit. Is it possible to notice both the two dimensional shape of the basins of attractions of the stable points and the curved transition path.
Finally the circuit is tested on the vibration signal from the experimental setup of Fig. 2.8. The signal is the same as in Section 2.3.1, consisting of 1500 data points

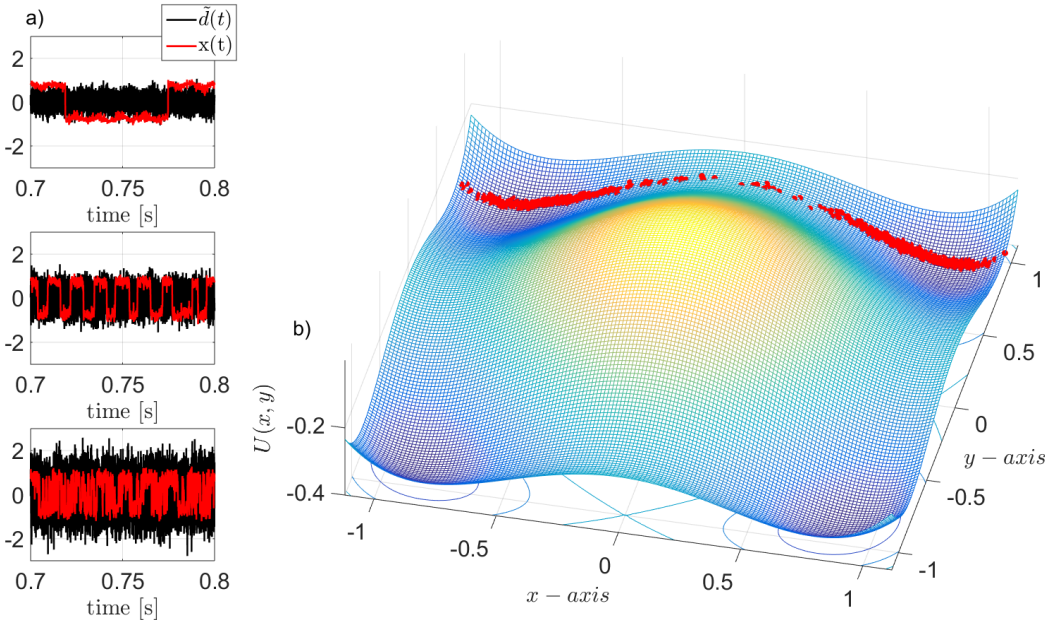

Figure 2.14: Test of the SR circuit on sinusoid of amplitude 0.1 V and frequency 80 Hz, $\delta = -0.4$. (a) Input signal in black and output x(t) in red for three different levels of noise. (b) Potential and output of the system when synchronised.

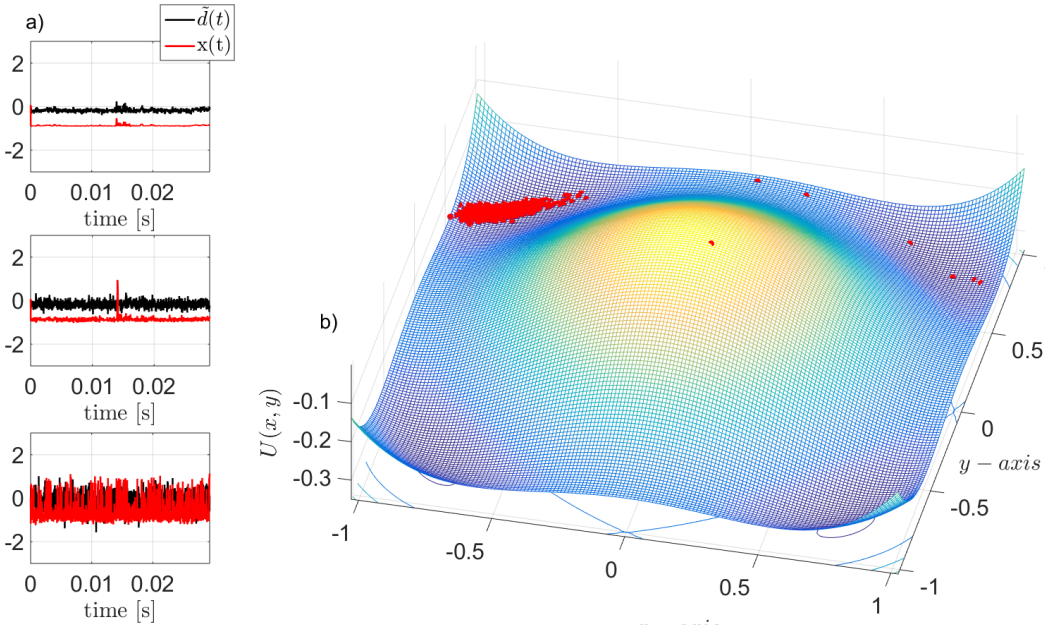

Figure 2.15: Test of the SR circuit on vibration data $\tilde{d}(t)$, $\delta = -0.65$. (a) Input signal in black and output x(t) in red for three different levels of noise. (b) Potential and output of the system when synchronised.

and the raw signal is normalised according to Eq. 2.1. In this case a Simulink circuit simulation is used instead of a real circuit, differently from the previous analysis. In the simulink model, the coupling constant is chosen as $\delta = -0.65$ and the values used for the components are R=4 $k\Omega$ and $C = 22\ pF$, giving a time constant $RC = 88\ ns$, which allows synchronisation with the sequence of impacts from the defective bearing. This value is selected following the analysis of Section 2.3.1 where the time integration step, after the time rescale, is $1/\left(Fs * k\right) \simeq 50\ ns$. Results of the circuit performance are shown in Figure 2.15 and they can be compared with the results from the numerical integration shown in Figure 2.11. Specifically three different values of the input noise $\varepsilon_x^{1/2} = \{0.0133, 0.20, 0.5\}$ are shown in Fig. 2.15(a) and the classical noise-driven SR synchronisation mechanism is observed. Figure 2.15(a) shows the potential landscape in the case of $\varepsilon_x^{1/2} = 0.20$ when the system shows a transition between two stable states at the occurrence time of the impact.

2.3.3 Analysis

The application of SR on a signal from a defective bearing presents several difficulties. The first problem is related to the temporal scale T_i at which the SR system synchronises. The inverse of the temporal scale of interest corresponds to the frequency at which the jumps between two stable states of the dynamical system should occur. Unfortunately T_i does not coincide with the interval of time between two impacts T_{im}, which is the only known variable related to the defective bearing. T_{im} is calculated from the shaft rotation speed and from the mechanical dimensions of the bearing, as described in Section 1.3.1. For the Flanders Make 2 setup the inner race defect produces impacts at $T_{im} \simeq 1/\left(5.43 \times f_{shaft}\right)$ and for the shaft rotational speed of $f_{speed} = 2.9\ Hz$ analysed here it corresponds to $T_{im} \simeq 60\ ms$. From Fig. 2.9 it is possible to verify that the separation between the two impacts corresponds to this estimate. On the other hand T_i clearly depends on uncontrolled factors such as the resonant frequency excited by the impact. As an example in Fig. 2.9(b) T_{im} and T_i are shown with red horizontal segments. Specifically T_i is shown for the second impact and T_{im} between the first and the second impacts. In order to have an estimate of T_i the interval of time between two impacts can be used, being:

$$T_i < T_{im} \tag{2.4}$$

However a blind search on a selected range of T_R in Eq. 2.2 is needed, as in Section 2.2, because the exact value of T_i is not known. This results in a computationally expensive and time consuming process, jeopardising a real time application of the SR mechanism

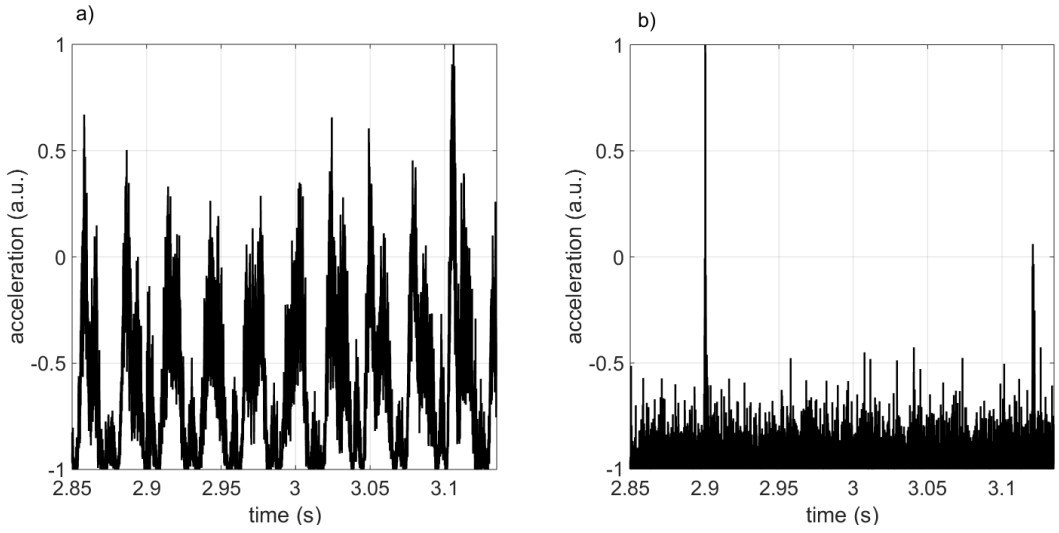

Figure 2.16: (a) The normalised signal $\tilde{d}(t)$ at lower shaft speed in respect to Fig. 2.9. (b) The same signal after the operation of cepstrum pre-whitening.

in vibration based condition monitoring.

The second issue with the SR approach is that for the same defective bearing successive impacts produce different results as can be seen in Fig. 2.9(b). For instance in the case of a machine operating at varying speed or varying load this aspect is even more pronounced. Intuitively the higher the shaft rotational speed or the load on the bearing, the bigger the impacts. Therefore the tuning of the spatial rescale S_R in Eq. 2.2 becomes particularly difficult. For the same value of S_R sections of the vibration signal might result in a supra-threshold stochastic resonance while others in a sub-threshold stochastic resonance. Therefore a step of signal pre-processing is needed. Specifically the signal should be divided into sections containing impacts of similar amplitudes.

The final issue is that the signal acquired by an accelerometer comprises both vibrations from the gears and from the defective bearing as shown in Eq. 1.8. Therefore the SR systems could synchronise with the gear meshing frequency or harmonics instead of the bearing fault frequency $1/T_{im}$, resulting in a missed detection. Ompusunggu et al. [Ompusunggu et al., 2013] address this problem and propose the use of cepstral pre-whitening to suppress components from the gears and use SR to enhance detection in the residual signal. Details of the cepstral pre-whitening are discussed in Section 1.3.3. An example of this procedure is presented in Fig. 2.16. The vibration signal is from the experimental setup of Fig. 2.8 but in this case the acceleration is measured when the shaft rotation speed is kept stationary at 0.87 Hz, which is different from Fig. 2.9 when the speed is 2.9 Hz. At this lower shaft speed the impacts from the defective bearing release less energy and the vibrations from the gear are predominant, Fig. 2.16(a).

The SR system applied directly to this signal synchronises with the vibrations from the gears. On the other hand Fig. 2.16(b) shows the signal after the operation of pre-whitening. The two impacts from the defective bearing are clearly visible. The application of SR to this signal will further enhance the presence of the defective bearing however it has to be recognised that the fundamental step towards detection is the cepstral pre-whitening. There are cases when SR can be applied directly on vibration signals. For example when there are no gearboxes in the machinery, as for instance in condition monitoring of the bearings supporting the shaft of a motor [He et al., 2012]. However this scenario is not likely to be realistic for an industrial use of SR, reducing drastically its range of applicability.

2.4 Summary

This chapter investigated the use of Stochastic Resonance (SR) in the field of vibration based condition monitoring.
Firstly, the classical one dimensional SR was compared, by means of a numerical simulation, to a two dimensional SR system. It was observed that the presence of the coupling constant between the modes of the two dimensional system, increases the tuning space for the SR and allows a better signal enhancement. As shown in Fig. 2.4 for four different input SNR, the performance of the two dimensional system doubles that of the classical one dimensional, according to the ratio between the square of the mean and the variance of the transition rates between stable states.
Secondly, this chapter showed results obtained from the application of the two dimensional SR to vibration data from an experimental setup. SR effectively enhanced the impact from a defective bearing as shown in Fig. 2.11. An analog circuit was used to produce the two dimensional SR system matching the results obtained by the numerical simulations, as shown in Fig. 2.15, proving that SR can be used directly in series with a vibration transducer.
Finally, problems related to the use of SR on vibration data have been discussed. The most important recognition is the need for implementing signal processing algorithms before the SR, in particular on vibration data from complex machinery. Furthermore, the tuning of the SR system can be highly time consuming and computationally expensive. Therefore SR does not accomplish the objectives detailed in Section 1.4 and despite the promising early results the work on SR was discontinued.
The focus of the research hereafter shifts towards the development of novel digital signal processing algorithms and the extension of existing methods. These algorithms will

be tested on numerical simulations and experimental data, from simple experimental setups to complex machinery, working both at stationary and non-stationary speed.

Chapter 3

Extension of common techniques

3.1 Introduction

This chapter investigates the use of two common techniques, Cepstral Editing (CE) and Spectral Kurtosis (SK), to enhance the component of the vibrations generated by a defective bearing on a machine operating at variable speed. Additionally it uses Order Tracking (OT) and the Squared Envelope Spectrum (SES) to obtain a stationary signal and subsequently perform diagnostics. The general background on the cepstrum and SK as well as on OT and the SES is discussed in Section 1.3.3.
In contrast to SR investigated in the previous chapter, CE and SK are well established methods in vibration based condition monitoring. They suppress the vibrations coming from the unwanted components, as for instance gears, resulting in the enhancement of the vibrations from the bearing. In the literature, they are introduced [Antoni and Randall, 2006, Randall and Sawalhi, 2011] as methods to be applied on machines operating at constant speed. When applied to signals from machines operating at variable speed, they follow a first step of OT [Randall and Antoni, 2011].
In the case of varying speed this two steps approach, of OT followed by enhancement of the defective bearing vibrations, is effective only for small fluctuations around the mean operating speed. Conversely, in the case of a machine undergoing large speed variations, the detection capability decreases drastically [Borghesani et al., 2013b, Abboud et al., 2017]. This is caused by the fact that OT does not preserve the spectral content of the transient dynamics of the impacts from the defective bearing, as discussed in Section 1.3.1. Figure 3.1 shows by means of a numerical simulation the effect of OT on a vibration signal modelled according to Eq.1.8, in the case of significant variation in

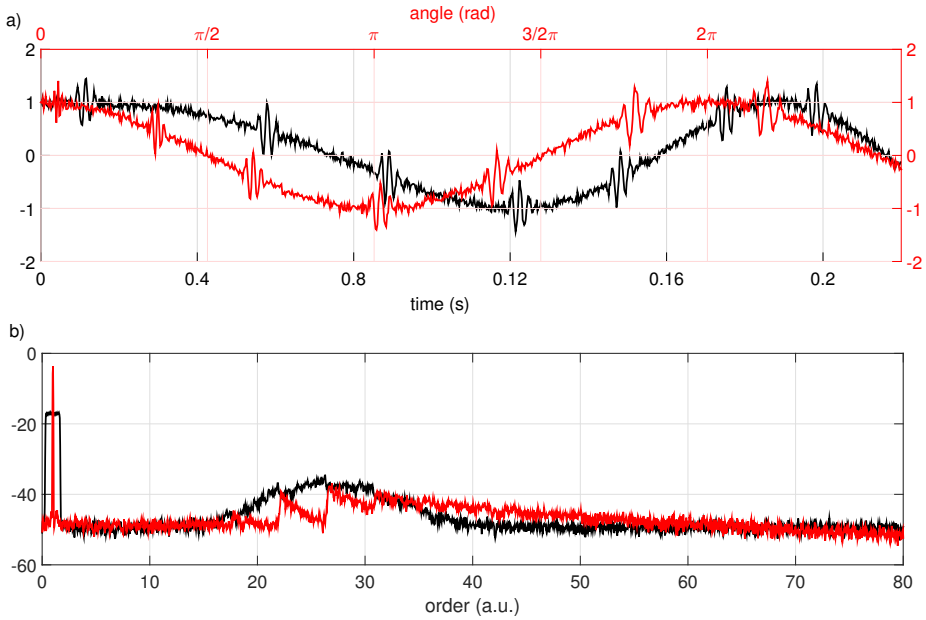

Figure 3.1: (a) Impacts from a defective bearing in the time (black) and angular (red) domain. (b) Power spectra

operating speed. Specifically, the signal comprises the vibrations from a gear and a sequence of impacts from a defect on the outer race of a bearing. Figure 3.1(a) shows the signal in the time and angular domain, in black and red respectively, in the case of a frequency varying from $f_{sh}(0) = 7$ Hz to $f_{sh}(0.1) = 20$ Hz. Figure 3.1(b) shows the power spectra in the case of a frequency varying linearly from $f_A(0) = 10$ Hz to $f_A(10) = 60$ Hz. It is possible to notice that after OT the chirp signal is transformed to a sinusoid and that the impacts occur at constant angular intervals as anticipated from Eq. 1.3. However, the excited resonant frequency becomes non-stationary and varies between two consecutive impacts. Recently, in order to overcome this drawback of OT, it has been proposed in a series of papers [Borghesani et al., 2013b, Randall and Smith, 2016b] to enhance the signal from the defective bearing directly in the time domain, where the vibration signal is cyclo-non-stationary, and only afterwards to re-sample in the angular domain. The work presented hereafter follows this line of research and shows, for the first time, that SK and CE are effective also when applied directly on cyclo-non-stationary signals. Therefore it extends the applicability of such widely used algorithms to a broader range of real world cases.

The chapter is organised as follows. Section 3.2 uses simulated and experimental data to compare the results obtained from the application of CE before and after the operation of OT. Section 3.2 is reproduced from the author's published work in the proceedings

of the 5^{rd} international conference on Condition Monitoring of Machinery in Non-stationary Operations (CMMNO) [Barbini et al., 2018][1]. Finally, Section 3.3 compares the performance of SK before and after OT showing that it is beneficial to apply SK to the non-stationary signal in the case of varying speed.

[1] In the literature it is implicit that the signal from the bearing is cyclic and the term was not included in the title of the paper. According to the models of Section 1.3.2 the signals are cyclo-non-stationary.

3.2 Application of cepstrum prewhitening on non-stationary signals

Article published in the Proceedings of the 5^{rd} international conference on Condition Monitoring of Machinery in Non-stationary Operations (CMMNO). Reprinted, with permission, from [Barbini et al., 2018].

Statement of contributions of joint authorship

L. Barbini (candidate): writing and compilation of manuscript, established methodology, data analysis, preparation of tables and figures. Presented results at the conference.

M. Eltabach : provided analysed data set, editing and co-author of manuscript.

J. L. du Bois (principal supervisor): supervised and assisted with manuscript compilation, editing and co-author

Copyright

Application of cepstrum prewhitening on non-stationary signals

L. Barbini[a,b,*], M. Eltabach[b], J. L. du Bois[a]

[a] *The University of Bath Department of Mechanical Engineering, Claverton Down, Bath, BA2 7AY, UK*
[b] *CETIM, avenue Félix-Louât - SENLIS 60300, France*

Abstract

In the field of vibration based condition monitoring a trusted symptom of a defective bearing is the observation of peaks, at characteristic frequencies, in the squared envelope spectrum (SES). If a machine is operating in a varying speed regime the SES is computed on the order tracked signal, i.e. the signal resampled at constant angular increments, and the SES can still be used for diagnostic. Despite its versatility a common problem with the SES is that peaks from other sources of vibrations, as for instance gears, can prevent the diagnosis of a defective bearing. Therefore pre-processing techniques are applied to the vibrational signal before the computation of the SES to enhance the signal from the bearings. Among these techniques cepstral pre-whitening (CPW) has gained much attention offering a remarkable capability of eliminating, in a blind way, both harmonics and modulation side-bands of the unwanted components. In the case of a varying speed regime the usual procedure consists of three steps: order track the signal, calculate the CPW, evaluate the SES. In this paper on the contrary the CPW is applied before the step of order tracking; therefore the proposed approach is: CPW the raw time signal, order tracking, evaluation of the SES. The remarkable observation is that for this approach the cepstrum does not present peaks at characteristic quefrencies, being the raw signal acquired in a varying speed regime. However this paper shows by means of numerical simulations and analysis of experimental data, that with the proposed methodology the masking components coming from the gears are suppressed and the signal from the defective bearing is enhanced.

1. Introduction

In a faulty bearing an impact occurs every time a rolling element hits a defect in the raceway or a defective rolling element hits the raceway. The detection of the shock generating from each impact is often a challenge due to the presence of other sources of vibrations, in particular gears, masking the presence of the defect. Therefore signal pre-processing methods have to be implemented before the evaluation of the widely established diagnostic technique of the squared envelope spectrum (SES). Cepstrum editing (CE) has been proposed as an efficient method for the suppression of gear components from a vibrational signal [1] and it performs well when compared with other techniques [2]. The working principle uses the fact that vibrations from gears result in a series of peaks at constant distances in the frequency spectrum. Therefore all these peaks can be eliminated suppressing, by means of a lifter, the corresponding peak in the cepstrum. Sawalhi et al. [3]

*Corresponding author
Email address: leo.barbini@bath.ac.uk (L. Barbini)

Preprint submitted to international Conference on condition Monitoring of Machinery in Non-stationary Operations

introduce the cepstral pre-whitening (CPW) as a further application of the cepstrum for the removal of all the discrete components from the spectrum, both vibrations from the gears and resonance effects.
When machines are operating at varying speed peaks corresponding to the vibrations from gears are smeared in the frequency domain and the cepstrum does not present significant peaks. In such cases the CPW is implemented in the order domain, after the operation of order tracking (OT)[4, 5]. However changing to a rotation angle basis smears the resonance frequencies excited by the impacts from the faulty bearing . Recently [6, 7] has been suggested to enhance the signal from the bearing directly in the time domain and to implement the OT only after this operation. Borghesani et al. [6] propose to band-pass filter the non stationary signal and Randall et al. [7] compare the performances of the application of three common techniques:spectral kurtosis for band selection, minimum entropy deconvolution and an exponential lifter.
The paper follows these methodologies and shows that CPW can be applied directly on time vibrational signals from machinery operating at varying speed conditions, before the operation of OT. The paper is organised as follows: section 3 presents the proposed method, section 2 evaluates its performance on a numerical simulation and section 3 on experimental data sets. Conclusions are presented in the final section.

2. Methods

In this paper two techniques will be used to pre-process, before the computation of the squared envelope spectrum (SES), vibrational signals from machines operating at varying speed. The two techniques are cepstral pre-whitening (CPW) and order tracking (OT). CPW can be implemented without the computation of the cepstrum [4], using only the Fourier transform:

$$x_{cpw} = IFT\left[\frac{FT(x)}{|FT(x)|}\right] \tag{1}$$

This operation is equivalent to setting to zero the real cepstrum and recombine it, in the frequency domain, with the phase of the original signal. The result is a white signal with a flat spectrum of amplitude one. OT is applied in the time domain implementing a digital re-sampling of the signal synchronously with the shaft rotation speed. In this paper the shaft rotation speed is considered to be provided by a tachometer. The envelope for the computation of the SES is calculated as the absolute value of the analytical representation of the full band signal. The SES is normalised by means of the ratio: $\tilde{SES}[l] = SES[l]/SES[0]$. In the following the $\tilde{}$ will be omitted. The common procedure using such techniques consists of a first step of OT and afterwards CPW the x_{OT} signal [4, 5], as it is shown in Fig. 1(a). However the resonant frequencies excited by the impacts from a faulty bearing are constant or vary more slowly than the operational speed of the machine. OT effectively produces a sequence of impacts equally spaced in the time domain, but the resonant frequencies excited by the impacts will be smeared [6] by the re-sampling. Therefore after OT the dynamic information is lost and the application of CPW may result in unwanted amplification of low signal to noise ratio bands [5].
To address this issue in this paper the CPW is applied directly on the non stationary signal and afterwards the OT is performed. The proposed approach is shown in Fig. 1(b). The central assumption is that the restriction of applying CPW only to signals showing periodic components in a spectrum can be relaxed. Eq. 1 is more generally effective and able for instance to enhance

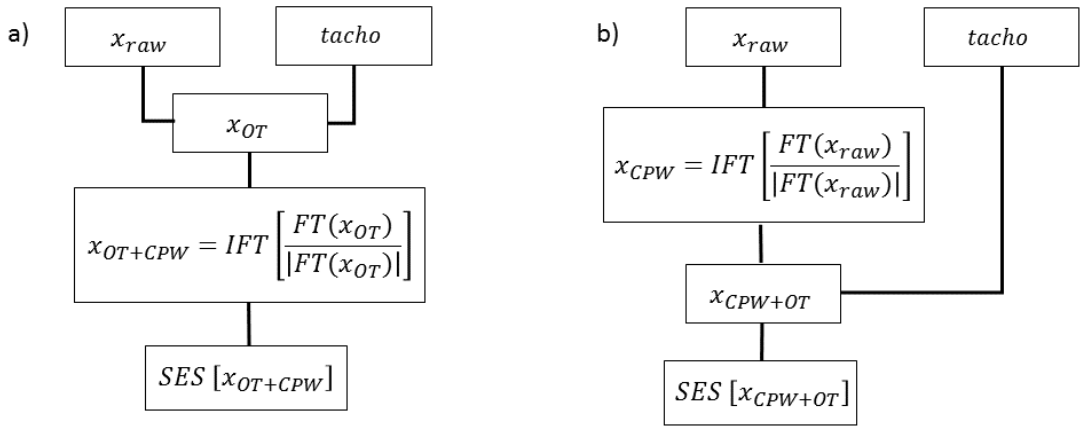

Figure 1: Schemes of the two processing methods

impacts masked by a strong non stationary signal, as shown by a numerical simulation in the next section. This follows from the observation that Eq. 1 is equivalent to what has been called the phase only signal [8] and used in [9] for detection of defects on surfaces.

3. Numerical investigation

The numerical simulation consists on the application of CPW to a signal constructed as the superposition of a deterministic non stationary component and a sequence of random impacts. Such signal does not show peaks in the cepstrum, nevertheless it will be shown that CPW is still capable of enhancing the sequence of impacts. A chirp signal with the frequency increasing linearly from 10 to $200Hz$ and amplitude 1 [a.u.], is used for the deterministic non stationary component. The impacts have mean occurrence frequency of $48.7Hz$ plus a random jitter of 2%, in order to resemble a random component coming from a defective bearing. The resonance frequency is simulated in the band $2200 - 3000Hz$ and the amplitude of the impacts is 0.1 [a.u.]. The signal is shown in Figure 2(a) in black, the total length is 2 seconds and the sampling frequency is $12.8kHz$, zoomed sections at different times are shown on the left and right sides, in yellow is superimposed only the sequence of impulses. As expected the real cepstrum of the simulated signal has no clear peaks, as shown in Figure 3(a). The real cepstrum is calculated as the inverse Fourier transform of the logarithm of the magnitude of the Fourier transform of the signal. The SES, shown in Figure 3(b), does not present indications of the presence of impulses, being masked by the high energy chirp.
The signal after the operation of CPW is shown in blue in Figure 2(b), the chirp is completely removed and the presence of the impacts is highly enhanced, for comparison in yellow it is shown the original sequence of impacts. The SES of the CPW signal is shown in Figure 3(c) where peaks are present at the expected mean occurrence frequency of the impacts and the first harmonic.

4. Experimental investigation

This section shows a benchmark comparison between the SES obtained using the proposed approach of Fig. 1(b) and the SES obtained from the usual procedure of applying CPW in the order domain Fig. 1(a). The data sets used in this section were provided by the Centre Technique des Industries Mécaniques (CETIM).

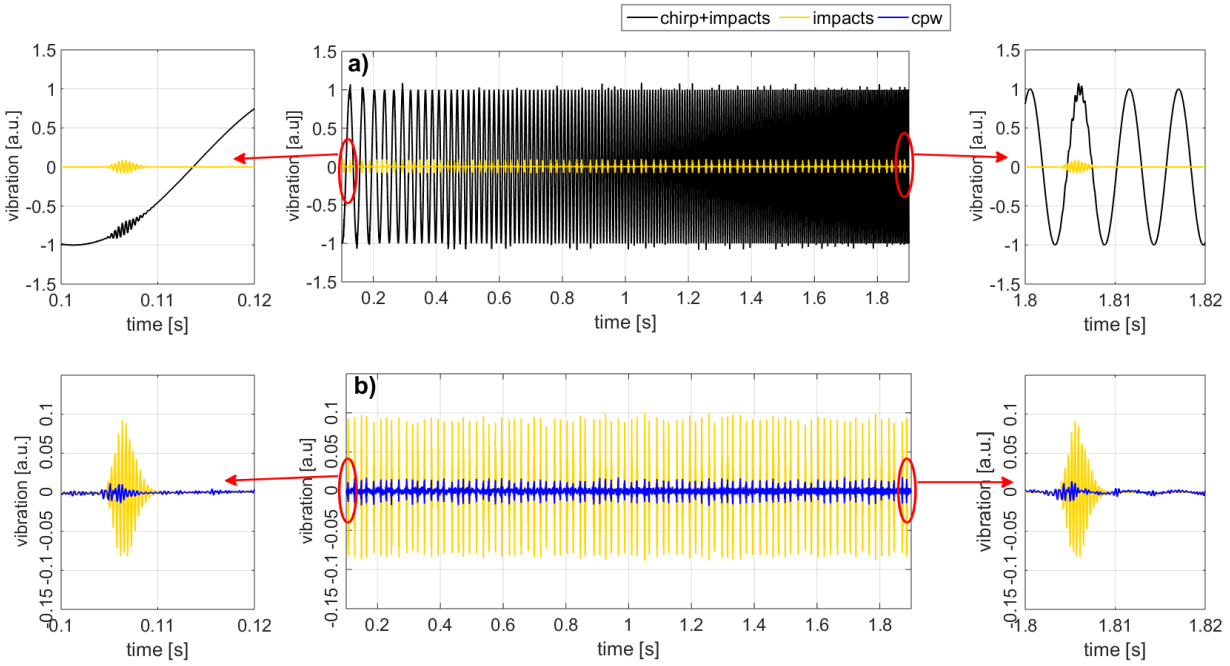

Figure 2: (a) Simulated non stationary signal. (b) Simulated non stationary signal after CPW. See legend for description of signals.

4.1. Test rig & data sets

Figure 4(a) shows the photograph of the test rig. A variable speed asynchronous electric motor drives the input shaft of a parallel spur-gear of ratio one and 18 teeth, and an alternator applies a constant load. The output shaft is supported by two rolling elements bearings of which the one close to the gearbox is in healthy conditions while the other one has an outer race defect with expected repetition of 3.04 orders: Ball Pass Outer race Order (BPOO). An accelerometer mounted on the casing of the healthy bearing is used as a vibration transducer.

Two signals are analysed in this paper: a run-up profile and a randomly varying speed, the lengths of the signals are of 15 seconds and 20 seconds respectively, both are sampled at Fs= $12.8kHz$. Figures 4(b-c) show the two speed profiles as a function of time: in the run-up the speed is varying approximately of 10 Hz increasing constantly from 25 to 35 Hz, while in the case of random variations the speed changes more drastically for example of approximately 30 Hz in 2.5 seconds. The SES of the run up signal is shown in Fig. 5(a) and for the random speed signal in Fig. 5(b). The speed variations are large in both cases therefore the SES are smeared and no clear peaks are present at the theoretical bearing fault order. The SES after OT the signals are shown in Fig. 5(c-d) and the presence of the defective bearing is revealed, however can be noticed disturbing components among which 1X has the highest energy and 2BPOO is almost masked. The real cepstra of the signals before and after OT are shown in Fig. 5(e) for the run up case and Fig. 5(f) for the random speed profile. In both cases after the operation of OT, in black, the gear components contribute a periodic spectrum resulting in a cepstrum with peaks separated by 1/X. On the other hand the cepstra for the raw non stationary signals, in blue, do not present peaks.

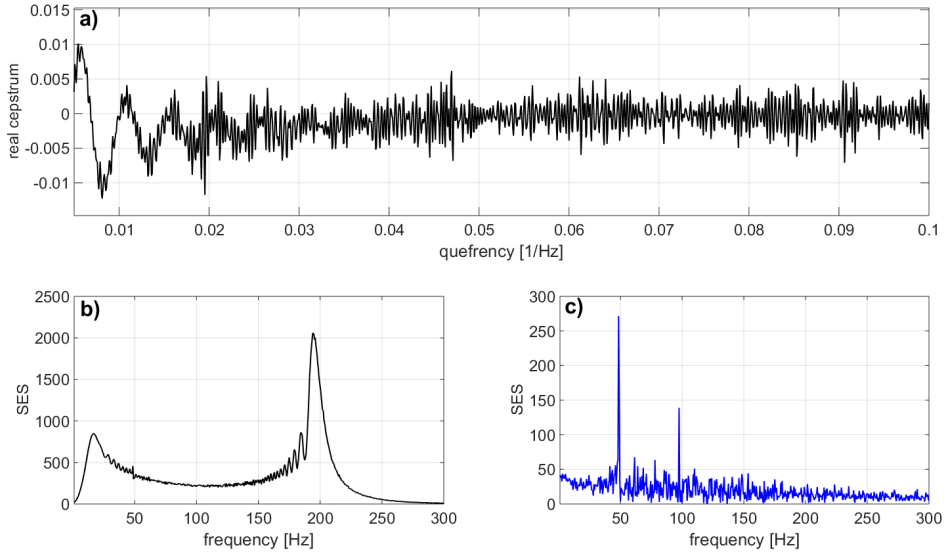

Figure 3: (a) Real cepstrum of the simulated non stationary signal comprising the two components, (b) corresponding SES. (c) The SES of the CPW signal.

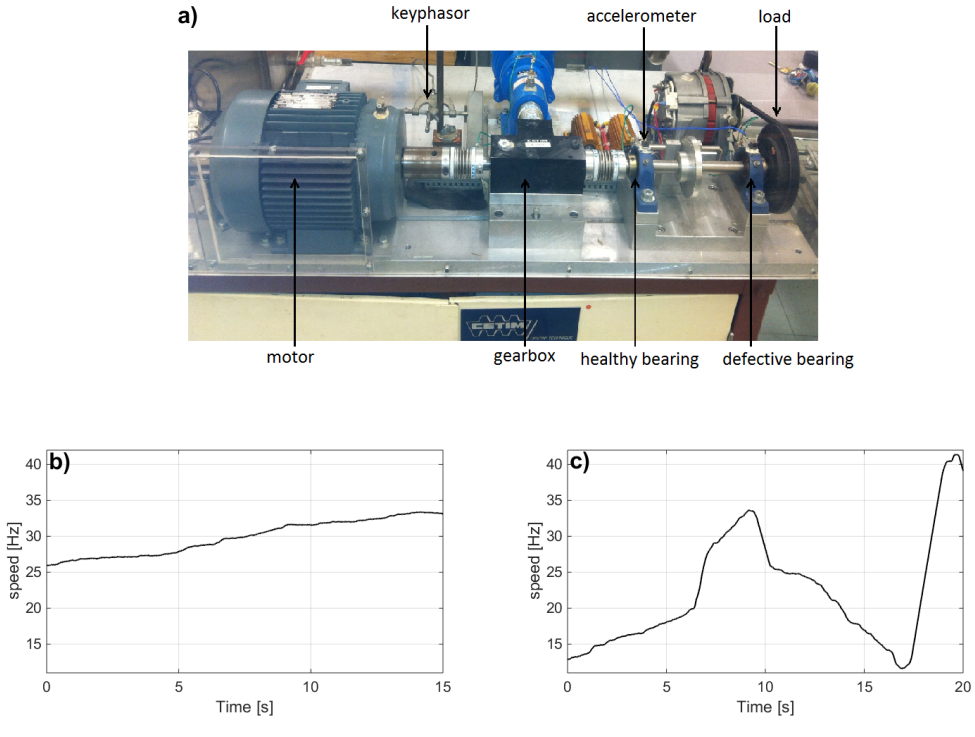

Figure 4: (a) The photograph of the test rig. (b) The run up speed profile. (c) The randomly varying speed profile

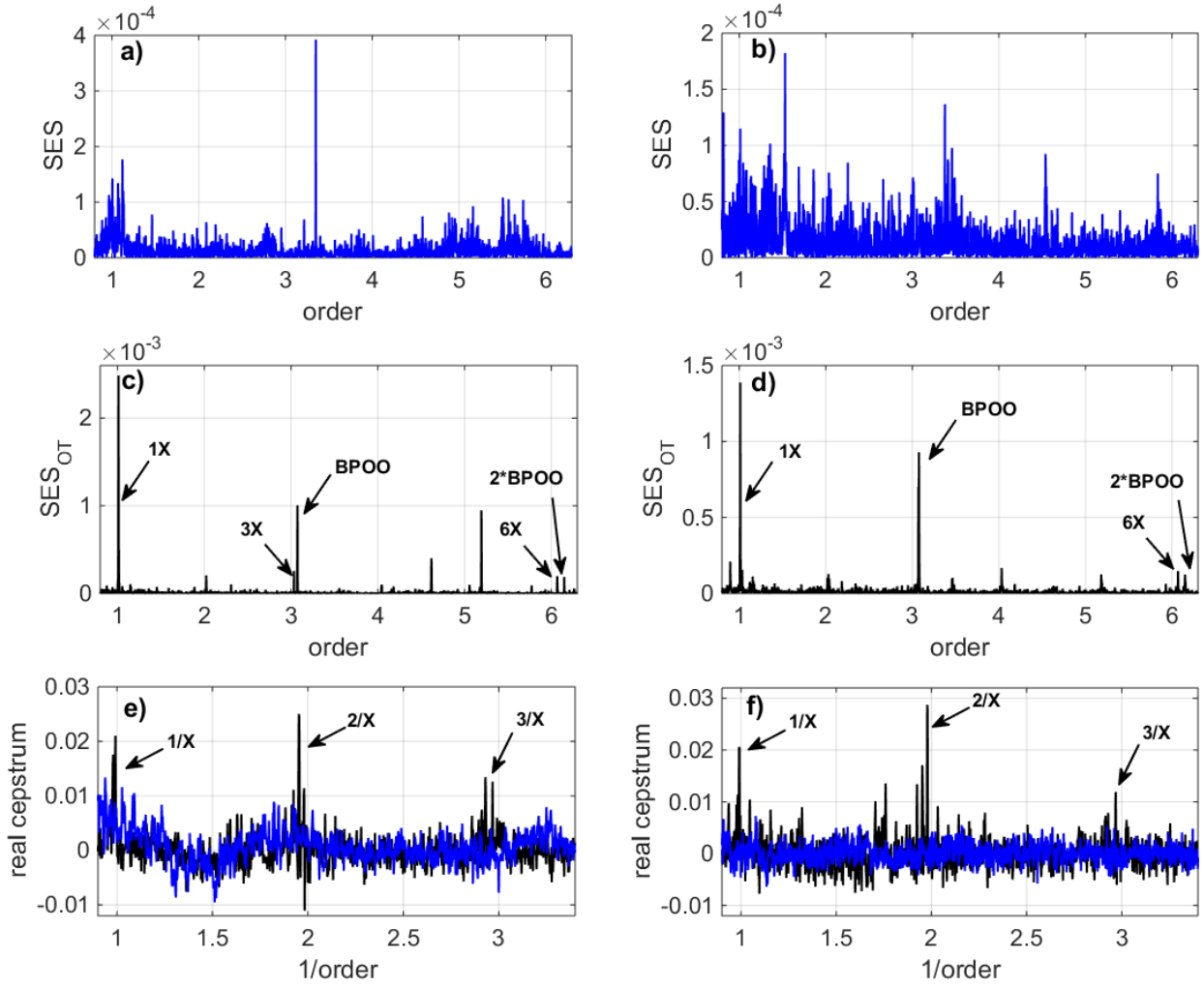

Figure 5: (a) SES of raw signal for the run-up speed and (b) randomly varying speed. (c-d) Corresponding SES after OT. (e-f) Real cepstra: in blue of the original signals and in black of the OT signals.

4.2. Results

The aim of the CPW step in the common procedure of Fig. 1(a), is that of removing the disturbing components from the SES of Fig. 5(c-d). After the operation of OT the spectrum shows periodicity contributing the peaks in the cepstra, as shown in Fig. 5(e-f) in black, therefore this is the typical application of cepstral pre-whitening on a non stationary signal [4].
In the method proposed in this paper, as shown in Fig. 1(b), the CPW is applied directly on the time non stationary signals for which the cepstra does not presents peaks at characteristic quefrencies, Fig. 5(e-f) in blue, and the SES Fig. 5(a-b) has smeared peaks. The SES resulting from the two methods are shown in Fig. 6 for the run up case and randomly varying speed respectively, top raw is the OT followed by CPW and bottom raw is CPW followed by OT. The vertical scales are defined, for a comparison, according to the SES of Fig. 5(c-d). The proposed method performs well when compared to the common procedure: the masking components are more suppressed and the peaks at characteristic fault frequencies have higher relative amplitude

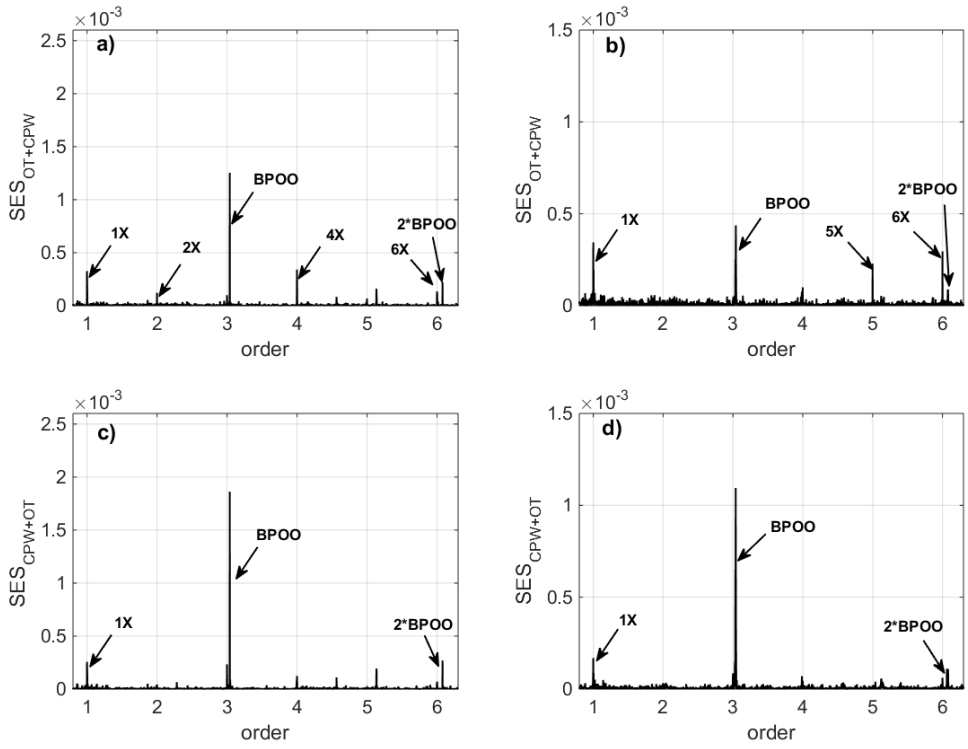

Figure 6: SES after processing the signals. OT followed by CPW for (a) run up speed, (b) randomly varying speed. CPW followed by OT for (c) run up speed, (d) randomly varying speed.

for both the analysed speed profiles.

5. Conclusion

The paper shows the effectiveness of cepstrum pre-whitening to enhance the presence of impacts from a faulty bearing when applied directly on acceleration signals from machinery operating at varying speed. The paper also shows that in variable speed situations it is beneficial to apply cepstrum pre-whitening directly to the time non-stationary signals instead of the order-tracked signals, because the resonant frequencies appear to change with speed in the order domain. The method proposed here consists of order tracking the signal only after the operation of whitening the time non-stationary signal, and finally calculating the squared envelope spectrum for diagnostics. Both numerical simulations and analysis of experimental data have been carried out. The proposed method has been compared with the common procedure of order tracking the signal as a first step and afterwards use the cepstrum pre-whitening in the order domain. The evaluation of the squared envelope spectra obtained by the two methods shows that, as proposed in this paper, the cepstrum pre-whitening performs well on the time non-stationary signal and that it is advisable to apply it before order tracking.

References

[1] R. B. Randall, N. Sawalhi, A new method for separating discrete components from a signal, Sound and Vibration 45 (5) (2011) 6.

[2] R. B. Randall, N. Sawalhi, M. Coats, A comparison of methods for separation of deterministic and random signals, The International Journal of Condition Monitoring 1 (1) (2011) 11 – 19.

[3] N. Sawalhi, R. B. Randall, Signal pre-whitening for fault detection enhancement and surveillance of rolling element bearings, in: The Eighth International Conference on Condition Monitoring and Machinery Failure Prevention Technologies, Cardiff, Wales, UK, June, 2011, pp. 19–22.

[4] P. Borghesani, P. Pennacchi, R. B. Randall, N. Sawalhi, R. Ricci, Application of cepstrum pre-whitening for the diagnosis of bearing faults under variable speed conditions, Mechanical Systems and Signal Processing 36 (2) (2013) 370 – 384.

[5] D. Abboud, M. Eltabach, J. Antoni, S. Sieg-Zieba, Envelope pre-processing techniques for rolling element bearing diagnosis in variable speed conditions, International Journal of Condition Monitoring 6 (2) (2016) 27–32.

[6] P. Borghesani, R. Ricci, S. Chatterton, P. Pennacchi, A new procedure for using envelope analysis for rolling element bearing diagnostics in variable operating conditions, Mechanical Systems and Signal Processing 38 (1) (2013) 23–35.

[7] R. B. Randall, W. A. Smith, M. Coats, Bearing diagnostics under widely varying speed conditions, in: Proceedings of the 4th Conference In Condition Monitoring of Machinery in Non-stationary Operations, Lyon, 2014.

[8] A. Oppenheim, J. Lim, The importance of phase in signals, Proceedings of the IEEE 69 (5) (1981) 529–541.

[9] D. Aiger, H. Talbot, The phase only transform for unsupervised surface defect detection, in: Computer Vision and Pattern Recognition (CVPR), 2010 IEEE Conference on, IEEE, 2010, pp. 295–302.

3.3 Application of the kurtogram on cyclo-non-stationary signals

This section tests the performance of the SK when applied to cyclo-non-stationary signals. Spectral kurtosis [Antoni, 2006] and its fast implementation the kurtogram [Antoni, 2007d], have been introduced as effective tools to determine the optimal demodulation band in the classical high resonant frequency approach for bearing fault detection [McFadden and Smith, 1984, Luo et al., 2010]. SK is a method used on the vibration signal from a machine operating at constant speed. In the case of varying speed, it is used following the procedure described in Section 3.2 for the CPW. Specifically, it is normally implemented after the operation of OT, so that the optimal demodulation band is found on the signal showing impacts at constant angular intervals [Randall and Antoni, 2011]. In the following, a numerical simulation shows that in the case of largely varying speed this procedure deteriorates the performance of the kurtogram and SK has to be used directly on the cyclo-non-stationary signal. The simulated vibration signal is modelled using Eq.1.7 and Eq.1.3. Specifically the following values are used for the vibrations from the gear:

$$\begin{array}{lll} r_m = [1,3] & N_A = 8 & N_B = 16 \\ \theta_{rm}^{A,B} = 0 & M_{r_m} = \frac{1}{2} & \\ E_{r_e}^{A,B} = 0 & C_{r_m,r_c}^{A,B} = 0 & D_{r_m,r_d}^{A,B} = 0 \end{array} \tag{3.1}$$

and the following values are used for the vibrations from the bearing:

$$\begin{array}{lll} \Theta = 1.81\ rad & D_p = 0.25 & a = 2e-4\ s \\ f_l = 2.4\ kHz & f_h = 3.2\ kHz & \end{array} \tag{3.2}$$

The total length of the simulated signal is 10 seconds and the sampling frequency is 12.8 kHz. The rotational speed of shaft A increases linearly from $f_A(0) = 7$ Hz to $f_A(0) = 14$ Hz. In addition the signal is buried in white Gaussian noise with SNR=15 dB. The signal corresponds to two linear chirps representing vibrations at gear meshing frequency and its third harmonic, superimposed to a sequence of impacts, produced by a defect on the outer race of the bearing supporting the shaft rotating at $f_A(t)$.
The results from the application of the kurtogram to this cyclo-non-stationary signal is shown in Fig. 3.7(a). The kurtogram correctly detects the demodulation band around 2600 Hz. As a matter of fact the impacts excite the same resonant band, irrespective of their occurrence at non-stationary intervals of time, as shown in Eq.1.3. On the other hand the result of the kurtogram applied to the OT signal is shown in Fig. 3.7(b)

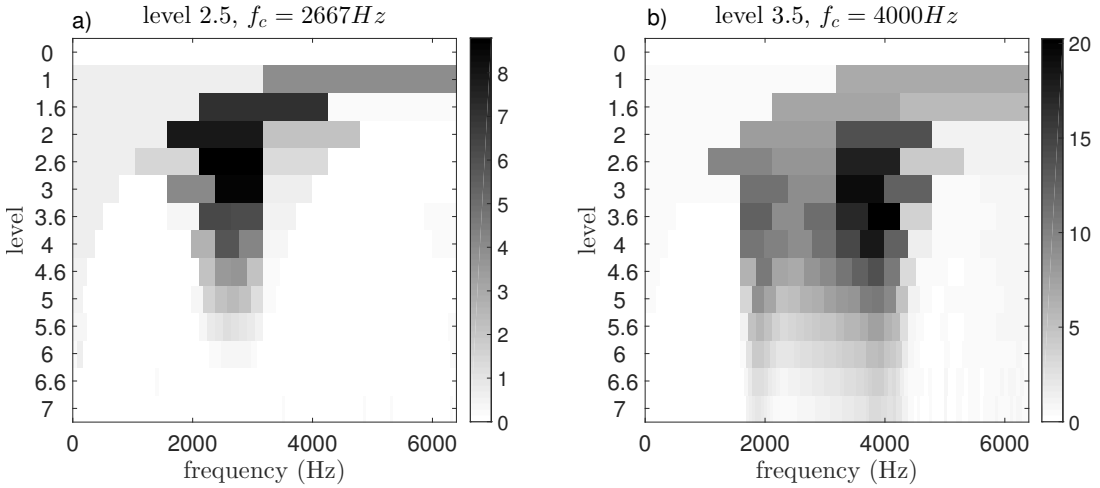

Figure 3.7: Kurtogram before (a) and after (b) order tracking the simulated cyclo-non-stationary vibration signal.

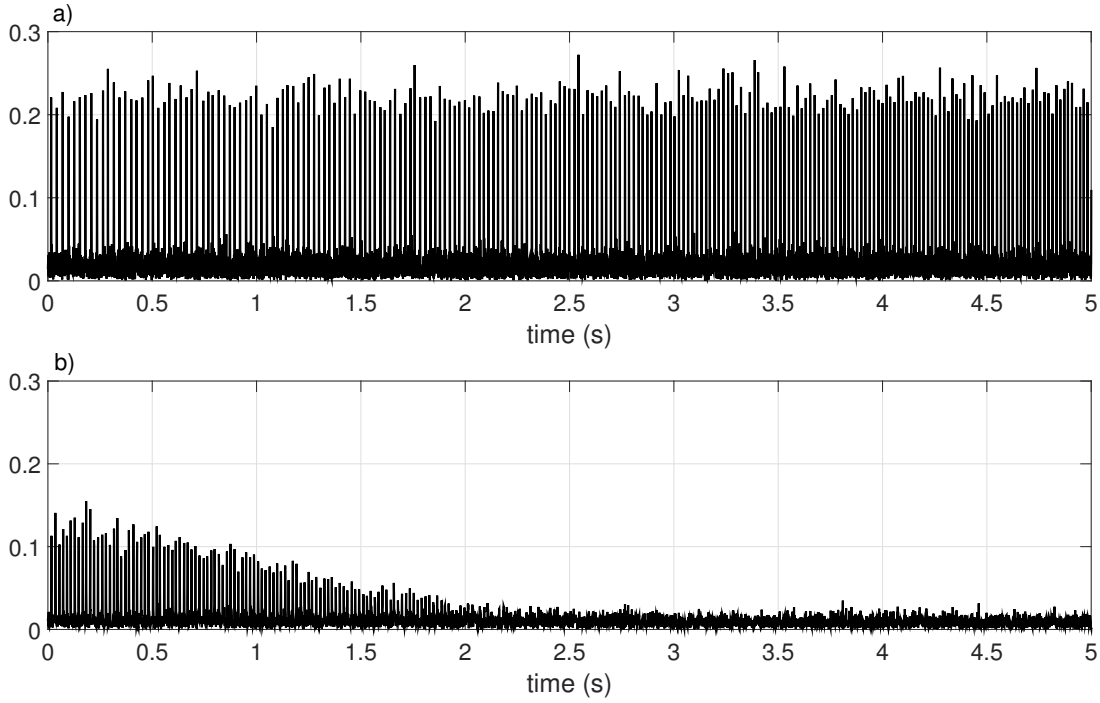

Figure 3.8: The demodulated signal before (a) and after (b) order tracking. The demodulation band are selected using the kurtograms

and the optimal demodulation band is wrongly estimated around 4000 Hz. In order to produce Fig. 3.7(b) the signal resampled in the angular domain is considered in the time domain. As shown in Section 1.3.3 the operation of re-sampling in the angular

domain has two consequences: the impacts occur at constant angular intervals and the excited resonance frequency becomes non-stationary. The latter consequence jeopardises the use of the kurtogram after the operation of OT.
The time domain signals after demodulation are shown in Fig. 3.8. For visualisation reasons only the first 5 seconds of the signal are displayed here. For the kurtogram applied directly on the cyclo-non-stationary signal, the demodulation is around 2600 Hz and the resulting signal is shown in Fig. 3.8(a). The sequence of impacts from the bearing is present for all the duration of the signal and the occurrence time of the impacts is non-stationary. As in Section 3.2, OT should be applied to this signal and the SES computed afterwards to allow detection. On the other hand, the result of demodulation around 4000 Hz as suggested by the kurtogram applied on the OT signal, is shown in Fig. 3.8(a). The impacts occur at constant time intervals, however due to the non-stationary resonant frequency they are present only in the first 2 seconds. In addition their amplitude is smaller in comparison with that of the impacts in Fig. 3.8(b). A better result could be achieved selecting a wider demodulation band, i.e. a smaller level number in Fig. 3.7(b). However this has two drawbacks: firstly it does not allow the use of the kurtogram in an automated procedure and secondly the vibrations from the gears could appear in this wider band. In conclusion it is beneficial to apply the kurtogram directly on the cyclo-non-stationary signal in order to preserve the impacts. Nevertheless, there are cases in which the resonant frequency excited by the impacts from the defective bearing changes as a function of speed and the kurtogram, even applied on the cyclo-non-stationary signal, is not able to select a proper demodulation band[2]. Therefore it is suggested that cepstral methods are preferred over SK, as introduced in Section 3.2, for the enhancement of cyclo-non-stationary vibration signals in the case of large speed variations.

3.4 Summary

This chapter showed how techniques introduced for the enhancement of bearing signals in machinery operating at a stationary speed are effective also on cyclo-non-stationary vibration signals. Specifically, the methods studied here are: Cepstral PreWhitening (CPW) and Spectral Kurtosis (SK). What is proposed is to invert the classical two step approach, consisting of OT followed by signal enhancement, such that firstly the cyclo-non-stationary signal is enhanced and only afterwards the signal is resampled in the angular domain. The analysis conducted here shows that this simple inversion has

[2]An example is shown in Fig. 4.15(b) in the next chapter

important consequences.
Firstly, it demonstrates the effectiveness of CPW and SK on cyclo-non-stationary signals. Secondly it improves the performance of the methods when applied to real world scenarios, when the speed of the machine is likely to vary. For CPW, comparison of the conventional procedure and the proposed procedure is shown in Fig 3.6, vibrations from the gears are suppressed more in the proposed approach. For SK, results are shown in Fig 3.8, the impacts from the defective bearing are enhanced better when the demodulation is implemented on the cyclo-non-stationary signal. Furthermore, when compared to techniques recently developed to deal with cyclo-non-stationary signals [Abboud et al., 2016b], the simple solution proposed here has two advantages: it is less computationally expensive and it is easier to interpret, relying only on existing methods. Therefore, it matches the objectives detailed in Section 1.4. Regarding the use of SK, it is worth noticing that an expert user should always check the kurtogram because the algorithm could select the band corresponding to impulsive noise, rather than impacts from a defective bearing.
In addition, the motivation behind the application of CPW to cyclo-non-stationary signals was to clarify the relationship to the phase only signal [Oppenheim and Lim, 1981]. To the best of the author's knowledge, this relationship is ignored in the field of condition monitoring. Interestingly, [Borghesani et al., 2013b] is among the first suggesting the enhancement of the component from the bearing directly on signals collected from machinery operating at varying speed. However, the same author in [Borghesani et al., 2013a] when applies CPW to cyclo-non-stationary signals, uses the classical approach as described here in Fig. 3.2(b), i.e. firstly OT to obtain a cyclo-stationary signal. Therefore we conclude that in the literature there is a misunderstanding on the requirement of the stationarity of a signal for the application of cepstral methods.
This chapter extended techniques already commonly used in vibration based condition monitoring; the next chapter introduces a novel signal processing technique and tests its performance on both cyclo-stationary and cyclo-non-stationary signals.

Chapter 4

Novel technique: phase editing

Nomenclature			
$\boldsymbol{x[k]}$	raw signal in time domain	$\boldsymbol{\hat{x}[l]}$	signal in frequency domain
$\boldsymbol{p[k]}$	phase edited signal	$\boldsymbol{x_{pe}[k]}$	phase edited residual signal
$\boldsymbol{L[l]}$	threshold vector of amplitude spectrum	$\boldsymbol{\lambda}$	threshold level of amplitude spectrum
$\boldsymbol{rc_{ed}[l]}$	edited real cepstrum	$\boldsymbol{x_{ce}[k]}$	signal after editing real cepstrum
$\boldsymbol{x_{ce+sk}[k]}$	signal after editing real cepstrum and spectral kurtosis filtering	$\boldsymbol{f_c}$	central frequency of spectral kurtosis filter
$\boldsymbol{B_w}$	bandwidth of spectral kurtosis filter	$\boldsymbol{x_{zc}[k]}$	signal after cepstral whitening
$\boldsymbol{K[n]}$	amplitude gain due to phase editing	$\boldsymbol{\theta[n]}$	phase delay due to phase editing
$\boldsymbol{l_b}$	frequency of maximum value of bearing signal	$\boldsymbol{l_g}$	frequency of maximum value of gear signal
$\boldsymbol{F_{d,h}}$	features estimated from the SES on the defective and healthy case	$\boldsymbol{N}$	total number of datapoints

4.1 Introduction

This chapter introduces a novel signal processing method for enhancing the detection of defective bearings from vibration data: phase editing (PE). The intuitive idea behind PE, is that the sequence of impacts generated by the non-smooth rotation of a defective bearing contributes very little power to the overall vibration signal, both for a machine operating at constant or varying speed. Surprisingly, this incontestable aspect has not been investigated by classical methods used in vibration-based condition monitoring as described in Section 1.3.3, while it will be seen that it can be exploited with remarkable results using PE. The approach proposed by PE is to filter the vibration signal

according to the amplitudes of different spectral bands, rather than their frequency. Specifically this unconventional filter in the spectral amplitudes is implemented using a simple FFT based algorithm. A qualitative demonstration of the algorithm was introduced by [Wójcicki et al., 2008] and applied to denoise a speech signal, while in the work presented here the mathematical formulation is subjected to rigorous analysis.
Besides the intuitive interpretation and the low computational complexity, another interesting aspect of PE is that it is implemented on the full band spectrum and its performance is not affected by changing the resonant band excited by the impacts from the defective bearing. This aspect will be verified both by means of a numerical simulation and analysis of experimental data. The only method matching this characteristic is the cepstral prewhitening (CPW), which deals equally with all the spectral bands, changing their amplitude to one. However, in contrast to PE, the flat amplitude spectrum resulting from CPW amplifies spectral bands containing only noise. Therefore the proposed method can be also seen as an extension of the CPW technique, resulting in less distortion of the original signal, because PE maintains the original shape of the amplitude spectrum. The superior performance of the proposed method to that of CPW has been investigated both on numerical simulations and analysis of experimental data. Please note that in what follows in this chapter the name zero cepstrum is used interchangeably with cepstral prewhitening, as it is in the literature on this topic.
Another important aspect of PE is its property of being effective both on cyclo-stationary and cyclo-non-stationary signals. Therefore it is possible to extend the procedure introduced in Chapter 3 to this novel method and the vibration from the defective bearing is enhanced directly on the cyclo-non-stationary signal, maintaining the spectral content of the transient dynamics, while OT is implemented afterwards to allow detection using the SES. This important aspect of PE has been investigated both on numerical simulated signals and experimental data, as shown in the following.
The chapter is organised as follows. Section 4.2 introduces the methodology, tests its performance and compares it with state of the art techniques: spectral kurtosis and cepstral editing. Section 4.2 is reproduced from the author's published work in the journal Mechanical Systems and Signal Processing [Barbini et al., 2017c]. Section 4.3 investigates the relationship between the operating speed of the machine and the performance of PE. The analysis is performed on experimental data from a machine operating at stationary speeds. Finally, Section 4.4 tests the effectiveness of PE to enhance cyclo-non-stationary vibration signals, both from a numerical simulation and from a machine operating at varying speed. Section 4.4 is reproduced from the author's published work in the proceedings of the 1^{st} World Congress on Condition Monitoring (WCCM) [Barbini et al., 2017a].

4.2 Phase editing as a signal pre-processing step for automated bearing fault detection

Article published in the journal Mechanical Systems and Signal Processing, [Barbini et al., 2017c].

Statement of contributions of joint authorship

L. Barbini (candidate): writing and compilation of manuscript, established methodology, data acquisition, data analysis, preparation of tables and figures.

A.P. Ompusunggu : assisted with manuscript compilation, editing and co-author

A. J. Hillis (associate supervisor): editing and co-author of manuscript

J. L. du Bois (principal supervisor): supervised and assisted with manuscript compilation, editing and co-author

A. Bartic : editing and co-author of manuscript

Copyright

Phase editing as a signal pre-processing step for automated bearing fault detection

L. Barbini[a,b,*], A. P. Ompusunggu[b], A. J. Hillis[a], J. L. du Bois[a], A. Bartic[b]

[a] *The University of Bath Department of Mechanical Engineering, Claverton Down, Bath, BA2 7AY, UK*
[b] *Flanders Make VZW, Celestijnenlaan 300, B-3001 Heverlee (Leuven), Belgium*

Abstract

Scheduled maintenance and inspection of bearing elements in industrial machinery contributes significantly to the operating costs. Savings can be made through automatic vibration-based damage detection and prognostics, to permit condition-based maintenance. However automation of the detection process is difficult due to the complexity of vibration signals in realistic operating environments. The sensitivity of existing methods to the choice of parameters imposes a requirement for oversight from a skilled operator. This paper presents a novel approach to the removal of unwanted vibrational components from the signal: phase editing. The approach uses a computationally-efficient full-band demodulation and requires very little oversight. Its effectiveness is tested on experimental data sets from three different test-rigs, and comparisons are made with two state-of-the-art processing techniques: spectral kurtosis and cepstral pre- whitening. The results from the phase editing technique show a 10% improvement in damage detection rates compared to the state-of-the-art while simultaneously improving on the degree of automation. This outcome represents a significant contribution in the pursuit of fully automatic fault detection.

Keywords: Phase spectrum, automated diagnostics of defective bearings, comparison with cepstrum pre-withening, comparison with spectral kurtosis

1. Introduction

Research into fully automated algorithms for the application of condition based maintenance on an industrial scale has gained much attention in recent years. There is a practical need for reliable diagnostic methods to help avoid human errors and to allow affordable implementations of multi-sensor architectures without employing expert users. In this field, vibration based condition monitoring is a well established approach, present in the literature since the 1980s, and a variety of vibration transducers are currently used: for example, accelerometers, acoustic emission and ultrasound [1, 2]. It is well known that bearings play a vital role in the health of many industrial machines and that they are particularly prone to failure [3]. This paper is concerned with automated algorithms for the assessment of bearing health using vibrational data.
The mathematical formulation of the second order cyclostationary nature of defective bearings signal and the clarification of its relationship with the high-frequency resonance technique [4] has

*Corresponding author
Email address: L.Barbini@bath.ac.uk (L. Barbini)

allowed the introduction of a widely accepted model of bearing faults [5, 6]. According to this model, features from defective bearings can be extracted by the squared envelope spectrum (SES) of the vibrational signal, as an estimation of the integrated cyclic coherence. The main difficulty in such feature estimation is that studying the SES of the full band raw signal usually does not provide a reliable assessment of the bearing condition and can result in defective bearings being classified as healthy. In complex machines, such as those used in industrial applications, this is due to the presence of vibration signals from other sources which are superimposed on those from the bearing itself. For instance, gears can contribute non-trivial vibration signals masking the presence of bearing defects. In such cases the SES of the raw vibrational signal shows various peaks, and the results are difficult to classify without the analysis of an expert user. From the point of view of an automated feature estimation there is then the need to find reliable methods to process the raw vibration signals, before the computation of the features from the SES, in order to simplify the diagnostic of a defective bearing.

Attempts have been made to automate common methods for the enhancement of bearing signals, however the results are not sufficiently reliable for industrial applications. For example the well established spectral kurtosis (SK) [7] is often used to select the frequency band containing bearing impact signals, but when automated there is a high risk of selecting the wrong demodulation band [8]. One solution to this problem is to edit the vibration signal such that the full frequency band is considered. This approach can be found in a method introduced by Borghesani [8], known as the zero cepstrum (ZC), where all the cepstral coefficients are set to zero and the SES is calculated for the full band edited signal. However this methods results highly sensitive to noise levels, as will be investigated in the following section. In the paper the focus is on an automated algorithms and cepstral approaches were preferred to other methods for removal of gear signals, as time synchronous averaging or discrete random separation, because somewhere else [9, 10] they performed comparably well but require a faster implementation and result easier to automate.

This paper presents a novel automated signal processing method for feature detection in bearing vibration signals, based on phase editing (PE). As with ZC, the PE method has the advantage of using the entire band for demodulation, so avoids the risk of selecting the wrong frequency band. The novelty lies in the procedure for the removal of vibrational signals not originating from bearings. In many enhancement techniques only the amplitude spectrum of a noisy signal is modified while the phase spectrum is unchanged. The PE approach on the other hand keeps the amplitude unchanged and recombines the signal with an edited phase spectrum. The result is a modified spectrum where small amplitude components are attenuated more than large amplitude components. It is well established that in a vibrational signal the energy from bearings is low compared to that from the other components [11], hence in order to discard the misleading information and enhance the weak signal from the bearings, the final step is to calculate the residual between the original signal and the PE signal. To the best of authors' knowledge the present paper is the first to propose the use of phase editing in the field of condition monitoring. The effectiveness of this novel technique has been tested by comparing its performance on experimental data sets with that of two state-of-the-art methods. The first consists of two steps: removal of discrete components, implemented by means of an automated cepstral editing procedure (ACEP) [12] and SK for selection of the band for demodulation; the second method tested in the comparison is the ZC.

The paper is structured as follows. Section 2 presents details and discussion of the three methods. Section 3 describes the experimental rigs. Results are presented in Section 4 and conclusions are drawn in Section 5.

2. Methods

In the signal acquired by an accelerometer positioned on a gearbox casing at least three components superimpose: vibration induced by gears, vibration from bearings and noise. Usually a suggested operation is that of order tracking for removal of speed fluctuations [11], however in this paper machines are operating at a constant speed and this step will be omitted. All the three methods described below are be intended as enhancement procedures implemented before bearings fault feature estimation by means of the SES. They are automated such that the user needs to provide only the bearing defect frequencies and the rotation speed of the shaft where the bearing is mounted. Diagrams of the three methods ACEP+SK, ZC, PE are shown respectively in Fig. 1-2-4.

2.1. Existing Method (I): ACEP+SK

Method I consists of two blocks, ACEP and SK. The first one minimises the components from the gears, which are likely to mask the weak signal from bearings. This is achieved using an edited version of the cepstrum. Advantages on editing the cepstrum are that it can be automated [12], without the need of adjustment from the user, and that it has performed well when compared with other methods for gears signal removal as time synchronous averaging, auto regressive modelling, self-adaptive noise cancellation, discrete/random separation [9, 10]. In more details three steps are involved in the ACEP block: spectral subtraction is applied to the high-pass liftered real cepstrum of the raw signal and afterwards a comb lifter is automatically generated for removal of impulses in

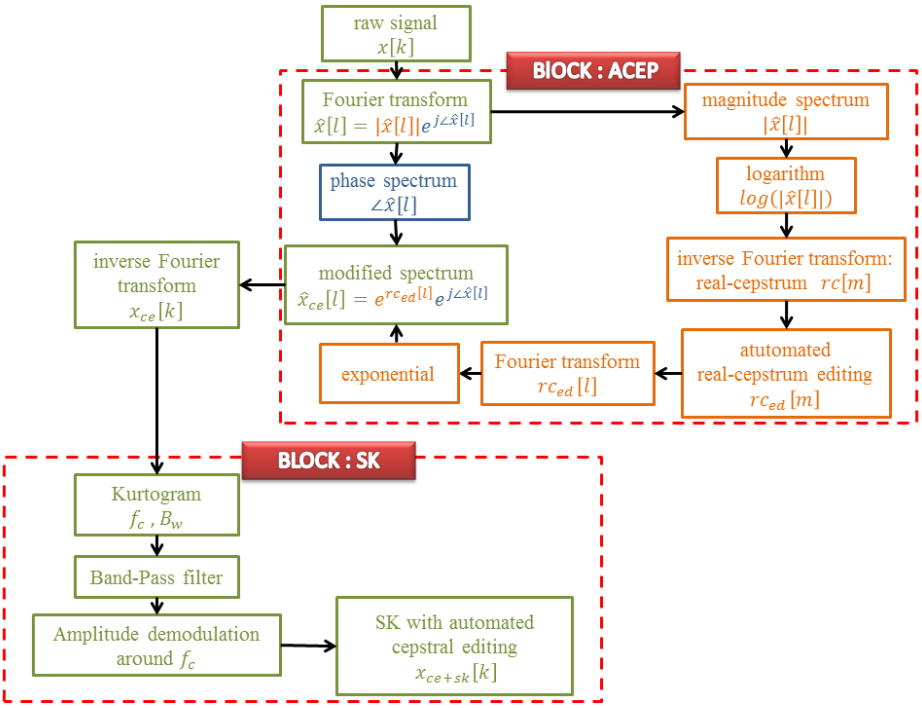

Figure 1: Scheme of method I: automated cepstral editing procedure (ACEP)+ spectral kurtosis (SK). Indexes k, l, m are for the time, frequency and quefrency domains. The green colour is for a signal where both magnitude and phase information are present while orange and blue are magnitude only and phase only.

the quefrency domain related to gear vibrations. This procedure provides an edited real cepstrum which is recombined with the original phase spectrum of the raw signal to obtain an edited vibration signal with enhanced bearing components x_{ce}.
The second step of Method I is the selection of the band of the spectrum where are present mainly vibrations from bearings, this is achieved using the SK. Its fast implementation was introduced by Antoni in [13], the algorithm gives as results: the bandwidth B_w and central frequency f_c of the demodulation band where the signal has the highest kurtosis and also the demodulated signal $x_{ce+sk}[k]$. From the perspective of automation two problems can be identified. Firstly the possible presence of vibration sources characterised by a kurtosis level higher then that of the defective bearings; secondly, the presence of peaks from gear harmonics in the selected narrow band for the demodulation. It should be noticed that the pre-processing with the ACEP algorithm increases the efficacy of the SK removing harmonics from gear components so to address the second of this problems. However the first problem is left unsolved and usually only human analysis of the kurtogram allows the right selection of demodulation band.

2.2. Existing Method (II): ZC

This method was described and exhaustively compared with other techniques by Borghesani et al. in [8]. ZC enhances the raw vibrational signal by means of editing the real cepstrum, however two differences with ACEP+SK can be found: firstly not only some impulses but the whole real cepstrum is set to zero; secondly no band pass filtering is implemented enabling full band demodulation. As remarked in [8] the computation of the $x_{zc}[k]$ can be accomplished without the calculation of the real cepstrum, as shown in Fig. 2, but simply modifying the Fourier transform

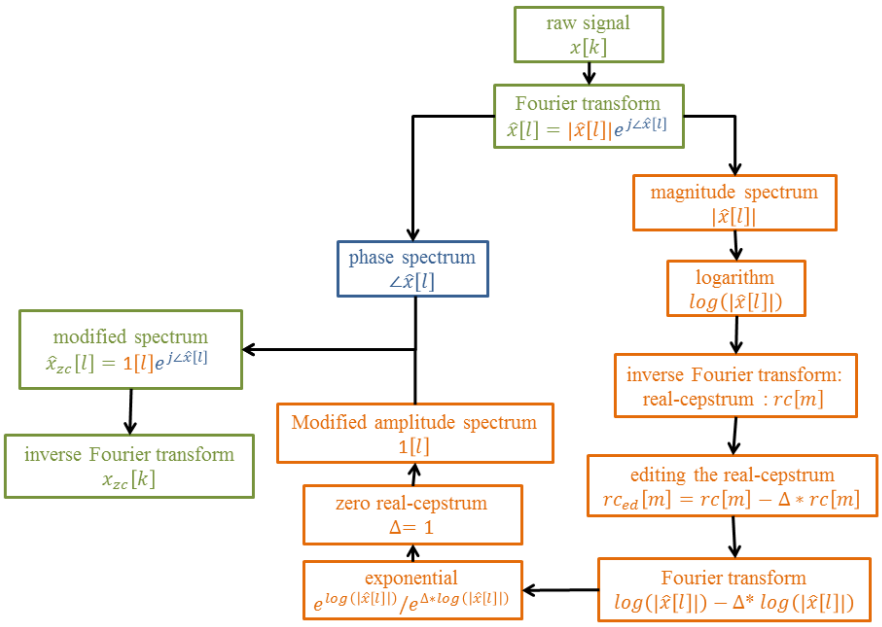

Figure 2: Scheme of method II: zero cepstrum (ZC). Indexes k, l, m are for the time, frequency and quefrency domains. The green colour is for a signal where both magnitude and phase information are present while orange and blue are magnitude only and phase only.

of the raw signal. The result of this procedure gives the so called 'phase only signal' [14].
In this framework the ZC edited signal is a filtered version of the raw signal, specifically the filter $g[k]$ is a function of the input and gives as output a signal with flat amplitude spectrum [15] and unchanged phase:

$$g[k] = IFT\left\{\frac{1}{|\hat{x}[l]|}\right\} \tag{1}$$

This procedure will perform equally well for a signal with no impulses in the real cepstrum. It can be interpreted as an amplitude distortion, implemented by means of the zero-phase filter $g[k]$, yielding to the enhancement of narrow time events. A numerical simulation is presented below in order to demonstrate the effect of this operation.

The simulated signal is the superposition of three unevenly spaced sinusoids at $11, 23$ and 31 $[Hz]$ with unity amplitudes, an outer race defective bearing with impact frequency $f_{od} = 80$ $[Hz]$ and a weak white noise of variance $\sigma = 0.05$. In the signal from the bearings a random jitter is considered for both the occurrence times and amplitudes of impacts, according to [5], and the excited resonance frequencies are in the band $15 - 17[kHz]$. The signal has a length of $7.5[s]$ and is sampled at $51kHz$. Figures 3(a) and (b) show respectively: a segment of the raw signal with seven recognisable impacts, the amplitude spectrum of the whole raw signal. The real cepstrum is shown in Fig.3(d) where the range of quefrencies is selected as 1 / $2f_{od}$ and 3 / f_{shaft} with the shaft frequency taken as the lowest of the sinusoids $f_{shaft} = 11$ $[Hz]$. As expected no clear peak is present in the real cepstrum at 0.1 $[1/Hz]$. Figure 3(c) shows the envelope of the zero

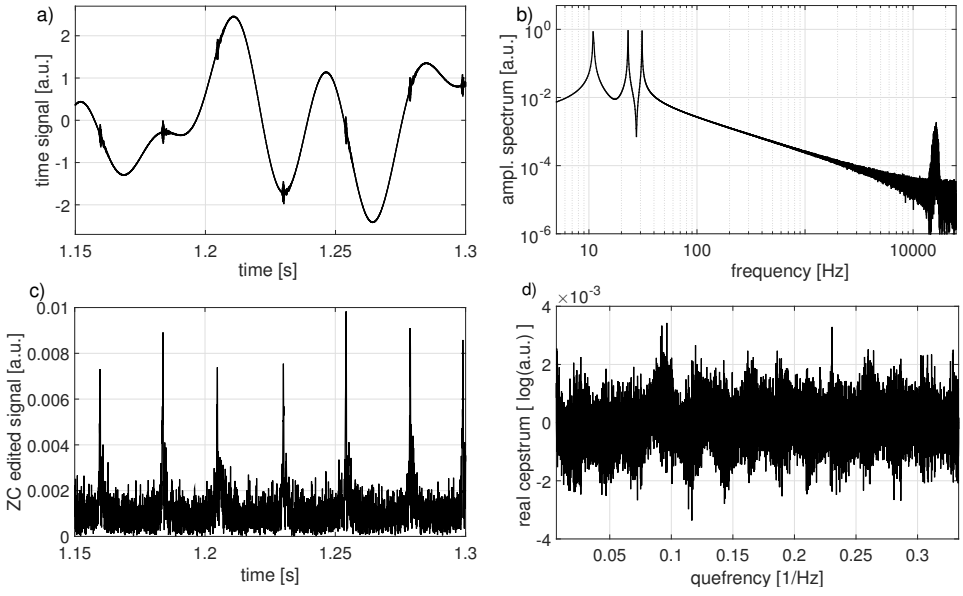

Figure 3: Application of the ZC method to a numerical simulation. The tested signal is realised as the superposition of three sinusoids at $11, 23$ and 31 $[Hz]$, a defective bearing signal and white noise. (a) Time domain: 7 impacts can be identified. (b) Amplitude spectrum of the raw signal: the tonal components have higher power than the defective bearing signal, the structural resonance excited by the impacts is in the band $15 - 17[kHz]$. (c) Absolute value of the analytic representation of the zero cepstrum edited signal $x_{zc}[k]$: sinusoidal components are removed while the impacts are enhanced. (d) Real cepstrum of the input signal: no clear peak can be identified in the quefrency range containing $1/10$ $[1/Hz]$.

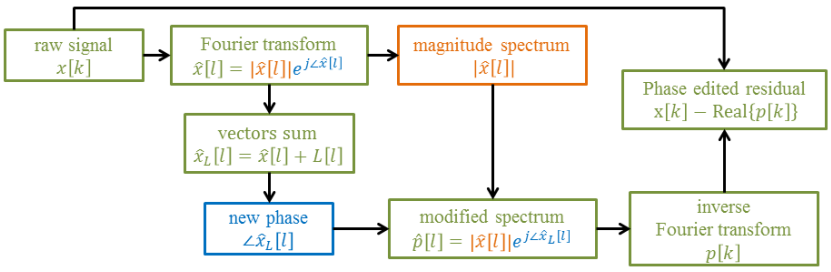

Figure 4: Scheme of method III: phase editing (PE). Indexes k, l are for the time and frequency domains. The green colour is for a signal where both magnitude and phase information are present while orange and blue are magnitude only and phase only.

cepstrum edited signal, calculated as the absolute value of the analytic representation of $x_{zc}[k]$. It is possible to identify the seven impacts and no presence of the sinusoids, confirming as anticipated the usefulness of method II for a signal with real cepstrum without impulses.

2.3. New Method (III): PE

The use of an edited phase spectrum, combined with the original magnitude spectrum, was first introduced by Wojcicki *et al.* [16] as a novel approach to speech enhancement. The method suppresses low-energy signal components through manipulation of the phase of the conjugate signal components in the frequency domain. In the original application it was used to clarify the high-energy spectral components and reduce noise. The methods are adapted here to use the residual from the original signal, thus rejecting the high-energy components and retaining the low-energy bearing signals of interest.

The schematic of Method III is shown in Fig.(4). The raw signal is first subject to a discrete Fourier transform. A real value $L[l]$ is then added to each complex component in the frequency domain, and normalised to the original component amplitude. The value $L[l]$ is of constant amplitude λ, and is positive for frequency components in the upper half of the imaginary plane and negative for those in the lower half-plane:

$$L[l] = \begin{cases} +\lambda & 0 \leq l < N/2 \\ -\lambda & N/2 \leq l \leq N-1 \end{cases} \tag{2}$$

with λ a positive real constant. The only parameter to tune in this procedure is λ, and this determines the amplitude threshold of the filter. The effect is shown in Figure 5(a). When the two complimentary signal components are recombined it serves to reduce the real part of the signal for small amplitude signal components. Upon transformation back to the time domain, the imaginary portion of the signal is discarded and the low-energy components are suppressed accordingly. The following analysis demonstrates the principle of operation.

The contribution of a frequency component $l = n \leq \frac{N}{2}$ to the real signal $x[k]$ having DFT $\hat{x}[l]$ with $k, l = 0, \ldots, N-1$ and $\hat{x}[N-n] = \hat{x}^*[n]$, is:

$$x_n[k] = \frac{1}{N}\left\{\hat{x}[n]e^{j\frac{2\pi}{N}nk} + \hat{x}[N-n]e^{j\frac{2\pi}{N}(N-n)k}\right\} = \frac{2\,|\hat{x}[n]|}{N} cos\left(\frac{2\pi}{N}nk + \angle(\hat{x}[n])\right) \tag{3}$$

For the phase edited signal the contribution of a frequency component n is:

$$\begin{aligned} Re\left\{p_n[k]\right\} &= \frac{|\hat{x}[n]|}{N} Re\left\{ \frac{\hat{x}_L^+[n]}{|\hat{x}_L^+[n]|} e^{+j\frac{2\pi}{N}nk} + \frac{\hat{x}_L^-[n]}{|\hat{x}_L^-[n]|} e^{-j\frac{2\pi}{N}nk} \right\} \\ &= \frac{|\hat{x}[n]|}{N} \Bigg[cos\left(\angle\hat{x}_L^+[n]\right) cos\left(\frac{2\pi}{N}nk\right) - sin\left(\angle\hat{x}_L^+[n]\right) sin\left(\frac{2\pi}{N}nk\right) + \\ &\quad + cos\left(\angle\hat{x}_L^-[n]\right) cos\left(\frac{2\pi}{N}nk\right) - sin\left(\angle\hat{x}_L^-[n]\right) sin\left(\frac{2\pi}{N}nk\right) \Bigg] \\ &= \frac{2\,|\hat{x}[n]|}{N} cos\left(\frac{2\pi}{N}nk + \frac{\angle\hat{x}_L^+[n] - \angle\hat{x}_L^-[n]}{2}\right) cos\left(\frac{\angle\hat{x}_L^+[n] + \angle\hat{x}_L^-[n]}{2}\right) \end{aligned} \tag{4}$$

where $\hat{x}_L^+[l] = \hat{x}[l] + L[l]$ and $\hat{x}_L^-[l] = \hat{x}^*[l] - L[l]$. For the enhancement of low-energy vibrational signals, in contrast to the case of speech signal denoising [17], the last step is the calculation of the residual. Using Eqs. (3) and (4), the new phase edited signal is given by

$$x_{pe,n}[k] = x_n[k] - Re\left\{p_n[k]\right\} = K[n]\frac{2\,|\hat{x}[n]|}{N} cos\left(\frac{2\pi}{N}nk + \angle\hat{x}[n] + \theta[n]\right). \tag{5}$$

where $K[n]$ and $\theta[n]$ are the gain and phase, respectively, of the PE residual filter, given by

$$\begin{aligned} K[n] &= \left[1 + cos^2\left(\frac{\alpha[n]+\beta[n]}{2}\right) - 2cos\left(\frac{\alpha[n]+\beta[n]}{2}\right) cos\left(\frac{\beta[n]-\alpha[n]}{2}\right)\right]^{1/2} \\ \theta[n] &= cos\left(\frac{\alpha[n]+\beta[n]}{2}\right) sin\left(\frac{\beta[n]-\alpha[n]}{2}\right) \Bigg/ \left[cos\left(\frac{\beta[n]-\alpha[n]}{2}\right) cos\left(\frac{\alpha[n]+\beta[n]}{2}\right) - 1\right] \end{aligned} \tag{6}$$

The angles $\alpha[n]$ and $\beta[n]$ are shown in Fig. 5(a) and defined as $\alpha[n] = \angle\hat{x}[n] - \angle\hat{x}_L^+[n]$, $\beta[n] =$

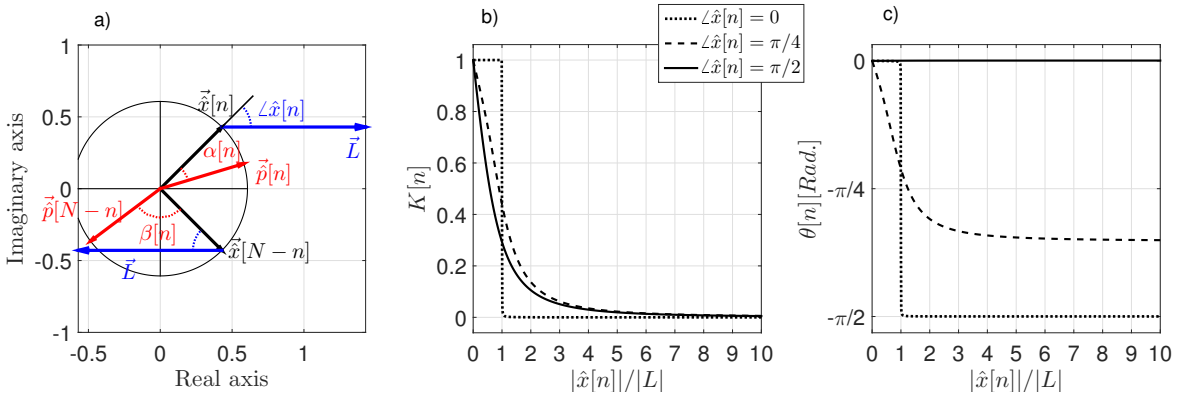

Figure 5: Effect of the proposed PE residual method on a single frequency component of a signal. (a) Example of vector rotation in the complex plane. In black the original vector and its complex conjugate, in blue the added vectors and in red the rescaled resultants. The angles $\alpha[n]$ and β in red, positive direction counterclockwise. (b) Variation of gain $K[n]$ with signal component amplitude. (c) Variation of phase modification $\theta[n]$ with signal component amplitude.

$\angle\hat{x}^*[n] - \angle\hat{x}_L^-[n]$ and for $0 \leq \angle\hat{x}[n] \leq \pi$

$$\alpha[n] = cos^{-1}\left[\frac{|\hat{x}[n]|/|L| - cos\left(\pi - \angle\hat{x}[n]\right)}{\left(1 + |\hat{x}[n]|^2/|L|^2 - 2cos\left(\pi - \angle\hat{x}[n]\right)|\hat{x}[n]|/|L|\right)^{1/2}}\right]$$
$$\beta[n] = cos^{-1}\left[\frac{|\hat{x}[n]|/|L| - cos\left(\angle\hat{x}[n]\right)}{\left(1 + |\hat{x}[n]|^2/|L|^2 - 2cos\left(\angle\hat{x}[n]\right)|\hat{x}[n]|/|L|\right)^{1/2}}\right] \tag{7}$$

while for $\pi < \angle\hat{x} < 2\pi$, $\alpha = -\alpha$ and $\beta = -\beta$. Figures 5(b-c) show respectively the gain $K[n]$ and the phase modification $\theta[n]$ as a function of the signal component amplitude $|\hat{x}[n]|/|L|$, for three different values of $\angle\hat{x}[n]$.
According to Eq.(5)

$$\begin{aligned} x_{pe,n}[k] &\simeq x_n[k] && for\ |\hat{x}[n]| \ll |L| \\ x_{pe,n}[k] &\simeq 0 && for\ |\hat{x}[n]| \gg |L| \end{aligned} \tag{8}$$

therefore PE can be interpreted as a thresholding in the amplitude of the spectral components where the level of the threshold is controlled setting $\lambda = |L|$. Spectral components with amplitude smaller than the threshold are decreased, independently of their frequency, since Eq. 5 is valid $\forall n$.

2.3.1. Application of PE to vibrational signals

This section describes the mechanism behind the efficacy of the proposed approach for enhancing bearing signals in gearbox vibrations. The vibrations from gears can be considered as amplitude and phase modulations of the fundamental tooth meshing frequency and its harmonics. In the frequency domain they will contribute a series of peaks [18] among which is possible to select

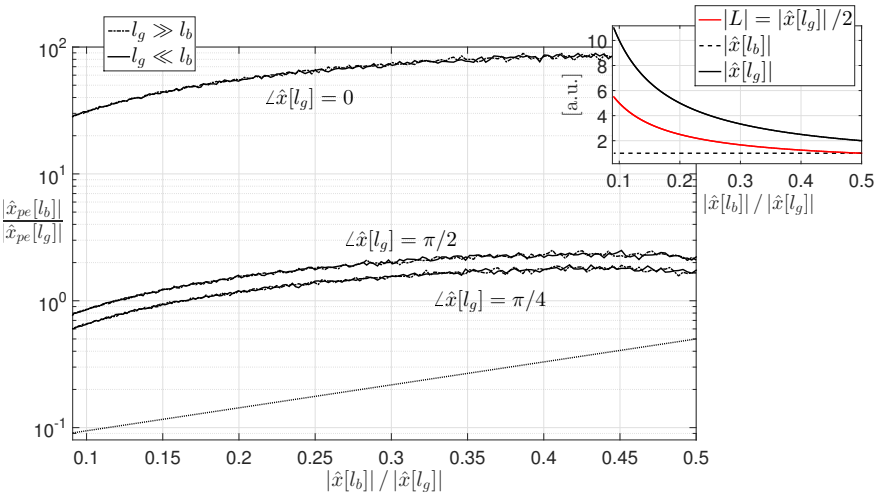

Figure 6: Performance of PE for different values of $\angle\hat{x}[l_g]$, $|\hat{x}[l_g]|/|L|$ and $|\hat{x}[l_b]|/|L|$. The dotted line is at the bisector and shows the level of no increase in the ratio $|\hat{x}[l_b]|/|\hat{x}[l_g]|$

the frequency l_g giving the peak with the smallest amplitude:

$$l_g = \min_{0<l\leq N/2} |\hat{x}[l]|$$

In contrast vibrations from a defective bearing will contribute a continuous spectrum around the resonant frequency of the impacts, among which the frequency l_b corresponds to the component with the biggest amplitude:

$$l_b = \max_{0<l\leq N/2} |\hat{x}[l]|$$

Most commonly, the gear meshing vibrations dwarf the signals from the bearings, and in the case of $|\hat{x}[l_g]| \gg |\hat{x}[l_b]|$ it is possible to select λ such that

$$|\hat{x}[l_g]| \gg \lambda \gg |\hat{x}[l_b]| \tag{9}$$

It is evident from Eqs. (8) that the result of applying the proposed PE residual filter in this case to almost completely suppress the high energy components from the gears while the low energy signal from the defective bearing is almost unchanged.

If, however, instead of Eq.(9) the vibrational composition is such that $|\hat{x}[l_g]| > \lambda > |\hat{x}[l_b]|$ the performance of PE depends on the phases of the spectral components of interest and on their ratios in respect to λ. A numerical investigation of the performance of PE for such a case is presented in Fig.(6). Three different values of $\angle\hat{x}[l_g]$ are considered: $0, \pi/4$ and $\pi/2$. For each of these phases the component from the bearing is considered to have a phase such that $\angle\hat{x}[l_b] = \angle\hat{x}[l_g] + \Delta\phi$. As shown in the inset plot, the amplitude of $|\hat{x}[l_b]|$ is kept constant while $|\hat{x}[l_g]|$ varies and $|L|$ is taken as $|\hat{x}[l_g]|/2$. The plot shows the mean of a Monte Carlo simulation comprised of 10^3 cases of $\angle\hat{x}[l_b]$ analysed for each value of $\angle\hat{x}[l_g]$. In the worst case, the ratio of the bearing signal over the gear signal, after the application of PE, is increased of a factor 4. Furthermore as expected from Eq.(5) the method does not depend on the frequency of the peaks and it shows the same performance for $l_b \gg l_g$ and $l_b \ll l_g$. Thus it is expected that the proposed method will provide useful signal conditioning wherever a separation in amplitudes exists between gear and bearing signals, and not only where that separation is large.

Finally a numerical investigation of PE on the same data as in Fig. 3 is presented, however in this simulation the level of noise is higher, with $\sigma = 0.2$. Figures 7(a) and (b), in black, show respectively a portion in the time domain and the amplitude spectrum of the raw signal. Firstly method II is implemented in order to check the performance in this noisy scenario. In Fig. 7(c) is shown the envelope of x_{zc}. It is not possible to identify the seven impulses from the bearing signal, unlike Fig. 3(c).
Fig. 7(d) shows the result of the application of the PE procedure as introduced in this paper. The absolute value of the analytic representation of $x_{pe}[k]$ allows the identification of the seven impulses in this noisy condition. The results of the application of method I for this numerical simulation are not shown here: SK selects the correct band for demodulation and the $x_{acep+sk}$ signal is comparable to x_{pe} in 7(d). The amplitude spectrum of x_{pe} is shown in Fig. 7(b) in yellow, as anticipated the phase editing method yields a signal with strongly decreased high energy components. In order to quantify the phase distortion due to the rotation of the Fourier vectors, Fig. 7(e) shows the difference between the unwrapped phases $\angle\hat{x}_{pe}[l]$ and $\angle\hat{x}[l]$, the frequency is zoomed around the resonance band $15 - 17[kHz]$. Phase differences of 2π are mainly identified,

yielding a good precision in the impulses occurrences as can be noticed by comparing Fig. 3(a-c) and Fig. 7(d).

3. Experimental setups

The experimental data sets used for the comparison between the three methods are collected from a gearbox dynamic simulator located in the laboratories of the Flanders Make VZW in Leuven, Belgium. The test bench is employed in two different configurations, namely Flanders Make 1 (FM1) and FM2. Also data sets publicly available on the websites of the Prognostics and Health Management Society (PHM) [19] and Machinery Failure Prevention Technology (MFPT) [20] are analysed.

Figures 8(a) and (b) show the photograph and schematic top view of the test setup FM1. The apparatus consists of two gearboxes, namely a parallel-shaft gearbox (2) and a perpendicular-shaft gearbox (3). The input shaft (8) of the parallel-shaft gearbox is driven through a flexible coupling, by an electric induction motor (1). The shaft rotational speed of the motor can be varied from 0 to 3000 rpm. The output shaft of the perpendicular shaft gearbox (9) is coupled with a magnetic-particle brake (4), where the torque can be adjusted from 0 to 50 Nm. The accelerometer $A\#1$ with sensitivity of $100[mV/g]$ and $\pm 5\%$ response deviation in the frequency range of $0.5[Hz]$ to $5[kHz]$ is used as vibrations transducer. The parallel-shaft gearbox (3) was designed and built with three parallel-shafts. Four helical gears are arranged in the gearbox such that it has two-stage reductions. Two straight bevel gears are assembled on their corresponding shaft, in the perpendicular-shaft

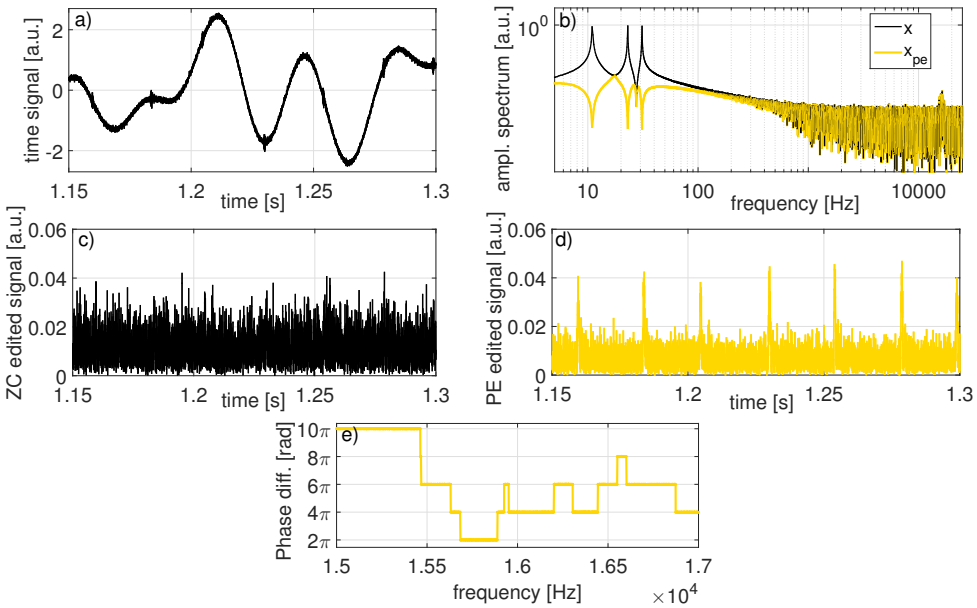

Figure 7: Application of the PE method to a numerical simulation. The tested signal is the same as in Fig. 3 with an increased level of noise. (a) The raw signal in time domain. (b) Amplitude spectrum of the raw and phase edited residual signals in black and yellow respectively. (c) Absolute value of the analytic representation of the ZC edited signal $x_{zc}[k]$: no clear impacts can be identified. (d) Absolute value of the analytic representation of the PE residual signal $x_{pe}[k]$: the seven impacts are clearly identified. (e) Phase difference between $x_{pe}[l]$ and $x[l]$ in the frequency range of the structural resonance excited by bearing impacts.

gearbox, so there is only one-stage reduction. Two different bearing types are assembled in the test setup, namely MB ER-14K and MB ER-16K. Two bearings ($B\#1$ and $B\#2$) of the former type are mounted in the parallel-shaft gearbox to support the input shaft (8) and the other bearings (from $B\#3$ to $B\#8$) of the latter type are mounted to support the other shafts. Details of the gears assembled in the two gearboxes and the bearings theoretical fault frequencies are listed in Table 1. For the setup FM1 two different types of defective bearings are tested separately, firstly a bearing with an inner race fault, secondly one with a rolling element fault, both are mounted on the input side of the second shaft of the parallel-shaft gearbox, namely ($B\#3$). Two different load conditions are tested for each configuration, $6[Nm]$ and $20[Nm]$ on the output shaft (9). Furthermore four constant speeds are investigated, on the shaft with the defective bearing they correspond to: $f_{shaft} = \{2.9;\ 8.7;\ 11.6;\ 14.5\}\ [Hz]$. The accelerometer of FM1 provides a total of 24 sets, 8 in healthy condition, 8 with inner race fault and 8 with rolling element faults. The length of each recorded vibrational signal is 5 seconds and the sampling rate is $51.2[kHz]$.
Figure 8(c) shows the schematic top view for the test setup FM2. The differences between FM1 and FM2 are that the perpendicular-shaft gearbox is removed and that the load is applied directly on the output shaft of the parallel-shaft gearbox. Gears and bearings are the same as in the FM1 setup and details are listed in Table 1. The accelerometer $A\#2$ has same specifications of $A\#1$ used in FM1, but is placed on the left side of the gearbox. For the setup FM2 a defective bearing

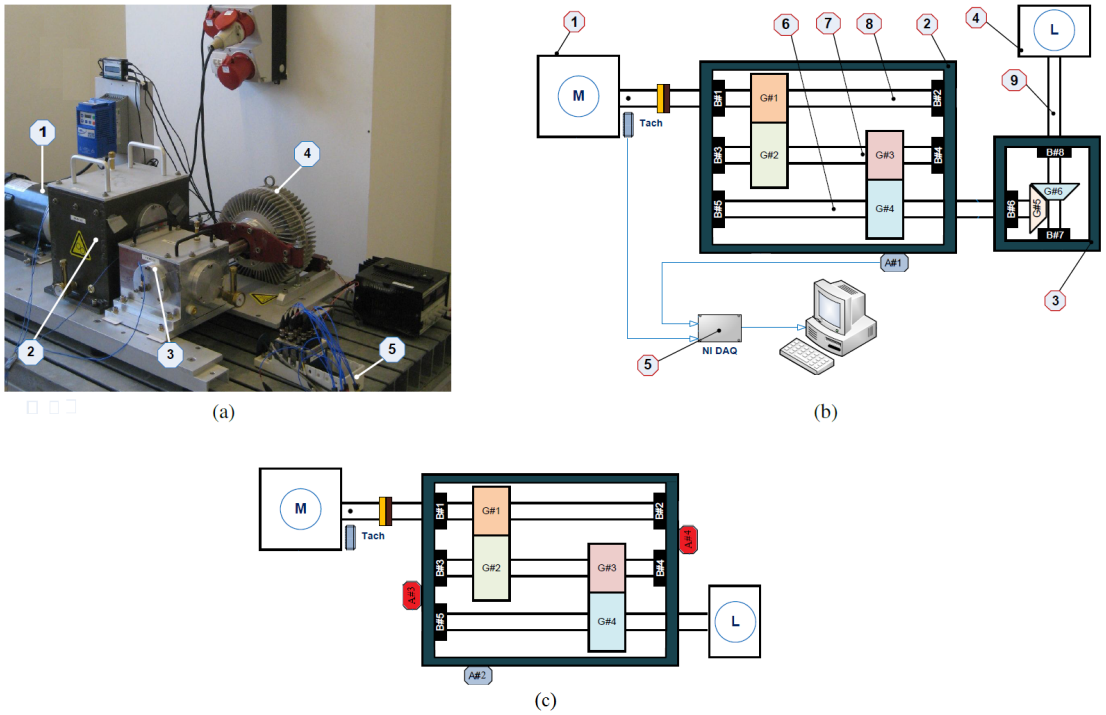

Figure 8: Experimental setups: (a) and (b) are respectively a photograph and the schematic top view of the setup Flanders Make 1 (FM1), the defective bearing is $B\#3$. (c) Schematic top view of FM2 and PHM. In blue the accelerometer used in the FM1 setup, with $B\#3$ as defective bearing. In red the accelerometers used in the PHM setup, with $B\#1$ as defective bearing.

Component	# of teeth	Type
G#1	29	Helical
G#2	100	Helical
G#3	36	Helical
G#4	90	Helical
G#5	20	Straight bevel
G#6	40	Straight bevel

Bearing defect	Cyclic Order $\times f_{shaft}$
Fundamental train freq. (FTF)	0.402
Ballpass freq. outer race (BPFO)	3.572
Ballpass freq. inner race (BPFI)	5.430
Ball spin freq. (BSF)	2.322

Table 1: Gears and defective bearing characteristics of the FM setups

MB ER-16K with an inner race fault is mounted on the input side of the second shaft of the parallel-shaft gearbox, namely ($B\#3$) and again two different load conditions are tested $6[Nm]$ and $20[Nm]$. Seven constant speeds are investigated, specifically on the shaft with the defective bearing they correspond to: $f_{shaft} = \{0.29;\ 0.58;\ 0.87;\ 1.16;\ 1.45;\ 1.74;\ 2.9\}\ [Hz]$. The length of the recorder vibrational signal is selected to obtain 15 revolutions for each f_{shaft} and the sampling rate is $51.2[kHz]$. The accelerometer of FM2 provides a total of 28 data sets, and 14 in healthy condition and 14 with inner race faults.
Figure 8(c) shows as well the schematic top view for the test setup used by the PHM. In this apparatus two accelerometers ($A\#3$-$A\#4$) are used as vibrations transducers with sensitivity of $10mV/g$, $\pm 1\%$ response deviation and resonant frequency $> 45[kHz]$. Furthermore all the bearings (from $B\#1$ to $B\#5$) assembled in the PHM test setup are MB ER-10K. Details of the gears and the bearings theoretical fault frequencies are listed in Table 2. Several combinations of faulty gears and bearings are present in the PHM dataset, here the following case is analysed: defective bearing with an inner race fault mounted on the input side of the first shaft, namely ($B\#1$) tested in two different load conditions. In this condition the gear on the output shaft, namely ($G\#4$), has a sheared key-way. Five constant speeds are investigated: $f_{shaft} = \{30;\ 35;\ 40;\ 45;\ 50\}[Hz]$, the length of each recorded vibrational signal is 4 seconds and the sampling rate is $200/3[kHz]$. Each accelerometer of the PHM setup provides a total of 20 data sets, 10 in healthy condition and 10 with inner race faults, only the data from the accelerometer on the input side, namely ($A\#3$), will be analysed.

Data sets from different types of defective bearings are stored in the MFPT database. Here three vibration signals from a bearing with an outer race defect and three from an healthy bearing are analised. The shaft rotational speed of the apparatus is $25[Hz]$, the sample rate is $97.656[kHz]$ and the length of each record is 6 seconds, only one load conditions is tested. The defective bearing is a NICE and the theoretical fault frequencies are listed in Table 3. The speed of the shaft with the defective bearings is $f_{shaft} = 25\ [Hz]$.

Component	# of teeth	Type
G#1	32	Spur
G#2	96	Spur
G#3	48	Spur
G#4	80	Spur

Bearing defect	Cyclic Order $\times f_{shaft}$
FTF	0.382
BPFO	3.052
BPFI	3.984
BSF	2.474

Table 2: Gears and defective bearing characteristics of the PHM setup

Bearing defect	Cyclic Order $\times f_{shaft}$
FTF	0.406
BPFO	3.245
BPFI	5.109
BSF	2.378

Table 3: Defective bearing characteristics of the MFPT setup

4. Results & discussion

This section presents the comparison of the three methods described in Section(1), the analysis is carried out on data sets taken from the setups detailed in Section(2). A fault feature value is calculated from the normalised $S\tilde{E}S$ of the three edited signals x_{ce+sk}, x_{zc}, x_{pe}. From each experimental configuration two feature values are calculated, one for the healthy case and one for the corresponding defective case. Features are calculated as the sum of the values of the $S\tilde{E}S[l]$ in a band around the theoretical fault frequency and up to a selected harmonic: $[k \cdot f_{defect} - 0.5 \cdot f_b,\ k \cdot f_{defect} + 0.5 \cdot f_b]$, with $k = 1, 2, \ldots, n$ with n =number of harmonics.
Specifically the SES is normalized by means of the ratio:

$$S\tilde{E}S[l] = SES[l]/SES[0] \tag{10}$$

and for the ACEP+SK signal the SES is the Fourier transform of the square of the absolute value of x_{ce+sk}, while for the zero-cepstrum and phase-edited methods the SES is implemented as the Fourier transform of the square of the absolute value of the analytic representation of x_{zc} and x_{pe}. The maximisation of the objective value $r(\lambda)$ has been defined as the criterion for determining the optimal parameter λ of Eq.2 in method III:

$$r(\lambda) = \frac{F_d(\lambda)}{F_h(\lambda)} \tag{11}$$

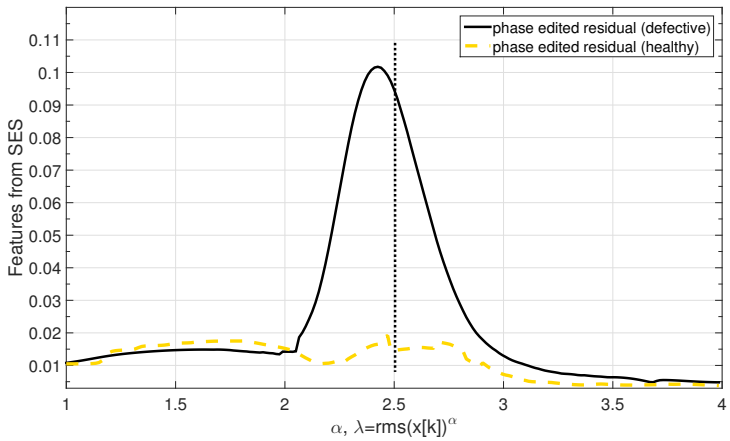

Figure 9: Tuning of the parameter λ in the PE method. Black and yellow are the features estimated from the squared envelope spectrum of the phase edited residual signal in healthy and faulthy bearing cases as a function of λ. Black vertical line is plotted at λ giving the max of the ratio $r(\lambda)$ between the features.

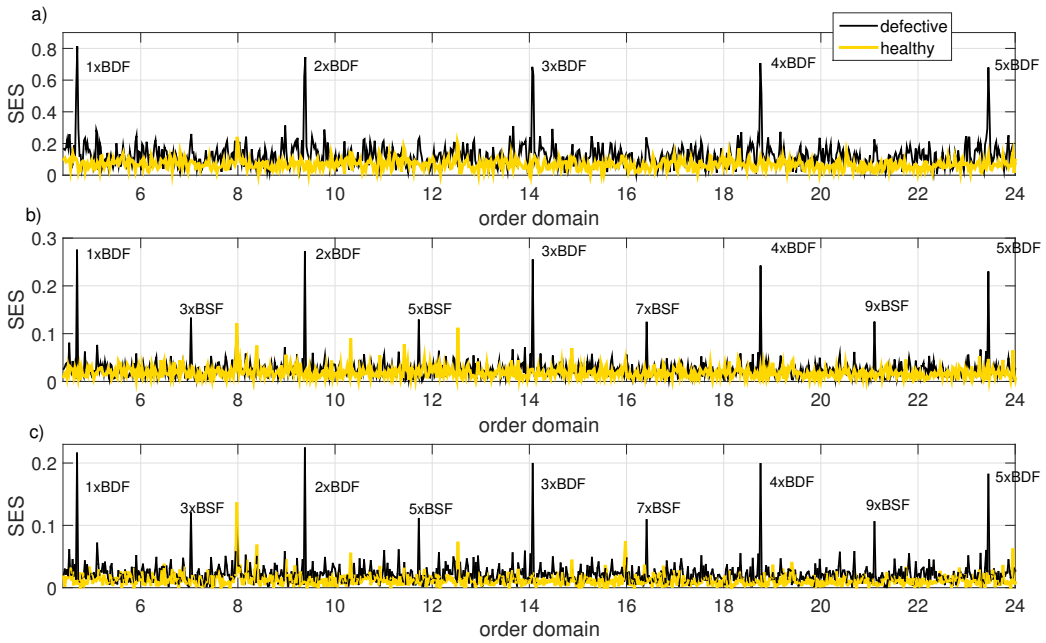

Figure 10: Performance comparison of the three methods on FM1 data set with a ball defect and $f_{shaft} = 8.7[Hz]$. SES of signal edited with (a) ACEP+SK, (b) ZC, (c) PE. Yellow and black are respectively healthy and defective conditions.

where $F_{h,d}(\lambda)$ are respectively the feature values calculated for an healthy and defective case. This is implemented in an automated way varying λ as a power α of the root mean square of the raw signal $x[k]$:

$$\lambda = rms\left(x[k]\right)^{\alpha} \tag{12}$$

Figure 9 shows an example of this procedure on a data set taken from FM1 setup with a shaft speed of $8.7[Hz]$ and a ball defect. Yellow and black lines are the features calculated from the SES of x_{pe} as a function of λ, respectively for the faulty and healthy conditions, while the vertical black line at the value of $\alpha = 2.5$ gives $max\left\{r\left(\lambda(\alpha)\right)\right\}$. For each couple of defective-healthy data sets the optimal parameter λ is computed in an automated way. In a practical application $F_h(\lambda)$ is a baseline, measured when the equipment is first commissioned and from this point onwards the signal processing can operate in a fully automated way with the estimation of features from each case to diagnose and the respective $r(\lambda)$. From all the 43 data sets tested in this paper the mean value of the tuning parameter is $\bar{\lambda} = 2.29$ with standard deviation $\sigma_\lambda = 0.13$.
Fig. 10-11-12-13 show the normalised SES in order domain for data sets from each of the four different setups, yellow is healthy case and black is defective case. The plots from top to bottom are the SES of methods I II and III, namely of x_{ce+sk}, x_{zc} and x_{pe} with the tuned λ.
In Fig. 10 the data is from the FM1 setup with a shaft speed of $8.7[Hz]$ and a ball defect, with all the methods peaks can be distinguished up to the fifth harmonic of the theoretical fault frequency $BDF = 2BSF$, as in Table 1. For the zero cepstrum and the phase edited residual signals peaks are also present at the odd harmonics of BSF, these are less clear in the SES of x_{ce+sk}. The ball spin frequency is the frequency with which the fault strikes the same race (inner or outer)

hence in general there are two impacts at BDF per basic period so that its expected that the even harmonics of BSF are dominant [11].
In Fig. 11 the data is from the FM2 setup with a shaft speed of $0.87[Hz]$ and inner race defect, with all the methods peaks can be distinguished up to the fifth harmonic of the theoretical fault frequency $BPFI$ as in Table 1. Typical sidebands due to the passing of the inner race fault into and out of the load zone are not clearly detected. This is attributable to the low speed and load conditions: the load on the shaft with the defective bearing is $20[Nm]$
Figure 12 shows the SES of the edited data from the MFPT setup. The shaft speed is $25[Hz]$ and the defect is on the outer race of the bearing. The ACEP+SK and phase editing methods, top and bottom respectively, allow the detection up to the fifth harmonic of the theoretical BPFO, Table 2, while x_{zc} up to the third harmonic. Furthermore can be noticed some spurious peaks in the ACEP+SK and that for the zero cepstrum edited signal the amplitude of peaks is one order of magnitude smaller. The SES is normalized as in Eq.10 hence the latter is the consequence of an higher value of the DC component and less pronounced impacts in the time domain envelope of x_{zc}.
In Fig. 13 the data is from the PHM setup with a shaft speed of $35[Hz]$ and an inner race defect, peaks up to the third harmonic of the theoretical fault frequency $BPFI$ as in Table 3 can be distinguished for the three methods, for this data set also the harmonics due to the load are present. The smearing of spectral peaks could be attributable to the presence of a sheared gear, or to speed fluctuations; the data is processed without applying order tracking.
Fig. 14 presents the comparison of the performance on all the available 43 data sets. It shows

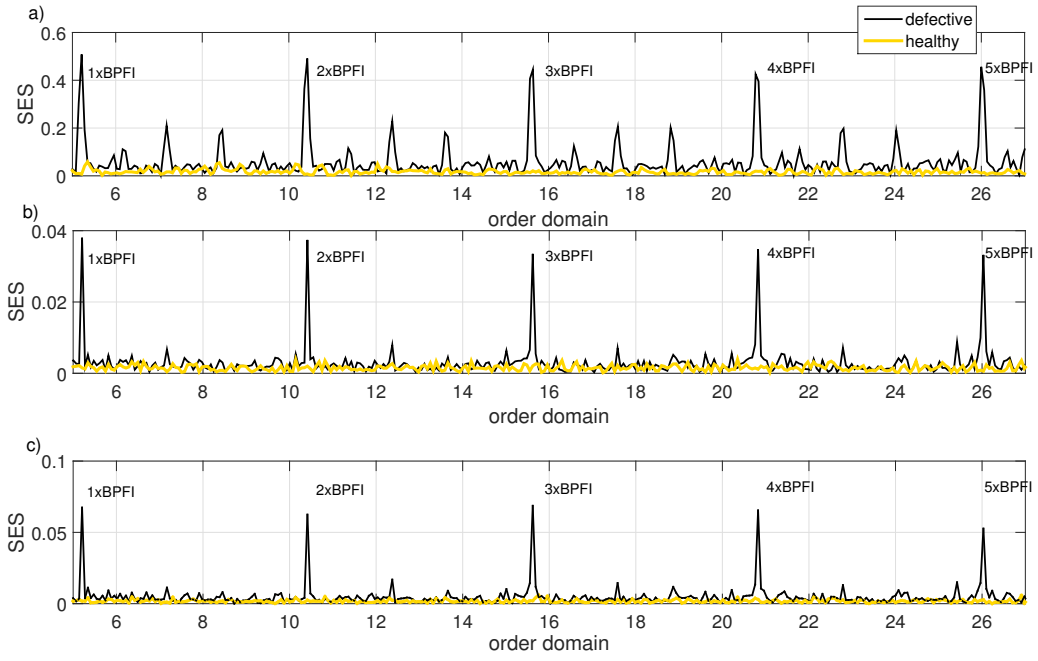

Figure 11: Performance comparison of the three methods on FM2 data set with a inner race defect and $f_{shaft} = 0.87[Hz]$. SES of signal edited with (a) ACEP+SK, (b) ZC, (c) PE. Yellow and black are respectively healthy and defective conditions.

for each case the normalised features of healthy and corresponding defective case in a scatter plot. The ideal detection of a defective bearing corresponds to the point $(1, 0)$. Features are normalised according to each set up type, defect and load. For example for FM1 in the case of a ball defect, with small load we normalise the features corresponding to the four frequencies $f_{shaft} = \{2.9;\ 8.7;\ 11.6;\ 14.5\}\ [Hz]$ and for the high load we normalise separately. Following a recent paper by Smith et al. [15] it is also studied the SES of the full bandwidth raw signals, Fig. 14 (a); as for method II and III the envelope is calculated as the absolute value of the analytic representation of the signal. Fig. 14(b) shows results from method I and Fig. 14(c-d) from method II, III. In green it is highlighted the portion of the square where the faulty features are at least three times bigger than the features of the corresponding healthy cases, providing an high confidence detection of the presence of a defect. In red the portion where the ratio between defective and healthy features is less then one; in orange where the ratio is between one and two and in yellow the portion where the ratio between defective and healthy features is between two and three and the detection is less reliable. The selection of the value three as good discriminant is made by the human inspection of the relative SES. Asterisk and triangle markers correspond respectively to data sets from FM2 and FM1 while circle and cross to PHM and MFPT data sets. The worst performance is of the envelope of the raw signal Fig. 14(a), in several cases the healthy condition has a feature higher than the faulty one, nevertheless 11 points reside in the green zone and the correct detection is accomplished. For the other three methods the results are comparable, with a slightly better performance of the proposed PE. Method I and II accomplish correct detection respectively in 31 and 30 cases, while the proposed method III in 34 cases, as shown in Fig. 14(b-

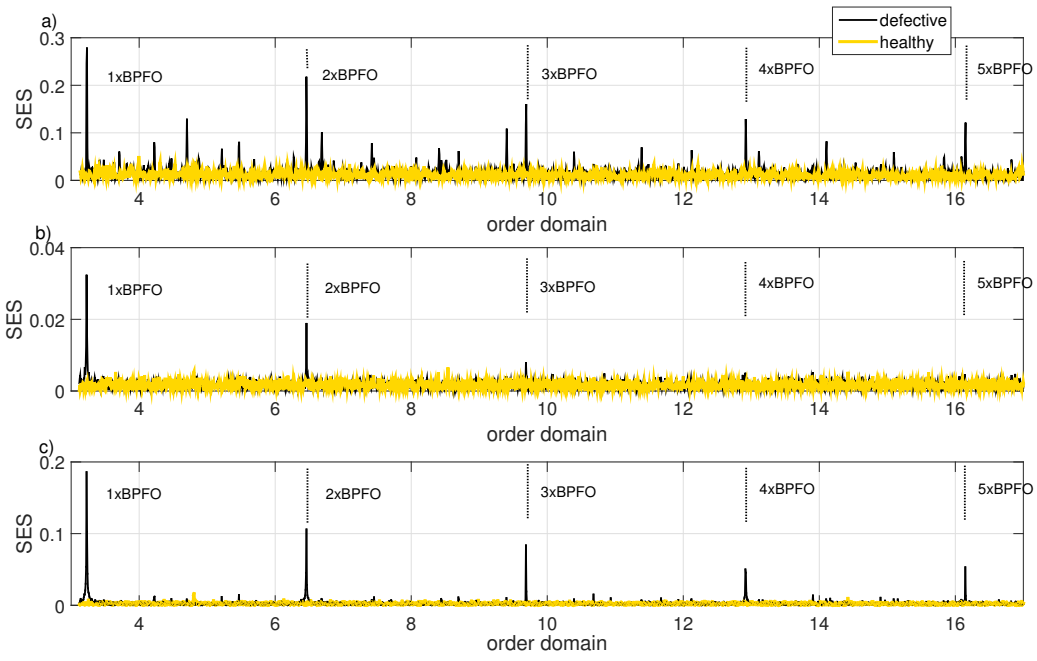

Figure 12: Performance comparison of the three methods on MFPT data set with a outer race defect and $f_{shaft} = 25[Hz]$. SES of signal edited with (a) ACEP+SK, (b) ZC, (c) PE. Yellow and black are respectively healthy and defective conditions.

c-d). Signals with a dominant bearing component can be identified in Fig. 14(a) because these are diagnosed successfully using the raw, unmodified signal only if the damage is severe. The data set from MFPT shows a case of dominant bearing damage signal, where the bearing damage was severe. This can be noticed from Fig. 14(a) with two of the three points in the green area and only one in the yellow one, indicating a good diagnosis. In Fig. 14(d) the disposition of the markers is almost unchanged, therefore when there is no need to suppress disturbing components the proposed method III is shown to be equally effective.

5. Conclusions

This paper proposed and tested a new method for the enhancement of bearing vibration signals to be used in automated condition monitoring: phase editing. The performance of the method is evaluated by means of feature estimation from the SES of the signals, with an overall correct detection rate of 79% when using the enhanced signals, compared with a rate of 25% when using the raw signals. For each case the ratio between the feature calculated from a faulty bearing and the feature from an healthy one was computed. The faulty bearing is considered correctly detected if the value of the ratio is greater than three. The effectiveness of the method compared favourably with that of two other promising contemporary enhancement approaches, which obtained performances of 72% (automated cepstral editing procedure with spectral kurtosis) and 69% (zero cepstrum). The proposed method was applied in an automated way in 43 experimental cases considering inner and outer race faults as well as ball faults, for machines operating at different speeds and loads. For each analysed case there is only one parameter to tune for a correct performance and this was

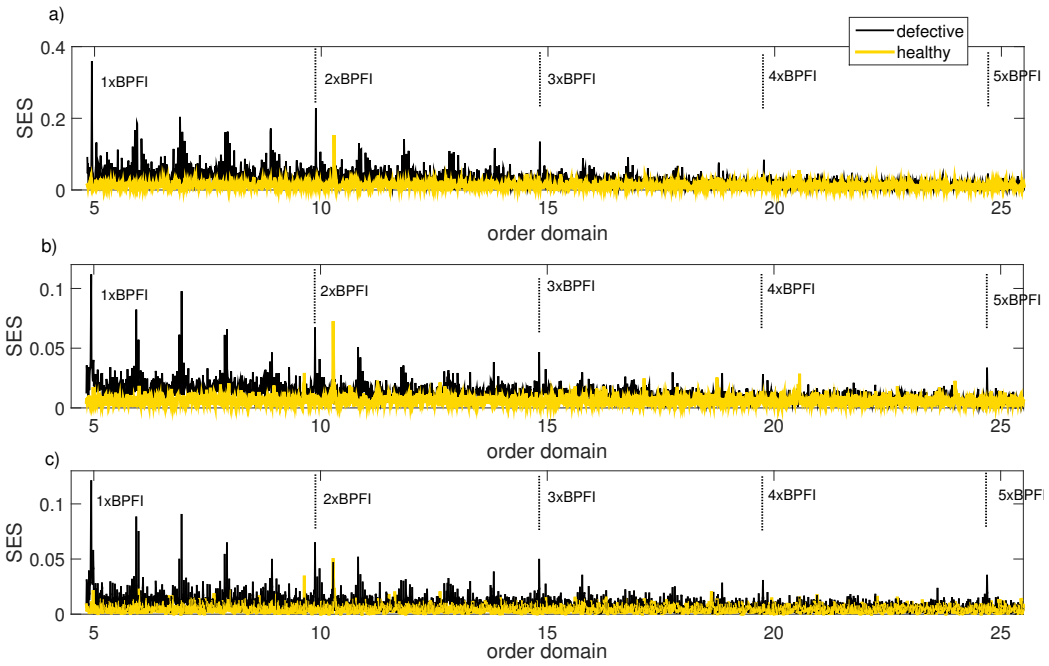

Figure 13: Performance comparison of the three methods on PHM data set with a inner race defect, a spur gear and $f_{shaft} = 35[Hz]$. SES of signal edited with (a) ACEP+SK, (b) ZC, (c) PE. Yellow and black are respectively healthy and defective conditions.

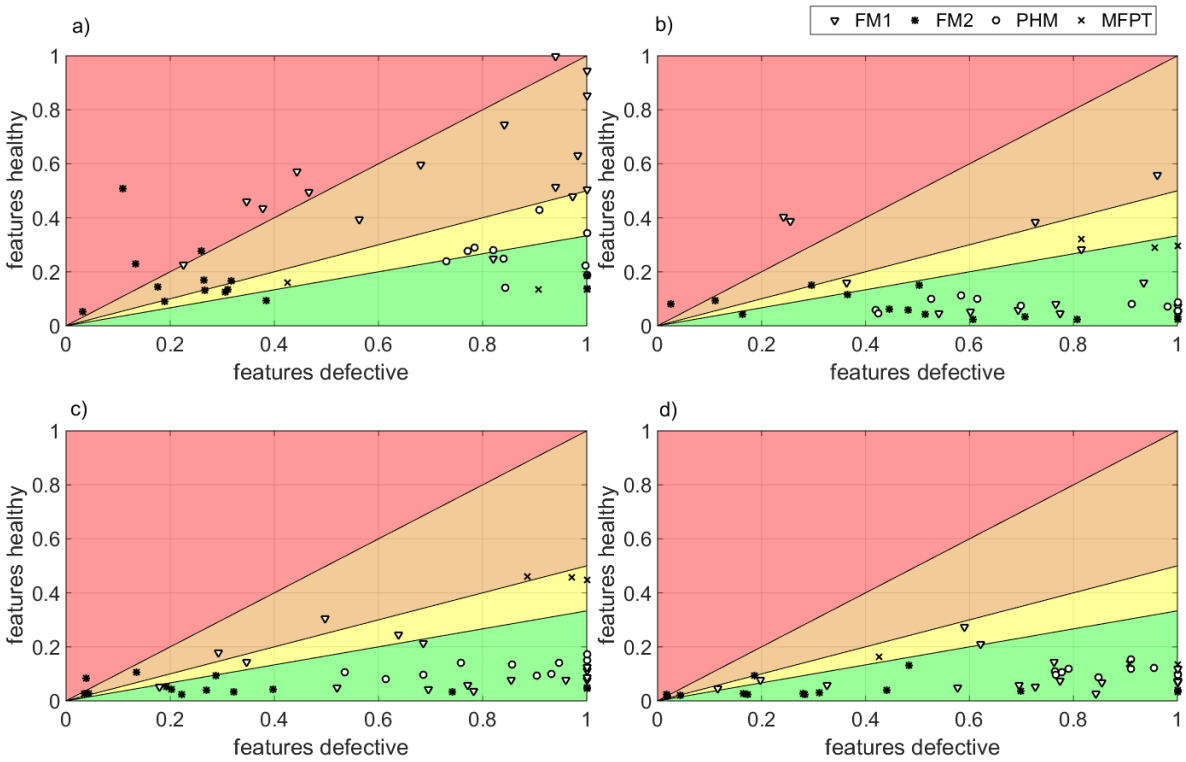

Figure 14: Healthy-defective scatter plots of features estimated from the SES: (a) of the raw signals, (b) of the signals edited with ACEP+SK, (c) ZC and (d) PE. Green represents the area where the ratio between the features is greater than 3 and the detection of the fault is very good. Yellow orange and red are the areas where the ratio is respectively between 2 and 3, 1 and 2 and smaller than 1. Triangle and asterisk pointers are FM1 and FM2 datasets while circle and cross to PHM and MFPT datasets

selected by a fully automated optimisation algorithm. Therefore only the bearing specification characteristics and rotation speed have to be adjusted for each case, so this method is suitable for use without specialist signal processing expertise from an operator. Furthermore phase editing uses the full band of the spectrum for demodulation and is computationally easy to implement, using mainly the FFT algorithm, so that it is a good candidate for an industrial application of vibration based bearing condition monitoring.

References

[1] D. Mba, B. K. N. Raj, Development of acoustic emission technology for condition monitoring and diagnosis of rotating machines: Bearings, pumps, gearboxes, engines, and rotating structures, The Shock and Vibration Digest 38 (1) (2006) 3–16.

[2] Y.-H. Kim, A. C. C. Tan, J. Mathew, B.-S. Yang, Engineering Asset Management: Proceedings of the 1st World Congress on Engineering Asset Management, Springer London, London, 2006, Ch. Condition Monitoring of Low Speed Bearings: A Comparative Study of the Ultrasound Technique Versus Vibration Measurements, pp. 182–191.

[3] I. El-Thalji, E. Jantunen, A summary of fault modelling and predictive health monitoring of rolling element bearings, Mechanical Systems and Signal Processing 6061 (2015) 252 – 272.

[4] P. McFadden, J. Smith, Vibration monitoring of rolling element bearings by the high-frequency resonance technique a review, Tribology International 17 (1) (1984) 3 – 10.
[5] J. Antoni, Cyclic spectral analysis of rolling-element bearing signals: Facts and fictions, Journal of Sound and Vibration 304 (35) (2007) 497 – 529.
[6] R. Randall, J. Antoni, S. Chobsaard, The relationship between spectral correlation and envelope analysis in the diagnostic of bearing faults and other cyclostationary machine signals, Mechanical Systems and Signal Processing 15 (5) (2001) 945 – 962.
[7] J. Antoni, The spectral kurtosis: a useful tool for characterising non-stationary signals, Mechanical Systems and Signal Processing 20 (2) (2006) 282 – 307.
[8] P. Borghesani, P. Pennacchi, R. Randall, N. Sawalhi, R. Ricci, Application of cepstrum pre-whitening for the diagnosis of bearing faults under variable speed conditions, Mechanical Systems and Signal Processing 36 (2) (2013) 370 – 384.
[9] R. B. Randall, N. Sawalhi, M. Coats, A comparison of methods for separation of deterministic and random signals, The International Journal of Condition Monitoring 1 (1) (2011) 11 – 19.
[10] B. Kilundu, A. P. Ompusunggu, F. Elasha, D. Mba, Effect of parameters setting on performance of discrete component removal (dcr) methods for bearing faults detection, in: Second European conference of the prognostics and health management (PHM) society, Nantes, France, 2014.
[11] R. B. Randall, J. Antoni, Rolling element bearing diagnostics a tutorial, Mechanical Systems and Signal Processing 25 (2) (2011) 485 – 520.
[12] A. P. Ompusunggu, T. A. Bartic, Automated cepstral editing procedure (acep) for removing discrete components from vibration signals, in: The twelfth International Conference on Condition Monitoring (CM) and Machinery Failure Prevention Technologies (MFPT), The Oxford Hotel, Oxford,UK, 2015.
[13] J. Antoni, Fast computation of the kurtogram for the detection of transient faults, Mechanical Systems and Signal Processing 21 (1) (2007) 108 – 124.
[14] A. Oppenheim, J. Lim, The importance of phase in signals, Proceedings of the IEEE 69 (5) (1981) 529–541.
[15] W. A. Smith, R. B. Randall, Rolling element bearing diagnostics using the case western reserve university data: A benchmark study, Mechanical Systems and Signal Processing 6465 (2015) 100 – 131.
[16] K. Wójcicki, M. Milacic, A. Stark, J. Lyons, K. Paliwal, Exploiting conjugate symmetry of the short-time fourier spectrum for speech enhancement, Signal Processing Letters, IEEE 15 (2008) 461–464.
[17] K. Paliwal, K. Wójcicki, B. Shannon, The importance of phase in speech enhancement, Speech communication 53 (4) (2011) 465–494.
[18] P. McFadden, J. Smith, A signal processing technique for detecting local defects in a gear from the signal average of the vibration, Proceedings of the Institution of Mechanical Engineers. Part C. Mechanical engineering science 199 (4) (1985) 287–292.
[19] Prognostics and health management society (phm) datasets, `http://www.phmsociety.org/references/datasets`, accessed: 2016-Feb.
[20] Machinery failure prevention technology (mfpt) datasets, `http://www.mfpt.org/FaultData/FaultData.htm`, accessed: 2016-Feb.

4.3 Speed dependence of the detection

The previous section introduced Phase Editing (PE) and compared its performance with that of state of the art techniques. This section investigates the relationship between detection and the operating speed of the machine[1]. Intuitively, the higher the shaft rotational speed, the higher the amount of energy produced by the impacts from the defective bearing, and detection is easier at higher rotational speeds. To the best of the author's knowledge, this relationship is only superficially investigated in the literature. For example [Al-Ghamd and Mba, 2006] use data at four different speeds, however the focus of their research is the comparison of acoustic emission versus accelerometer data and they examine only time domain features, as for instance root mean square and kurtosis.

In order to conduct the analysis, the FM2 experimental set up of Fig.4.8(c) is used in a broader range of operating conditions. Specifically

$$\begin{aligned} f_{shaft} = &\{0.29;\ 0.58;\ 0.87;\ 1.16;\ 1.45;\ 1.74;\ 2.9;\ 4.35; \\ &5.80;\ 7.25;\ 8.70;\ 10.15;\ 11.6;\ 13.05;\ 14.5\} \quad [Hz] \end{aligned}$$

for the shaft with the defective bearing. Two load conditions of 6 and 20 $[Nm]$ are considered. Both data for the healthy and defective cases are collected, the defect being on the outer race of $(B\#3)$ in Figure 4.8(c). Note that the speed is kept constant during the measured window of time for each of the f_{shaft}, therefore the signals are cyclo-stationary.

The phase editing method as introduced in the previous section is applied to the raw signals. For each f_{shaft} speed the best value for λ is selected in an automated way by maximising $r(\lambda) = F_d(\lambda)/F_h(\lambda)$ where $F_{d,h}$ are respectively the features calculated from the SES for a healthy and defective case. Figure 4.15(a) shows the resulting maximum value of $r(\lambda)$, in black for the 6 Nm load on the output shaft while in red for the 20 Nm load. The same four confidence bands as in Fig. 4.8 are used here. The results show that there is no strong dependence of the detection on the load. On the other hand, the detection depends strongly on the speed of the shaft. Very good detection, green area $F_d/F_h > 3$, is achieved for values of the shaft speed of at least 0.87 Hz. A logarithmic increase in the ratio of the features is observed for the lowest values of the speed up to 1.74 Hz, while for higher speeds values fluctuate between 10 and 20. Therefore it is concluded that transition from missed to very good detection occurs by varying the speed over a small range. As mentioned in the previous section, one

[1]The analysis is restricted to PE, however similar results are obtained using the ZC and ACEP+SK.

of the advantages of PE rests on its implementation on the full band of the vibration signal. Therefore PE does not depend on the band containing the resonant frequency excited by the impacts from the defective bearing. This important characteristic of the PE method was shown, by means of a numerical simulation, in Fig.4.6 and here is verified on experimental data. For the dataset analysed the resonant frequency excited by the impacts is identified using the Kurtogram, as introduced in Section 1.3.3. The resulting optimal central frequency for demodulation, for each of the f_{shaft} speeds, is shown in Figure 4.15(b) and the resonant frequency varies by more than 20 kHz. The comparison with Fig. 4.15(a) shows, as expected, that the performance of PE is not affected by the variation of the resonant frequency.

In addition, from this analysis emerges that methods depending on demodulation are difficult to apply in the case of large speed variations, i.e. for a speed varying in the same range of the f_{shaft}. For instance, the approach described in Section 3.3 would result in selecting a low level number giving a filter of $\sim$ 20 kHz bandwidth. However components from the gears are likely to be present in such a wide band of the spectrum, jeopardising the demodulation. Therefore we conclude that it is advisable to use a full band approach, such as PE, for the enhancement of the vibrations from the bearing in non-stationary speed conditions.

The next section addresses this issue and shows that PE is effective when directly applied to cyclo-non-stationary signals.

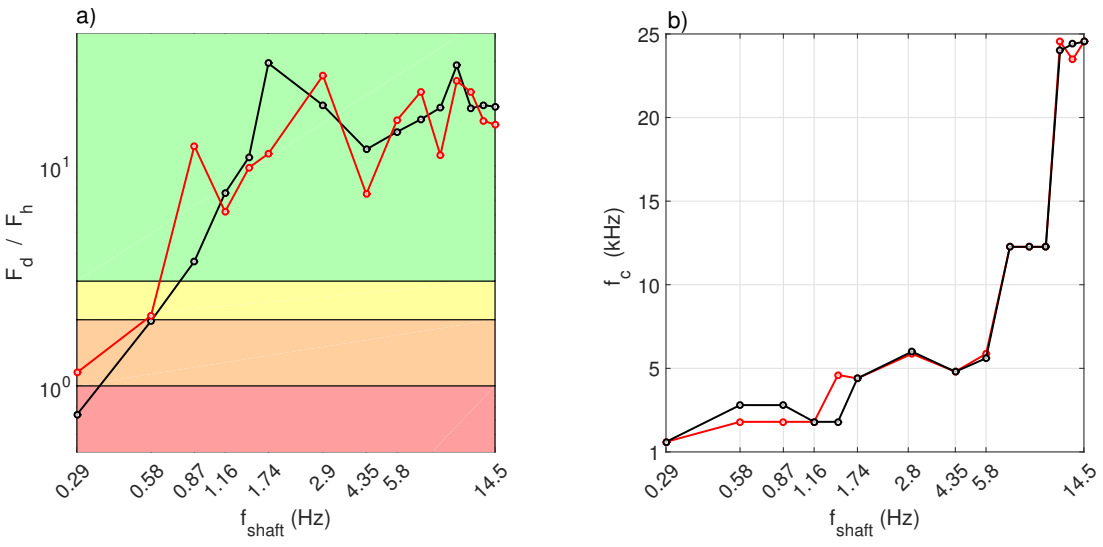

Figure 4.15: (a) Maximum value of ratio between defective and healthy features at different speeds, red load of 20 Nm and black load of 6 Nm. (b) Optimal central frequency for demodulation calculated with SK for different speeds.

4.4 Phase editing to enhance bearing fault detection in variable speed condition

Article published in the Proceedings of the 1^{st} World Congress on Condition Monitoring (WCCM), cited as [Barbini et al., 2017a].

Statement of contributions of joint authorship

L. Barbini (candidate): writing and compilation of manuscript, established methodology, data analysis, preparation of tables and figures. Presented results at the conference.

M. Eltabach : provided analysed data set, editing and co-author of manuscript.

J. L. du Bois (principal supervisor): supervised and assisted with manuscript compilation, editing and co-author

Copyright

Phase editing to enhance bearing fault detection in variable speed condition

L. Barbini[a,b,*], M. Eltabach[b], J. L. du Bois[a]

[a] *The University of Bath Department of Mechanical Engineering, Claverton Down, Bath, BA2 7AY, UK*
[b] *CETIM, avenue Félix-Louât - SENLIS 60300, France*

Abstract

The computation of the squared envelope spectrum (SES) on vibration data collected from a rotating machine is a common tool used to diagnose a defective bearing. To enhance the diagnosis, pre-processing methods have to be implemented, before the evaluation of the SES, to suppress vibrations from sources other than the bearings. Conventionally suppression of the spurious components is achieved by exploiting either their separation in the frequency domain or the contrast between deterministic signals and the random vibration components from a defective bearing. Recently the phase editing method (PE) was used to exploit another characteristic of the vibration signal to improve diagnosis in stationary speed conditions. PE caters to, and exploits the scenario where vibrations from a defective bearing have small amplitude compared to vibrations from other components, effectively thresholding the amplitudes of the spectral components of a signal. In this paper the PE method is applied analytically and experimentally to a broader class of machinery, encompassing machines with varying speed conditions. It is demonstrated that the separation of the bearing component and masking components is equally effective in the non-stationary case.

1. Introduction

The diagnosis of a defective bearing on a rotating machinery can be carried out by analysing vibration data. A defective bearing produces a series of impacts throughout its rotation and each impact generates a burst of energy which propagates in the machine, from the bearing to the vibration transducer. The detection of such impacts is the signature of a defective bearing and is commonly realised in the spectral domain. However the occurrence time of the impacts is not periodic, even for a machine operating at constant speed, but is characterised by a random jitter. For this reason it is recognised that the squared envelope spectrum (SES) has to be preferred to spectral analysis for bearing diagnosis [1]. A problem with the SES is that vibration transducers gather vibrations from all the components of the machinery, including for example the gears, and therefore the SES presents several peaks and the results are difficult to analyse. Several envelope pre-processing techniques have been introduced to suppress unwanted components. One approach exploits the separation between the high resonant frequency of the impacts versus the lower gear meshing frequencies. Common methods include a high pass filter, a kurtosis maximising band-pass filter [2] or the calculation of the residual after time synchronous averaging (TSA), corresponding to a comb filter [3]. A different approach exploits the statistical difference between the deterministic

*Corresponding author
Email address: leo.barbini@bath.ac.uk (L. Barbini)

Preprint submitted to First World Congress on Condition Monitoring

components from gears versus the random component from the bearing, as in the discrete random separation (DRS) [4] and the cepstrum pre-whitening [5].
Recently Barbini et al. [6] proposed phase editing (PE) as a novel method to enhance the vibration component from a defective bearing, as a modification of a speech denoising algorithm [7]. PE uses the fact that the component from the bearing has a small amplitude compared to the masking components. It consists of a threshold in the amplitude of the spectral components, independent of their frequency or statistical properties: components with a spectral amplitude above a threshold are suppressed. Therefore the remaining signal contains the weak vibration from the defective bearing.
In this paper, PE is applied to vibration signals from machinery operating at varying speed, in contrast to the stationary signals analysed in previous work [6]. It is shown that PE is effective regardless of the non-stationary speed, as long as the signal exhibits separation in spectral amplitude between the unwanted components and the bearing component. The paper is organised as follows: section 1 presents the proposed methodology, section 2 shows a numerical example while section 3 presents results from the analysis of real operational data. Finally conclusions are presented in section 4.

2. Methods

For the vibration signal $x[k]$ with Fourier transform (FT) $\hat{x}[l]$ where $k, l \in \{0, \cdots, N-1\}$ are the indexes of time and frequency, the phase editing (PE) method consists of the calculation of the

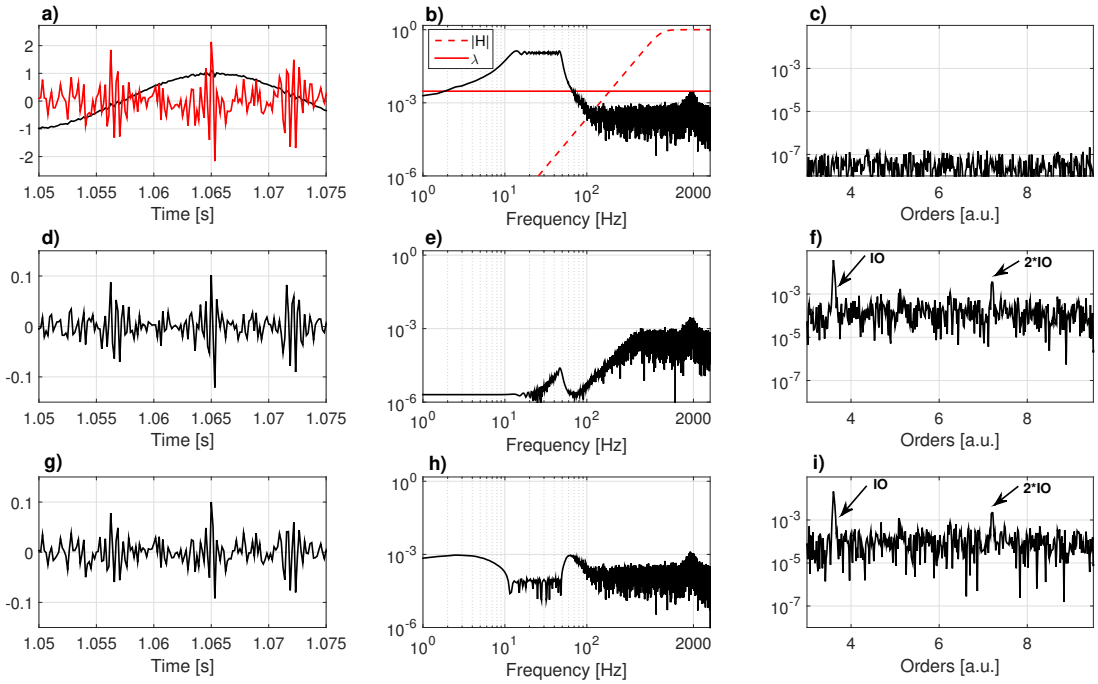

Figure 1: Numerical simulation. First row the original signal, second row the signal after high pass filtering, third row the signal after PE. First column time domain, second column amplitude spectra, third column SES after OT.

residual with its denoised version $p[k]$. The denoised signal is given by

$$p[k] = Real\left\{IFT\left\{|\hat{x}[l]|\, e^{\angle \hat{x}_L[l]}\right\}\right\} \tag{1}$$

where $\hat{x}_L[l] = \hat{x}[l] + L[l]$ and

$$L[l] = \begin{cases} +\lambda[l] & 0 \leq l < N/2 \\ -\lambda[N-1-l] & N/2 \leq l \leq N-1. \end{cases} \tag{2}$$

For each frequency index n PE returns a sinusoidal component [6]:

$$x_{pe,n}[k] = x_n[k] - Re\left\{p_n[k]\right\} = K[n]\frac{2\,|\hat{x}[n]|}{N} cos\left(\frac{2\pi}{N}nk + \angle\hat{x}[n] + \theta[n]\right) \tag{3}$$

The differences between the original sinusoid $x_n[k]$ and $x_{pe,n}[k]$ are the terms $K[n]$ and $\theta[n]$. In particular the term $K[n]$ vanishes [6] for $|\hat{x}[n]| \gg |L[n]|$ while is unitary for $|\hat{x}[n]| \ll |L[n]|$. Therefore PE suppresses all the spectral components with amplitude greater than a threshold, independently from the frequency index. The value of the threshold is defined by $\lambda[l]$ which is a function selected by the user and in the simplest case is a constant. However the threshold can also be chosen to suppress entire frequency bands of the signal as in a common filter.
Equation 3 is valid also in the case considered in this paper of a machine operating at varying speed and PE can be applied directly on the time non-stationary signal provided that $\lambda[l]$ is chosen as

$$\hat{x}_b[l] \ll \lambda[l] \ll \hat{x}_g[l] \tag{4}$$

Where $\hat{x}_b[l]$ and $\hat{x}_g[l]$ are the spectral amplitudes of the non-stationary vibrations from the bearing and from the gears. The approach of enhancing the bearing component directly from the time non-stationary signal avoids problems with the suppression of masking components after order tracking (OT)[8]. Recently this approach has been implemented using classical signal separation techniques such as band-pass filtering [9], spectral kurtosis and cepstral pre-whitening [10], while it is proposed using PE for the first time in this paper. Only after the enhancement of the bearing components the signal is subjected to OT and the SES is evaluated in the order domain. The envelope is calculated on the full band analytical representation of the signal and the SES is normalised as $\tilde{SES}[l] = SES[l]/SES[0]$, the tilde is omitted in the following. The selection of the best threshold is achieved maximising the peaks in the SES at the bearing characteristic fault orders by user inspection.
Therefore the proposed approach comprises in total three steps: PE the time non-stationary signal, re-sample the signal at constant angular increments using a tachometer signal (OT), evaluate the SES in order domain.

3. Numerical investigation

The proposed methodology is applied on a time non-stationary signal comprising a masking component, a sequence of impacts and background noise. The masking component is a chirp with frequency increasing linearly from 10 Hz to 50 Hz. The sequence of impacts has occurrence time at 3.57 orders of the chirp instantaneous frequency and a random jitter of 1%, and the resonant frequency is in the band $1700 - 2200$ Hz. Total length of the signal is 20 seconds and sampling

frequency 6.4 kHz. The amplitude of the chirp is ten times that of the sequence of impacts. Figure 1(a) shows the signal in time domain, in black the simulated signal comprising the three components, while in red the sequence of noisy impacts multiplied by a factor 10. Figure 1(b) shows the amplitude spectrum of the signal, with the disturbing chirp and the peak around the resonant frequency representing the random and time non-stationary sequence of impacts. Fig. 1(c) shows the normalised SES of the full band signal in the order domain after OT. As expected no peak at the impacts order (IO) is seen. In the simulated signal the resonant frequency band and the varying frequency of the chirp are separated, therefore a classical high-frequency filter is sufficient for the enhancement of the impacts. As an example this is done with a fourth order Butterworth filter of cut-off frequency 400 Hz. The amplitude response $|H[l]|$ of the filter is shown with the red dashed line in Fig. 1(b). Figure 1(d) shows the filtered signal in time domain, and Fig. 1(e-f) the amplitude spectrum and the SES after OT. The masking chirp is suppressed and the SES displays peaks at the IO and harmonic. We address the question whether similar results are achievable using the PE method.

Figure 1(b) displays the characteristic which is the key point for the application of PE: the separation in spectral amplitude between the disturbing components and the impacts for the time

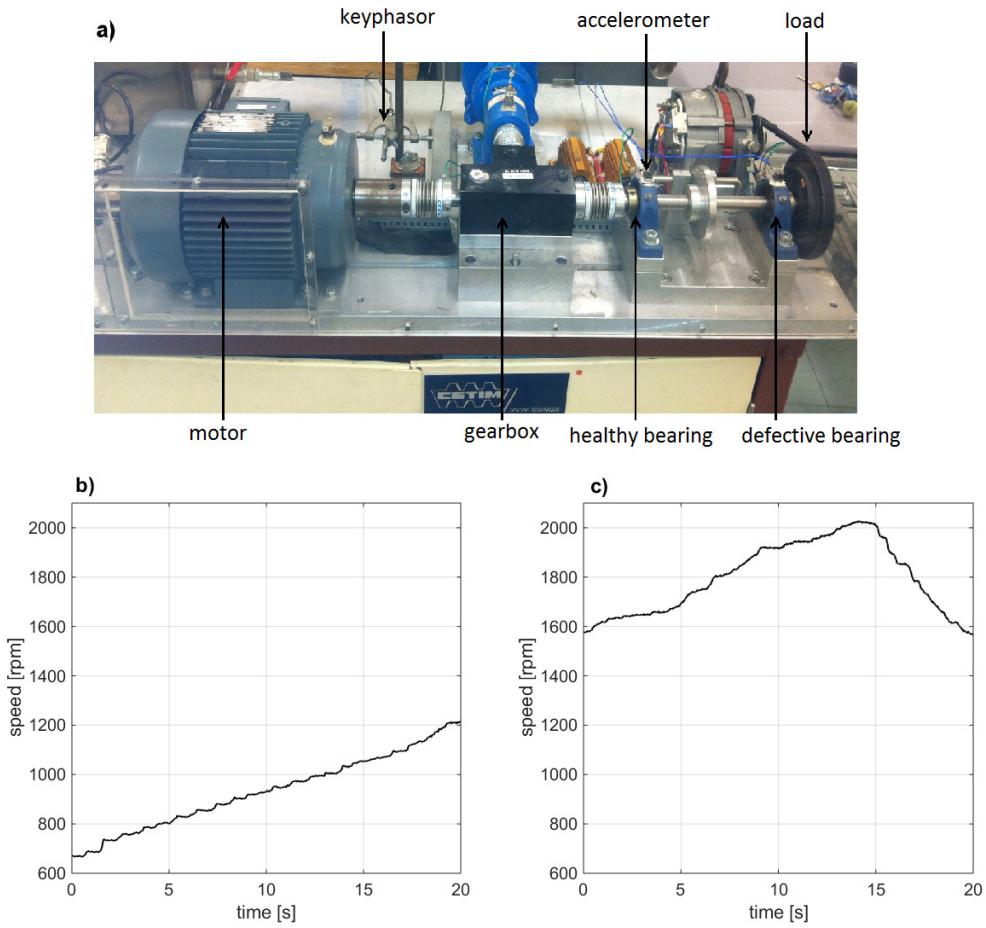

Figure 2: Photograph of the test rig (a). Run-up speed profile (b). Run-up and run-down speed profile (c).

non-stationary signal. Therefore the enhancement of the impacts can be achieved by a threshold in the spectral amplitudes and PE results are effective also for machinery operating at varying speed. In particular for the simulated signal it is sufficient to use a constant value for λ, as shown in Fig. 1(b) with the red line. The resulting phase edited signal is presented in Fig. 1(g-h-i) with impacts revealed in the SES at the IO and its harmonics. The amplitude spectrum of the PE signal, Fig. 1(h), displays the suppression of the spectral components above the selected threshold. Comparison with the high frequency filtered signal shows a good agreement as well as comparison with the noisy impacts in time domain, Fig. 1(a) in red.

4. Experimental investigation

4.1. Test rig & data sets

A photograph of the test rig is presented in Fig. 2(a). It consists of a variable speed asynchronous electric motor, a parallel spur-gear of ratio one, and an alternator applying a constant load. The shaft rotational speed is measured by a keyphasor mounted close to the motor. Two rolling elements bearings support the output shaft and the one far from the gearbox has an outer race defect with expected repetition of 3.04 orders (BPOO). An accelerometer mounted on the casing of the bearing close the gearbox is used as a vibration transducer.
Two varying speed profiles are analysed in this paper as shown in Fig. 2(b-c). The first one is a run-up profile with a doubling of the rpm, the second one a run-up and run-down of the motor. The recorded data sets are 20 s long and are sampled at 25.6 kHz. The Welch power spectra of

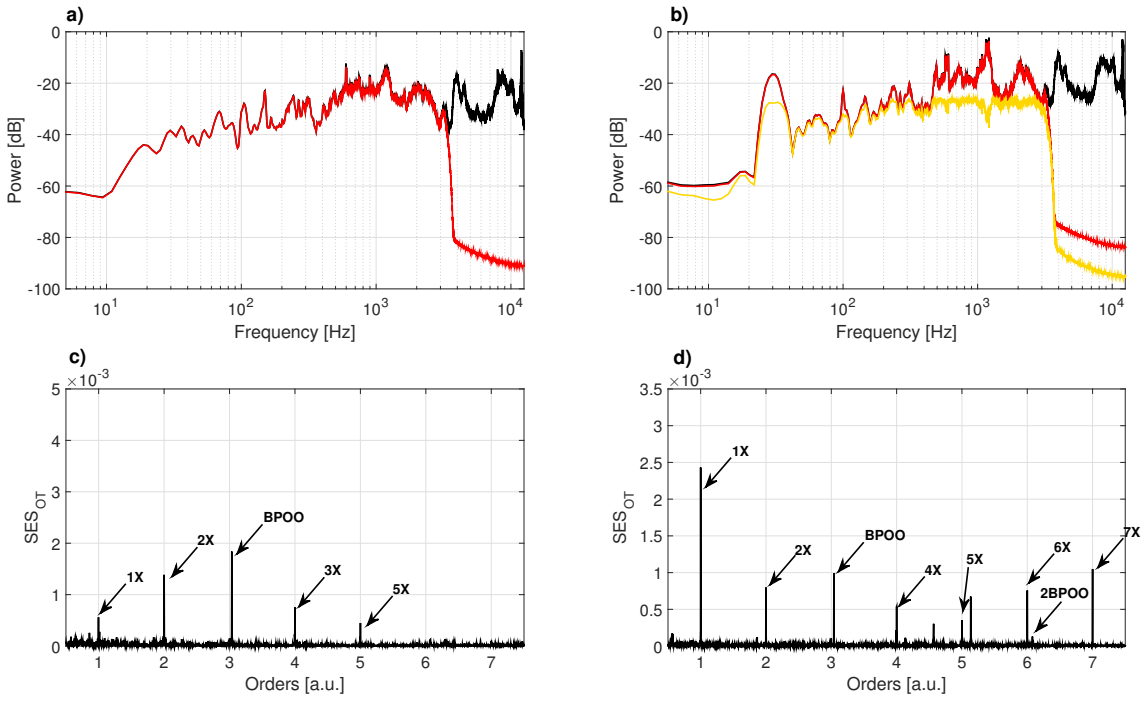

Figure 3: Welch power spectra for the run-up speed profile (a) and run-up run-down speed profile (b). In black raw signal and in red PE signal with α_1, in yellow PE signal with α_2. Squared envelope spectrum after OT the raw signals, run-up (c) run-up run-down (d)

the data sets are shown respectively in Fig. 3(a-b), black line, with Hamming window of 10000 samples and 50% overlapping.

4.2. Results

The speed variations for both cases are strong enough to smear out spectral peaks and the SES computed directly on the time non-stationary signals does not allow diagnosis. On the contrary after OT peaks appear in the SES as shown in Figure 3(c-d). Peaks at order 1 and harmonics correspond to vibrations from the gearbox while at orders 3.04 and harmonics correspond to impacts from the defective bearing. In both cases despite the peak at the characteristic defective bearing frequency, the diagnosis could be misleading due to the presence of the vibrations from the gearbox, particularly for the closeness of the BPOO and 3X. Therefore PE is applied for the suppression of the unwanted peaks.

For the analysed data the resonant frequency of the bearing appears in a band around 2000 kHz while vibrations from the gears occur at higher frequencies [11]. For this reason a logistic function was chosen as the threshold for PE, akin to low pass filtering:

$$\lambda[l] = \alpha \left(1 - \frac{1}{1 + e^{-\beta(v[l]-1)}}\right) \tag{5}$$

where α is the value above which the spectral amplitudes are suppressed and β controls the steepness of the curve. The vector $v[l]$ linearly increases from 0 to r, where r selects the cutoff frequency. Substitution of Eq. 5 in Eq. 2 gives the anti-symmetric threshold function $L[l]$ as shown in Fig. 4, with $r = 4$ and $\beta = 20$.

Firstly the high frequency components are suppressed to check whether the detection is enhanced. In Eq. 5 parameters are chosen as $\alpha_1 = max\{|\hat{x}[l]|\}$ and $r = 4$ so that PE acts similarly to a low pass filter with cut off frequency of $3200Hz$. Figure 3(a-b) in red shows the Welch power spectra of the time non-stationary PE edited signals. As expected the low frequency amplitudes coincide with the original, in black. The edited signals are subjected to OT and the SES are computed. The corresponding SES are shown in figure 3(a-b) respectively for the run-up case and the run-up run-down case. The suppression of the high frequency components removes all the unwanted peaks from the SES for the first speed profile, compared to Figure 3(c). On the other hand for the second

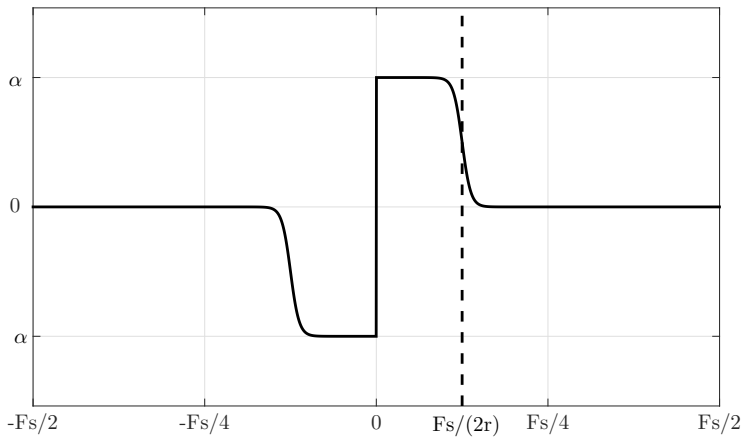

Figure 4: Threshold function $L[l]$ for $\lambda[l]$ with $\beta = 20$ and $r = 4$.

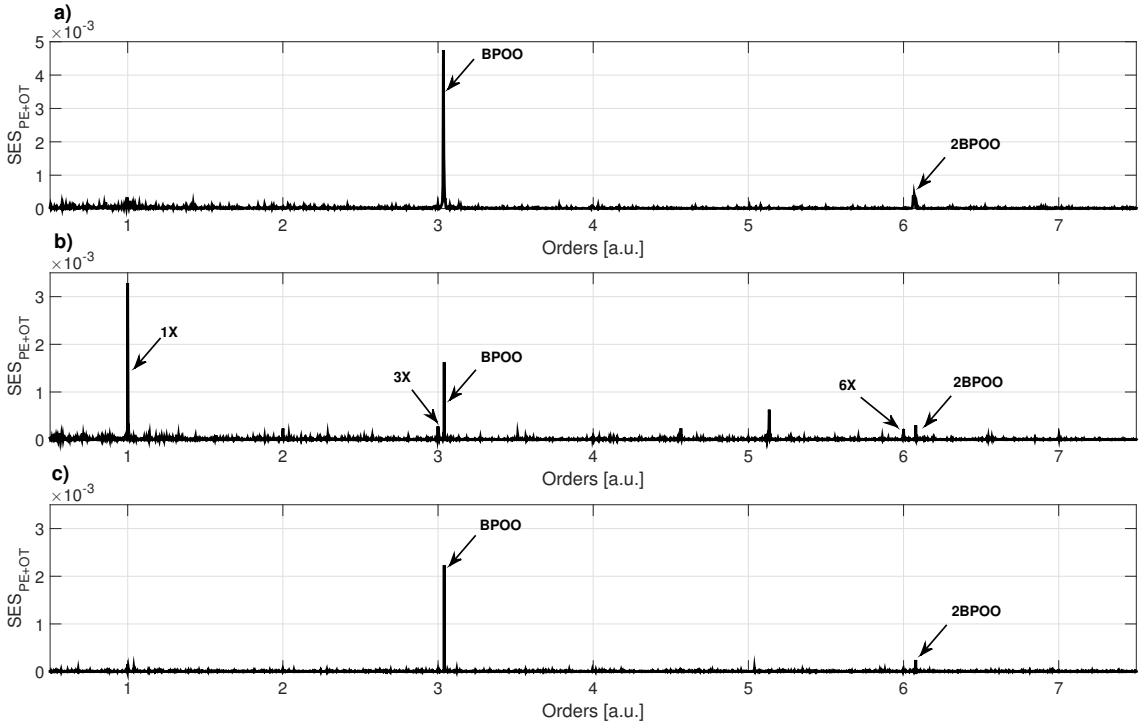

Figure 5: Squared envelope spectrum after PE with α_1 followed by OT, for run-up (a) and run-up run-down speed profile (b). PE with α_2 for run-up run-down (c).

speed profile, peaks are still present other than the BPOO and its harmonics. These peaks can be suppressed by exploiting the separation in amplitude between gears and bearing components. The value of the parameter α in Eq. 5 is decreased so that PE implements simultaneously a threshold in the spectral amplitudes and a low pass filter. Figure 3(c) in yellow shows the Welch power spectrum of the resulting PE signal with $\alpha_2 = 0.07\ max\{|\hat{x}[l]|\}$. The SES computed after performing OT on the PE signal is shown in Fig. 5(c). The unwanted peaks are removed, compared to Figure 3(d), leaving only the BPOO and its harmonic.

5. Conclusion

This paper tested the effectiveness of phase editing (PE) as an envelope pre-processing method to enhance the diagnosis of defective bearings from a machine operating in non-stationary speed conditions. The procedure consists of applying PE to the time non-stationary signal, order tracking the edited signal, and finally computing the SES. The performance was tested both on a simulated signal and on experimental data.

PE implements a threshold on the amplitude of spectral components. It was shown that if there is separation between spectral amplitudes, PE works irrespective of the stationary/non-stationary properties of the signal. It was also shown that the threshold function used for the PE can be selected to obtain a combination of frequency filtering and suppression of components with higher spectral amplitudes.

References

[1] R. B. Randall, J. Antoni, S. Chobsaard, The relationship between spectral correlation and envelope analysis in the diagnostics of bearing faults and other cyclostationary machine signals, Mechanical systems and signal processing 15 (5) (2001) 945–962.

[2] J. Antoni, R. Randall, The spectral kurtosis: application to the vibratory surveillance and diagnostics of rotating machines, Mechanical Systems and Signal Processing 20 (2) (2006) 308–331.

[3] R. B. Randall, Vibration-based condition monitoring: industrial, aerospace and automotive applications, John Wiley & Sons, 2011.

[4] J. Antoni, R. Randall, Unsupervised noise cancellation for vibration signals: part iia novel frequency-domain algorithm, Mechanical Systems and Signal Processing 18 (1) (2004) 103–117.

[5] N. Sawalhi, R. B. Randall, Signal pre-whitening for fault detection enhancement and surveillance of rolling element bearings, in: The Eighth International Conference on Condition Monitoring and Machinery Failure Prevention Technologies, Cardiff, Wales, UK, June, 2011, pp. 19–22.

[6] L. Barbini, A. P. Ompusunggu, A. Hillis, J. du Bois, A. Bartic, Phase editing as a signal pre-processing step for automated bearing fault detection, Mechanical Systems and Signal Processing 91 (2017) 407–421.

[7] K. Wójcicki, M. Milacic, A. Stark, J. Lyons, K. Paliwal, Exploiting conjugate symmetry of the short-time fourier spectrum for speech enhancement, IEEE Signal processing letters 15 (2008) 461–464.

[8] D. Abboud, M. Eltabach, J. Antoni, S. Sieg-Zieba, Envelope pre-processing techniques for rolling element bearing diagnosis in variable speed conditions, International Journal of Condition Monitoring 6 (2) (2016) 27–32.

[9] P. Borghesani, R. Ricci, S. Chatterton, P. Pennacchi, A new procedure for using envelope analysis for rolling element bearing diagnostics in variable operating conditions, Mechanical Systems and Signal Processing 38 (1) (2013) 23–35.

[10] R. Randall, Vibration-based diagnostics of gearboxes under variable speed and load conditions, Meccanica 51 (12) (2016) 3227–3239.

[11] D. Abboud, S. Baudin, J. Antoni, D. Rémond, M. Eltabach, O. Sauvage, The spectral analysis of cyclo-non-stationary signals, Mechanical Systems and Signal Processing 75 (2016) 280–300.

4.5 Summary

This chapter introduced Phase Editing (PE) as a novel signal processing method for enhancing the detection of a defective bearing from a vibration signal, PE was previously used in speech denoising while here it for the first time applied to vibration signals. Its mathematical formulation was thoroughly discussed in Section 4.2, showing that from a theoretical point of view PE accomplishes the objectives detailed in Section 1.4 extremely well, being intuitive, of low computational complexity and effective on both cyclo-stationary and cyclo-non-stationary signals.

The method was then implemented in an automated way, with no need for supervision by an expert user. Its performance was tested on numerical simulated signals and experimental data, from different types of machines operating both at stationary and varying speed, respectively in Section 4.2 and Section 4.4. The machines contained defective bearings with different types of faults, in the inner race, outer race and rolling element. PE performed well in the enhancement of the weak vibrations from the defective bearings masked by the strong vibrations from the gears and in comparison to state of the art techniques, provided a 10% improvement in detection capability. Furthermore it was recognised that missed detection occurred in the case of low operating speeds of the machine, as shown in Section 4.3. Specifically PE detected the defective bearings mounted on shafts rotating at speeds above 3 Hz. This suggests that missed detection is caused by the use of accelerometers as vibration transducers, rather than the specific signal processing method, for instance the literature advises the use of acoustic emission sensors for condition monitoring of machines operating at slow speeds, as discussed in Section 1.3.4.

The data used in this chapter were collected from laboratory setups of relatively simple complexity and despite the excellent results obtained here, PE has to be tested on data from real world machines. This situation will be investigated in the next Chapter, which introduces a novel signal processing method based on PE and applies it to data from complex machines.

Chapter 5

Novel technique: amplitude - cyclic frequency decomposition

Nomenclature			
$\boldsymbol{x[k]}$	raw signal in time domain	$\boldsymbol{x_{AD}[k,l]}$	amplitude-cyclic frequency decomposition
$\boldsymbol{\hat{x}[j]}$	Fourier transform of raw signal	$\boldsymbol{p[k]}$	phase edited signal
$\boldsymbol{N_l}$	number of threshold levels	$\boldsymbol{\hat{x}_{m,M}}$	min,max of $\lvert\hat{x}[j]\rvert$
$\boldsymbol{\lambda}$	threshold level	$\boldsymbol{SES_{AD}[m,l]}$	squared envelope spectrum of $x_{AD}[k,l]$
$\boldsymbol{g[k]}$	vibrations from gears	$\boldsymbol{b[k]}$	vibrations from bearing
$\boldsymbol{A_r}$	amplitude of meshing	$\boldsymbol{f_{sh}}$	shaft frequency
$\boldsymbol{n_t}$	number of teeth	$\boldsymbol{g}$	harmonic order of amplitude modulation
$\boldsymbol{r}$	harmonic order of meshing	$\boldsymbol{B_{rg}}$	amplitude of amplitude modulation
$\boldsymbol{T_{bd}}$	occurrence time of impacts	$\boldsymbol{\tau_p}$	random time jitter of p^{th} impact
$\boldsymbol{BPOO}$	ball pass order outer race	$\boldsymbol{DSES_{x_{AD}}[m]}$	decomposition sqaure envelope spectrum
$\boldsymbol{BPOI}$	ball pass order inner race	$\boldsymbol{CO}$	cage order
$\boldsymbol{L[j]}$	asymmetric threshold vector	$\boldsymbol{\gamma[j]}$	threshold function

5.1 Introduction

This chapter introduces a method to decompose a vibration signal into a two dimensional map showing the cyclic content calculated on a set of threshold levels of the amplitude spectrum: Amplitude-cyclic frequency Decomposition (AD). The method is implemented using Phase Editing and uses the same principle of separating vibrations from different mechanical components of the machine based on their amplitude rather than their spectral frequency. AD is the direct extension of PE, with the advantage of

showing the cyclic content on all the calculated thresholds, thus with no need for the selection of the best level. For instance, in the previous chapter the selection was implemented through an automated method which maximises features calculated on the squared envelope spectrum and it needs vibration signals collected when the machine is in healthy conditions. In addition the performance of PE was tested in the previous chapter using data sets coming from relatively simple experimental setups. Here the AD will be tested on vibration signals from complex machinery, such as a wind turbine gearbox and a civil engine aircraft, thus proving the effectiveness of PE on real world scenarios.
In the literature the only method which offers a type of analysis comparable to that of AD is the Spectral Correlation (SC), as introduced in Section 1.3.3. SC similarly decomposes the signal into a two dimensional map, but in this case it shows the cyclic content contained in a set of spectral frequency bands. The two methods differ from a theoretical point of view, but as shown in the following, the resulting two dimensional maps are highly comparable and offer the same detection capabilities in all the analysed data sets. However the proposed AD has a lower computational complexity resulting in a faster implementation.
The chapter is organised as follows. Section 5.2 describes the experimental setup from which vibration data will be analysed. Section 5.3 introduces the methodology, tests it both on numerical simulated signals and real world data and compares it with the SC. Section 5.3 is reproduced from the author's published work in the journal Mechanical Systems and Signal Processing [Barbini et al., 2017b]. Section 5.4 addresses the computational cost of AD and finally Section 5.5 shows two cases of missed detection of a defective bearing.

5.2 Experimental setups

This section describes two of the three experimental setups from which vibration data is analysed in Section 5.3, the third experimental setup is from Centre Technique des Industries Mécaniques (CETIM) and it was already described in Section 3.2.

Wind turbine gearbox

The data on the wind turbine gearbox were provided by the National Renewable Energy Laboratory (NREL) of the United States. The data were collected under the wind turbine gearbox condition monitoring round robin study [Sheng, 2012]. Figure 5.1

shows the configuration of the turbine drive train, with the gearbox in blue. The turbine has a rated power of 750 kW. Figure 5.2 shows the details of the components of the gearbox and Figure 5.3 the schematics with corresponding number of teeth of the gears. The gearbox comprises on the downwind side a low speed planetary stage and on the upwind side two parallel stages. The planetary stage is connected to the intermediate speed stage and the high speed stage is connected to the generator. The complete drive train was first installed in the NREL dynamo-meter test facility and run-in. Later it was sent to a wind farm for field testing. In the field test, it experienced two loss of oil events that damaged its internal bearings and gear elements. At this point it was brought back to the dynamo-meter test facility and run under controlled loading conditions, in order to avoid catastrophic failure of the gearbox. After collection of data for condition monitoring purposes, the turbine was disassembled and a failure analysis was conducted on the gearbox [Errichello and Muller, 2012]. The analysis found four defective bearings, respectively A, B, C and D in Figure 5.3. The four bearings presented the following defects:

1. A dents on the outer race and possible damage due to assembly error
2. B overheating on the inner race
3. C dents and scuffing on the inner race and possible damage due to assembly error
4. D scuffing, polishing and fretting corrosion on the outer race.

In addition, the gear of the parallel stage presented scuffing, the gear of the intermediate stage presented fretting corrosion, scuffing and polishing wear. The annulus of the planetary stage presented scuffing, polishing and fretting corrosion.

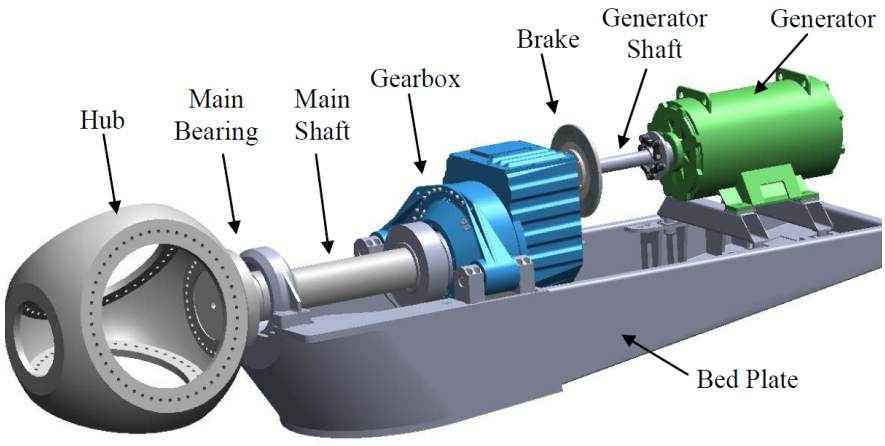

Figure 5.1: Wind turbine drive train, reproduced from [Sheng, 2012]

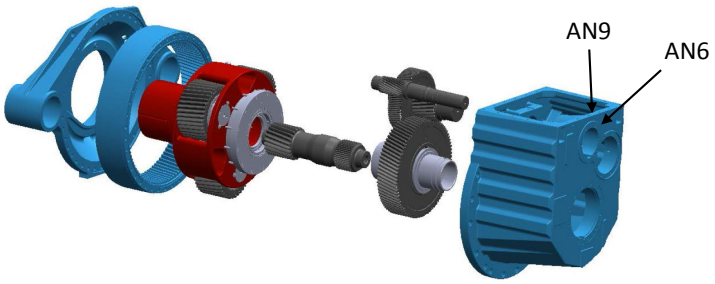

Figure 5.2: Wind turbine gearbox components, reproduced from [Sheng, 2012]

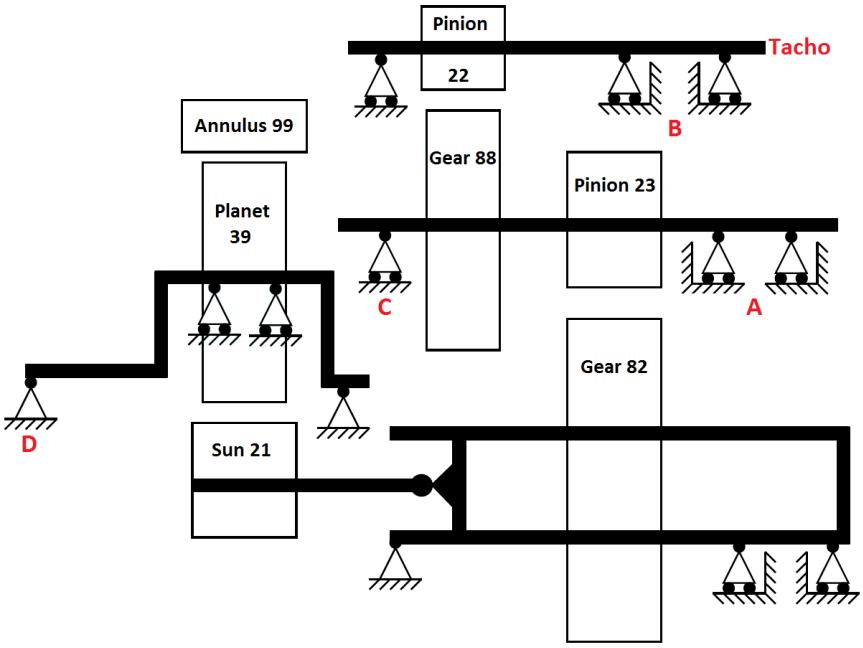

Figure 5.3: Schematic of wind turbine gear box with number of teeth and locations of defective bearings

Vibration data was collected by 8 piezoelectric accelerometers IMI 622B01 and Figure 5.2 shows the locations of the sensors AN6 and AN9 used in the analysis of Section 5.3. Both the sensors are placed on the downwind side of the gearbox: AN6 radially on the intermediate speed shaft and AN9 radially on the high speed shaft. Data sets are 1 minute long and the sampling rate is 40 kHz. Finally, a tachometer was placed on the high speed shaft to measure the rotational speed, as shown in Figure 5.3. For all the length of the measurement the speed was kept constant at 30 Hz with small variations.

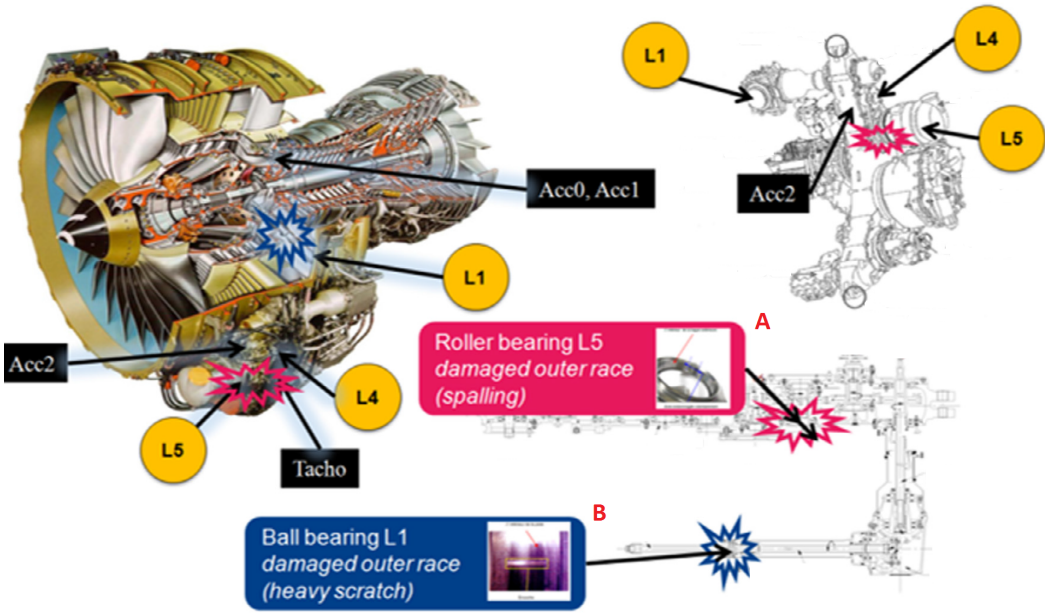

Figure 5.4: General overview of the aircraft engine and the accessory gearbox, reproduced from [Antoni et al., 2017a]

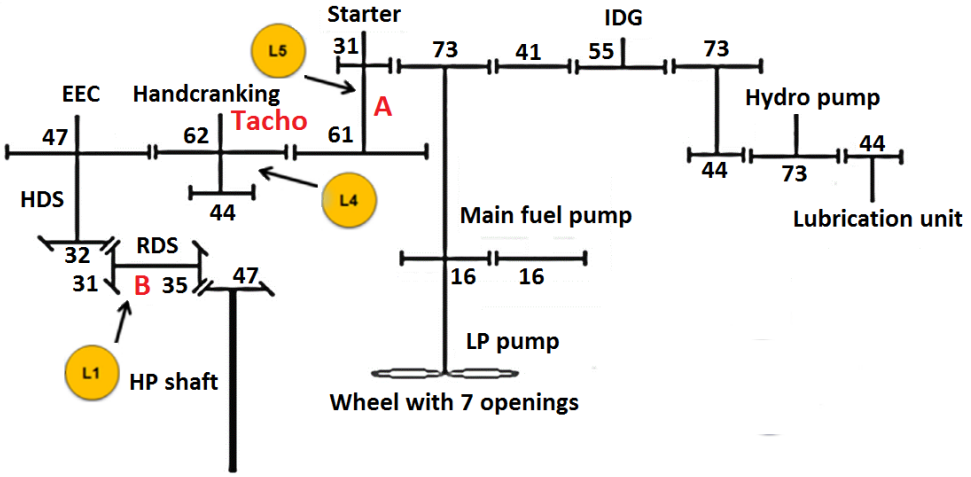

Figure 5.5: Schematic of the aircraft accessory gearbox, with locations of defective bearings. Reproduced from [Antoni et al., 2017a]

Aircraft engine

The data on the aircraft engine was provided by Safran for the 8^{th} Conference Surveillance held in Roanne, France, October 2015 [Safran, 2017]. The data were collected during a ground test on a civil aircraft engine which comprises two main shafts and an

accessory gearbox with equipment such as pumps, starter, Integrated Drive Generator (IDG) and Electronic Engine Control (EEC) alternator. The general overview of the engine is shown in Figure 5.4, while Figure 5.5 shows the schematics of the gearbox. The gearbox is linked to the High Pressure (HP) shaft by a Radial Drive Shaft (RDS) and a Horizontal Drive Shaft (HDS). Two defective bearings are present on the shafts L5 and L1 and in the analysis of Section 5.3 they are respectively A and B. The defect on bearing A is a wide spalled area on the outer race, in a sector of 32° along all the functional line of the race, with a depth of approximately 0.1 mm. While the defect on bearing B the defect is a scratch on the outer race with a depth of about 0.3 mm and a width of about 1 mm [Antoni et al., 2017a]. Vibration data were collected by means of three accelerometers, as shown in Fig. 5.4. Acc0 and Acc1 are located near the RDS and Acc2 is located on the flange of the accessory gearbox, in the vicinity of shaft L5. The data is acquired[1] at 50 kHz for a total length of 200 s while the engine is performing an acceleration from idle to full power and the speed was recorded by a tachometer placed on the shaft L4 as shown in Fig. 5.5. Figure 5.6 shows the non stationary speed reconstructed from the tachometer signal.

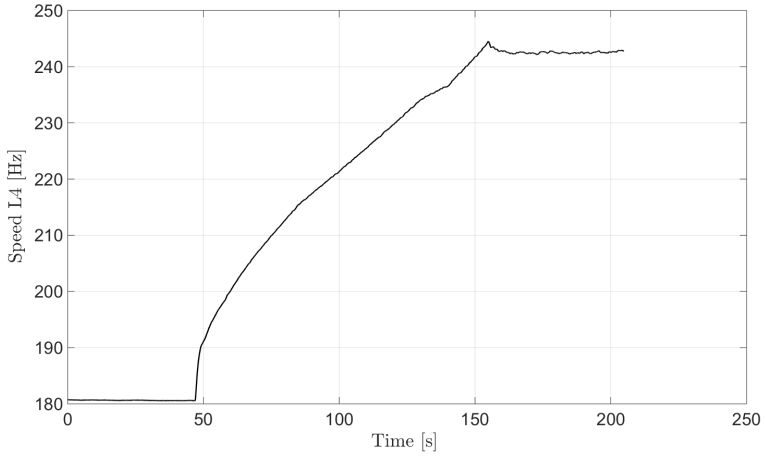

Figure 5.6: Instantaneous rotational speed of the shaft L4 of the aircraft engine

[1]Please notice that the data downloaded from the supplementary material of [Antoni et al., 2017a] is in mp3 format and has a sampling rate of 44.1 kHz and a total length of 204.8 s

5.3 Amplitude-cyclic frequency decomposition of vibration signals for bearing fault diagnosis based on phase editing

Article published in the journal Mechanical Systems and Signal Processing, [Barbini et al., 2017b]

Statement of contributions of joint authorship

L. Barbini (candidate): writing and compilation of manuscript, established methodology, data analysis, preparation of tables and figures. Presented results at the conference.

M. Eltabach : provided analysed data set, editing and co-author of manuscript.

A. Hillis : editing and co-author of manuscript.

J. L. du Bois (principal supervisor): supervised and assisted with manuscript compilation, editing and co-author

Copyright

Amplitude-cyclic frequency Decomposition of vibration signals for bearing fault diagnosis based on phase editing

L. Barbini[a,*], M. Eltabach[b], A. J. Hillis[a], J. L. du Bois[a]

[a] *The University of Bath Department of Mechanical Engineering, Claverton Down, Bath, BA2 7AY, UK*
[b] *Centre Technique des Industries Mécaniques, Félix-Louât, Senlis 60300, France*

Abstract

In rotating machine diagnosis different spectral tools are used to analyse vibration signals. Despite the good diagnostic performance such tools are usually refined, computationally complex to implement and require oversight of an expert user. This paper introduces an intuitive and easy to implement method for vibration analysis: amplitude cyclic frequency decomposition. This method firstly separates vibration signals accordingly to their spectral amplitudes and secondly uses the squared envelope spectrum to reveal the presence of cyclostationarity in each amplitude level. The intuitive idea is that in a rotating machine different components contribute vibrations at different amplitudes, for instance defective bearings contribute a very weak signal in contrast to gears. This paper also introduces a new quantity, the decomposition squared envelope spectrum, which enables separation between the components of a rotating machine. The amplitude cyclic frequency decomposition and the decomposition squared envelope spectrum are tested on real word signals, both at stationary and varying speeds, using data from a wind turbine gearbox and an aircraft engine. In addition a benchmark comparison to the spectral correlation method is presented.

Keywords: phase editing, diagnostics of defective bearings, spectral correlation, enhanced squared envelope spectrum, variable speed

1. Introduction

In a rotating machine when a rolling element bearing has a defect it does not operate smoothly but produces a series of impacts throughout its rotation. The impacts generate vibrations which propagate through the machine from the bearing to the vibration transducer. Diagnosis of a defective bearing is subject to the observation of such vibrations. The literature on signal processing methods for the ad-hoc treatment of vibrational signals is abundant, as are mathematical models for the expected vibrations from defective bearings [1, 2]. In particular it is commonly accepted that the signal from a defective bearing is cyclostationary and that the most appropriate tool for its analysis is Spectral Correlation (SC). Specifically [3] shows that the integral over all spectral frequencies of the SC is equivalent to the spectrum of the squared envelope, therefore it is related to the high resonant frequency technique [4]. Recently Antoni et al. [5] introduced an algorithm for the fast computation of the SC. The algorithm was successfully used to detect faulty bearings

*Corresponding author
Email address: L.Barbini@bath.ac.uk (L. Barbini)

on machines operating both at stationary and non-stationary speeds.
The SC achieves detection of a defective bearing exploiting two aspects of a vibrational signal, namely its statistical properties and the separation of the vibrations in spectral frequency. The first aspect uses the presence of peaks in the cyclic domain for a series of impacts from the defective bearing. The latter exploits the fact that vibrations from different components of the machine occupy different spectral bands. Usually gears contribute peaks at low frequencies versus the high resonant frequencies excited by the impacts from a defective bearing. The combination of these two aspects in the SC allows detection of the defective bearing without any preceding steps for suppression of vibrations from gears or other unwanted components. Therefore a 2-dimensional decomposition simplifies, conceptually and practically, the usual procedure of first pre-processing the vibration signal and afterwards calculating the Squared Envelope Spectrum (SES) [6].
This paper introduces a novel method to decompose a vibrational signal in a 2-dimensional map. The method is implemented using Phase-Editing (PE) [7] to threshold spectral amplitudes at different levels. It exploits the fact that components of a vibrational signal can be separated according to their amplitudes independently from their frequency in the spectrum. For instance, in the case of a small defect on a bearing, vibrations from the gears contribute a series of high amplitude peaks, while the impacts from the bearing contribute a low amplitude resonance around the excited resonant frequency. The SES is then calculated for each threshold level, in order to observe peaks in the cyclic domain. Therefore the proposed method decomposes the vibrational signal in a 2-dimensional map of which the characteristic dimensions are: the spectral amplitude level up to which the signal has been thresholded and its corresponding cyclic content. The name of the proposed method is Amplitude-cyclic frequency Decomposition (AD).
Differently from phase editing [7], AD does not require the optimisation step for the selection of the best threshold level, in addition the 2-dimensional map allows the simultaneous visualisation of the cyclic content of vibrations from gears and bearings at different spectral amplitudes. The method does not require any pre-processing of the vibration signal and it can be applied also to machines operating at non-stationary speeds. Only one parameter has to be tuned, namely the number of thresholds. In addition the computational cost for each threshold level of the AD consists of four computations of the fast Fourier transform of the vibration signal. For these reasons AD is well suited for an automated detection scheme.
The paper is structured as follows: Section 2 introduces the method and, by means of a numerical simulation, compares the performance of AD with that of SC. Section 3 presents the results of AD applied to three experimental data sets: a laboratory set-up characterised by largely varying speed, a wind turbine gearbox, and a civil aircraft engine. Comparison with the results obtained from SC is presented for the three cases. Section 4 draws some conclusions.

2. Methods

This section shows how to obtain the amplitude-cyclic frequency decomposition of the raw vibration signal $x[k]$, with Fourier transform $\hat{x}[j]$ where $k, j = \{0, \cdots, N_k - 1\}$ are the indices in the time and frequency domains, respectively.
Firstly $x_{AD}[k, l]$ is computed using the phase editing method to threshold $|\hat{x[j]}|$ at N_l levels [7]:

$$x_{AD}[k, l] = x[k] - \text{Real}\left(p^{(l)}[k]\right). \tag{1}$$

where $l = \{0, \cdots, N_l - 1\}$ is the index of the threshold level and $p^{(l)}[k]$ is the phase edited vector obtained for the l level. For each level the phase editing method suppresses spectral components

with amplitude smaller than the selected threshold and can be seen as a denoising procedure. This is achieved rotating in the complex plane pairs of conjugate vectors of $\hat{x}[j]$. The degree of rotation is defined by the ratio between the amplitude of the vector and the value of the threshold level. Specifically, if the conjugate vectors have an amplitude smaller than the threshold they are significantly rotated, while in the opposite scenario, the vectors are rotated of a small quantity. As a final step the Inverse Fourier Transform (IFT) is calculated on this modified spectrum, adding pairs of complex vectors which cancel out or reinforce accordingly to the degree of rotation. The result of this operation is a denoised complex signal in the time domain of which the real part only is retained. Following this procedure, in Eq. (1) $p^{(l)}[k]$ is defined as the IFT of the modified amplitude spectrum of the raw vibration signal:

$$p^{(l)}[k] = \text{IFT}\left\{\hat{p}^{(l)}[j]\right\} = \text{IFT}\left\{|\hat{x}[j]| \exp\left\{i\angle\left(\hat{x}[j] + L^{(l)}[j]\right)\right\}\right\} \tag{2}$$

where $L^{(l)}[j]$ is the threshold vector for the level l. In Eq. (2) $L^{(l)}[j]$ is an antisymmetric vector:

$$L^{(l)}[j] = \begin{cases} +\lambda^{(l)} & 0 \leq j < N_k/2 \\ -\lambda^{(l)} & N_k/2 \leq j \leq N_k - 1 \end{cases} \tag{3}$$

where for each l the constant $\lambda^{(l)}$ is found in an automated way from $\hat{x}[j]$:

$$\lambda^{(l)} = \hat{x}_M \left(\frac{\hat{x}_m}{\hat{x}_M}\right)^{l/(N_l-1)} \tag{4}$$

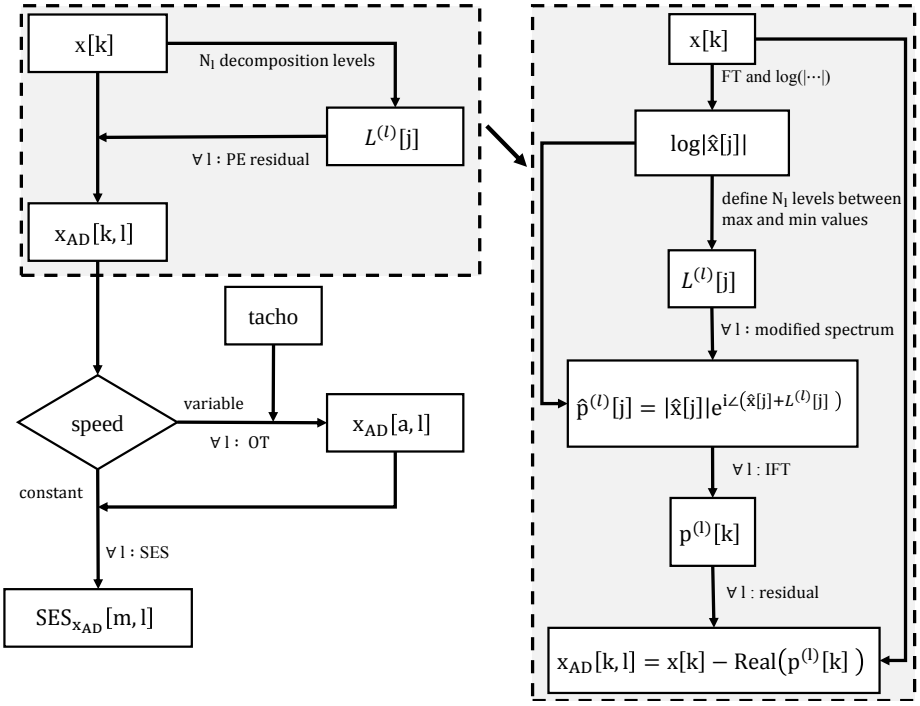

Figure 1: Scheme of proposed method for the Amplitude-cyclic frequency Decomposition (AD).

with $\hat{x}_M = \max_{0 \le j < N_k/2} \{|\hat{x}[j]|\}$ and $\hat{x}_m = \min_{0 \le j < N_k/2} \{|\hat{x}[j]|\}$.
Barbini et al. in [7] showed that in the case of a single threshold level, for each frequency index $j = n \le N_k/2$, PE returns the sinusoidal component:

$$x_{pe,n}[k] = x_n[k] - \text{Real}\{p_n[k]\} = K[n]\frac{2\,|\hat{x}[n]|}{N} cos\left(\frac{2\pi}{N}nk + \angle\hat{x}[n] + \theta[n]\right) \tag{5}$$

where the differences with the original sinusoid $x_n[k]$ are the terms $K[n]$ and $\theta[n]$, representing the gain and phase modifications, respectively. In particular,

$$\begin{array}{ll} K[n] \simeq 0, & |\hat{x}[n]| \gg |L[n]| \\ K[n] \simeq 1, & |\hat{x}[n]| \ll |L[n]|. \end{array} \tag{6}$$

Equations (5) and (3) are valid for all the N_l threshold levels of Eq. (4). Therefore $x_{AD}[k,l]$ of Eq. (1) is interpreted as N_l vibration signals from which are systematically removed components with spectral amplitude above a threshold logarithmically decreasing from $\hat{x}_M$ to $\hat{x}_m$. For instance $x_{AD}[k,0]$ is equivalent to the original vibration signal and $x_{AD}[k,N_L-1]$ can be interpreted as being similar to the cepstral pre-whitened signal [8] where instead of unity, the spectral amplitude is $\hat{x}_m$. As a final step the squared envelope spectrum is computed, giving the $SES_{x_{AD}}[m,l]$, with $m = \{0,\cdots,N_k-1\}$ the index in the cyclic order domain. The envelope is calculated as the absolute value of the analytical representation of the signal. For each l the SES is normalised according to $\tilde{SES}_{x_{AD}}[m,l] = SES_{x_{AD}}[m,l]/SES_{x_{AD}}[0,l]$, and henceforth the tilde ($\tilde{}$) is omitted. The above methodology is applied as described to a time stationary signal. For time non-stationary signals order tracking (OT) is required. Specifically in the case of large speed variations [9] shows that separation of vibrations from the gears and from the defective bearing should be performed directly on the time non-stationary signal, before order tracking (OT). This paper deals with non-stationary signals in a similar manner, computing OT after the thresholding in the spectral amplitude domain. Eq. (5) is also valid for frequency components in the case of non-stationary speeds, therefore OT is computed for each of the N_L vectors of $x_{AD}[k,l]$ yielding $x_{AD}[a,l]$ where $a = \{0,\cdots,N_k-1\}$ is the index in the angle domain. Finally the $SES_{x_{AD}}[m,l]$ is calculated from $x_{AD}[a,l]$.
A schematic depicting the proposed methodology is shown in Fig.1.

2.1. Numerical investigation

This section presents the performance of $SES_{x_{AD}}[m,l]$ on a numerically simulated signal. The signal is the superposition of three components. It comprises vibrations from a defective gear

Gear	Value	Bearing	Value	Noise	Value
f_{sh}	8 [Hz]	T_{bd}	58.10 [ms]	$\text{E}\{n[k]\}$	0 [a.u.]
n_t	33 [a.u.]	$\text{E}\{\tau_p\}$	0 [s]	$\text{E}\{n[k]\}^{1/2}$	0.65 [a.u.]
r	[7, 8, 9]	$\text{E}\{\tau_p^2\}^{1/2}$	2.50 [ms]		
g	[1, 2]	a	2.00 [ms]		
A_r	[1, 2, 1]	f_1	1.70 [kHz]		
B_{rg}	$\begin{bmatrix} 0 & 0 \\ 0.5 & 0.25 \\ 0 & 0 \end{bmatrix}$	f_2	2.70 [kHz]		

Table 1: Values used in the numerical simulation.

$g[k]$ from a defective bearing $b[k]$ and Gaussian noise $n[k]$.
The defective gear has n_t teeth and rotates at f_{sh} contributing vibrations of the form:

$$g[k] = \sum_r A_r \cos\left(2\pi r f_{sh} n_t \frac{k}{Fs}\right)\left[1 + \sum_g B_{rg} \cos\left(2\pi g f_{sh} \frac{k}{Fs}\right)\right] \tag{7}$$

where $f_{sh} n_t = f_{mg}$ is the meshing frequency and the values of $r,\ A_r\ g,\ B_{rg}$ depend on the defect. In contrast to [10], Equation (7) includes only amplitude modulations and the phases of all the sinusoids are set to zero.
The defective bearing contributes a series of impulses occurring every T_{bd} plus a random jitter τ_p:

$$b[k] = m[\tilde{k}] * \left[\sum_p \delta\left(\frac{k}{Fs} - pT_{bd} - \tau_p\right)\right] \tag{8}$$

where $*$ is the convolution operator and $m[k]$ represents the excited waveform equal for all the impacts, with $\tilde{k} = \left\{0, \cdots, N_{\tilde{k}} - 1 = T_{bd} Fs\right\}$. The excited waveform is a colored noise decaying exponentially:

$$m[\tilde{k}] = \left(w[\tilde{k}] * h[\tilde{k}]\right) e^{-\tilde{k}/(aFs)} \tag{9}$$

where $a < T_{bd}$ to ensure temporal separation between successive impacts, $w[\tilde{k}]$ is a Gaussian noise and $h[\tilde{k}]$ is a second order band pass filter of cut-off frequencies $f_1,\ f_2$. In contrast to [3] the

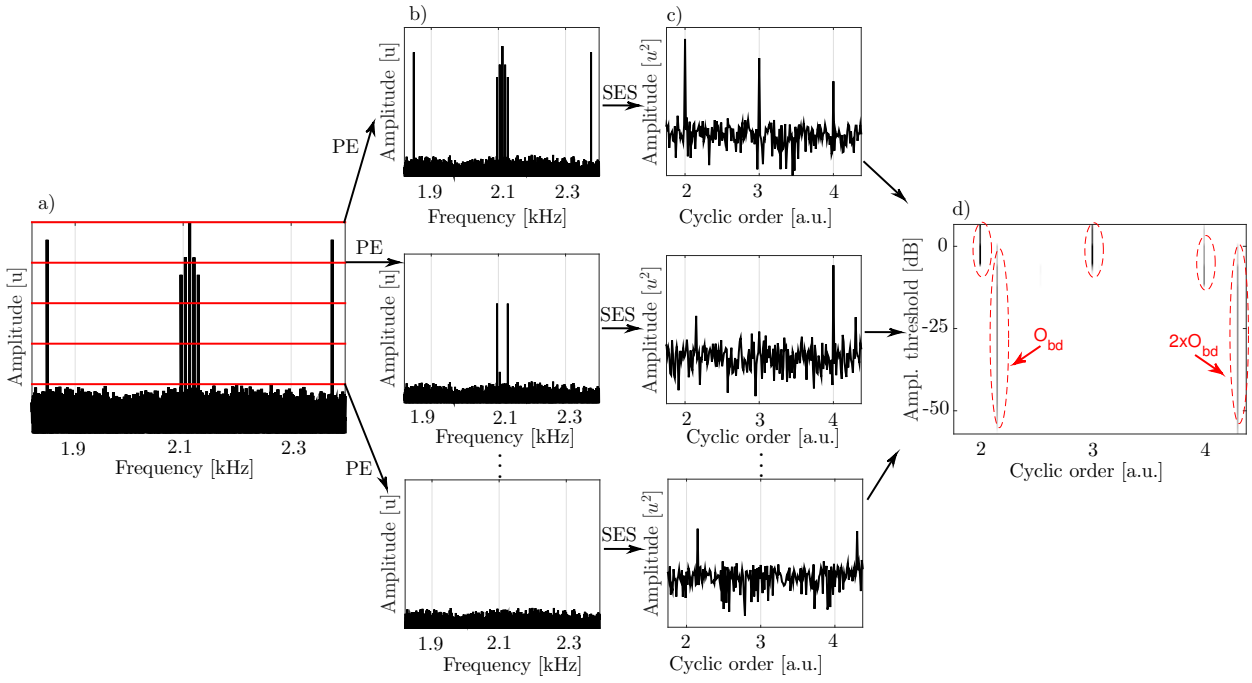

Figure 2: Numerical simulation. (a) Amplitude spectrum of b[k]+n[k]+g[k] in black and N_l=5 tresholds $L^{(l)}[j]$ in red. (b) Amplitude spectrum of the amplitude thresholded signals. (c) The SES for the amplitude thresholded signals. (d) $SES_{x_{AD}}[m, l]$ for $N_L = 50$.

amplitude of all the impacts is unitary and Eq. (8) models an outer race fault.
The values used in the numerical simulation can be found in Table 1, the signal is sampled at Fs=5.12 $\times$ 10+4 [Hz] and the total length is $T_s = 10[s]$. The amplitude spectrum obtained for the signal $g[k] + b[k] + n[k]$ is shown in black in Fig.2(a), the frequency is zoomed around the three meshing harmonics, and 5 threshold functions $L^{(l)}[j]$ are shown in red. Fig.2(b) shows the amplitude spectrum of the signal after the thresholding; the peaks from the gears are systematically suppressed. For each component the next step is to compute the SES as shown in Fig.2(c). It is possible to notice how after the thresholding the SES reveals gradually the presence of peaks at the expected bearing fault order $O_{bd} = (f_{sh}T_{bd})^{-1} = 2.15\ [orders]$ and harmonic, while the peaks from the gears at integer orders are removed.
The $SES_{x_{AD}}[m, l]$ obtained applying the proposed algorithm with $N_l = 50$ threshold levels, to the signal $g[k] + b[k] + n[k]$ is shown in Fig.2(d). For displaying purposes a lower limit in the colour map was implemented. Firstly it is noticed that the presence of the defective bearing is displayed by the two vertical lines at 2.15 and harmonic cyclic orders, extending roughly from the amplitude threshold $\lambda^{(l)} = -10$ [dB] to $\lambda^{(l)} = -60$ [dB]. Secondly the component from the gear contributes lines at integer cyclic orders for threshold levels from roughly $\lambda^{(l)} = 6$ [dB] to $\lambda^{(l)} = -10$ [dB]. Therefore this 2D map shows that the $g[k]$ has higher spectral amplitude then $b[k]$, in addition it shows the decreasing amplitudes of the modulation in Eq. (7) as expected from B_{rg}, with the harmonics at 3rd and 4th cyclic order reaching smaller spectral amplitudes.
Figure 3(a) shows the spectral coherence of the signal $g[k] + b[k] + n[k]$, obtained by applying the fast spectral correlation (SC) algorithm. For display purposes a lower limit in the color map was implemented and for comparison the $SES_{x_{AD}}[m, l]$ of Fig2(d) is shown in Fig.3(b). The size of the window for the short time Fourier transform (STFT) of the fast spectral correlation algorithm was selected as $N_w = 2^{11}$. For this selection the spectral frequency resolution is $\Delta f = 25$ [Hz]. The component $b[k]$ contributes the two vertical spectral lines at Cyclic orders 2.15 and harmonic. While $g[k]$ contributes the three horizontal cyclic lines around the harmonics of the gear meshing frequency as well as the peaks at integer cyclic orders from the amplitude modulation in Eq. (7). It is interesting to notice from Fig.3(a) that what masks the defective bearing in the integral over all the frequencies, as for instance in the top SES of Fig.2(c), are the horizontal lines from the meshing frequency components which contribute a peak at 33 cyclic orders. This was further verified by repeating the numerical simulation with the matrix $B_{rg} = 0$. Also in this case the SES does not show peaks at the bearing defect orders, not shown here.
Figure 4 shows the envelope spectra obtained from sections of the 2D maps of Fig.3. Specifically Fig.4(a) shows the Enhanced Envelope Spectrum (EES) obtained from the integral over the spectral frequencies in the band (1.90, 2.03) [kHz] while Fig.4(c) in the band (2.07, 2.15) [kHz]. The selected bands exploit the spectral frequency separation to distinguish between $g[k]$ and $b[k]$. Figure 4(b-d) shows the sum in spectral amplitude bands of the $SES_{x_{AD}}[m, l]$ obtained from the proposed amplitude-cyclic frequency decomposition:

$$DSES_{x_{AD}}[m] = \sum_{l_1}^{l_2} SES_{x_{AD}}[m, l] \tag{10}$$

Decomposition Squared Envelope Spectrum (DSES) is computed for the thresholds in the range (-20, -40) [dB] in Fig.4(b) and (6, 0) [dB] in Fig.4(d). The selected bands exploit the spectral amplitude separation to distinguish between $g[k]$ and $b[k]$. The DSES calculated on the band at high spectral amplitudes shows peaks at the gear cyclic orders, on the other hand the DSES of the

band comprising low spectral amplitudes shows the peaks at the defective bearing orders. In the case of a signal dominated by vibrations from a bearing the bands in the DSES are interchanged. Therefore DSES gives information on the magnitude of the vibrations from a defective bearing, relative to vibrations from other components.

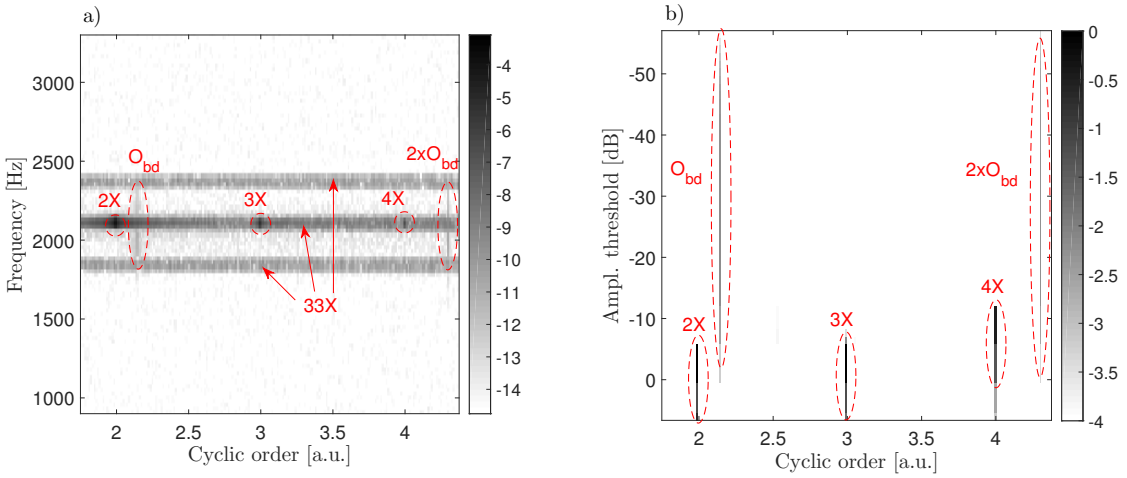

Figure 3: Numerical simulation. Spectral coherence $N_w = 2^{11}$ in (a). Amplitude-cyclic frequency Decomposition $N_l = 50$ in (b).

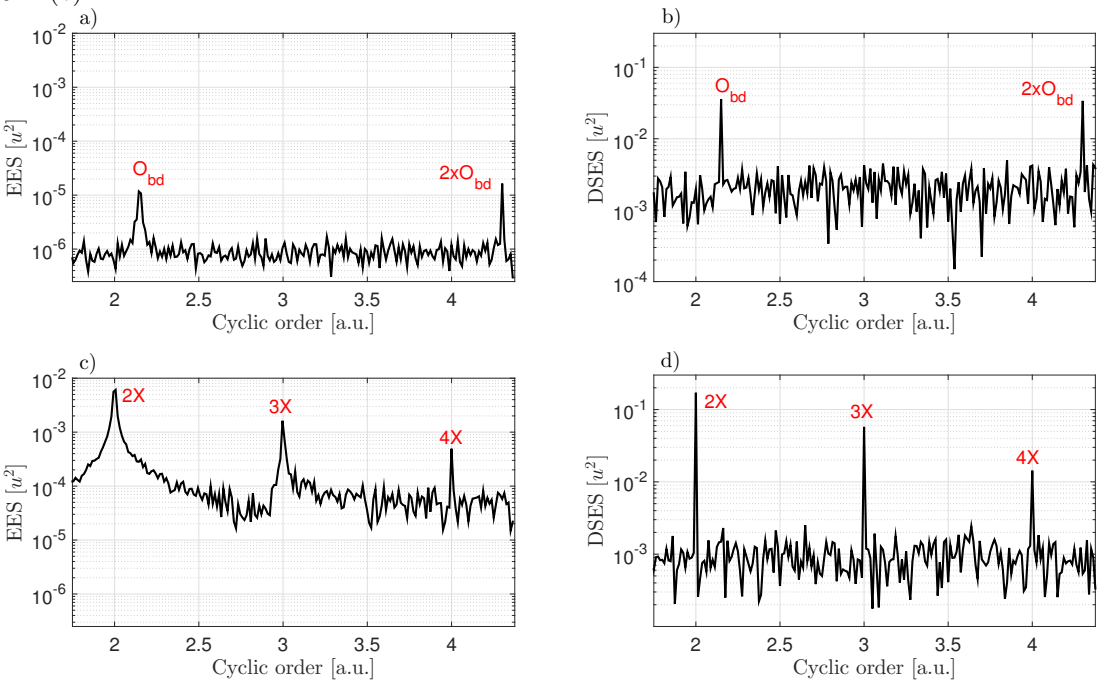

Figure 4: Numerical simulation. First row shows the bands containing the defective bearing signal. (a) EES in (1.90, 2.03) [kHz]. (b) DSES in (-20, -40) [dB]. Second row shows the bands containing gear signal. (c) EES in (2.07, 2.15) [kHz]. (d) DSES in (6, 0) [dB].

CETIM	NREL		Safran
Sensor Acc1 Fs=25.60 [kHz] T_i=25 [s] T_f=45 [s] BPOO =3.04 [orders]	Sensor AN9 Fs=40.00 [kHz] T_i=0 [s] T_f=20 [s] $BPOO_A$=3.52 [orders] $BPOI_B$=11.51 [orders]	Sensor AN6 Fs=40.00 [kHz] T_i=0 [s] T_f=60 [s] $BPOI_C$=2.46 [orders] $BPOO_D$=0.29 [orders]	Sensor Acc2 Fs=44.10 [kHz] T_i= 113[s] T_f= 133[s] $BPOO_A$=7.76[orders] CO_A= 0.43 [orders] $BPOO_B$=4.00 [orders]

Table 2: Values describing the analysed data sets.

3. Experimental Results & discussion

This section presents results from the application of the proposed method to real world data. First, data sets from a laboratory set-up are analysed, provided by the Centre Technique des Industries Mécaniques (CETIM), France. Second, data sets from a wind turbine gearbox are analysed, provided by the National Renewable Research Laboratory (NREL), United States. Last, data sets from an aircraft engine are analysed, provided by Safran.
These three data sets are well documented in other publications[11, 12, 13] with diagrams of the machines, explanations of sensor locations, descriptions of faults and diagnostics challenges. In this paper, for simplicity, only the values used for each data set are stated, sufficient for the reproduction of results. Specifically Table 2 summarises for each data set the sampling rate Fs, the initial and final times T_i and T_f, the sensor specification and the expected fault orders. BPOO is the ball pass order on the outer race while BPOI is that on the inner race, and CO are the cage orders.
In the following, the results obtained applying the amplitude-cyclic frequency decomposition to the three datasets are shown. A comparison with the results obtained from the spectral correlation is presented as well.

3.1. CETIM: Benchmark of bearing faults in large speed variations

The data set provided by CETIM is characterised by a motor operating at largely varying speed, specifically the random-speed profile in [14]. In this paper the dataset is used to show the effectiveness of the amplitude-cyclic frequency decomposition in non stationary speed regimes. The dataset comprises a signal from a tachometer for computation of order tracking.
The $SES_{x_{AD}}[l, m]$ with $N_l = 50$ threshold levels is shown in Fig.5(a-b), with zoomed in sections around BPOO=3.04 and 2xBPOO cyclic orders. As can be noticed the method performs well allowing detection of the defective bearing. In addition the method achieves separation between the vibrations from the gears, at integer cyclic orders, and the bearing. For this data set it is observed that vibrations from the bearing have greater amplitude than vibrations from the gears. Figure5(c-d) shows for comparison the spectral coherence obtained with the fast SC algorithm with the size of the window for the STFT $N_w = 2^8$, giving spectral frequency resolution of $\Delta f = 100$ [Hz]. In this paper the the fast-SC algorithm is modified such that it uses a STFT resampled in the angular domain for each spectral frequency. The SC is also effective in the diagnosis of the defective bearing. The excited resonant frequency appears in the spectral band around 2 [kHz], as observed also in the order-frequency spectral correlation [12]. In addition SC achieves separation of gear and bearing vibrations and the results are comparable with the proposed AD.
Figure 6(a-b) shows the DSES and EES around the bands containing the component from the

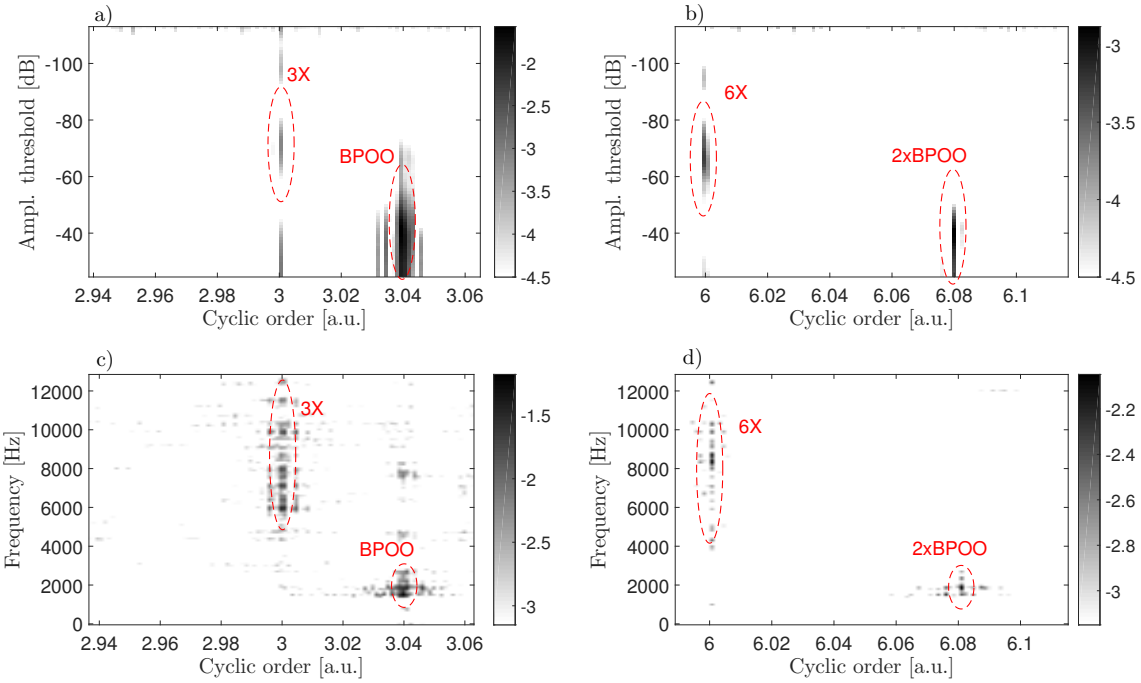

Figure 5: CETIM dataset. First row $SES_{x_{AD}}$ with N_l=50 levels, zoom around BPOO=3.04 in (a) and 2xBPOO in (b). Second row spectral coherence with $N_w = 2^8$, zoom around BPOO in (c) and 2xBPOO in (d).

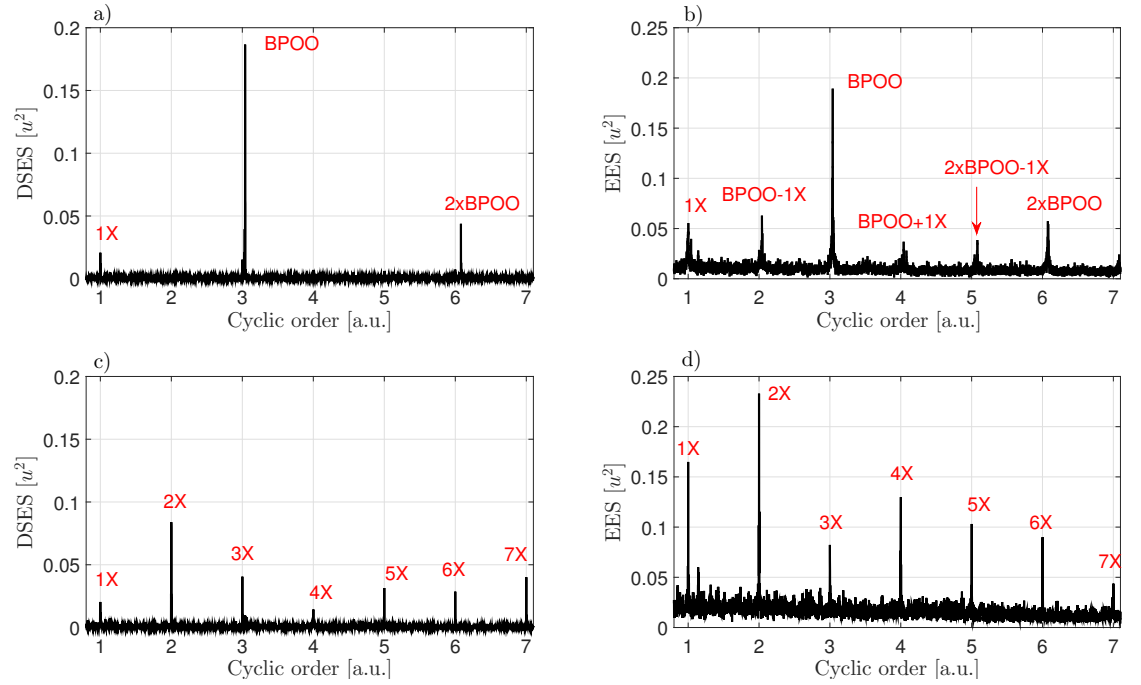

Figure 6: CETIM dataset. First row shows the bands containing the defective bearing signal. (a) DES in (-50, -55) [dB]. (b) EES in (1.8, 2.1). Second row shows the bands containing gear signal. (c) DES in (-75, -80) [dB]. (d) EES in (7.5, 8.0) [kHz].

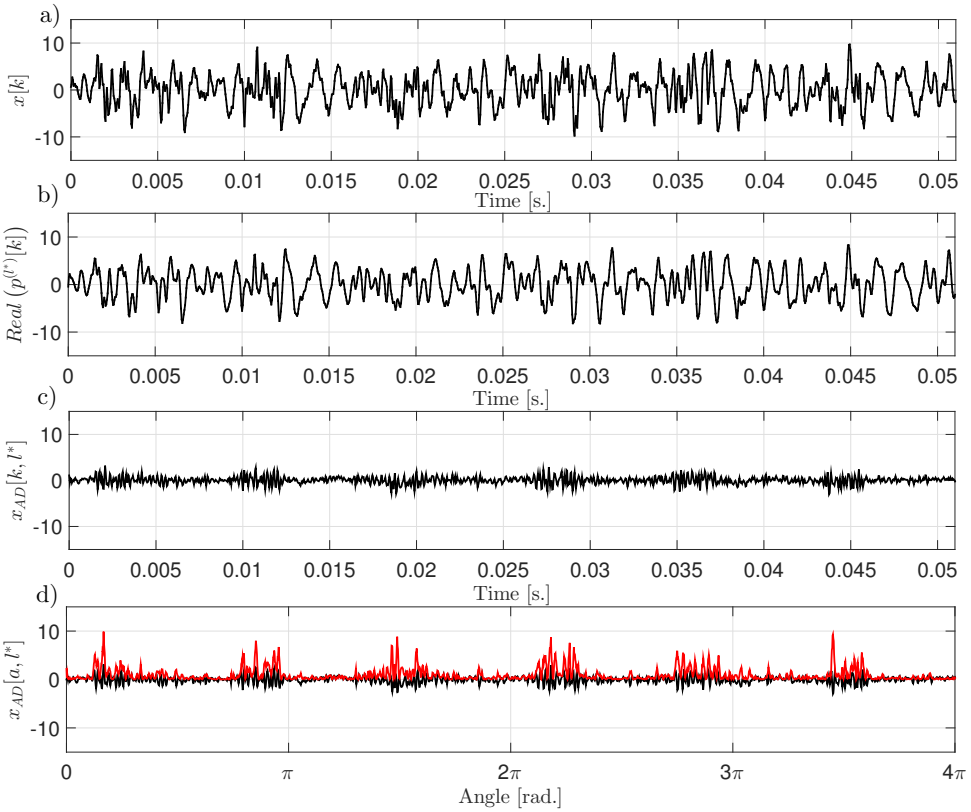

Figure 7: CETIM dataset, example of intermediate steps of AD. (a) The raw vibrational signal. (b) PE signal and (c) PE residual signal, threshold level is $l^* = 8$. (d) PE residual signal after OT in black, squared envelope in red.

defective bearing. The DSES is in the band (-50, -55) [dB] while the SES is in the band (1.8, 2.1) [kHz] and the peaks at BPOO and 2xBPOO are evident in both plots. For the SC the peaks around 2, 4 cyclic orders are modulation sidebands of the BPOO at $\pm$ 1 order of shaft frequency. Such modulations are absent in the DSES, however the detection of the defective bearing is still evident. Figure6(c-d) shows the bands containing the component from the gears. The DSES is in the band (-75, -80) [dB] while the EES is in the band (7.5, 8.0) [kHz].
Finally, for visualization of the operational workflow of AD on a real world dataset, Fig.7 shows the signals resulting from each step of Fig.1. Fig.7(a-b-c) shows respectively: the raw acquired signal, the real part of the PE signal thresholded at the level $l^* = 6$ and the PE residual signal of Eq.(1). It is possible to notice how in the PE residual signal the impacts from the defective bearing are clearly visible, showing the effectiveness of the PE algorithm when applied to non stationary signals. On the other hand Fig.7(d) shows the PE residual signal in the angular domain as well as the square of the absolute value of the analytical representation of the signal in red, used for the computation of $SES_{X_{AD}}[m, l^*]$. In the angular domain it can be verified that there are three impacts per revolution of the shaft according to BPOO.

3.2. NREL: Benchmark of bearing faults in a wind turbine gearbox

The dataset provided by NREL is from a wind turbine gearbox with both multiple defective bearings and gears. The defects are due to assembly damage as well as working wear. The dataset

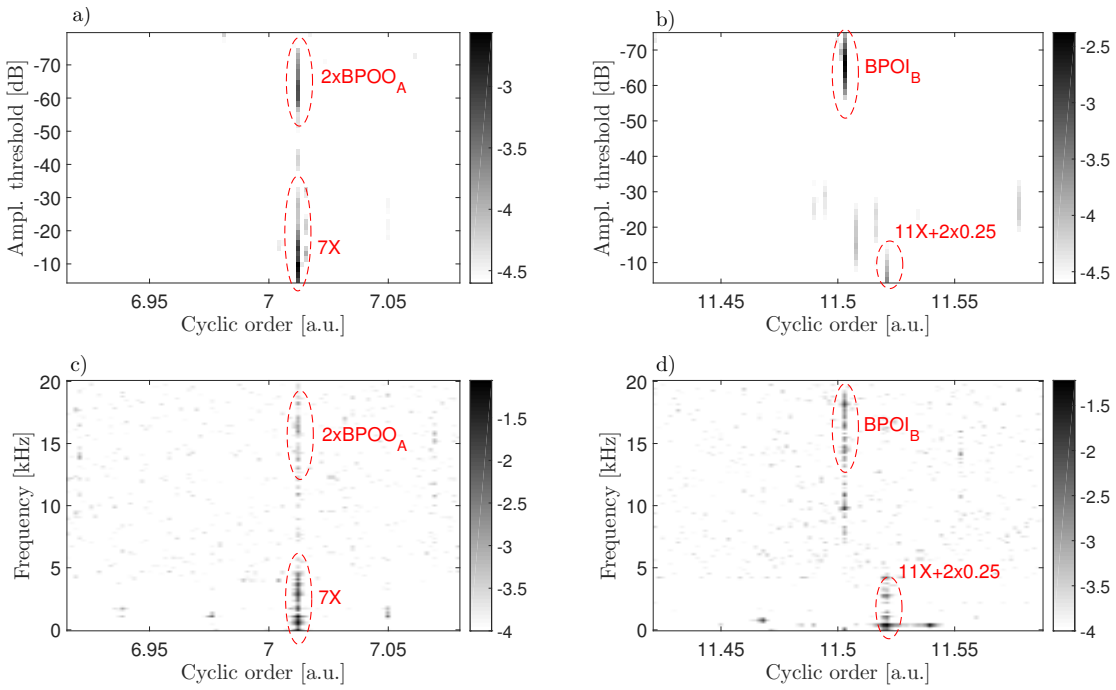

Figure 8: NREL dataset. First row $SES_{x_{AD}}$ with N_l=50 levels. (a) zoom around 2xBPOO$_A$=7.04, (b) BPOI$_B$=11.51. Second row spectral coherence with $N_w = 2^8$. (c) zoom around 2xBPOO$_A$, (d) BPOI$_B$.

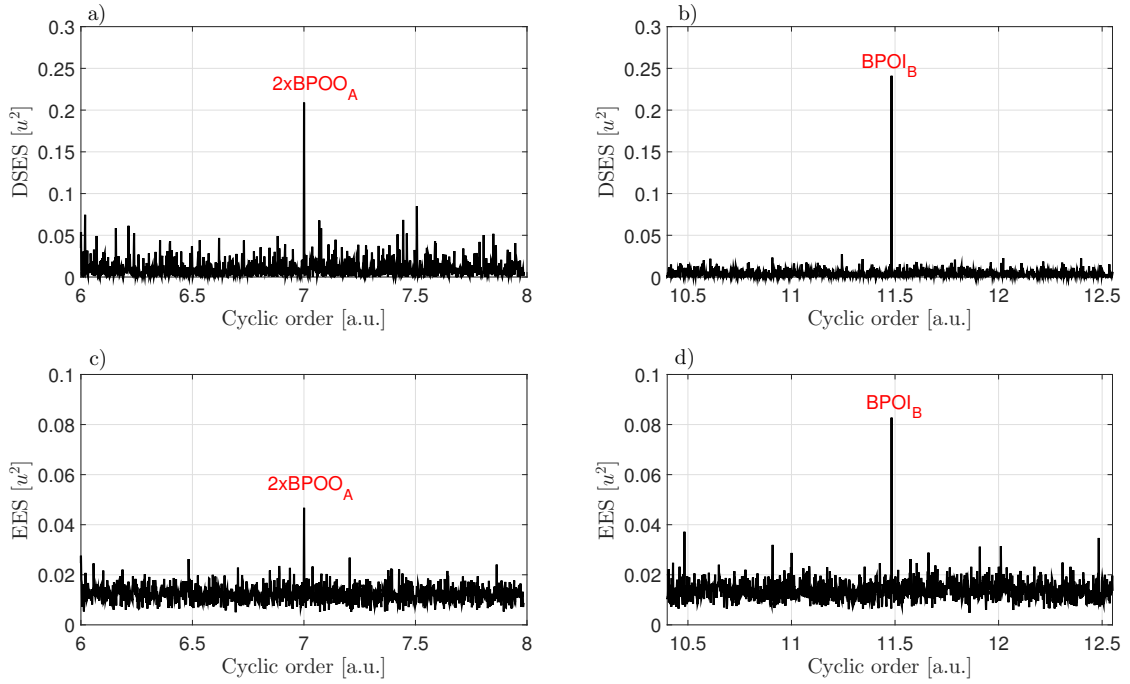

Figure 9: NREL dataset, DSES and EES in the bands containing the defective bearing signal. First row DSES in the band (-65, -70) [dB]. Second row EES in the band (1.55, 1.75) [kHz].

includes a signal from a tachometer for the computation of order tracking. The operating speed of the wind turbine is almost constant for the selected interval of time but OT was computed also in this case. However due to the limited variation of the speed OT is computed directly on the $x[k]$ and afterwards is used the algorithm of Fig. 1 for a signal at constant speed.
Table 2 gives four defective rolling element bearings, respectively named A B C D, however from the analysis conducted in this paper only three are identified. The proposed amplitude-cyclic frequency decomposition misses the detection of the defect at BPOO_D=0.29 cyclic orders. In addition the defect at BPOO_A is not found at the fundamental but at even harmonics, in particular $2\times\text{BPOO}_A$=7.04. The results obtained here corroborate the findings of [11, 15].
Figure 8(a-b) shows respectively the $SES_{x_{AD}}[m,l]$ around the $2\times\text{BPOO}_A$ and BPOI_B cyclic orders; the number of threshold levels is $N_l = 50$. In Fig. 8(a) the cyclic order of the defective bearing at $2\times\text{BPOO}_A$ is close to the 7X harmonic of the gear component. However the different sources of vibration can be separated according to their spectral amplitudes. Vibrations from the gears contribute high spectral amplitudes around -10 [dB] while vibrations from the bearing contribute small spectral amplitudes around -65 [dB]. This example shows how a 2-dimensional map simplifies the detection of a defective bearing in the case of components contributing peaks at the same cyclic order. In particular there is no need to pre-process the signal to suppress masking vibrations before the computation of the SES. Similar results are obtained for the defect at BPOI_B as shown in Fig.8(b). For this case the component from the gears, at high spectral amplitudes, is at $\sim$ 11.52 cyclic orders. It is due to modulation at 0.25 orders from a defective gear and therefore it corresponds to $11\text{X}+2\times0.25$. Vibrations for the defective bearing on the other hand correspond to the line at BPOI_B cyclic orders around -70 [dB]. Figure 8(c-d) shows the spectral coherence zoomed in around the same cyclic orders, the window size of the STFT is $N_w = 2^8$, giving Δf= 156 [Hz]. The results match those obtained with the proposed methodology. The spectral coherence in Fig. 8(c) shows that around the 7X cyclic order there are two sources of vibrations, with the gears at lower frequencies than the defective bearing. Similarly in Fig. 8(d) the gears contribute a peak at $\sim$ 11.52 cyclic orders at low spectral frequencies. On the other hand the defective bearing excites a resonance around 17 [kHz] contributing a clear line around BPOI_B cyclic orders. Further analysis of the second harmonic can be found in Appendix A. Figure 9(a-b) shows the DSES in the band (-65, -70) [dB] where the component of vibrations from the defective bearing is found. The peaks at 2xBPOO_A and BPOI_B are observed respectively in Fig. 9(a) and Fig. 9(b). Figure 9(c-d) shows for comparison the EES in the band (15.5, 17.5) [kHz]. The peaks from the two defective bearings are also clearly present in this case.
A first investigation of $SES_{x_{AD}}[l,m]$ did not reveal the presence of the defect at BPOI_C, therefore in this case spectral frequency separation was also used to achieve detection. The set of constants $\lambda^{(l)}$ of Eq.4 is multiplied by a function of frequencies $0 \leq \gamma[j] \leq 1$ so that to implement simultaneously a filter in the spectral frequencies and a threshold in the spectral amplitudes:

$$L^{(l)}[j] = \begin{cases} +\lambda^{(l)}\gamma[j] & 0 \leq j < N_k/2 \\ -\lambda^{(l)}\gamma[N-1-j] & N_k/2 \leq j \leq N_k - 1. \end{cases} \tag{11}$$

The function $\gamma[j]$ is chosen as a 6^{th} order band-pass Butterworth filter of bandwidth 2 [kHz] and central frequency 10 [kHz]. The band of interest was chosen by the user after investigation of the $SES_{x_{AD}}[l,m]$ for different values of the central frequency.
Figure 10(a) shows the resulting $SES_{x_{AD}}[l,m]$ around the BPOI_c cyclic orders. The spectral frequency filtering in the thresholds of Eq. 11 shifts the component from the defective bearing at

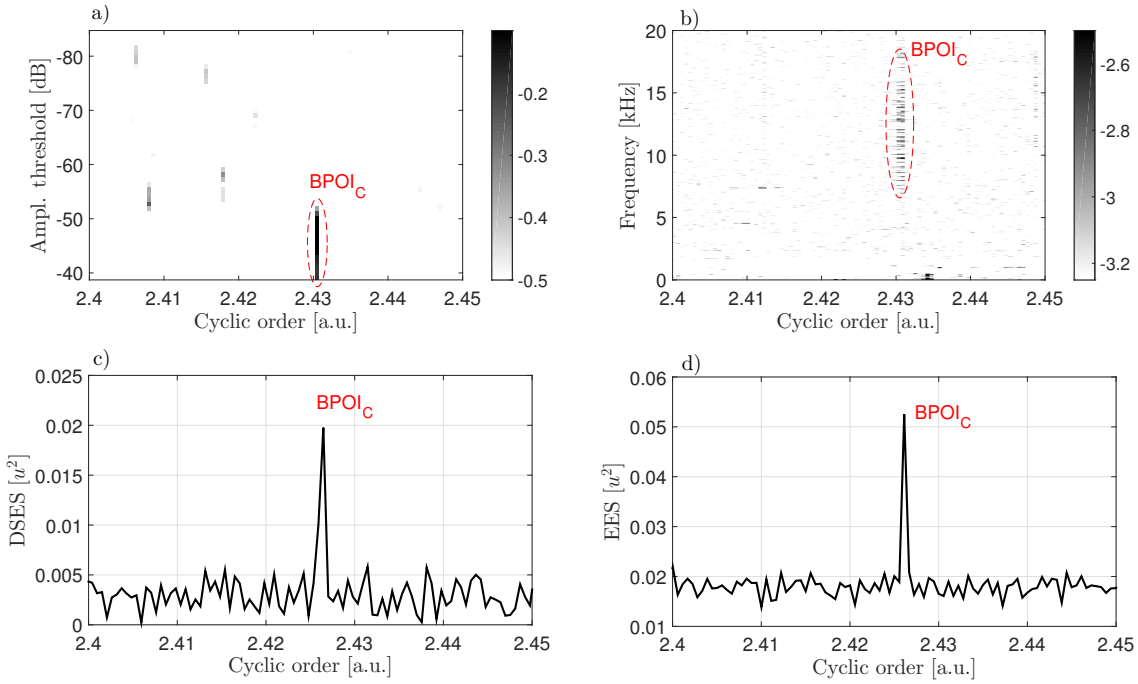

Figure 10: NREL dataset. (a) $SES_{x_{AD}}$ with N_l=50 levels, zoom around BPOI$_C$=2.34. (b) spectral coherence with $N_w = 2^{11}$, zoom around BPOI$_C$. (c) DSES in the band (-45, -50) [dB]. (d) EES in the band (8.5, 11) [kHz].

high spectral amplitudes, around -45 [dB] from Fig. 8(a-b), meaning that in this spectral frequency band vibrations from the bearing have dominant amplitudes. For comparison the spectral coherence is shown in Fig. 10(b), the window size for the STFT is $N_w = 2^{11}$ giving a frequency resolution Δf=20 [Hz]. The defect at BPOI$_c$ cyclic orders is observed around 9 [kHz], corresponding to the selected central frequency for the spectral filter of Eq. 11. Further analysis of the second harmonic can be found in Appendix A.

Finally Fig. 10(c-d) shows the DSES and EES around the band containing the defective bearing vibrations, respectively (-45, -50) [dB] for the $SES_{x_{AD}}[l, m]$ and (8.5, 11) [kHz] for the spectral coherence.

3.3. Safran: Benchmark of bearing faults in an aircraft engine

The dataset provided by Safran was acquired on a civil aircraft engine with multiple damaged bearings. The defects are seeded. The dataset includes a signal from a tachometer for the computation of order tracking. Table 2 shows two defective bearings, respectively A and B, however from the analysis conducted in this paper only one is found. The proposed amplitude-cyclic frequency decomposition misses the detection of the defect at BPOO$_B$=4.00 cyclic orders. This results corroborates the analysis of [13].

Figure 11(a) shows the $SES_{x_{AD}}$ with N_l=50 levels, zoomed around BPOO$_A$=7.76 cyclic orders. A clear line at the expected fault order extends up to -100 [dB] showing that the defective bearing contributes strong vibrations. Sidebands at the OC$_A$ can be seen around the line at BPOO$_A$. The presence of such sidebands at the cage orders is unusual for an outer race fault, however can be confirmed by the findings of [13] where it was shown an amplitude spectrum characterised by a

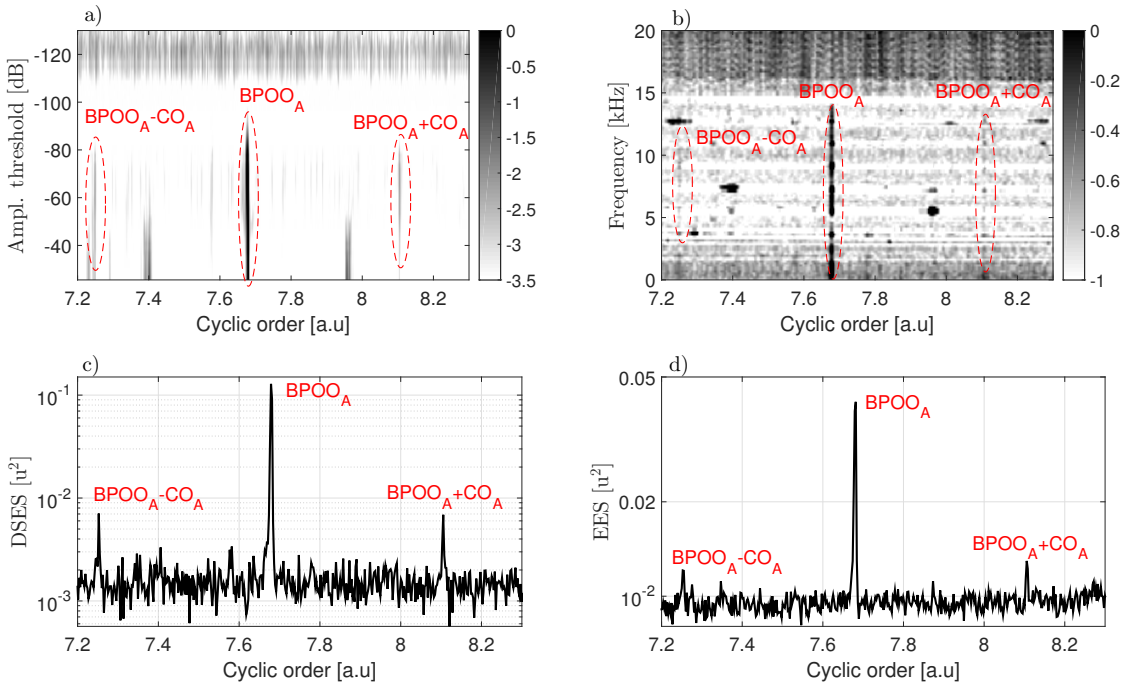

Figure 11: Safran dataset. (a) $SES_{x_{AD}}$ with N_l=50 levels, zoom around BPOO$_A$=7.76 comprising sidebands at CO$_A$=0.43. (b) spectral coherence with $N_w = 2^8$. (c) DSES in the band (-60, -80) [dB]. (d) EES in the band (8, 12) [kHz].

series of peaks at BPOO$_A$ and harmonics, with sidebands equispaced by OC$_A$. Figure 11(b) shows for comparison the spectral coherence calculated with a STFT window size $N_w = 2^8$, giving a frequency resolution Δf=175 [Hz]. The defective bearing is found also in this case with the sidebands at the cage orders less evident but still present. Further analysis of the second harmonic can be found in Appendix A.

Finally Fig. 11(c-d) shows respectively the DSES and EES in the bands containing the defective bearing vibration. The plots are smoothed in the cyclic order domain, so that the cyclic resolution for both plots is $\Delta\alpha = 2.60 \times 10 - 3$ [a.u.]. The DSES is in the band (-60, -80) [dB] while the EES is in the band (8, 12) [kHz], peaks at BPOO$_A$ and sidebands at CO$_A$ are present in both plots.

4. Conclusions

This paper has introduced a new method to decompose a vibration signal in a 2-dimensional map: the Amplitude-cyclic frequency Decomposition (AD). The method can be used to analyse vibration signals of rotating machines operating in both stationary and non stationary speed regimes. In addition, the Decomposition Squared Envelope Spectrum (DSES) has been computed as the sum over the spectral amplitudes of the AD. It is proved that the DSES is as an enhancement of the usual SES.

In this paper the AD and DSES have been applied on three vibration signals in order to show their ability to detect defective bearings. The analysed data sets are from a wind turbine gearbox, a civil aircraft engine and a laboratory set-up characterised by large speed variations. These three

data sets are well documented in the literature and the results obtained by other methods can be used for comparison. In this paper the performances of AD and DSES have been compared with those of the fast Spectral Correlation algorithm and the Enhanced Envelope Spectrum. Matching results were obtained for all the analysed data sets. The proposed methodology is computationally easy to implement, relying only on the fast Fourier transform algorithm. In addition it requires the selection of only one parameter, which for all the data sets analysed in the paper was kept constant at $N_l = 50$, therefore it is proposed as a good candidate for an automatic industrial application.

Acknowledgment

The authors would like to thank the Centre Technique des Industries Mécaniques, the National Renewable Energy Laboratory and Safran for sharing the data analysed in this study.

Appendix A. Second harmonic

The first column of Fig. A.12 shows a zoomed in section of the $SES_{x_{AD}}[m, l]$ for the data from NREL, the second column shows for comparison shows a zoomed in section of the spectral coherence. The cyclic orders are zoomed in around the expected second harmonics of the defective bearings, from top to bottom for BPOO_A, BPOI_B and BPOI_C according to Fig. 8 and Fig. 10.

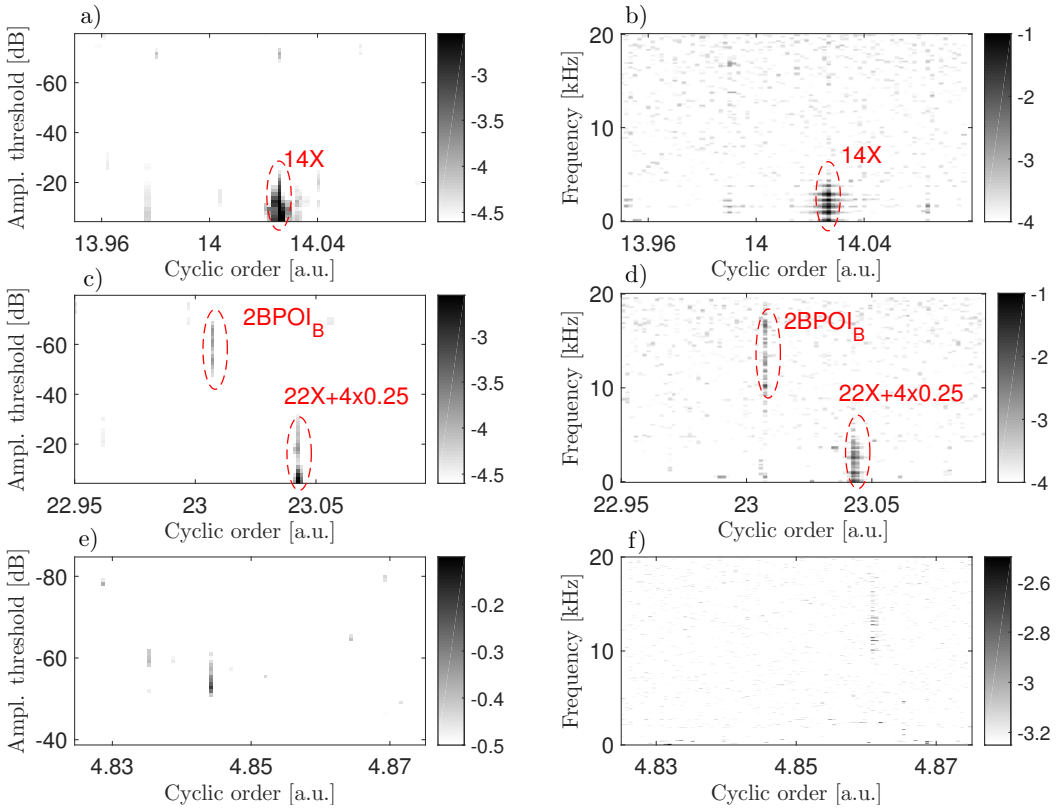

Figure A.12: NREL dataset, zoomed in section around second harmonics. (a-c-e) AD, (b-d-f) spectral coherence.

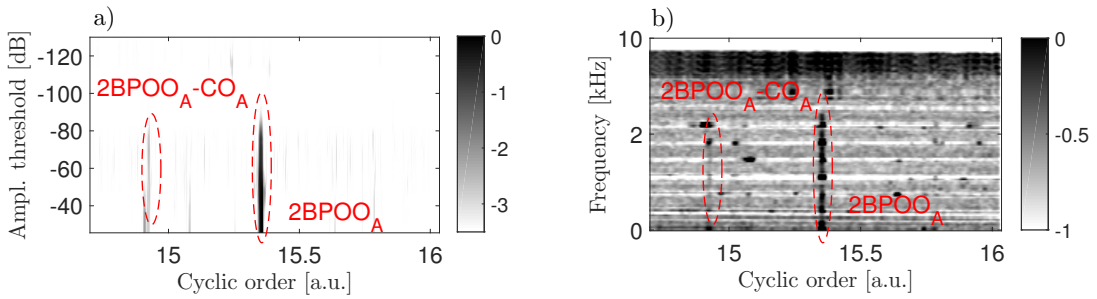

Figure A.13: Safran dataset, zoomed in section around second harmonic. (a) AD, (b) spectral coherence.

For BPOO$_A$ there is no clear evidence of the higher harmonic. Following the analysis of Fig. 8, the vertical line close to 14 cyclic orders in Fig. A.12(a-b) has been assumed from the gears. On the other hand the second harmonic of BPOI$_B$ is found by both methods, Fig. A.12(c-d). Finally, for BPOI$_C$ there is no clear evidence of the second harmonic from AD while there is a weak indication from the spectral coherence.

Figure A.13 shows zoomed in section of the data from Safran, respectively $SES_{x_{AD}}[m, l]$ in Fig. A.13(a) and for comparison the spectral coherence in Fig. A.13(b). The cyclic orders are zoomed in around the expected second harmonic of the defective bearing BPOO$_A$, according to Fig. 11. Both methods clearly reveal the presence of the second harmonic, in addition they give a weak indication on the presence of the sideband at CO$_A$.

References

[1] R. B. Randall, Vibration-based Condition Monitoring, John Wiley & Sons, 2011.

[2] J. Antoni, Cyclic spectral analysis of rolling-element bearing signals: Facts and fictions, Journal of Sound and Vibration 304 (3–5) (2007) 497 – 529.

[3] R. Randall, J. Antoni, S. Chobsaard, The relationship between spectral correlation and envelope analysis in the diagnostic of bearing faults and other cyclostationary machine signals, Mechanical Systems and Signal Processing 15 (5) (2001) 945 – 962.

[4] P. McFadden, J. Smith, Vibration monitoring of rolling element bearings by the high-frequency resonance technique — a review, Tribology International 17 (1) (1984) 3 – 10.

[5] J. Antoni, G. Xin, N. Hamzaoui, Fast computation of the spectral correlation, Mechanical Systems and Signal Processing 92 (2017) 248 – 277.

[6] R. B. Randall, J. Antoni, Rolling element bearing diagnostics — a tutorial, Mechanical Systems and Signal Processing 25 (2) (2011) 485 – 520.

[7] L. Barbini, A. Ompusunggu, A. Hillis, J. du Bois, A. Bartic, Phase editing as a signal pre-processing step for automated bearing fault detection, Mechanical Systems and Signal Processing 91 (2017) 407 – 421.

[8] N. Sawalhi, R. B. Randall, Signal pre-whitening for fault detection enhancement and surveillance in rolling element bearings, in: Eighth International Conference on Condition Monitoring and Machinery Failure Prevention Technologies, Cardiff, UK, 2011.

[9] P. Borghesani, R. Ricci, S. Chatterton, P. Pennacchi, A new procedure for using envelope analysis for rolling element bearing diagnostics in variable operating conditions, Mechanical Systems and Signal Processing 38 (1) (2013) 23 – 35.

[10] P. McFadden, J. Smith, A signal processing technique for detecting local defects in a gear from the signal average of the vibration, Proceedings of the Institution of Mechanical Engineers, Part C: Journal of Mechanical Engineering Science 199 (4) (1985) 287–292.

[11] Wind turbine gearbox condition monitoring round robin study – vibration analysis, `http://www.nrel.gov/docs/fy12osti/54530.pdf`, accessed: 2017-March.

[12] D. Abboud, S. Baudin, J. Antoni, D. Rémond, M. Eltabach, O. Sauvage, The spectral analysis of cyclo-non-stationary signals, Mechanical Systems and Signal Processing 75 (2016) 280 – 300.

[13] J. Antoni, J. Griffaton, H. André, L. D. Avendaño-Valencia, F. Bonnardot, O. Cardona-Morales, G. Castellanos-Dominguez, A. P. Daga, Q. Leclère, C. M. Vicuña, D. Q. Acuña, A. P. Ompusunggu, E. F. Sierra-Alonso, Feedback on the surveillance 8 challenge: Vibration-based diagnosis of a safran aircraft engine, Mechanical Systems and Signal Processingdoi:http://dx.doi.org/10.1016/j.ymssp.2017.01.037.

[14] D. Abboud, M. Eltabach, J. Antoni, S. Sieg-Zieba, Envelope preprocessing techniques for rolling element bearing diagnosis in variable speed conditions, in: Twelfth International Conference on Condition Monitoring and Machinery Failure Prevention Technologies (MFPT), Oxford, UK, 2015.

[15] C. Peeters, P. Guillaume, J. Helsen, Vibration-based bearing fault detection on experimental wind turbine gearbox data.

5.4 Computational cost

The proposed AD is a computationally inexpensive method and this section investigates an interesting aspect: evaluating the computational cost of AD and comparing it with that of the SC, implemented with the fast-SC algorithm [Antoni et al., 2017a]. In the following AD and SC are implemented in Matlab 2014b on a i5-4590 CPU with up to 3.3 GHz clock cycles.
The computational cost of the AD is addressed in terms of the number of complex multiplications. For a signal of length N_k the implementation of AD consists of 5 FFT for each of the N_l threshold levels, where the 5 FFT are respectively 2 from the PE, 2 from the Hilbert transform and 1 from the computation of the spectrum of the envelope, thus giving a complexity of

$$C_{AD} \sim N_k log_2(N_k) 5 N_l. \tag{5.1}$$

Figure 5.20(a) shows in black the Elapsed Time (ET) for the implementation of AD on $N_k = 8 \times 10^5$ samples, for different numbers of thresholds N_l, while in red it shows the expected ET from Eq. 5.1. This can be seen as a common application, with the vibration signal consisting of a measurement of 20 seconds sampled at 40 kHz.
Figure 5.20(b) shows the ratio between the ET of the SC and the ET of the AD, for a signal of different lengths and for different threshold levels. In red it shows the ratio equal to one as a reference. The ratio is calculated in such a way that the 2D matrix computed by the AD and SC have respectively the same number of threshold levels

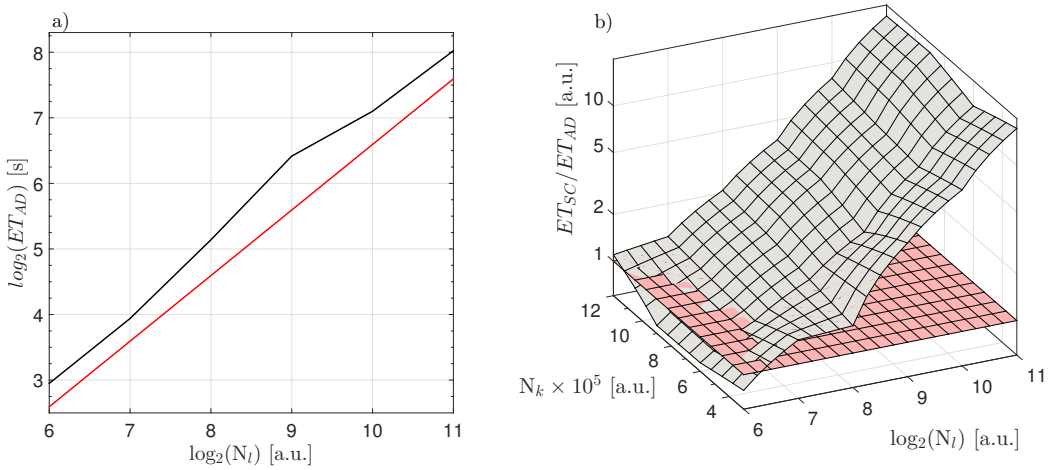

Figure 5.20: (a) Elapsed time of AD on a signal of $N_k = 8 \times 10^5$. (b) Ratio of the elapsed time between SC and AD.

and the same number of frequency (spectral) bands:

$$N_l = \frac{Fs/2}{\Delta f} \tag{5.2}$$

where Δf of the FastSC for a window length of N_w is $\Delta f = Fs/N_w$. Figure 5.20(b) shows that the AD is significantly faster than SC for increasing number of thresholds, while the relative performances do not depend as heavily on the length of the analysed signals. Another aspect qualifying AD as a computationally superior method compared to SC is that the SES calculated for a threshold level in AD computes all the cyclic orders from 0 to $Fs/\left(2\bar{f}_{shaft}(t)\right)$, where $\bar{\cdot}$ denotes the mean value. In contrast the SC computes up to a maximum pre-selected cyclic order value, because the computational cost increases quadratically with it. Thus the computation time of SC varies significantly with the mean operating speed of the machine, while that of AD is fixed.

5.5 Missed detection

This section shows two cases of missed detection of defective bearings from the analysis of vibration data from the experimental setups described in Section 5.2. Following the analysis of Section 5.3 the defects which can not be detected by vibration analysis are respectively:

1. the outer race defect in the bearing D supporting the planet carrier of the wind turbine gearbox, as shown in Fig.5.3
2. the outer race defect in the bearing B on the shaft L1 of the accessory gearbox of the civil aircraft engine, as shown in Fig.5.4.

For both cases results are shown from the application of the proposed AD and for comparison from the fast-SC. In addition, analysis of the same data sets can be found in [Sheng, 2012, Peeters et al., 2016] and [Antoni et al., 2017a, Gryllias et al., 2017], respectively for the data sets from NREL and Safran, confirming that such faults are not detectable by existing vibration analysis methods.
Figure 5.21 shows the AD and spectral coherence[2], respectively top and bottom, for the NREL data set zoomed into the cyclic orders around the expected $\text{BPOO}_D = 0.29$ of Table 5.2. The data analysed here is from the sensor AN7 and the total length is 60s. The AD is calculated for $N_l = 2^6$ levels and the SC for $N_w = 8$. Similar results are obtained from the analysis of data from the other sensors. It can be seen that in the

[2]The spectral coherence is a normalised version of the spectral correlation [Antoni et al., 2017b].

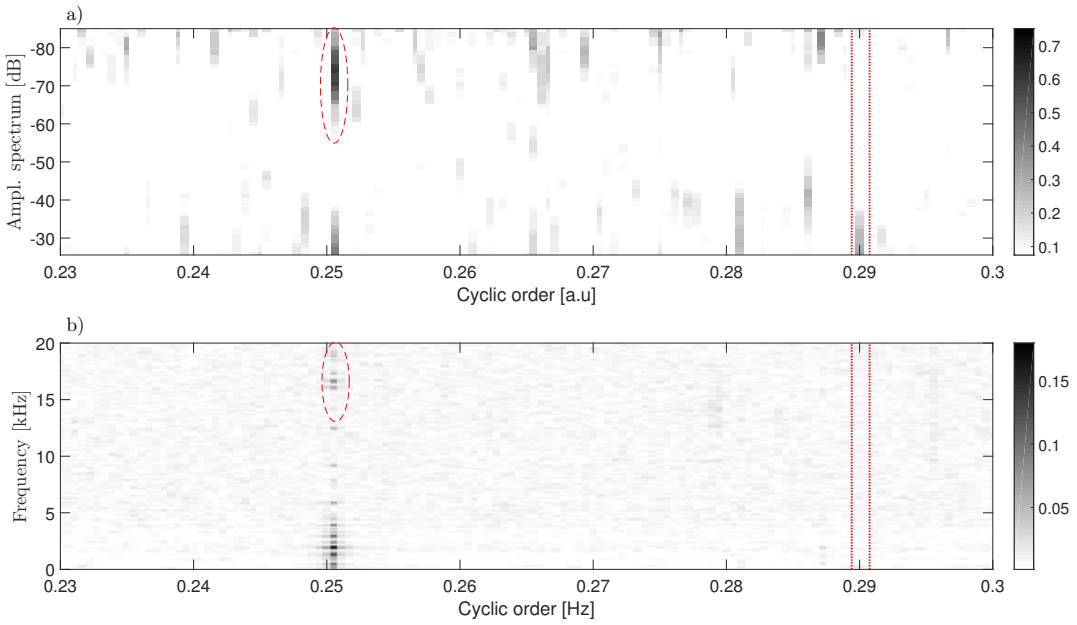

Figure 5.21: Missed detection in the wind turbine gearbox. (a) $SES_{x_{AD}}$ with $N_l = 2^6$ levels, zoom around BPOO$_D$=0.29. (b) spectral coherence with $N_w = 2^8$.

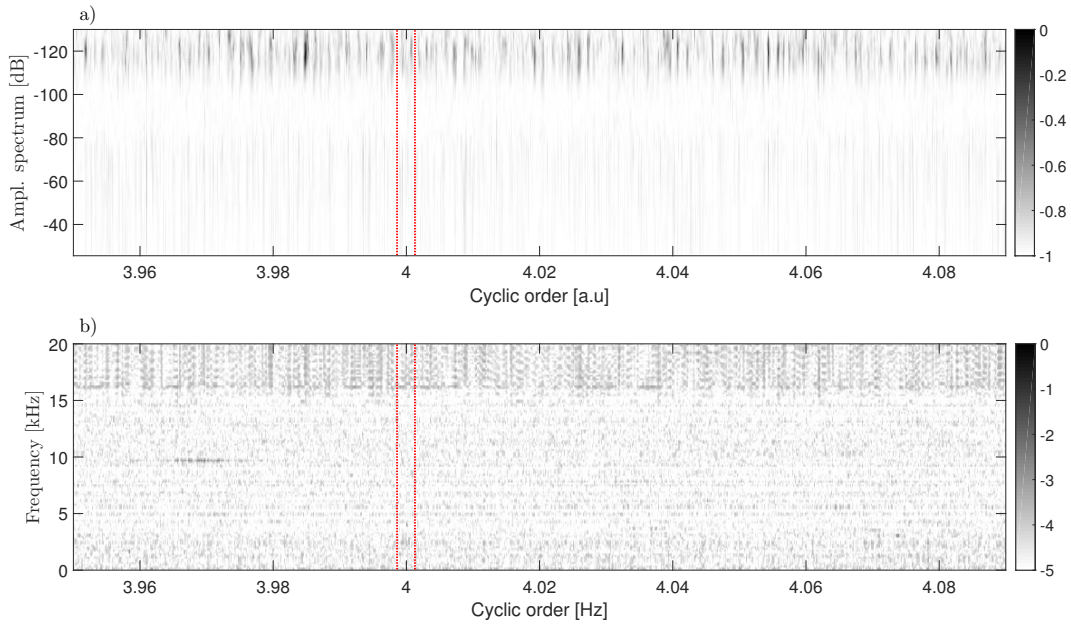

Figure 5.22: Missed detection in the Aircraft engine. (a) $SES_{x_{AD}}$ with $N_l = 2^6$ levels, zoom around BPOO$_B$=4.00. (b) spectral coherence with $N_w = 2^8$.

region highlighted by the red vertical dotted lines around BPOO_D, there is no evidence of the defect from either of the two methods. On the other hand, Figure 5.21 shows a vertical line at around 0.25 orders, which corresponds to the rotational frequency of the pinion in the intermediate gear set of Figure 5.3. Both the methods show that this line is present simultaneously at high spectral amplitude/low frequency and low spectral amplitude/high frequency. This situation is similar to the analysis of $2\times\text{BPOO}_A = 7$ orders for the NREL data set in Section 5.3, suggesting that the cyclic content highlighted by the red circles is due to the presence of impacts with a small amplitude in the vibration signal. However the relative deviation from the expected BPOO_D is too large therefore is not attributed to the defective bearing.
Finally, Fig. 5.22 shows the AD and spectral coherence for the data from Safran, zoomed into the cyclic orders around the expected $\text{BPOO}_B = 4.00$ of Table 5.2. The data analysed here is from sensors Acc1 for a total length of 20 seconds with $T_{i,f}$ as in Table 5.2 and the AD is calculated for $N_l = 2^6$ levels while the SC for $N_w = 8$. Vertical red dotted lines highlight the region of interest, showing no evidence of the defective bearing. A possible motivation for these missed detection, even by the combined analysis with AD and SC, is the presence of structural damping between the location of the defects and the position of the accelerometers.

5.6 Summary

This chapter introduced a novel signal processing method for the detection of defective bearings from vibration measurements: Amplitude-cyclic frequency Decomposition (AD). The proposed method thresholds the amplitude spectrum of the signal on a set of N_l values and for each threshold level shows the corresponding cyclic content, thus decomposing the vibration signal into a two dimensional map. The algorithm is described in detail in Section 5.3.
AD uses the PE algorithm of Chapter 4 to threshold the signal, from which it follows that it is applicable to both vibration signals from machines operating at constant and variable speed. In addition, AD needs very little supervision by an expert user, N_l being the only parameter to be selected. In this regard, it was noticed that AD is not particularly sensitive to the number of levels, for instance the same $N_l = 50$ was used in all the analysed data sets.
The performance of AD has been tested on data from three different experimental setups, as described in Section 5.2 and compared to that of the Spectral Correlation (SC) algorithm, which among the state of the art techniques is the most similar one,

decomposing the vibration signal into a two dimensional map. The results are shown in Fig. 5.11, Fig. 5.13, Fig. 5.15, Fig. 5.16 from which it is possible to conclude that the detection capability of AD is comparable to that of SC.
Finally, regarding the computational complexity, AD is a fast algorithm and being based on PE it only performs 5 calls of the FFT for each threshold level. As shown in Fig. 5.20, it is up to 10 times faster than the fast-SC algorithm for the range studied. For these reasons it can be concluded that the proposed method shows all the key characteristics detailed in Section 1.4 and is believed to be one of the best performing techniques currently available for the detection of bearing damage from vibration signals.

Chapter 6

Conclusions

This thesis introduces novel signal processing methods to monitor the condition of rotating machines from their vibration signature, specifically to perform diagnostics of rolling element bearings. The aim throughout the work was to provide practical and applicable tools to the industry and the focus was the development of methods both applicable without supervision by an expert user and capable of monitoring machines operating in non-stationary conditions. The strategy adopted during the research work was twofold, encompassing both analog and digital signal processing methods. In a first stage the work focused on the development of a circuit capable of enhancing the signal to noise ratio of the analog signal from an accelerometer, while in a second stage the strategy shifted towards the introduction of digital signal processing algorithms for feature extraction. The following discusses separately for both of the strategies the main results and future research perspectives.

The analog circuit described in Chapter 2 uses the phenomenon of Stochastic Resonance (SR) to enhance the cyclic content of vibration signals. SR is already a well established method in the field of vibration based condition monitoring and in its classical implementation the vibration data, after analog to digital conversion, is used as the input of a 1D SR system. The SR system then resonates at the cyclic frequency of the vibrations generated by the defective bearing and its output is a signal showing enhanced diagnostic information. With respect to this conventional procedure, the thesis contributes two novelties. Firstly, it uses a 2D SR system instead of the 1D system, the advantage being that the 2D system, due to the presence of the coupling constant between the two modes allows a finer tuning of the resonance, and shows superior enhancement capabilities [Barbini et al., 2015]. Secondly, it implements SR in an electrical circuit capable of reproducing the software based system, allowing its use

directly on analog signals in series with an accelerometer.
Despite the promising results obtained during the research on SR, it was observed that its application on real world vibration signals needs a time consuming tuning of several parameters and requires pre-processing methods, otherwise SR applied on the raw signal resonates with the vibrations coming from components different from the defective bearing. These drawbacks jeopardise the advantage resulting from the easy implementation achieved with the analog circuit, and force the user to prefer the use of SR in its digital version where pre-processing methods can be implemented. However in the domain of digital signal processing, the state of the art algorithms for cyclic spectral analysis perform better than SR, being specifically developed for such a purpose. For these reasons the research on the SR circuit was discontinued and the focus was shifted towards the development of digital signal processing methods other than SR.
Further investigations on SR in the field of condition monitoring must take into account the drawbacks identified in this thesis and discard both the software and circuit based systems. The author believes that the only possible direction for research is on the implementation of SR in a digital processing unit, in order to enhance the signal before its analysis with dedicated software.
Regarding the research on digital signal processing methods, the thesis both investigates the extension of conventional techniques in Chapter 3 and introduces two novel approaches in Chapter 4 and Chapter 5.
The extension of the conventional techniques addresses an actual need of the industry for condition monitoring methods applicable in real world scenarios, when machines operate under varying loads and speeds. This topic has attracted the attention of researchers during recent years, following the mathematical modelling of the vibration signature of a defective machine as a cyclo-non-stationary signal. In this respect, the contribution of this thesis is the observation that two techniques commonly used in the cyclo-stationary case for the suppression of masking vibrations, cepstral prewhitening [Barbini et al., 2018] and spectral kurtosis, can be directly applied to cyclo-non-stationary signals. This demonstrates to the condition monitoring community that there is no need to develop sophisticated and computationally expensive techniques to address the non-stationarity.
The main contribution of the thesis is the introduction of two novel methods to enhance diagnostics of defective bearings. The underlying idea of the proposed approaches is both simple and distinctive with respect to the current state of the art: separation of the vibrations from different components of the machine by exploiting their diverse amplitude rather than their frequency. This is achieved by suppressing all the values lower than a chosen threshold in the amplitude spectrum, independent of their position

in the frequency spectrum. Two remarkable aspects can be recognised: firstly this approach works on the full band of the spectrum, without the need for selecting a spectral band of interest. On the contrary this is the main problem encountered by the classical methods. Secondly it works for machines operating in non-stationary conditions. As a matter of fact in the non-stationary case the peaks in the amplitude spectrum will be smeared but are still separated in their amplitude levels.

Regarding the first novel method, the algorithm used to threshold the vibration signals is called Phase Editing (PE) and its mathematical description and application to real world signals is discussed in [Barbini et al., 2017c]. The proposed technique is firstly implemented in an automated way on a set of cyclo-stationary signals, with the selection of the best threshold level achieved by the maximisation of cyclic features. It is then extended to the case of cyclo-non-stationary signals [Barbini et al., 2017a]. When compared with state of the art techniques PE showed a 10% improvement in the performance of detection. Combined with its simple implementation, based on the fast Fourier Transform, and intuitive interpretation, this makes it a method suitable for industrial applications.

The final method introduced by this thesis is the Amplitude - cyclic frequency Decomposition (AD) which uses PE to produce a two dimensional map of the vibration signal, showing its cyclic content calculated on a set of threshold levels. The method is fully automated with the threshold linearly chosen between the maximum and minimum value of the log amplitude spectrum and the user has only to pre-select how many levels to compute. AD inherits all the benefits of PE and is effective both on cyclo-stationary and cyclo-non-stationary signals, works on the full spectral band of vibration signals and is computationally inexpensive. AD is mathematically introduced and tested on a set of experimental data sets in [Barbini et al., 2017b]. Its performance has also been thoroughly compared to that of the fast Spectral Correlation (SC) algorithm, showing very similar detection capabilities and smaller computation times, thus proving that the results obtained here are remarkable and unmatched by the current state of the art.

Regarding future research on PE and AD it is of interest to investigate the use of thresholds for simultaneously suppressing spectral amplitudes and specific spectral bands. Here this concept was introduced in Chapter 4 where in [Barbini et al., 2017a] a threshold level dependent on the frequency was also used to implement a low pass filter. However this was manually chosen by the author while it is preferable to study automated algorithms to optimise the shape of the threshold. Furthermore, in the proposed algorithms the instantaneous speed of the machine in the cyclo-non-stationary case was taken as input data, but in some industrial contexts this is not available and

it might be difficult to place an encoder on the machine. For this reason it is suggested to use one of the methods for instantaneous speed estimation from the vibration signals before the implementation of PE or AD, in such a way as to offer a more ductile tool to the industry. In a broader perspective, it is also of interest to use the proposed methods on condition monitoring applications other than diagnostics of defective bearings, for example of internal combustion engines or in modal analysis, and to test them on currents or pressure signals.

Finally, the two cases of missed detection described at the end of Chapter 5 suggest possible directions for increasing the reliability of a condition monitoring system. From the analysis conducted here, it appeared that the vibrations occurring on the location of the defect do not reach the transducer, presumably due to structural and material damping along the transfer path. Thus physical phenomena other than vibrations should be simultaneously measured, for instance acoustic emissions and temperature, maximising the probability of gathering diagnostics information and further allowing sensor fusion. In addition this limitation suggests a change to the view of the condition monitoring system. Currently this is seen as a tool to be applied to an existing machine, whereas its presence has to be planned at the design stage, placing transducers inside the machine close to components subjected to failures. From the broader perspective of condition based maintenance, this will also allow the collection of large data sets for evaluation of prognostics methods, which is currently the fundamental problem for the researchers in the field. Such a change of view will therefore dramatically extend the performance of the maintenance system and will open new research frontiers for the community.

Bibliography

[Abboud, 2015] Abboud, D. (2015). *Vibration-based condition monitoring of rotating machines in nonstationary regime*. PhD thesis, Lyon, INSA.

[Abboud et al., 2017] Abboud, D., Antoni, J., Sieg-Zieba, S., and Eltabach, M. (2017). Envelope analysis of rotating machine vibrations in variable speed conditions: A comprehensive treatment. *Mechanical Systems and Signal Processing*, 84, Part A:200 – 226.

[Abboud et al., 2016a] Abboud, D., Baudin, S., Antoni, J., Rmond, D., Eltabach, M., and Sauvage, O. (2016a). The spectral analysis of cyclo-non-stationary signals. *Mechanical Systems and Signal Processing*, 75:280 – 300.

[Abboud et al., 2016b] Abboud, D., Eltabach, M., Antoni, J., and Sieg-Zieba, S. (2016b). Envelope pre-processing techniques for rolling element bearing diagnosis in variable speed conditions. *International Journal of Condition Monitoring*, 6(2):27–32.

[AD, 2017] AD (2017). Analog multiplier AD633 datasheet. `http://www.analog.com/en/products/linear-products/analog-multipliers-dividers/ad633.html#product-overview`. Accessed: May.

[Akhand and Upadhyay, 2016] Akhand, R. and Upadhyay, S. H. (2016). A review on signal processing techniques utilized in the fault diagnosis of rolling element bearings. *Tribology International*, 96(Supplement C):289 – 306.

[Al-Ghamd and Mba, 2006] Al-Ghamd, A. M. and Mba, D. (2006). A comparative experimental study on the use of acoustic emission and vibration analysis for bearing defect identification and estimation of defect size. *Mechanical Systems and Signal Processing*, 20(7):1537 – 1571.

[Al-Najjar, 2007] Al-Najjar, B. (2007). The lack of maintenance and not maintenance which costs: A model to describe and quantify the impact of vibration-based maintenance on company's business. *International Journal of Production Economics*, 107(1):260–273.

[Analog Devices, 2017] Analog Devices (2017). MEMS Accelerometer Performance Comes Of Age. `http://www.analog.com/media/en/technical-documentation/tech-articles/mems-accelerometer-performance-comes-of-age.pdf`. Accessed: August.

[Antoni, 2006] Antoni, J. (2006). The spectral kurtosis: a useful tool for characterising non-stationary signals. *Mechanical Systems and Signal Processing*, 20(2):282 – 307.

[Antoni, 2007a] Antoni, J. (2007a). Cyclic spectral analysis in practice. *Mechanical Systems and Signal Processing*, 21(2):597 – 630.

[Antoni, 2007b] Antoni, J. (2007b). Cyclic spectral analysis of rolling-element bearing signals: Facts and fictions. *Journal of Sound and Vibration*, 304(3):497 – 529.

[Antoni, 2007c] Antoni, J. (2007c). Cyclic spectral analysis of rolling-element bearing signals: Facts and fictions. *Journal of Sound and Vibration*, 304(35):497 – 529.

[Antoni, 2007d] Antoni, J. (2007d). Fast computation of the kurtogram for the detection of transient faults. *Mechanical Systems and Signal Processing*, 21(1):108 – 124.

[Antoni, 2009] Antoni, J. (2009). Cyclostationarity by examples. *Mechanical Systems and Signal Processing*, 23(4):987 – 1036.

[Antoni et al., 2004] Antoni, J., Bonnardot, F., Raad, A., and El Badaoui, M. (2004). Cyclostationary modelling of rotating machine vibration signals. *Mechanical systems and signal processing*, 18(6):1285–1314.

[Antoni et al., 2017a] Antoni, J., Griffaton, J., André, H., Avendao-Valencia, L., Bonnardot, F., Cardona-Morales, O., Castellanos-Dominguez, G., Daga, A., Leclére, Q., Molina Vicuña, C., Acuña, D., Ompusunggu, A., and Sierra-Alonso, E. (2017a). Feedback on the surveillance 8 challenge: Vibration-based diagnosis of a safran aircraft engine. *Mechanical Systems and Signal Processing*.

[Antoni and Randall, 2004] Antoni, J. and Randall, R. (2004). Unsupervised noise cancellation for vibration signals: part iia novel frequency-domain algorithm. *Mechanical Systems and Signal Processing*, 18(1):103–117.

[Antoni and Randall, 2006] Antoni, J. and Randall, R. (2006). The spectral kurtosis: application to the vibratory surveillance and diagnostics of rotating machines. *Mechanical Systems and Signal Processing*, 20(2):308 – 331.

[Antoni et al., 2017b] Antoni, J., Xin, G., and Hamzaoui, N. (2017b). Fast computation of the spectral correlation. *Mechanical Systems and Signal Processing*, 92:248 – 277.

[Antoniadou et al., 2015] Antoniadou, I., Manson, G., Staszewski, W. J., Barszcz, T., and Worden, K. (2015). A time–frequency analysis approach for condition monitoring of a wind turbine gearbox under varying load conditions. *Mechanical Systems and Signal Processing*, 64:188–216.

[Apostolico et al., 1997] Apostolico, F., Gammaitoni, L., Marchesoni, L., and Santucci, S. (1997). Resonant trapping: A failure mechanism in switch transitions. *Physical Review E*, 55(1):36.

[Bagavathiappan et al., 2013] Bagavathiappan, S., Lahiri, B. B., Saravanan, T., Philip, J., and Jayakumar, T. (2013). Infrared thermography for condition monitoring a review. *Infrared Physics & Technology*, 60:35 – 55.

[Barbini et al., 2013] Barbini, L., Bordi, I., Fraedrich, K., and Sutera, A. (2013). The stochastic resonance in a system of gradient type. *European Physical Journal Plus*, 128:13.

[Barbini et al., 2015] Barbini, L., Cole, M., Hillis, A., and du Bois, J. (2015). Weak signal detection based on two dimensional stochastic resonance. In *23rd European Signal Processing Conference (EUSIPCO)*, pages 2147–2151. `https://doi.org/10.1109/EUSIPCO.2015.7362764`.

[Barbini et al., 2017a] Barbini, L., Eltabach, M., and du Bois, J. L. (2017a). Phase editing to enhance bearing fault detection in variable speed condition. In *Proceedings of the 1st World Congress on Condition Monitoring (WCCM)*, ILEC Conference Centre, London, UK.

[Barbini et al., 2018] Barbini, L., Eltabach, M., and du Bois, J. L. (2018). Application of cepstrum prewhitening on non-stationary signals. In *Advances in Condition Monitoring of Machinery in Non-Stationary Operations. Applied Condition Monitoring*, volume 9, pages 275–283. Springer.

[Barbini et al., 2017b] Barbini, L., Eltabach, M., Hillis, A., and du Bois, J. (2017b). Amplitude-cyclic frequency decomposition of vibration signals for bearing fault diag-

nosis based on phase editing. *Mechanical Systems and Signal Processing*. Accepted, in print.

[Barbini et al., 2017c] Barbini, L., Ompusunggu, A., Hillis, A., du Bois, J., and Bartic, A. (2017c). Phase editing as a signal pre-processing step for automated bearing fault detection. *Mechanical Systems and Signal Processing*, 91:407 – 421. `https://doi.org/10.1016/j.ymssp.2016.12.004`.

[Benzi et al., 1983] Benzi, R., Parisi, G., Sutera, A., and Vulpiani, A. (1983). A theory of stochastic resonance in climatic change. *SIAM Journal on Applied Mathematics*, 43(3):565–578.

[Benzi et al., 1981] Benzi, R., Sutera, A., and Vulpiani, A. (1981). The mechanism of stochastic resonance. *Journal of Physics A: Mathematical and General*, 14(11):L453.

[Bonnardot et al., 2005] Bonnardot, F., El Badaoui, M., Randall, R., Danire, J., and Guillet, F. (2005). Use of the acceleration signal of a gearbox in order to perform angular resampling (with limited speed fluctuation). *Mechanical Systems and Signal Processing*, 19(4):766 – 785.

[Borghesani et al., 2013a] Borghesani, P., Pennacchi, P., Randall, R. B., Sawalhi, N., and Ricci, R. (2013a). Application of cepstrum pre-whitening for the diagnosis of bearing faults under variable speed conditions. *Mechanical Systems and Signal Processing*, 36(2):370 – 384.

[Borghesani et al., 2013b] Borghesani, P., Ricci, R., Chatterton, S., and Pennacchi, P. (2013b). A new procedure for using envelope analysis for rolling element bearing diagnostics in variable operating conditions. *Mechanical Systems and Signal Processing*, 38(1):23–35.

[Bouillaut, 2001] Bouillaut, L.and Sidahmed, M. (2001). Cyclostationary approach and bilinear approach: comparison, applications to early diagnosis for helicopter gearbox and classification method based on hocs. *Mechanical Systems and Signal Processing*, 15(5):923–943.

[Braun, 1986] Braun, S. (1986). *Mechanical signature analysis: theory and applications*. Academic Pr.

[Cardenas Cabada et al., 2017] Cardenas Cabada, E., Leclere, Q., Antoni, J., and Hamzaoui, N. (2017). Fault detection in rotating machines with beamforming: Spatial visualization of diagnosis features. *Mechanical Systems and Signal Processing*, 97:33 – 43. Special Issue on Surveillance.

[Cardona-Morales et al., 2014] Cardona-Morales, O., Alvarez-Marin, D., and Castellanos-Dominguez, G. (2014). *Condition Monitoring Under Non-Stationary Operating Conditions using Time-Frequency Representation-Based Dynamic Features*, pages 441–451. Springer Berlin Heidelberg, Berlin, Heidelberg.

[Cempel, 1991] Cempel, C. (1991). *Vibroacoustic condition monitoring*. Ellis Horwood Limited.

[Chapeau-Blondeau and Godivier, 1997] Chapeau-Blondeau, F. and Godivier, X. (1997). Theory of stochastic resonance in signal transmission by static nonlinear systems. *Physical Review E*, 55(2):1478.

[Collis et al., 1998] Collis, W. B., White, P. R., and Hammond, J. K. (1998). Higher-order spectra: the bispectrum and trispectrum. *Mechanical systems and signal processing*, 12(3):375–394.

[Dai and He, 2012] Dai, D. and He, Q. (2012). Multiscale noise tuning stochastic resonance enhances weak signal detection in a circuitry system. *Measurement Science and Technology*, 23(11):115001.

[Dai et al., 2011] Dai, D., He, Q., Liu, Y., Wang, J., and Gong, C. (2011). An improved bistable circuitry system for weak signal detection. In *2011 IEEE International Conference on Information and Automation*, pages 79–84.

[Dalpiaz et al., 2000] Dalpiaz, G., Rivola, A., and Rubini, R. (2000). Effectiveness and sensitivity of vibration processing techniques for local fault detection in gears. *Mechanical systems and signal processing*, 14(3):387–412.

[Dwyer, 1983] Dwyer, R. (1983). Detection of non-gaussian signals by frequency domain kurtosis estimation. In *Acoustics, Speech, and Signal Processing, IEEE International Conference on ICASSP'83.*, volume 8, pages 607–610. IEEE.

[Dyer and Stewart, 1978] Dyer, D. and Stewart, R. M. (1978). Detection of rolling element bearing damage by statistical vibration analysis. *Journal of mechanical design*, 100(2):229–235.

[El-Thalji and Jantunen, 2015] El-Thalji, I. and Jantunen, E. (2015). A summary of fault modelling and predictive health monitoring of rolling element bearings. *Mechanical Systems and Signal Processing*, 6061:252 – 272.

[Elforjani and Mba, 2008] Elforjani, . and Mba, D. (2008). Monitoring the onset and propagation of natural degradation process in a slow speed rolling element bearing with acoustic emission. *Journal of Vibration and Acoustics*, 130(4):041013.

[Errichello and Muller, 2012] Errichello, R. and Muller, J. (2012). Gearbox reliability collaborative gearbox 1 failure analysis report. *Contract*, 303:275–3000.

[Fauve and Heslot, 1983] Fauve, S. and Heslot, F. (1983). Stochastic resonance in a bistable system. *Physics Letters A*, 97(1-2):5–7.

[Flandrin et al., 2004] Flandrin, P., Rilling, G., and Goncalves, P. (2004). Empirical mode decomposition as a filter bank. *IEEE signal processing letters*, 11(2):112–114.

[Fyfe and Munck, 1997] Fyfe, K. and Munck, E. D. S. (1997). Analysis of computed order tracking. *Mechanical Systems and Signal Processing*, 11(2):187 – 205.

[Gammaitoni et al., 1998] Gammaitoni, L., Hänggi, P., Jung, P., and Marchesoni, F. (1998). Stochastic resonance. *Reviews of modern physics*, 70(1):223.

[Gang et al., 1992] Gang, H., De-chun, G., Xiao-Dong, W., Chun-Yuan, Y., Guang-Rong, Q., and Rong, L. (1992). Stochastic resonance in a nonlinear system driven by an aperiodic force. *Physical review A*, 46(6):3250.

[Gardner, 1994] Gardner, W. A. (1994). An introduction to cyclostationary signals. *Cyclostationarity in communications and signal processing*, pages 1–90.

[Gebraeel et al., 2004] Gebraeel, N., Lawley, M., Liu, R., and Parmeshwaran, V. (2004). Residual life predictions from vibration-based degradation signals: a neural network approach. *IEEE Transactions on industrial electronics*, 51(3):694–700.

[Godivier et al., 1997] Godivier, X., Rojas-Varela, J., and Chapeau-Blondeau, F. (1997). Noise-assisted signal transmission via stochastic resonance in a diode nonlinearity. *Electronics Letters*, 33(20):1666–1668.

[Gryllias et al., 2017] Gryllias, K., Moschini, S., and Antoni, J. (2017). Application of cyclo-non-stationary indicators for bearing monitoring under varying operating conditions. In *ASME Turbo Expo 2017: Turbomachinery Technical Conference and Exposition*, pages V006T05A021–V006T05A021. American Society of Mechanical Engineers.

[Gryllias and Antoniadis, 2013] Gryllias, K. C. and Antoniadis, I. A. (2013). Estimation of the instantaneous rotation speed using complex shifted morlet wavelets.

Mechanical Systems and Signal Processing, 38(1):78 – 95. Condition monitoring of machines in non-stationary operations.

[Guoji et al., 2014] Guoji, S., McLaughlin, S., Yongcheng, X., and White, P. (2014). Theoretical and experimental analysis of bispectrum of vibration signals for fault diagnosis of gears. *Mechanical Systems and Signal Processing*, 43(1):76–89.

[Hänggi et al., 1993] Hänggi, P., Jung, P., Zerbe, C., and Moss, F. (1993). Can colored noise improve stochastic resonance? *Journal of Statistical Physics*, 70(1):25–47.

[He et al., 2012] He, Q., Wang, J., Liu, Y., Dai, D., and Kong, F. (2012). Multi-scale noise tuning of stochastic resonance for enhanced fault diagnosis in rotating machines. *Mechanical Systems and Signal Processing*, 28:443–457.

[Hedin, 2014] Hedin, L. O. E. (2014). Method and apparatus for analysing the condition of a machine having a rotating part. US Patent 8,762,104.

[Heng et al., 2009a] Heng, A., Tan, A. C. C., Mathew, J., Montgomery, N., Banjevic, D., and Jardine, A. K. S. (2009a). Intelligent condition-based prediction of machinery reliability. *Mechanical Systems and Signal Processing*, 23(5):1600–1614.

[Heng et al., 2009b] Heng, A., Zhang, S., Tan, A. C. C., and Mathew, J. (2009b). Rotating machinery prognostics: State of the art, challenges and opportunities. *Mechanical systems and signal processing*, 23(3):724–739.

[Howard, 1994] Howard, I. (1994). A review of rolling element bearing vibration 'detection, diagnosis and prognosis'. Technical report, DEFENCE SCIENCE AND TECHNOLOGY ORGANIZATION CANBERRA (AUSTRALIA).

[Huang et al., 1998] Huang, N. E., Shen, Z., Long, S. R., Wu, M. C., Shih, H. H., Zheng, Q., Yen, N. C., Tung, C. C., and Liu, H. H. (1998). The empirical mode decomposition and the hilbert spectrum for nonlinear and non-stationary time series analysis. In *Proceedings of the Royal Society of London A: mathematical, physical and engineering sciences*, volume 454, pages 903–995. The Royal Society.

[IMS, 2017] IMS (2017). IMS University of Cincinnati, NASA Ames Prognostics Data Repository. `http://ti.arc.nasa.gov/project/prognostic-data-repository`. Accessed: August.

[Janssens et al., 2015] Janssens, O., Schulz, R., Slavkovikj, V., Stockman, K., Loccufier, M., Van de Walle, R., and Van Hoecke, S. (2015). Thermal image based fault diagnosis for rotating machinery. *Infrared Physics & Technology*, 73:78 – 87.

[Jardine et al., 2006] Jardine, A. K. S., Lin, D., and Banjevic, D. (2006). A review on machinery diagnostics and prognostics implementing condition-based maintenance. *Mechanical Systems and Signal Processing*, 20(7):1483 – 1510.

[Kilundu et al., 2014] Kilundu, B., Ompusunggu, A., Elasha, F., and Mba, D. (2014). Effect of parameters setting on performance of discrete component removal (dcr) methods for bearing faults detection. In *Second european conference of the prognostics and health management (PHM) society, Nantes.*

[Klamecki, 2005] Klamecki, B. E. (2005). Use of stochastic resonance for enhancement of low-level vibration signal components. *Mechanical Systems and Signal Processing*, 19(2):223 – 237.

[Kloeden and Platen, 1992] Kloeden, P. and Platen, E. (1992). *Numerical Solution of Stochastic Differential Equations.* Springer Science & Business Media.

[Leclere et al., 2016] Leclere, Q., André, H., and Antoni, J. (2016). A probabilistic approach for the estimation of the instantaneous angular speed of rotating machines from vibration measurements: application to fault diagnosis. In *Proceedings of ISMA 2016*, Leuven, Belgium.

[Lu et al., 2014] Lu, S., He, Q., Hu, F., and Kong, F. (2014). Sequential multiscale noise tuning stochastic resonance for train bearing fault diagnosis in an embedded system. *IEEE Transactions on Instrumentation and Measurement*, 63(1):106–116.

[Lu et al., 2016] Lu, S., He, Q., Hu, F., and Kong, F. (2016). Online fault diagnosis of motor bearing via stochastic-resonance-based adaptive filter in an embedded system. *IEEE Transactions on Systems, Man, and Cybernetics: Systems*, PP(99):1–12.

[Luchinsky et al., 1999a] Luchinsky, D. G., Mannella, R., McClintock, P., and Stocks, N. G. (1999a). Stochastic resonance in electrical circuits. i. conventional stochastic resonance. *IEEE Transactions on Circuits and Systems II: Analog and Digital Signal Processing*, 46(9):1205–1214.

[Luchinsky et al., 1999b] Luchinsky, D. G., Mannella, R., McClintock, P., and Stocks, N. G. (1999b). Stochastic resonance in electrical circuits. ii. nonconventional stochastic resonance. *IEEE Transactions on Circuits and Systems II: Analog and Digital Signal Processing*, 46(9):1215–1224.

[Lumme, 2012] Lumme, V. (2012). *Intelligent Interpretation of Machine Condition Data.* PhD thesis, Julkaisu-Tampere University of Technology.

[Luo et al., 2010] Luo, H., Qiu, H., Ghanime, G., Hirz, M., and van der Merwe, G. (2010). Synthesized synchronous sampling technique for differential bearing damage detection. *Journal of Engineering for Gas Turbines and Power*, 132(7):072501.

[Malhi and Gao, 2004] Malhi, A. and Gao, R. X. (2004). Pca-based feature selection scheme for machine defect classification. *IEEE Transactions on Instrumentation and Measurement*, 53(6):1517–1525.

[Mallat, 1999] Mallat, S. (1999). *A wavelet tour of signal processing*. Academic press.

[Mba and Raj, 2006] Mba, D. and Raj, B. K. N. (2006). Development of acoustic emission technology for condition monitoring and diagnosis of rotating machines: Bearings, pumps, gearboxes, engines, and rotating structures. *The Shock and Vibration Digest*, 38(1):3–16.

[McFadden and Smith, 1984] McFadden, P. and Smith, J. (1984). Vibration monitoring of rolling element bearings by the high-frequency resonance technique a review. *Tribology International*, 17(1):3 – 10.

[McFadden and Smith, 1985] McFadden, P. D. and Smith, J. D. (1985). A signal processing technique for detecting local defects in a gear from the signal average of the vibration. *Proceedings of the Institution of Mechanical Engineers Part C Mechanical engineering science*, 199(4):287–292.

[Moss and McClintock, 1988] Moss, F. and McClintock, P. V. E. (1988). *Noise in Nonlinear Dynamical Systems*. Cambridge University Press.

[National Instruments, 2017] National Instruments (2017). Sensors for condition monitoring. `http://www.ni.com/white-paper/52461/en/`. Accessed: August.

[Nectoux et al., 2012] Nectoux, P., Gouriveau, R., Medjaher, K., Ramasso, E., Chebel-Morello, B., Zerhouni, N., and Varnier, C. (2012). Pronostia: An experimental platform for bearings accelerated degradation tests. In *IEEE International Conference on Prognostics and Health Management, PHM'12.*, pages 1–8. IEEE Catalog Number: CPF12PHM-CDR.

[Nikias and Mendel, 1993] Nikias, C. L. and Mendel, J. M. (1993). Signal processing with higher-order spectra. *IEEE Signal processing magazine*, 10(3):10–37.

[Ompusunggu et al., 2013] Ompusunggu, A. P., Devos, S., and Petre, F. (2013). Stochastic-resonance based fault diagnosis for rolling element bearings subjected to

low rotational speed. *International Journal of Prognostics and Health Management*, 4:1–15.

[Oppenheim and Lim, 1981] Oppenheim, A. and Lim, J. (1981). The importance of phase in signals. *Proceedings of the IEEE*, 69(5):529–541.

[Peeters et al., 2016] Peeters, C., Guillaume, P., and Helsen, J. (2016). Vibration-based bearing fault detection on experimental wind turbine gearbox data. In *Third european conference of the prognostics and health management (PHM) society, Bilbao*.

[Peeters et al., 2017] Peeters, C., Guillaume, P., and Helsen, J. (2017). A comparison of cepstral editing methods as signal pre-processing techniques for vibration-based bearing fault detection. *Mechanical Systems and Signal Processing*, 91:354–381.

[Pylvänen and Elfström, 2013] Pylvänen, M. and Elfström, J. (2013). *Remote Diagnostics with Distributed Intelligence and Centralised Data Storing*. moventas, EWEA.

[Randall, 2011] Randall, R. (2011). *Vibration-based Condition Monitoring*. John Wiley & Sons.

[Randall et al., 2001] Randall, R., Antoni, J., and Chobsaard, S. (2001). The relationship between spectral correlation and envelope analysis in the diagnostic of bearing faults and other cyclostationary machine signals. *Mechanical Systems and Signal Processing*, 15(5):945 – 962.

[Randall and Smith, 2016a] Randall, R. and Smith, W. (2016a). Use of the teager kaiser energy operator to estimate machine speed. In *Third european conference of the prognostics and health management (PHM) society, Bilbao, Spain*, pages 5–8.

[Randall, 2016] Randall, R. B. (2016). A history of cepstrum analysis and its application to mechanical problems. *Mechanical Systems and Signal Processing*, pages –.

[Randall and Antoni, 2011] Randall, R. B. and Antoni, J. (2011). Rolling element bearing diagnostics a tutorial. *Mechanical Systems and Signal Processing*, 25(2):485 – 520.

[Randall and Sawalhi, 2011] Randall, R. B. and Sawalhi, N. (2011). A new method for separating discrete components from a signal. *Sound and Vibration*, 45(5):6.

[Randall et al., 2011] Randall, R. B., Sawalhi, N., and Coats, M. (2011). A comparison of methods for separation of deterministic and random signals. *The International Journal of Condition Monitoring*, 1(1):11 – 19.

[Randall and Smith, 2016b] Randall, R. B. and Smith, W. A. (2016b). New cepstral methods for the diagnosis of gear and bearing faults under variable speed conditions. In *ICSV23 conference, Athens*.

[Ribrant and Bertling, 2007] Ribrant, J. and Bertling, L. (2007). Survey of failures in wind power systems with focus on swedish wind power plants during 1997-2005. In *Power Engineering Society General Meeting, 2007. IEEE*, pages 1–8. IEEE.

[Safran, 2017] Safran (2017). Surveillance 8 international conference. `https://surveillance8.sciencesconf.org/`. Accessed: September.

[Samuel and Pines, 2005] Samuel, P. D. and Pines, D. J. (2005). A review of vibration-based techniques for helicopter transmission diagnostics. *Journal of sound and vibration*, 282(1):475–508.

[Sato et al., 1977] Sato, T., Sasaki, K., and Nakamura, Y. (1977). Real-time bispectral analysis of gear noise and its application to contactless diagnosis. *The Journal of the Acoustical Society of America*, 62(2):382–387.

[Sawalhi and Randall, 2011] Sawalhi, N. and Randall, R. B. (2011). Signal pre-whitening for fault detection enhancement and surveillance of rolling element bearings. In *The Eighth International Conference on Condition Monitoring and Machinery Failure Prevention Technologies, Cardiff, Wales, UK, June*, pages 19–22.

[Schoen et al., 1995] Schoen, R., Habetler, T., Kamran, F., and Bartfield, R. G. (1995). Motor bearing damage detection using stator current monitoring. *IEEE transactions on industry applications*, 31(6):1274–1279.

[Sheng, 2012] Sheng, S. (2012). Wind turbine gearbox condition monitoring round robin study-vibration analysis. Technical report, National Renewable Energy Laboratory (NREL), Golden, CO.

[Siegel et al., 2014] Siegel, D., Zhao, W., Lapira, E., AbuAli, M., and Lee, J. (2014). A comparative study on vibration-based condition monitoring algorithms for wind turbine drive trains. *Wind Energy*, 17(5):695–714.

[Singleton et al., 2017] Singleton, R. K., Strangas, E. G., and Aviyente, S. (2017). The use of bearing currents and vibrations in lifetime estimation of bearings. *IEEE Transactions on Industrial Informatics*, 13(3):1301–1309.

[Sohoel, 1985] Sohoel, E. O. (1985). Method and instrument for determining the condition of an operating bearing. US Patent 4,528,852.

[Spectral Kurtosis, 2017] Spectral Kurtosis (2017). Code for fast implementation of the kurtogram. `https://uk.mathworks.com/matlabcentral/fileexchange/48912-fast-kurtogram`. Accessed: 2017-May.

[Stack et al., 2006] Stack, J. R., Habetler, T. G., and Harley, R. G. (2006). Fault-signature modeling and detection of inner-race bearing faults. *IEEE Transactions on Industry Applications*, 42(1):61–68.

[Stack et al., 2004] Stack, J. R., Harley, R. G., and Habetler, T. G. (2004). An amplitude modulation detector for fault diagnosis in rolling element bearings. *IEEE Transactions on Industrial Electronics*, 51(5):1097–1102.

[Stocks, 2000] Stocks, N. G. (2000). Suprathreshold stochastic resonance in multilevel threshold systems. *Physical Review Letters*, 84(11):2310.

[Tan et al., 2009] Tan, J., Chen, X., Wang, J., Chen, H., Cao, H., Zi, Y., and He, Z. (2009). Study of frequency-shifted and re-scaling stochastic resonance and its application to fault diagnosis. *Mechanical systems and signal processing*, 23(3):811–822.

[Vachtsevanos et al., 2006] Vachtsevanos, G. J., Lewis, F., Hess, A., and Wu, B. (2006). *Intelligent fault diagnosis and prognosis for engineering systems*. Wiley Online Library.

[Widrow et al., 1986] Widrow, B., Stearns, S. D., and Burgess, J. C. (1986). Adaptive signal processing edited by bernard widrow and samuel d. stearns. *The Journal of the Acoustical Society of America*, 80(3):991–992.

[Wójcicki et al., 2008] Wójcicki, K., Milacic, M., Stark, A., Lyons, J., and Paliwal, K. (2008). Exploiting conjugate symmetry of the short-time fourier spectrum for speech enhancement. *IEEE Signal processing letters*, 15:461–464.

[WoS, 2017] WoS (2017). Stochastic resonance used in bearing fault detection. `http://www.webofknowledge.com`. Accessed: May.

[Zimroz et al., 2014] Zimroz, R., Bartelmus, W., Barszcz, T., and Urbanek, J. (2014). Diagnostics of bearings in presence of strong operating conditions non-stationaritya procedure of load-dependent features processing with application to wind turbine bearings. *Mechanical systems and signal processing*, 46(1):16–27.